The Role of Oxidative Stress in Age-Related Changes to Ionic Currents Regulating Cerebral Giant Cell Excitability in the Pond Snail, *Lymnaea stagnalis*

Lamia Hachoumi

A thesis submitted in partial fulfilment of the requirements of the University of Brighton for the degree of Doctor of Philosophy

June 2018

The University of Brighton

Abstract

The increase in mean human lifespan since 1900 has been an incredible feat; however, ageing is a challenging issue faced by society. CNS ageing is accompanied by cognitive decline and is the major risk factor for conditions such as Alzheimer's disease. The understanding of the neuronal ageing process in mammalian species has been significantly hampered due to the complexity of the mammalian brain and restrictions of non-invasive experimental techniques in humans.

Many of the changes associated with neuronal ageing are evolutionarily conserved, which raises the possibility of using simpler organisms to investigate this process. This study utilised the pond snail, *Lymnaea stagnalis,* to perform a top-down analysis of the effects of age on *Lymnaea* feeding behaviour with a focus on age-related changes to voltage-gated outward currents in an identified pair of neurons, known as the cerebral giant cells (CGCs).

The observed decrease in feeding frequency with age was accompanied with reduced spontaneous and evoked CGC firing frequency, an increase in the after-hyperpolarisation, hyperpolarisation of the resting membrane potential and narrowing of action potentials. These changes were associated with underlying alterations to the kinetics and voltage sensitivity of the A-type K^+ current. Ageing suppressed a previously uncharacterised voltage-gated outward chloride current and enhanced a newly discovered voltage-gated TEA/4-AP/NPPB insensitive outward current in the CGCs. There were no age-related changes to the conductance of the delayed rectifier or recently identified inward rectifier. The use of selective pharmacological channel blockers inferred that many of the age-related changes to CGC action potential waveform could be explained by the altered A-type K^+ current. Ageing of the CGCs was also associated with an increase in MDA and protein carbonyl levels in the CNS, which suggested that oxidative stress might be an important determinant of these changes. Acute exposure to AAPH, a pro-oxidant generator, in young *Lymnaea* altered feeding frequency and mimicked many of the age-related changes to CGC firing properties that could be prevented or reversed with the antioxidant combination of Vitamins C and E. Furthermore, acute AAPH treatment remarkably replicated the effects of age on the voltage-gated outward currents in the young CGCs.

In conclusion, this study has characterised the age-related changes to CGC firing properties and has shown that many of these changes can be explained by alterations to the A-type K^+ current. These changes can be largely mimicked by acute AAPH treatment in young CGCs, which strongly suggests that oxidative stress is a major driver of CGC ageing.

Table of Contents

List of Tables

Table of Figures

Abbreviations and Definitions

4-HNE	4-Hydroxynonenal
5-HT	Serotonin
AA	Arachidonic acid
AAcid	Aristolochic acid
AAPH	2,2'-Azobis (2-amidinopropane) dihydrochloride
AD	Alzheimer's disease
AHP	After-hyperpolarisation
AP	Action potential
BG	Buccal ganglia
BK	Large conductance calcium activated potassium channel
CAMK	Calcium/Calmodulin-dependent kinase
CBC	Cerebral buccal connective
CC	Current clamp
CDK	Cyclin-dependent kinase
CG	Cerebral ganglia
CGC	Cerebral giant cells
CLC	Chloride-conducting ion channels
CNS	Central nervous system
COX	Cyclooxygenase
CPG	Central pattern generator/generating
CS	Conditioned stimulus
DR	Delayed rectifier
E_{rev}	Reversal potential
f_0	Initial instantaneous firing frequency
F_{adap}	Strength of adaptation
fAHP	Fast after-hyperpolarisation
FFA	Free fatty acids
f_{ss}	Steady state instantaneous firing frequency
G	Conductance
HVA	High-voltage activated calcium channel
I	Current
$I_{Na(P)}$	Persistent sodium current
$I_{Na(T)}$	Transient sodium current
I_A	A-type potassium current
I_{Cl}	Chloride current
ICS	Intracellular calcium stores
I_{DR}	Delayed rectifier current
IL	Interleukin
I_R	Inward rectifier current
I_{sAHP}	Slow after-hyperpolarisation current

L&M	Learning and memory
LCGC	Left CGC
LOX	Lipoxygenase
LTD	Long-term depression
LTM	Long-term memory
LTP	Long-term potentiation
LVA	Low-voltage activated calcium channels
mAHP	Medium after-hyperpolarisation
MDA	Malondialdehyde
mTOR	Mammalian Target of Rapamycin
NADPH	Nicotinamide adenine dinucleotide phosphate
NCX	Sodium calcium exchanger
NF-kB	Nuclear factor kappa-light-chain-enhancer of activated B cells
NO	Nitric oxide
NOS	Nitric oxide synthase
OS	Oxidative stress
PC	Protein carbonyl
PCGC	Paired CGCs
PD	Parkinson's disease
PLA_2	Phospholipase A_2
RCGC	Right CGC
RMP	Resting membrane potential
ROS	Reactive oxygen species
RyR	Ryanodine receptors
sAHP	Slow after-hyperpolarisation
SASP	Senescence-associated secretory phenotype
SFA	Spike frequency adaptation
SF	Selectivity filter
SK	Small conductance calcium-activated potassium channels
TEVC	Two-electrode voltage clamp
V	Voltage
VC	Voltage clamp
VGCC	Voltage-gated calcium channels
VGKC	Voltage-gated potassium channels
V_m	Membrane potential
VSD	Voltage sensor domain
$\tau_{activation}$	Time constant of activation
τ_{adap}	Time constant of adaptation
$\tau_{calcium}$	Time constant of calcium clearance
$\tau_{deactivation}$	Time constant of deactivation
$\tau_{inactivation}$	Time constant of inactivation

Acknowledgments

First and foremost, I would like to thank my principle supervisor, Dr Mark Yeoman, for his unwavering support, encouragement, optimism and patience that has helped make this thesis possible. The last few years have truly been an invaluable and inspiring experience as I have learnt so much from his knowledge and skills about electrophysiology, ageing and the research process- all of which will serve me in good stead throughout my career. I have been lucky to have such a fantastic supervisor to conduct research with and thus, thank you again for all that you have done for me.

I would also like to say a massive thank you to my other wonderful supervisors, Dr Greg Scutt and Dr Marcus Allen, for all their support, expertise and very insightful discussions.

Thank you to Dr Jon Mabley and Dr Bhavik Patel for the interesting conversations regarding oxidative stress and non-scientific related stuff in the lab. I would also like to thank the technical staff in the Bioresources Unit for tending to the snails utilised in this thesis.

Lastly, I would like to thank my family. An enormous thanks to my incredibly patient parents who are undoubtedly my biggest supporters and have always encouraged me to follow my passion. Thank you to my two brothers, Ayoub and Ousama, who have also supported me throughout this whole process. Thanks for generally putting up with me!

Author's Declaration

I declare that the research contained in this thesis, unless otherwise formally indicated within the text, is the original work of the author. The thesis has not been previously submitted to this or any other university for a degree, and does not incorporate any material already submitted for a degree.

Signed

Dated   **27/06/2018**

"Hard work is only a prison sentence if you lack motivation"

- Malcolm Gladwell

Chapter 1: Introduction

1.1 Ageing

In multicellular organisms, the moment of conception signals the commencement of growth and development leading to a stage of reproductive competence during adulthood (**Figure 1.1**). With time, however, facets associated with a process described as ageing begin to emerge. Ageing is commonly defined by biologists as the deterioration of physiological integrity, resulting from the accumulation of deleterious changes with advancing age[448]. In humans, ageing is a familiar aspect of life that is characterised by a progressive decline in function, loss of fecundity, increased risk of disability, chronic or degenerative diseases and eventually death as the final end point[333].
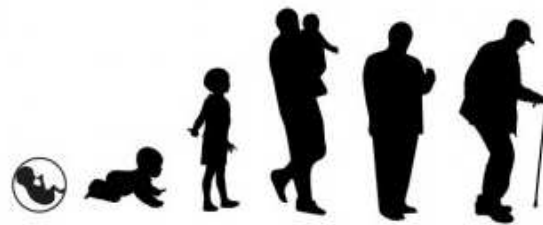
Figure 1.1| Human Ageing. The ageing process is an intrinsic process that occurs in every individual and leads to a physiological decline[271]**.**

1.1.1 The ageing population dilemma

The increase in human lifespan expectancy is one of the most remarkable achievements of the 20th century. In fact, in most developed countries including the United Kingdom (UK) there has been more than a doubling in life expectancy[77]. Before 1900, most individuals did not exceed the age of 50 years old- a trend that had changed very little since the times of the Roman Empire. Mortality was exceptionally high, particularly during childhood because of infectious diseases[334,275]. By mid-19th century, however, improvements in sanitation and medical advances such as the development of antibiotics aided the control of infectious diseases and led to a significant decrease in childhood mortality and improvement in life expectancy. In the UK in 1985, only 15% of the population was aged 65 years old and over[275]. At present, this figure has increased to 24%, which is approximately 11 million people in the population. It is projected that by 2035, 16 million people (29%) will be aged 65 years old and over. The 'oldest old', individuals aged 85 years old and over, have seen the fastest increase of more than a doubling in their population from 0.7 million in 1985 to over 1.5 million people in 2010.

By 2035, it is expected that 3.5 million people (or 5%) will be aged 85 years old and over in the UK[334,77,4]. The number of centenarians (those aged 100 years old and over) has also increased significantly over the last 30 years from 2,500 in 1985 to 13,350 in 2012[491]. Improvement in health, decreases in birth rate and ageing of the 'baby boomers' has been so significant that for the first time in history the proportion of individuals aged 65 years old and over in the UK is larger than the under 16 years old age group[4].

This accomplishment of human lifespan extension in the developed world has been accompanied by a transition in mortality- from a great reduction in childhood mortality caused by poor infection control to a rise in adulthood mortality (as well as morbidity) caused by chronic and degenerative diseases such as cancer and Alzheimer's disease (AD). For example, it is estimated that around 800,000 people aged 65 years old and over are currently suffering from dementia[4]. It is projected by 2025, this figure will increase to 1.14 million people[4]. Undoubtedly, this will have a huge economic and social impact. Currently two-thirds of patients receiving medical care on the NHS are 65 years old and over. In 2012, ~ £9.4 billion of the NHS budget was spent on elderly care[358]. With the NHS suffering from its worst ever financial crisis there are deep concerns about the quality of care that the elderly will receive. To compound the situation, government cuts in social care has increased the burden on the NHS to care for the elderly population. Indeed, a recent report published by Sir Michael Marmot at University College London highlighted that the rise in life expectancy may actually be grinding to a halt due to this recession of governmental funding to health and social care for the elderly population[289].

Whilst the government has pledged to increase the NHS budget by £10 billion in 2021 for the care of elderly patients they will also need to heavily invest in ageing research to prevent the collapse of the NHS in future[114]. Ageing research is very important especially as no cures currently exist for a large number of age-related conditions such as AD. Thus, gaining an understanding of the ageing process will facilitate the future development of therapeutics that may delay or prevent the progression of age-related diseases and potentially ageing itself.

1.2 Normal brain ageing

Normal brain ageing is an intrinsic process that occurs in every human[108]. A decline in cognitive and motor functioning as well as balance impairment and hearing loss are some of the common phenotypic changes associated with normal brain ageing. The extent of

these manifestations varies between individuals and in some, these phenotypes may not even be obvious. Typically, these impairments are not serious enough to cause disability and in fact over 60% of the population aged 65 years old and over are considered as ageing normally (or healthy)[362].

1.2.1 Learning and memory changes during normal brain ageing

Memory impairment is the clinical condition that is most frequently observed during normal brain ageing and is specifically referred to as age-associated memory impairment (AAMI). The diagnostic criteria for AAMI include the following: 1) Individual aged 50 years old and over; 2) Score 1 SD (standard deviation) lower in memory test than the mean for young adults, and; 3) absence of dementia and other conditions such as depression[421]. It has been found that AAMI affects approximately 38% and 80% of the elderly population aged 65-80 years old and >80 years old, respectively[421,238]. Interestingly, AAMI appears to be a relatively evolutionarily conserved feature of ageing as invertebrate species such as *Aplysia californica, Lymnaea stagnalis* and *Drosophila melanogaster* also exhibited such behavioural changes[163,149,228,477].

Long-term memories are those that can last for days, months and years and are categorised as either explicit or implicit. Explicit (or declarative) memories involve the conscious retrieval of information such as facts (semantic memories) and events (episodic memories). In contrast, implicit (non-declarative) memories are those that are stored and retrieved without conscious recollection and is evident while performing tasks such as walking or riding a bike[389].

It has been well established from explicit memory tasks in humans that older individuals encounter difficulties in their ability to remember information learned recently, whereas younger subjects do not experience such difficulties[475,98]. In particular, it has been observed that episodic memory performance begins to display signs of impairment from middle age onwards. Semantic memory remains relatively stable from middle age to young elderly, but performance is hindered in very old individuals[170]. Implicit memory appears to be unaffected by the ageing process[475].

1.2.2 Neuroanatomical changes during normal brain ageing

It has been consistently found in humans that there is a reduction in the volume and/or weight of the brain during normal ageing, particularly in the frontal lobes and

hippocampus[15,343]. This decrease in volume was previously attributed to neuronal death; however, advances in stereological techniques have shown that neuronal loss is actually very minimal (approximately 10%) in healthy old individuals[15]. For example, Gómez-Isla *et al.* (1996) used stereological cell-counting techniques in human post-mortem brains and discovered that in the entorhinal cortex there was no neuronal loss in this region with age. However, in brains from AD patients there was a neuronal loss of ~50% in this region when compared to the healthy age-matched controls[153]. Indeed, numerous studies in ageing mammalian models have now corroborated such findings[153,328,343,15].

With neuronal loss being very small in the healthy ageing brain, it is therefore only responsible for a small reduction in brain volume. Due to such findings, the focus has shifted to examine whether decreases in brain volume arise as a result of morphological alterations to neurons with age. Investigations in the hippocampus have shown *via* immunoblot and proteomic experiments that the levels of synapse-specific proteins decreases with age[454]. Canas *et al.* (2009), for example, showed that the presynaptic terminal protein, synaptophysin and SNAP-25, were significantly reduced in old rats when compared to young rats[63]. Such findings indicate that there is a decrease in the number of pre- and post-synaptic terminals with age. Studies using electron microscopy with synaptic immunolabeling have supported these findings by illustrating the loss of synaptic terminals and even a decrease in perforated synapses in the ageing hippocampus[304,345,100]. Interestingly, the animals used in all these studies displayed deficits when performing learning and memory tasks such as the Morris water maze and it has been shown that the magnitude of synaptic terminal loss is correlated with the severity of memory impairment[304,345,100].

Other studies in mammals have shown that in the ageing neocortex, hippocampus, cerebellum and substantia nigra there is a decrease in the density of dendritic spines by approximately 20-40%[100]. This loss of spines is accompanied with a decrease in axospinous synapses[345,100]. In ageing rats it has been reported that decreases in dendritic spines in the hippocampus is associated with impairment of spatial memory tasks, as young rats with intact memory did not exhibit such morphological changes[100]. Shorter apical dendrites and reduced dendritic arborisation have also been observed in CA1 hippocampal neurons and neocortical neurons in old mice, monkeys and humans[109,100,342]. Structural image analysis in the cerebellum and substantia nigra have shown not only is there a regression of dendritic arbors, but that there is also atrophy of the neuronal soma in old mammalian models[100].

Interestingly, morphological changes to neurons with increasing age is a conserved evolutionarily feature as such alterations have also been documented in invertebrate species. For example, in *Caenorhabditis elegans* (*C. elegans*) it has been found that there is ectopic branching from the soma and axonal blebbing with increasing ageing[437,74]. In the pond snail, *Lymnaea stagnalis,* Janse *et al.* (1999) demonstrated axonal branching was significantly reduced in ageing neuroendocrine caudodorsal cells[528].

1.2.3   Age-related changes in neuronal firing

A decline in neuronal firing frequency is commonly associated with ageing of neurons and is believed to be a contributing factor underlying AAMI[364,310]. For example, Kaczorowski *et al*. (2009) demonstrated the relationship between an age-related decrease in neuronal firing and alterations to learning and memory[215]. In this study, mice were trained on a fear conditioning task to assess memory formation and it was observed that old mice displayed a mild specific deficit in spatial learning when compared to young mice[215]. Furthermore, current clamp recordings from CA1 hippocampal neurons in these old mice revealed that there was a significant decrease in neuronal firing frequency that was accompanied with an increase in the amplitude and duration of the after-hyperpolarisation (AHP)[215].

Numerous studies involving invertebrate species have also shown that hypoexcitability is an evolutionarily conserved manifestation of the ageing process. For example, investigations by Patel *et al*. (2006) and Scutt *et al*. (2012) in the cerebral giant cells (CGCs) of ageing *Lymnaea*, revealed that there was as significant decrease in both spontaneous and evoked firing rates[393,336]. This, as often reported in ageing mammalian neurons, was accompanied with an increase in the AHP duration. Experiments conducted by Hermann *et al*. (2013) and Watson *et al*. (2012) not only showed that neuronal firing rates decreased in *Lymnaea* with age, but also found that old snails were unable as a consequence to consolidate learned behaviour into LTM[175,477].

A clear consistent finding from both ageing mammalian and invertebrate species is that the decrease in neuronal firing is accompanied with an increase in the AHP. This contributes to the slowing of neuronal firing frequency by increasing the inter-spike interval[393,292,364,325]. The AHP is composed of three distinct components. The initial component is the fast AHP (fAHP) that lasts for ~2-10 ms, this is followed immediately by the medium AHP (mAHP) that lasts ~50-100 ms and finally the slow AHP (sAHP),

which has a time course of seconds[292]. Specifically, changes to the mAHP and sAHP duration have typically been reported in studies examining the decline in neuronal firing frequency with age[393,503,364,292].

Generation of the AHP is partly mediated by calcium (Ca^{2+})-activated potassium K^+ currents[364,292]. Indeed, it has been well recognised that Ca^{2+}-activated K^+ currents are vulnerable to the ageing process particularly due to the dysregulation of Ca^{2+} homeostasis[447,445]. This is often reflected as an increase to their conductance, which has partially been able to explain the increase to the AHP duration with age[352,392,292].

It is also known, however, that other conductances such as voltage-gated K^+ currents can have an important role in regulating the AHP[212,146,457,416]. Such currents have not been as extensively examined in relation to the age-related increase of the AHP duration. The likely reason for this is that they are not dependent on Ca^{2+} and therefore, often presumed to be unaffected by alterations to Ca^{2+} homeostasis with age[318,151]. This also appears to have led to a general assumption that ionic currents not dependent on Ca^{2+} are not significantly impaired with age, irrespective of the knowledge that they could be affected indirectly by altered Ca^{2+} homeostasis and/or altered by other detrimental processes involved in ageing such as oxidative stress (OS) and inflammation[398,399,364].

1.2.4 Age-related changes in synaptic transmission

In addition to a decline in neuronal firing, subtle alterations occurring at the synapse with age are also believed to lead to the development of AAMI. Synapses are specialized cell-to-cell junctions that enables neurons to communicate with each other and thus, mediate a variety of cognitive processes in the brain such as learning and memory[431,464].

The process of synaptic transmission begins at the presynaptic terminal following the arrival of an action potential. This depolarisation stimulates Ca^{2+} influx *via* voltage-gated Ca^{2+} channels (VGCCs), which subsequently triggers the migration and fusion of synaptic vesicles to the active zone of the terminal. Neurotransmitters released from the vesicles during exocytosis diffuse across the synaptic cleft and bind to their target receptors located on the postsynaptic membrane. Excitatory neurotransmitters will cause the membrane potential to depolarise and thus propagate the electrical signal, whilst inhibitory neurotransmitters will hyperpolarise the membrane potential to attenuate the propagation of electrical signals[364]. Synaptic transmission is perhaps the most

fundamental process in the brain that enables it to achieve all of its functions and therefore, any alterations to this process can have detrimental ramifications[464].

So, what happens to synaptic transmission with age? In relation to glutamate neurotransmission, a few studies have observed that glutamate uptake is significantly reduced in the ageing hippocampus and cerebral cortex of rodents[384,24,394]. This has been cited as one of the principle factors impeding glutamate neurotransmission[394,482,350]. Another study by Latour *et al.* (2012), for example, demonstrated that glutamate release was also altered with age[255]. In this study, the paired-pulse facilitation ration (an index of change in presynaptic glutamate release) was higher in the ageing hippocampus of rats and thus, suggesting that there is a reduction in presynaptic glutamate release[255]. Furthermore, Western-blot analysis also showed significant decreases in the vesicular glutamate transporters, VGlut-1 and VGlut-2, in the presynaptic membranes of these older animals[255].

Even in simpler models of ageing there have been a few studies examining changes to neurotransmission. For example, Patel *et al.* (2012) utilised carbon fibre amperometry to investigate serotonin (5-HT) release from the CGCs in the ageing *Lymnaea* CNS[337]. It was observed that there was an increase in spontaneous 5-HT release and a decrease in 5-HT clearance in the old CGCs[337]. This reduction in clearance, as reflected by an increase in the time constant of decay (t), may have been due to dysfunction of the serotonin transporter (SERT)[337]. Interestingly, it was found that blocking SERT in old CGCs with fluoxetine decreased t[337]. However, it would have been expected that inhibiting SERT would further increase t in the old CGCs rather than decrease it. It was postulated that the inhibition of SERT may have triggered a compensatory mechanism(s) in old CGCs to reduce 5-HT content in the extracellular space[337].

1.2.5 Age-related changes in synaptic plasticity

Synaptic plasticity is the modification of the efficacy of synaptic transmission, i.e. its synaptic strength. Studies have revealed that alterations to neuronal firing and synaptic transmission with age contribute towards alterations in synaptic plasticity[310,91,247].

Hebbian forms of synaptic plasticity, including long-term potentiation (LTP) and long-term depression (LTD), have been proposed as cellular correlates for specific types of memories[10,93]. LTP is the enhancement of synaptic strength lasting for hours or even days, whilst LTD is the decrease in synaptic strength[10,290].

N-methyl- D-aspartate receptor (NMDAR)-dependent LTP is triggered by the strong depolarisation of the postsynaptic membrane in order to relieve the Mg^{2+} block of NMDA receptors and thus, allow for its activation by presynaptically released glutamate[290]. Both Ca^{2+} and Na^+ can then enter the postsynaptic dendritic spine[290]. The significant rise in postsynaptic Ca^{2+} triggers LTP *via* the activation of signalling transduction molecules such as Ca^{2+}/calmodulin(CaM)-dependent protein kinase II (CaMKII)[93,10,290]. The primary mechanism involved in LTP expression at hippocampal synapses is the alteration in α-amino-3-hydroxy-5-methyl-4-isoxazolepropionic acid (AMPA) receptor trafficking, which results in an increase in the number of AMPA receptors expressed within the postsynaptic density[10,290]. The persistence of synaptic enhancement for hours to days (late phase of LTP), requires protein synthesis[10,290].

The induction of NMDAR-dependent LTD requires only a smaller rise in postsynaptic Ca^{2+}[290,78]. This activates serine/threonine phosphatases during signal transduction, which dephosphorylates synaptic substrates[290]. For example, Ser845 on GluR1 is a protein kinase A (PKA) substrate site that has been shown to be dephosphorylated during LTD[10,290,78]. This decreases the probability of AMPA receptor channel opening and thus, contributes to the expression of LTD (**Figure 1.2**). The removal of AMPA receptors *via* dynamin- and clathrin-dependent endocytosis is also involved in LTD expression [290,78].
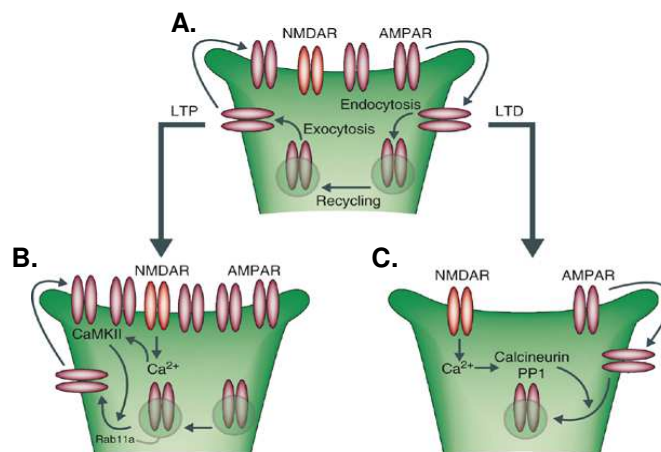
Figure 1.2| Hippocampal LTP and LTD [78]. (A) During the basal state, NMDA receptors are non-active due to the Mg^{2+} block (not shown) and AMPA receptors cycle between the intracellular compartments and postsynaptic membrane. (B) The induction of LTP is signalled with a robust influx of Ca^{2+} *via* NMDA receptors. CaMKII is then activated and enhances LTP by increasing AMPA receptor translocation to the postsynaptic membrane. (C) During LTD, endocytosis is enhanced to remove AMPA receptors from the postsynaptic membrane, a Ca^{2+}-dependent process involving calcineurin.[10,290,78]

It has been recognised that the age-related decline in synaptic plasticity may be due to an increase in the LTP threshold[360]. Studies by Barnes *et al.* (1996) and Foster *et al.* (2007) found that this was partly caused by insufficient postsynaptic depolarisation, which consequently led to a reduction in NMDA receptor activation[128,27,245]. It is thought that the larger AHP also observed in these ageing neurons hinders the integration of postsynaptic potentials and therefore decreases depolarisation of postsynaptic neurons[129,245,252]. Other studies involving the ageing CA1 hippocampal region of rodents have also shown that there are deficits to the NMDA receptor itself due to oxidative modifications and/or alterations in subunit expression[245]. This diminishes the Ca^{2+} contribution to LTP made by the NMDA receptors and thus, LTD is favoured over LTP[129,245,252].

Studies investigating the ageing prefrontal cortex in rats, have also reported that there is disinhibition of PKA signalling[360]. It was observed that increasing PKA activity in these animals exaggerated cognitive deficits, whilst inhibition ameliorated such deficits[360]. In invertebrates such as *Drosophila melanogaster* and *Aplysia californica,* it has also been shown that the decline in synaptic plasticity with age is caused by a chronic increase in PKA activity and that this could be reversed by reducing its activity[499,23,228].

1.3   Oxidative stress: The mechanism driving neuronal ageing?

In order to understand how the phenotypic changes observed during normal brain ageing manifests, an understanding of the mechanistic basis of neuronal ageing is required. Such knowledge could also facilitate the development of therapeutic treatments in the future that could potentially ameliorate the detrimental effects associated with brain ageing. This would significantly improve the quality of life for individuals and may even extend longevity.

At present, OS is considered a critical mediator of neuronal ageing[503,445,295,470]. Numerous studies from mammalian to invertebrate models have demonstrated that there is a significant increase in OS in the ageing CNS, which suggests that this may be an evolutionarily conserved facet of the neuronal ageing process[503,445,295,470,87,176,32]. Such studies have implicated the increase in OS responsible for the functional alterations observed in ageing neurons[503,445,295,470,87,176,32].

The initial theory regarding the role of OS in ageing was the "free radical theory of ageing", which had been proposed by Denham Harman in 1956[168]. Here, it was

postulated that ageing and age-related diseases manifest as a result of cumulative changes/damage to cell and tissues inflicted by an increase in the production of free radicals[150,168].

Under normal physiological conditions, redox homeostasis establishes a dynamic balance between pro-oxidants and antioxidants whereby excess free radicals are scavenged by antioxidants to attenuate any potential damage. With age, however, this balance between pro-oxidants and antioxidants is compromised and there is a shift to the former that results in the excessive generation of free radicals (**Figure 1.3**)[463,135]. This imbalance, as described by the theory, induces OS- a state where endogenous antioxidant defence systems are overwhelmed- and thus, eventually causes oxidative damage[463,135,168].

Figure 1.3| Ageing and OS. There is a loss of homeostatic control in the body with age, which consequently affects the dynamic balance between pro-oxidants and antioxidants. This shift results in the excessive generation of free radicals.

1.3.1   Generation of reactive oxygen species

A free radical is any molecular species capable of independent existence that contains an unpaired electron in its outer shell[346]. Free radicals chemically alter biological molecules because their unpaired electrons makes them highly reactive and unstable molecules[265,135]. In aerobic organisms, oxygen is critically important for normal functioning and thus, the majority of free radicals produced are oxygen-centred radicals. Such radicals are commonly referred to as reactive oxygen species (ROS) and include some of the following: superoxide ($O_2^{\bullet-}$), hydroxyl radical (•OH), nitric oxide (NO•), peroxyl radicals (ROO•), hydroperoxyl (HO2•), and alkoxyl radicals (RO•). Importantly, the term ROS does not just encompass free radicals but also includes non-free radical species. Such molecules are reactive, but are not classified as free radicals due to their lack of unpaired electrons. Hydrogen peroxide (H_2O_2), peroxynitrite ($ONOO^-$), ozone and hypochlorous acid are examples of non-free radical species.[7,346]

Cells can generate ROS in several ways. NADPH oxidases in cells are responsible for electron transfer across biological membranes and in doing so generate superoxide from the reduction of oxygen[329,127]. This formation of superoxide undergoes further reactions to generate hydrogen peroxide, hydroxyl radicals and hypochlorous acid[329,127]. Both phagocytic and non-phagocytic NADPH oxidases are one of the few intracellular sources that generate ROS as part of their primary function rather than as by-product[33].

Nitric oxide synthase (NOS) is another important intracellular source of ROS[45]. By utilising L-arginine, O_2 and NADH, NOS produces nitric oxide (NO), which has a number of physiological functions[45]. There are three types of NOS: 1) endothelial NOS (eNOS); 2) neuronal NOS (nNOS); and 3) inducible NOS (iNOS)[45]. NO produced by eNOS in endothelial cell is involved in vasodilation of the arterial wall[64]. NO generated by nNOS in nitrergic neurons is involved in maintaining LTP during learning and memory as well as relaxing smooth muscle in the gastrointestinal tract[339]. NO produced by iNOS is an effector molecule in the inflammatory and immune response and thus beneficial; however, overproduction is detrimental and can result in oxidative damage to tissues under pathological conditions and/or ageing[73].

Xanthine oxidases utilise xanthine as a substrate as well as O_2 as its electron acceptor in synthesis of $O_2^{\cdot-}$, which can then undergo subsequent reactions to form additional ROS[371,265]. This ROS generated (at low levels) is involved in second messenger signalling and the synthesis of antimicrobial molecules[465]. Other intracellular generators of ROS include, for example, the endoplasmic reticulum, peroxisomes, lipoxygenases and cyclooxygenases[33]. Additionally, it has been demonstrated that exogenous environmental factors such as ultraviolet light and toxins such as rotenone have the capacity to cause ROS generation in cells[41].

The mitochondrial respiratory chain, however, is the site responsible for the vast majority of ROS produced in cells under normal conditions (**Figure 1.4**). In cellular respiration, the two electron carrier molecules, NAD^+ and FAD, accept electrons from reactions occurring during glycolysis and the Krebs cycles and thus are reduced to NADH and $FADH_2$, respectively. These electrons then enter the mitochondrial electron transport chain, which consists of several events that occur on five protein complexes located on the inner mitochondrial membrane. During the first stage, NADH specifically donates electrons to complex I and $FADH_2$ donates its electrons to complex II. Electrons are passed from these complexes to ubiquinone (coenzyme Q). Reduced ubiquinone donates

the electrons to complex III, which subsequently passes them to peripheral cytochrome *c*. These electrons are relayed to complex IV to mediate the formation of water from O_2 and hydrogen ions (H^+). The flow of electrons through complex I, III and IV is coupled to the pumping of protons from the mitochondrial matrix to the intermembrane space. This generates a proton-motive force utilised by complex V (ATP synthase) to produce ATP from ADP and inorganic phosphate.[260,82]
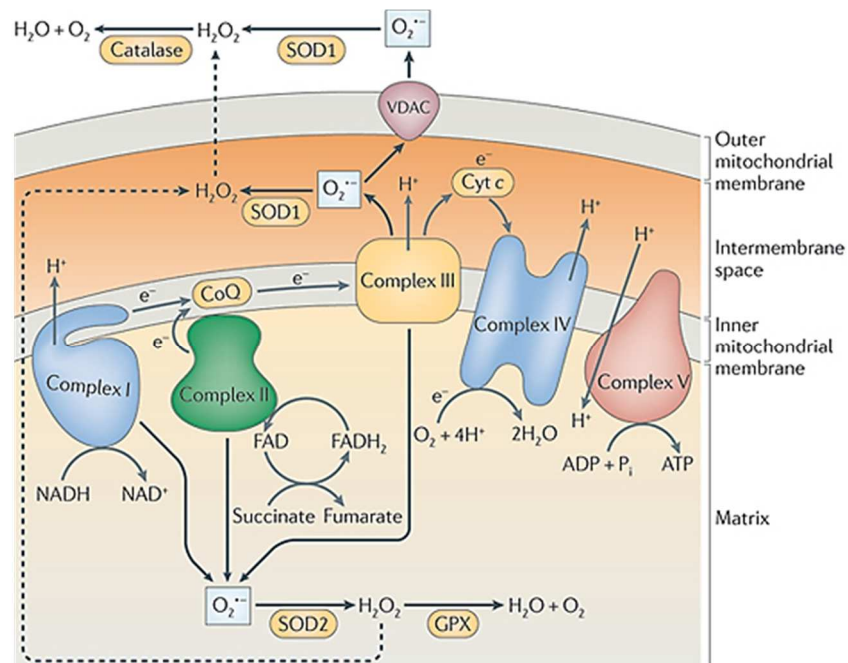
Figure 1.4| The mitochondrial electron transport chain[481]. During this process, electrons are transferred to complex I and II of the electron transport chain (on the inner membrane) from NADH and FADH₂, respectively. These electrons are then transferred from coenzyme Q to complex III to complex IV and finally to complex V, where ATP is synthesized. Superoxide generation can occur, at very low levels, due to electron leakage across complex I-III and can be converted to H₂O₂ by SOD1 and 2 enzymes. Subsequently, H₂O₂ can be broken down to H₂O and O₂ by either catalase or glutathione peroxidase.[481,202,82]

1.3.1.1 Potent intracellular ROS generators during neuronal ageing

In the 1970s, Denham Harman's 'the free radical theory of ageing' was updated to incorporate the role of the mitochondria in OS during ageing[302]. This theory is now referred to as the 'mitochondrial free radical theory of ageing (MFRTA)'[302,463]. Here, it was proposed that mitochondria are primarily responsible for the excessive production of free radicals with age due to their involvement in oxidative phosphorylation, which requires them to consume approximately 90% of the cell's oxygen supply[82].

Since this proposal, studies investigating the ageing CNS have shown that the mitochondria indeed continue to be the main intracellular source of ROS in neurons, but their output is severely enhanced[161,445]. This is problematic for two main reasons. First, mitochondria regulate a number of important cellular functions such as ATP synthesis, Ca^{2+} buffering, fatty acid oxidation and apoptosis[218]. Second, neurons are highly metabolic cells and require large numbers of mitochondria in order to perform critical processes including neuronal firing and neurotransmission[218]. Thus, impairment to the functioning of mitochondria with age due to their increase in ROS production will ultimately have detrimental effects on the properties and lifespan of neurons.

Mitochondria are very interesting organelles as they, like the nucleus, possess their own DNA and genetic machinery[52]. Its genome is a circle, of approximately 16.5 kb, double-stranded mitochondrial DNA (mtDNA) that encodes for 13 proteins of the oxidative phosphorylation system, 2 ribosomal RNAs (rRNAs) and 22 transfer RNAs (tRNAs)[52]. The rest of the genes required for the functioning of the mitochondria are encoded by nuclear DNA (nDNA)[52].

A growing body of evidence has implicated mtDNA damage specifically responsible for the increase in mitochondrial ROS generation during normal neuronal ageing and even in neurodegenerative diseases[156,161,295,297]. mtDNA are regularly attacked by ROS throughout an organisms lifetime due to their close proximity to the respiratory chain[52,500]. This leads to an accumulation of mutations, which is exacerbated by the lack of protective histones on mtDNA as well as the decline incurred to DNA repair mechanisms with increasing age[500].

Damaged mtDNA contributes to the age-related increase in mitochondrial ROS production by primarily hindering oxidative phosphorylation[376,161]. This causes more electrons to prematurely leak from the ETC and subsequently augments superoxide production[376,161]. Studies have consistently shown that mtDNA damage during normal neuronal ageing specifically reduces complex I and IV activity in rodents[295]. Typically these alterations appear to be profound in regions vulnerable to the ageing process and implicated in AAMI, such as the hippocampus and cerebral cortex[295]. Overall, it appears that a viscous cycle manifests within the mitochondria between mtDNA damage and ROS generation that leads to the increase in OS during neuronal ageing.

1.3.1.2 Potent extracellular ROS generators during neuronal ageing

The properties of neurons with age are also profoundly affected by the increase in ROS generated *via* extrinsic non-neuronal sources in the CNS[276,38]. This other source is glial cells, which form intimate contacts with neurons and are critical for their proper functioning[20,199]. Glial cells, for example, can modulate neurons by releasing various neurotransmitters and neurotrophic factors[204,20,199]. They also have an integral role in maintaining homeostasis in the CNS by removing excess ions such as K^+ (a process referred to as K^+ spatial buffering) as well as neurotransmitters such as glutamate from the extracellular environment to minimise/prevent neurotoxicity[270,236,72,90].

Glial cells, particularly microglia, are the most potent cellular sources of ROS in the CNS[276,38]. Under healthy conditions, ROS levels in glia are kept at relatively low levels in order to conduct important processes such as second messenger signalling and phagocytosis[276,38]. With increasing age, however, glial cell dysfunction due to a decrease in antioxidant capacity, mitochondrial dysfunction, inflammation and senescence, exacerbates the production of ROS[269,470,142,217,429,75]. Consequently, this increases OS in the ageing CNS and the ROS-mediated attacks on neurons by glial cells impairs their properties and functioning[276,38].

1.3.2 ROS-mediated attacks on DNA, lipid and proteins in ageing neurons

It has been shown in ageing neurons that elevation of ROS causes substantial oxidative modifications/damage to biomolecules including DNA, lipids and proteins. Consequently, this impairs important neurophysiological processes such as neuronal excitability and neurotransmission[176,134,470,478].

ROS in ageing neurons attacks nuclear and mitochondrial DNA in several different ways. Hydroxyl radicals, in particular, appear to be major mediators of DNA damage under conditions such as OS. Studies have shown that $^\bullet$OH addition can occur at the electron rich C5=C6 pyrimidine bonds, where it preferentially adheres to the C5 position[81]. This generates C6-yl thymidine radicals, which have the ability to abstract a hydrogen atom from deoxyribose either from its own or a neighbouring base. These abstractions are believed to cause a break in the DNA strand or lead to base release[81,53].

The base radical adduct formed by $^\bullet$OH at C5 can subsequently be attacked (reduced) by radicals such as superoxide or molecular oxygen to form 5-hydroxy-6-hydrothymine

residue and peroxyl radicals, respectively[140]. Peroxyl radicals can also then be reduced to form hydroperoxyl, which subsequently undergoes thiol-mediated reduction. This produces thymine glycol, which is another major DNA damage product that is extremely toxic[171].

DNA guanine residues are also vulnerable targets to ROS-mediated attacks. For example, the addition of $^\bullet$OH at the C8 position of guanine residues yields the mutagenic lesion, 8-hydroxyguanine (8-oxo-G), that consequently leads to the misincorporation of adenine during DNA replication[171,140].

As ROS concentrations are very low under normal conditions, any damage caused to DNA is minimal and can be efficiently resolved by DNA repair mechanisms. Studies have shown, however, that there is a decline in DNA repair with age that contributes to the accumulation of DNA damage products in neurons[219,466]. If cells are unable to repair damaged DNA then this can have a devastating impact. For example, mutations in the mitochondrial genome have been found to hinder the synthesis of proteins involved in oxidative phosphorylation (**section 1.3.1.1**) such as complex I in ageing neurons[161]. This can lead to a decline in ATP levels and impair processes that are dependent on ATP such as the Na^+/K^+-ATPase and Ca^{2+}-ATPase[55]. Oxidative damage to DNA has also been shown to induce a senescent-like phenotype in neurons (**section 1.3.3.4**) during normal brain ageing and if extensive can cause neurodegeneration[213].

Free radicals can attack membrane lipids in a process specifically referred to as lipid peroxidation. The neuronal membrane is particularly prone to ROS-mediated attacks due to their high content of polyunsaturated fatty acids (PUFAs), which contain carbon-carbon double bonds[99,478]. Examples of PUFAs includes the omega-6 fatty acid, arachidonic acid (AA), and the omega-3 fatty acid, docosahexaenoic acid (DHA)[3,67,122]. These fatty acids can be liberated from the *sn-2* position of membrane phospholipids by phospholipase A_2 (PLA$_2$) enzymes. Studies investigating post-mortem samples of human frontal cortex from elderly patients have shown that PLA$_2$ and AA levels are elevated[361].

In the invertebrate, *Lymnaea stagnalis,* it has been documented that there is an increase in neuronal PLA$_2$ activity during normal brain ageing[478,32]. This suggests that this may be a conserved age-related change. An increase in PLA$_2$ is problematic because it will liberate more AA, for example, from the plasma membrane. Follow this, AA can be subjected to enzymatic oxidation[30]. Here, AA is metabolised by cyclooxygenase (COX), lipoxygenase (LOX) and cytochrome p450 to produce eicosanoids (prostaglandins,

thromboxanes and leukotrienes), which are pro-inflammatory mediators[30,122]. A by-product generated by the eicosanoid pathway is ROS, which can cause further damage to the membrane by attacking lipids and thus, leads to a vicious cycle[122].

The biosynthesis of thromboxane A_2 can lead to the formation of malondialdehyde (MDA), which is an advance lipid peroxide end product (or reactive aldehyde) that has been shown to form adducts on DNA and proteins in neurons[313]. The formation of MDA is a non-enzymatic process whereby radicals, particularly peroxyl and hydroxyl radicals, act upon AA by adding molecular oxygen[134,22]. This is subsequently followed by a Hock cleavage, which is the chemical degradation of C-C and O-O bonds[134]. This reaction also results in the formation of other reactive aldehydes such as 4-HNE, which is very cytotoxic and can lead to severe protein damage and even cell death[406].

In addition to exerting detrimental effects upon other biomolecules, damage of lipids by ROS can affect the structural and physiological properties of neuronal plasma membranes[258]. Increased liberation of PUFAs by PLA_2 reduces membrane fluidity[258]. This could affect the behaviour of ion channels localised in the neuronal membrane and consequently alter neuronal excitability and synaptic transmission.

In the brain it has also been shown that ROS can cause damage to proteins by oxidizing their side chains of amino acids[414]. The sulphur-containing amino acids, cysteine and methionine, are particularly prone to oxidation, although other side chains such as arginine, tryptophan and tyrosine can also be oxidised in ageing neurons[184].

Oxidation of the side-chain amine groups can transform them into carbonyls and result in protein cross-linking[89]. Indeed, protein carbonyl levels are typically assessed in experimental investigations to measure the extent of protein oxidation in cells and thus is a common marker of OS[89]. During normal brain ageing, protein carbonyl levels have been shown to be significantly elevated in the hippocampus and the cerebral cortex of mice displaying deficits in learning and memory[188].

Nitration of tyrosine residues to form 3-nitrotyrosine (3-NT) is another type of oxidative modification that can occur to proteins[143]. 3-NT is a post-translational oxidative modification and is generated by nitrating agents such as peroxynitrite, nitrogen dioxide and nitrous acid[359]. The formation of 3-NT can significantly alter protein structures and function and with age has been shown to be increased in the cerebral cortex and

hippocampus of rodents as well as in the cerebrospinal fluid (CFS) and brain (post-mortem) of humans[143].

1.3.3 The wider implications of OS during normal neuronal ageing

Neuronal ageing is a complex dynamic progression that is not solely mediated by OS[445,15,503,295]. Indeed, studies have implicated *via* experimental observations that other mechanisms are also involved in the manifestation of the neuronal ageing phenotype. Most notably, this includes processes such as inflammation, cellular senescence, Ca^{2+} dysregulation and altered nutrient sensing[148,447,397,51,138,75,213]. However, evidence from such studies have consistently demonstrated that OS is a common feature in all these different processes and thus, may lie at the helm of linking these different entities together to drive neuronal ageing.

1.3.3.1 OS and altered nutrient sensing

It has been discovered over recent years that simple genetic mutations can substantially extend lifespan and delay the manifestation of age-related changes and diseases in laboratory model organisms[271,210,296]. It has been found that mutations in many of these so-called "longevity genes" decrease the activity of nutrient-sensing pathways[335,271]. The mammalian target of Rapamycin (mTOR) is an example of an evolutionarily conserved nutrient sensing pathway that has been extensively linked to organismal ageing[271]. mTOR is a large serine/threonine protein kinase that belongs to the phosphatidylinositol 3 kinase-related kinase (PI3KK) family and is a central regulator of cellular metabolism and growth[471,496,253]. It exists as two complexes in cells: mTOR complex 1 (mTORC1) and mTOR complex 2 (mTORC2)[166,471].

The mTORC1 pathway is stimulated by various nutrients (particularly amino acids) and hormones, and is negatively regulated by cellular stressors[471]. mTORC1 phosphorylates the translational molecules, eukaryotic translation initiation factor 4E (eIF4E) binding protein 1 (4E-BP1) and S6 kinase 1 (S6K1), to promote protein synthesis[471,253]. The binding of rapamycin to mTORC1 inhibits its function *via* FK506-binding protein (FKBP12)[503,166]. Inactivation of mTORC1 also induces autophagy[166]. Conversely, the role of mTORC2 remains largely elusive, but there has been some evidence demonstrating that it may be involved in suppressing autophagy *via* Akt signalling[253].

So, does OS alter mTOR signalling during normal brain ageing? Some studies have shown that the age-related increase in ROS activity enhances mTOR signalling[210,166]. This results in an increase in protein synthesis, but also decreases autophagy[210,166]. The resultant accumulation of erroneous proteins in the ageing CNS caused by inherent translational errors as well as oxidative modifications contributes to the functional decline of neurons[210,166]. A study by Majumder *et al.* (2012) revealed that the age-related increase in hippocampal mTOR activity contributed to spatial memory deficits in ageing mice[284]. Interestingly, it has been shown that treatment with antioxidants and free radical scavengers can reverse this increase in mTOR activity with age and subsequently ameliorate such deficits to memory formation[372,116].

1.3.3.2   OS and inflammation

Numerous studies have revealed that a chronic low-grade inflammatory status manifest with age, which is referred to by the term coined by Franceschi *et al.* (2000) as "inflammaging"[131,132]. This chronic inflammation increases the expression of pro-inflammatory mediators such as TNF-α, IL-6 and COX-2, which go onto damage cells/tissues and consequently impair fundamental neuronal processes such as excitability and synaptic plasticity[131,113].

It has been documented that the persistent NF- κB signalling incurred in ageing neurons has a central role in enhancing inflammation through its ability to induce the transcription of pro-inflammatory genes[405,518,113]. For example, Maqbool *et al.* (2013) showed that persistent NF- κB signalling in an ageing mouse model increased the expression of pro-inflammatory mediators and subsequently impaired hippocampal-dependent spatial learning[287]. Another study involving neuronal IKKβ (an activator of NF-κB) knockout mice, found that at old age these mice performed significantly better than wild-type mice during the Morris Water Maze task[518].

Interestingly, studies have revealed that OS significantly elevates the levels of pro-inflammatory mediators in ageing neurons by directly activating NF-kB signalling[378]. Others have also shown that oxidation of lipids increases inflammation in ageing mammalian neurons *via* the generation of prostaglandins[248,211]. This increase in inflammation induced by OS in the CNS, will go onto to generate more ROS at the site of inflammation and thus, further exacerbate OS[43].

1.3.3.3 OS and Ca²⁺ dysregulation

Ca^{2+} is the most common intracellular second messenger in neurons and is responsible for regulating many critical processes[447]. Notably, Ca^{2+} is involved in neurotransmitter release, neuronal firing, synaptic plasticity, gene expression and even apoptosis[446,527,479]. Transient fluctuations in the intracellular calcium ($[Ca^{2+}]_i$) concentration act as signals to trigger these events and thus, $[Ca^{2+}]_i$ is tightly regulated in neurons to prevent the deterioration of these fundamental functions[479]. However, the mechanisms involved in maintaining $[Ca^{2+}]_i$ homeostasis in the CNS appears to be comprised with age[318].

Numerous mechanisms exist in neurons to maintain Ca^{2+} homeostasis[479,461,447,446,318,151]. When an increase in $[Ca^{2+}]_i$ is required, this can be accomplished *via* ligand-gated ion channels (LGICs) or voltage-gated Ca^{2+} channels (VGCCs) [479,527]. Ca^{2+} can also be released from intracellular organelles, including the mitochondria and endoplasmic reticulum (ER)[151,479]. To reduce $[Ca^{2+}]_i$ following the activation of neuronal signal transduction pathways, ionic pumps such as the Ca^{2+}-ATPase (PMCA) and Na^+/Ca^{2+} exchanger (NCX) on the plasma membrane facilitate Ca^{2+} removal from the intracellular space to the extracellular environment[446,479,447]. The ER *via* sarco-endoplasmic reticulum Ca^{2+}-ATPase (SERCA) and mitochondria *via* VGCCs and the mitochondrial Ca^{2+} uniporter (MCU) can sequester intracellular Ca^{2+}, whilst calcium binding proteins (CaBPs) transport Ca^{2+} ions to extrusion sites to lower $[Ca^{2+}]_i$[446,447,461,151].

It is known that an increase in OS can directly impair Ca^{2+} homeostasis and lead to Ca^{2+} overload in ageing neurons[527,515,294]. In the cerebellum of old rats, for example, it has been shown that OS causes major structural changes to the PMCA (adduct formation *via* oxidation of cysteine residues) that decreases their activity and causes a significant increase in $[Ca^{2+}]_i$.[515]. It has also been demonstrated that ROS oxidises SERCA to attenuate the ER's capacity to sequester Ca^{2+} in ageing neurons[247,154,446,318]. Other studies have detailed that mitochondrial dysfunction caused by the age-related increase in OS, not only exaggerates ROS release but also hinders the ability of the mitochondria to remove Ca^{2+} from the cytosol[494,495,446].

1.3.3.4 OS and cellular senescence

Cellular senescence- a state of permanent cell cycle arrest- is typically considered to be a powerful tumour suppression mechanism in young organisms[206]. Studies, however, have

shown that senescent cells accumulate with increasing age and develop a more sinister role that contributes to the manifestation of age-related diseases[61,308].

Neurons cannot undergo cellular senescence because they are post-mitotic cells[213]. Despite this, recent studies have revealed that ageing mammalian neurons can display a senescent-like phenotype[435,40,213]. Features include, for example, an increase in the expression of senescence-associated beta-galactosidase (SA-βgal), p16[INK4a] tumour suppressor protein and senescence-associated DNA-damage foci (SDF)[213,247]. These senescent-like neurons can also produce a senescence-associated secretory phenotype (SASP), which is composed of pro-inflammatory cytokines, chemokines, growth/remodelling factors, proteases and ROS[213,439]. It is thought that the adverse alterations inflicted to the microenvironment *via* the SASP secretome causes significant modifications to neurons, which then propels the ageing process[62,213,249].

At present, there is very limited evidence demonstrating that OS directly induces a senescent-like phenotype in ageing neurons. However, it has been well established in young animal models and cell culture experiments that increasing ROS has the capacity to induce senescence primarily *via* DNA damage, but also by causing mitochondrial dysfunction[71,348]. A study by Jurk *et al*. (2012), for example, showed that OS was higher in senescent-like Purkinje and cortical neurons from old mice[213]. Additionally, it was found that the intensity of SDFs markers such as γH2AX was significantly greater in these neurons, which indicated the occurrence of DNA damage[213]. Based on such findings, it is entirely plausible that OS may be responsible for inducing a senescent-like phenotype in ageing neurons by causing DNA damage.

Regardless of whether OS is responsible for initiating the manifestation of a senescent-like phenotype in ageing neurons, it is clear that generation of the SASP will increase OS in neurons and hinder their properties by oxidising cellular components[83,439,213].

1.4 The use of invertebrate animal models to study neuronal ageing

One of the most fundamental goals in neuroscience research is to understand how the human brain ages. This is particularly important as the elderly population is rapidly expanding and thus, the number of individuals suffering from AAMI and more devastating conditions such as AD is also increasing.

Whilst information about human brain ageing and its associated pathologies has increased significantly over the last few decades, there are huge obstacles that have prevented researchers from deepening current understanding of brain ageing, particularly at a network and single-cell level. One of the reasons for this is that it is currently not possible to record neuronal activity in a live human brain without causing severe injuries to the patient. This has restricted researchers to the use of non-invasive brain imagining techniques or post-mortem samples, which predominately provides information about the brain regions attributed to certain behaviours or areas that are structurally affected with age[400].

Another barrier encountered is that the human brain contains approximately 100 billion neurons that form incredibly complex synaptic connections. This has made it extremely difficult to attribute age-related behavioral changes to deficits in the functioning of specific neurons or synapses[355]. Even the brains of other vertebrate models such as mice and rats are substantially complex and so this challenging issue is still encountered. As a result of this dilemma, researchers have opted to use invertebrate animal models as their relatively simple nervous system allows for the examination of easily traceable neuronal networks and specific neurons[355,386]. Importantly, many of the neurophysiological and behavioural alterations that manifest in ageing mammalian models have also been observed in ageing invertebrates[503,393,364,151,295]. This suggests that the cellular and molecular mechanisms mediating these changes are evolutionarily conserved in the ageing CNS across different species.

1.4.1   Why use the invertebrate pond snail, *Lymnaea stagnalis*, as a model of neuronal ageing?

The pond snail, *Lymnaea stagnalis,* has served successfully as an invertebrate model of neuronal ageing because of the capacity to conduct electrophysiological studies[336,507,316,416,476,478]. The *Lymnaea* CNS is relatively simple and composed of approximately 20,000 neurons and thus is substantially less complex than a mammalian brain[124]. Many of these neurons are relatively large in size (ranging from ~10-100 um in diameter) and are brightly pigmented orange, which makes it easier to identify specific neurons of interest during electrophysiological recordings[124,169]. Their CNS is divided into 11 ganglia, 9 of which (the paired cerebral, pedal, parietal, pleural and the unpaired visceral) are arranged in a ring-like structure surrounding the oesophagus[124,169]. The

buccal ganglia are the remaining two and are located anteriorly attached to the buccal mass[124,169].

Another advantage with using the *Lymnaea* model is that the neuronal networks involved in regulating behaviours such as feeding, respiration and locomotion have been identified and well described[438,274,282,35,506,509,427]. Importantly, the characteristics of these behaviours can be traced to specific neurons and synaptic connections[35]. Investigating the link from behaviour to the properties of identified neurons is referred to as a top-down approach.

One particular network in the *Lymnaea* CNS that has been heavily examined in ageing studies is the feeding network[21,507,336,392]. The reason for this is that the neurons involved in feeding behavior have been well defined in terms of their firing patterns, their ionic currents, their synaptic connections and the neurotransmitters they release[35,417,508,21]. All of these features have been related to specific aspects of feeding behaviour. Some of the neurons within this network are not only involved in feeding behaviour, but have also been shown to be involved in regulating learning and memory[507,146,432,433].

Importantly, a number of age-related changes that have been observed in mammalian models have also been detailed in the *Lymnaea* feeding network. Such changes include some of the following: 1) a decrease in firing frequency; 2) an increase in the AHP; 3) alterations in synaptic connectivity; 4) OS; 5) Ca^{2+} dysregulation; 6) increase in PLA_2 activity and generation of free fatty acids, and; 7) impaired LTM retention[507,21,174,393,478].

1.5   The feeding network in *Lymnaea stagnalis*

The *Lymnaea* feeding cycles consists of the following three phases: a protraction phase and two phases of retraction, which can be subdivided into the rasp and swallow phases[35]. These three phases are the active phases of the *Lymnaea* feeding cycle during which food enters the mouth and is then swallowed. Additionally, there is a fourth distinct phase known as the rest or inactive phase that occurs between cycles following the active phases[35].

Prior to the initiation of the feeding cycle (**Figure 1.5**), the radula is positioned away from the mouth by the ondotophore in the rest phase[453,529,530]. Feeding in *Lymnaea* begins with the protraction phase[112,35]. During this phase, the mouth is opened to allow for the forward rotation and protraction of its ondotophore out of the mouth. Simultaneously, the

radula is also protracted out of the open mouth as it is drawn over the bending plane of the ondotophore thus bringing it into contact with food at the end of this phase[35,453]. The rasp phase immediately follows the protraction phase and signals the first of the two phases of retraction (R1)[366]. During rasp, food is scrapped into the cavity of the buccal mass as the ondotophore with the radula is retracted back through the open mouth[453,529]. In the swallow phase, the second phase of retraction (R2), the radula is positioned back to the anterior portion of the mouth as it closes[366,529,453]. There is a strong retraction that causes the ondotophore to rotate back past its resting position and this forces food into the oesophagus[453,35]. At the end of the feeding cycle, the buccal mass relaxes and the ondotophore returns to its original position and is held at rest phase.
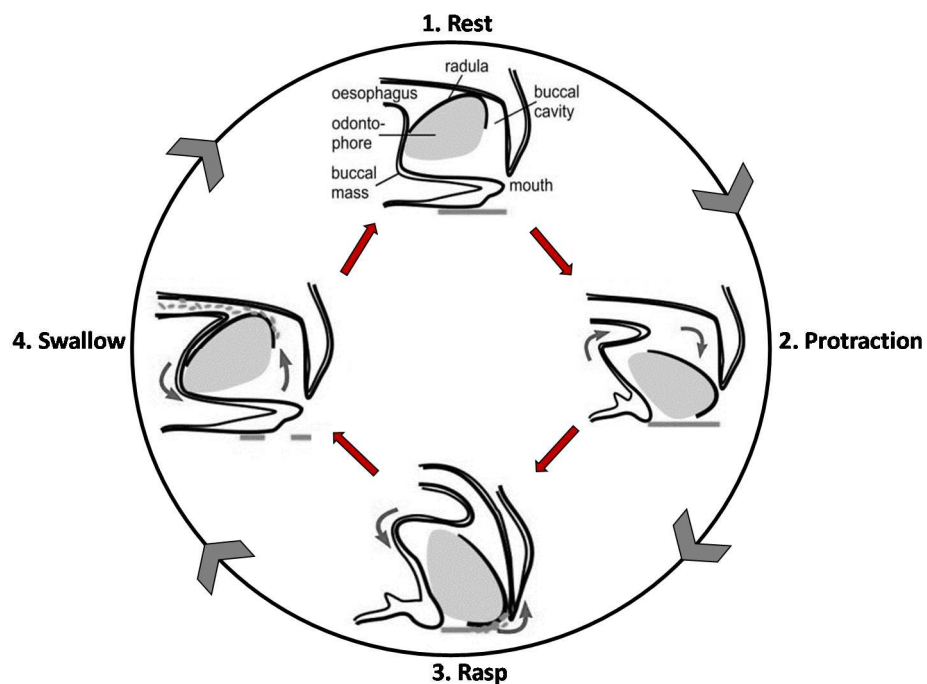
Figure 1.5| *Lymnaea stagnalis* feeding cycle[112]. This cycle consists of the following four phases: 1) rest; 2) protraction; 3) rasp, and; 4) swallow phase. During the active phases (2-4), structural components of the feeding apparatus undergo various movements to allow for the ingestion of food in snails[112,453,529,530,35].

1.5.1   The neuronal network underlying feeding behaviour in *Lymnaea*

Feeding behaviour in *Lymnaea* arises due to the activity of central pattern generator interneurons, modulatory interneurons and motor neurons in the CNS[427]. These neurons underlying feeding are predominately distributed between the buccal ganglia and the cerebral ganglia (**Figure 1.6**).
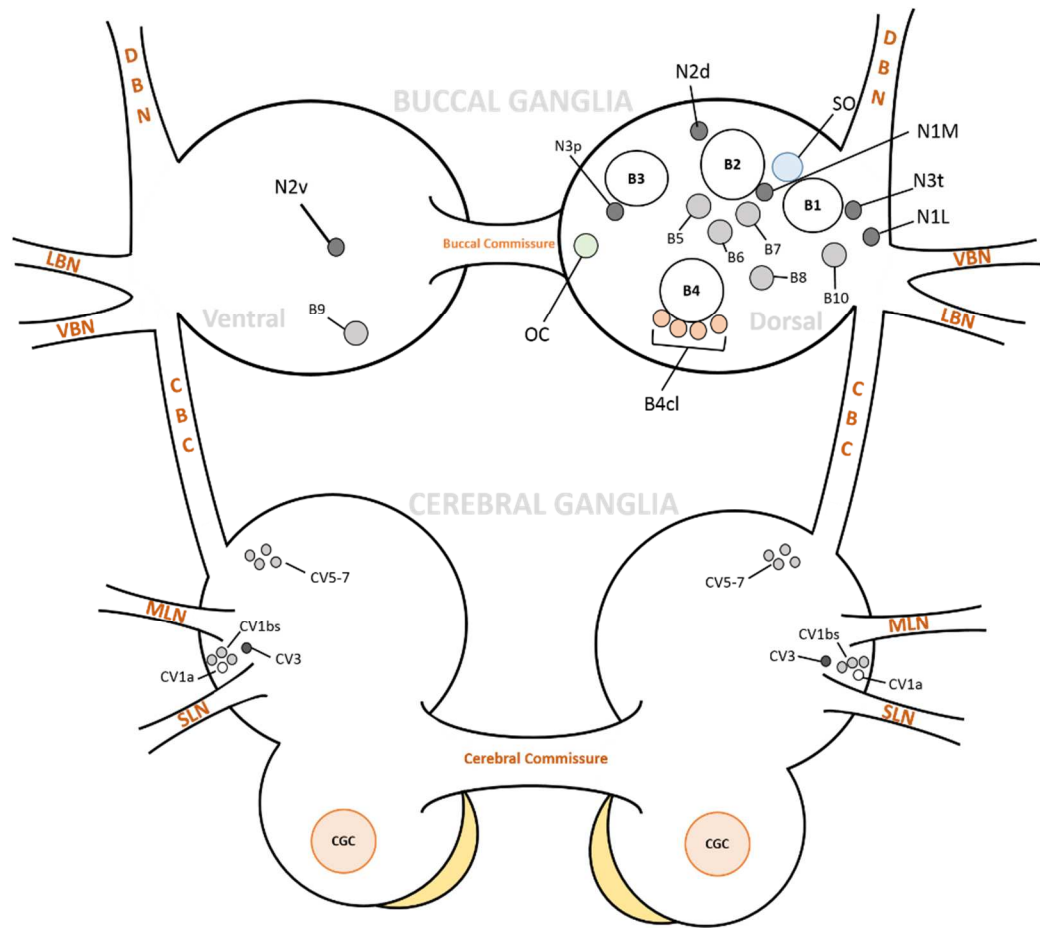
Figure 1.6| The feeding neuronal network in *Lymnaea*. This diagram illustrates the locations of identified neurons in the buccal and cerebral ganglia known to be involved in feeding behaviour. Abbreviations: CBC – cerebral buccal connective, DBN – dorsal buccal nerve, LBN- lateral buccal nerve, VBN- ventral buccal nerve, MLN- median lip nerve and SLN- superior lip nerve. Diagram adapted from Benjamin *et al*. (2012)[35].

1.5.1.1 The central pattern generator interneurons

The CPG interneurons located in the buccal ganglia (**Figure 1.7**) are critical cells of the feeding neuronal circuit as they are the major source of rhythmicity in *Lymnaea* feeding behaviour[427,35]. There are three classes of CPG interneurons: N1, N2 and N3. These three interneuron classes align with the three active phases of the feeding cycle. The N1 interneurons are responsible for the protraction phase, the N2 interneurons for the rasp phase and the N3 interneurons for the swallow phase[427]. Each interneuron class contains two subtypes: N1 medial (N1M) and N1 lateral (N1L) in the N1 class, N2 dorsal (N2d) and N2 ventral (N2V) in the N2 class, and N3 phasic (N3p) and N3 tonic (N3t) that forms the N3 class[35,505,427]. Studies have revealed that N1M, N2v and N3t are the most important cells from each group for the generation of the triphasic rhythm underlying normal feeding behaviour in *Lymnaea*[35].

Electrophysiological recordings from the intact *Lymnaea* CNS have shown that stimulation of N1Ms, which produces plateau potentials, during protraction drives fictive feeding by exciting N2vs and inhibiting the N3ts[36,427]. Activation of the N2vs in the rasp phase hyperpolarises N1Ms to inhibit their activity, whilst also inhibiting N3t[54,505,35]. Spontaneous cessation of the N2v plateau marks the entry into swallow phase. Here, the N3ts, which fire a post-inhibitory rebound (PIR) rasp phase inhibition, send a strong inhibitory input to the N1Ms (but not to the N2vs) to delay their re-activation and therefore allowing for a separate swallow phase to occur during the feeding cycle[505,35].
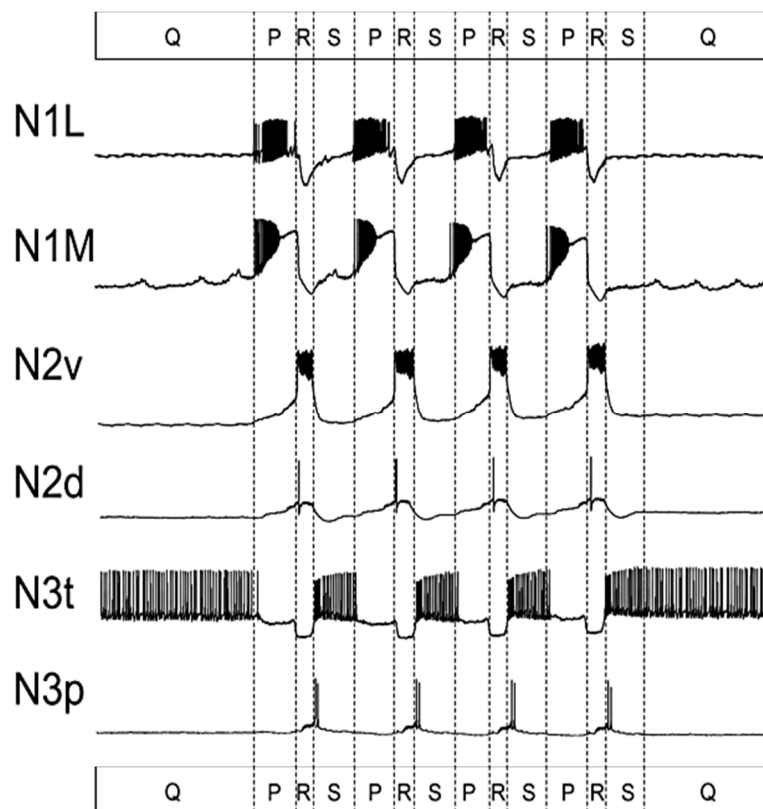
Figure 1.7| CPG interneurons in the *Lymnaea* feeding network[85]. Intracellular recordings illustrating the firing patterns of CPG interneurons during four fictive feeding cycles. Prior to the initiation of the feeding cycle is the quiescence (or rest) phase. In fast rhythms, as demonstrated here, the rest phase does not occur. In the protraction (P) phase, only N1 interneurons (N1M and N1L) are active. N2 interneurons (N2v and N2d) are only active during the rasp (R) phase, whilst in the swallow (S) phase only N3 interneurons (N3t and N3p) are active[35,427,458].

1.5.1.2 Motor neurons

Following activation by interneurons, the motor neurons located in the buccal ganglia innervate the muscles responsible for mediating the protraction, rasp and swallow phases. There are 10 motor neurons, B1-B10, that have been identified and their characteristic firing patterns are displayed in **Figure 1.8**. B1, B6 and B7 specifically stimulate the muscles involved in protraction[35,336,459]. The B3 and B10 motor neurons enables the contraction of muscles that mediate the rasp phase[35]. The swallow phase muscles are controlled predominately by the activity of the B4/B4cl motor neurons[336,35].

With regards to B2, this motor neuron is weakly entrained to the feeding rhythm as it is not directly involved in facilitating the coordination of the feeding cycle[341,418]. It has been shown that the primary function of B2 is to regulate oesophageal motility and gut tissues for digestion when activated upon feeding[341,418].

The cerebral ganglia contains an additional five motor neurons, CV3-7, that are rhythmically active and responsible for innervating muscles involved in opening and closing the mouth during feeding[35].

Interestingly, it has been shown that some motor neurons are involved in rhythm generation due to their synaptic connections with CPG interneurons[417,35]. This strictly applies to motor neurons and CPG interneurons that are active in the same phases[35]. For example, this includes the following: 1) In the protraction phase, B7 motor neurons are electrically coupled to N1Ms; 2) In the rasp phase, B10 motor neurons are electrically coupled to N2 interneurons, and; 3) In the swallow phase, B4/B4Cl motor neurons are electrically coupled to N3 interneurons[417].

The B7 motor neuron, in particular, has been reported to have a very important role in rhythmicity[417,35]. Persistent artificial depolarisation of B7 has been shown to initiate fictive feeding by activating N1M, whilst suppression of B7 firing has been found to inhibit SO-driven feeding cycles[417,35].
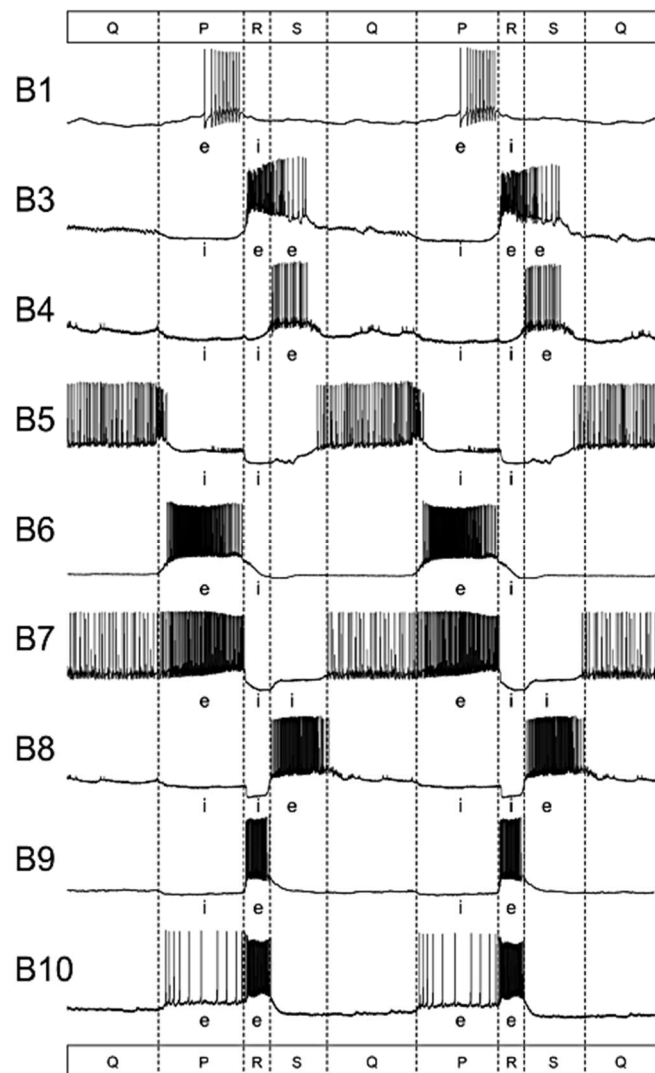
Figure 1.8| The buccal ganglia motor neurons in the *Lymnaea* feeding network[85]. This diagram illustrates the firing patterns of the buccal motor neurons during two fictive feeding cycles. The activity of these motor neurons is controlled by either excitatory (e) or inhibitory (i) inputs in the protraction (P), rasp (R) and swallow (S) phases of the feeding cycle[35,36]. Note, the B2 motor neuron is not shown as it is weakly entrained to the feeding rhythm[341,418].

1.5.1.3 Modulatory interneurons

The firing of the feeding CPG can be modulated by several types of neurons. The slow oscillator (SO) is an example of a modulatory interneuron. The SO is a single cell that can be located in either the right or left buccal ganglion and when activated can drive a feeding rhythm in the feeding CPG[35]. The SO is able to do this through its excitatory monosynaptic connection with N1Ms[35,505]. The SO fire prior to the protraction phase to provide a component of the excitatory input that stimulates N1M[427]. Once fictive feeding has commenced, the SO becomes entrained in the feeding rhythm due to the inhibitory

inputs that it receives from N2 and N3 interneurons[35,505,427]. Inhibition of SO firing has been found to cause CPG rhythmical activity to become irregular and to decrease its frequency[223]. The SO, however, is not required for the activation of sucrose-evoked fictive feeding[35,223].

The cerebral giant cells (CGCs) are another important type of modulatory interneurons in the *Lymnaea* feeding system. They are a large pair of serotonergic interneurons that are located on the ventral surface in the anterior lobe of each cerebral ganglion[35]. The two (left and right) CGCs fire synchronously due to their mixed electrical and chemical connection with each other[336]. They fire tonically and *in vivo* fine wire recordings of the CGCs performed by Yeoman *et al.* (1994) showed that they had firing rates between 1-20 spikes/min, which was considerably lower than CGC firing rates recorded from isolated CNS preparations (60-120 spikes/min)[508]. It is only at these higher non-physiological firing rates in the isolated CNS that the CGCs have been shown to initiate fictive feeding[508,35]. Instead, the CGCs at physiological firing rates have a gating function in the feeding network[508,35]. The firing of CGCs, for example, depolarises N1Ms and N2vs to lower their threshold required for the generation of a plateau[505,35]. Additionally, it has also been shown that in order for SO to drive a fictive feeding rhythm *via* the feeding CPG, the CGCs must be firing[35,506,508]. As the CGCs have synaptic connections to every interneuron as well as many motor neurons to provide a background depolarisation, this indicates that gating by the CGCs is a fundamental aspect of the feeding rhythm[35].

The cerebral ventral 1a (CV1a) cells are also an important type of modulatory neuron. They are located on the ventral surface of the cerebral ganglia and occur as pair of bilaterally symmetrical interneurons[35,223]. When depolarised, CV1a's have been shown to activate and maintain fictive feeding cycles due to their monosynaptic excitatory synaptic connections with N1Ms[223]. CV1a, like the SO, is not necessary for the initiation of sucrose-evoked fictive feeding. When sucrose driven cycles are activated, however, inhibition of CV1a firing has been shown to disrupt the rasp phase by decreasing the duration of B3 motor neuron spiking activity[223]. Thus, CV1a is thought to maintain the stability of this important phase that typically does not exhibit a lot of variability unlike the other active feeding phases under normal conditions[223]. Other modulatory interneurons involved in feeding include the N1Ls, octopamine cells (OC) and cerebral ventral 1b (CV1bs) cells[459,509,35]. **Figure 1.9** display traces of intracellular recordings of the SO, CV1a and CGCs.

A. SO-driven rhythm

N1 N2 N3

N1M

N2d

N3p

SO

current to SO

30 mV

10 secs

B. CV1a-driven rhythm

N1 N2 N3

N1M

N2d

N3p

CV1a

current to CV1a

30 mV

10 secs

C.

Moto-neurons: B4, B6, B1

Inter-neurons: SO, N3p, N3t

mono

CGC

poly

Inter neurons: N1M, N2d, N2v

Moto-neurons: B7, B5, B2

Di.

SO

N1
N2
N3

CGC

BL10

10s

Dii.

SO

N1
N2
N3

CGC

BL10

10s

29
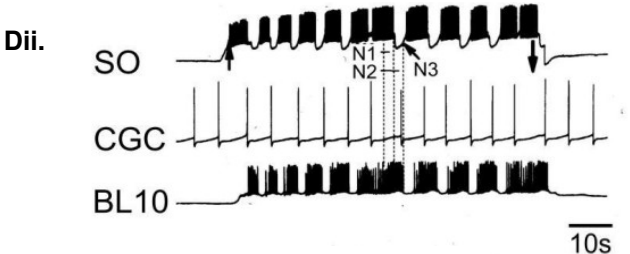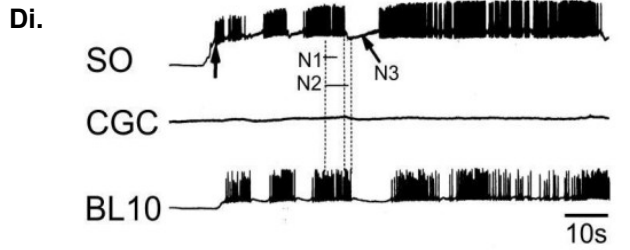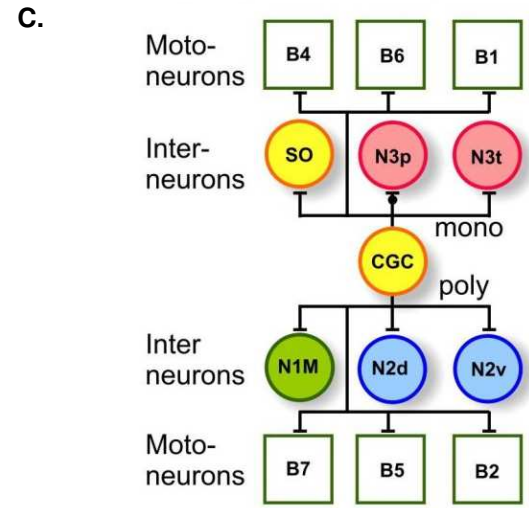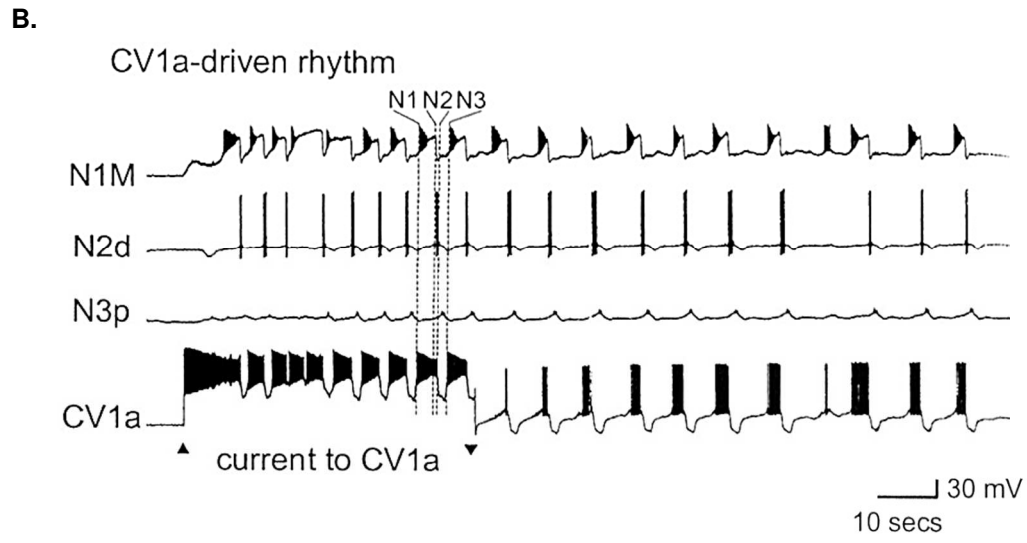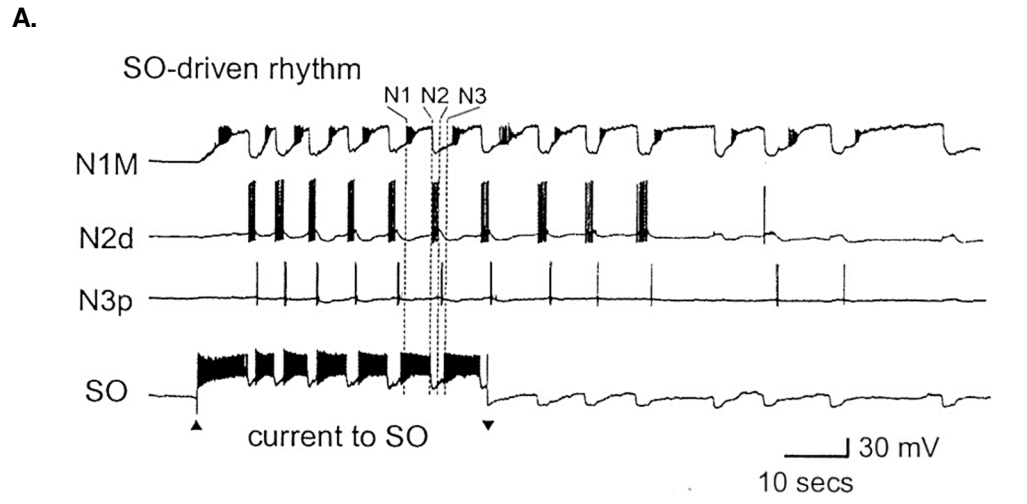
Figure 1.9 | Modulatory interneurons in the *Lymnaea* feeding network[223,35]**. Stimulation of (A) SO and (B) CV1a by a depolarising current drives a fictive feeding rhythm due to their monosynaptic excitatory connection with N1M, which gives rise to the protraction phase**[35]**. Both SO and CV1a are then inhibited by N2 and N3 interneurons to allow for rasp and swallow phases, respectively. (C) CGCs form synaptic connections with all interneurons and numerous motor neurons to gate feeding** [35]**. (Di) Inhibition of CGC firing by a hyperpolarising current disrupts the ability of the SO to drive fictive feeding cycles, as observed in B10 motor neurons recording. (Dii) Depolarisation of the CGCs enables SO to drive fictive feeding cycles in a B10 motor neuron**[223]**.**

1.6 The Cerebral Giant Cells

1.6.1 The role of the CGCs in learning and memory in *Lymnaea*

The CGCs gating mechanism is an essential modulatory component of the neuronal network underlying feeding behaviour. Interestingly, the CGCs have been shown to be involved in LTM formation when *Lymnaea* are classically conditioned to generate a feeding response[35,240,224]. The experimental appetitive conditioning paradigm involves a single pairing of two chemosensory stimulus, amyl acetate (the conditioned stimulus, CS) to sucrose (the unconditioned stimulus, UC)[428]. This training in *Lymnaea* results in the associative conditioning of feeding, which can last over three weeks and is classed LTM formation[35,240,224].

In *Lymnaea,* the neurotransmitter nitric oxide (NO) is required for the activation of feeding by a chemosensory input[240]. It has also been revealed that NO is critically involved in LTM formation as disruption of NO signalling after appetitive conditioning of feeding results in the impairment of LTM consolidation[240]. Korneev *et al.* (2005) showed that there were changes to the expression of *Lymnaea* nitric oxide synthase genes (*Lym-nNOS)* in the CGCs following the conditioning of feeding behaviour[240]. They found that the expression of an *anti-NOS gene* (a negative translation regulator of NOS) decreased 4 hours post-conditioning and that two hours after this, the *Lym-nNOS1* gene was upregulated in the CGCs[240]. Another study by Kemenes *et al.* (2006) showed that in the CGCs there was a delayed (16-24 hours) persistent depolarisation of its membrane potential that developed following associative conditioning of feeding[226]. This depolarisation enhanced the CS response in cerebro-buccal interneurons such as CV1a as well as elevated presynaptic Ca^{2+} levels, which were thought to significantly increase the amplitude of CGC postsynaptic potentials[224]. These findings demonstrate that the CGCs are not only important in gating feeding behaviour, but are also central to LTM formation.

1.6.2 Does ageing alter CGC associated behaviours in *Lymnaea*?

The feeding neuronal circuit in *Lymnaea* is subjected to age-related changes, which not only causes deficits to feeding behaviour but also impairs LTM formation[21,336,176,477,478]. For example, Watson *et al.* (2012) found that LTM consolidation (assessed *via* an appetitive reward conditioning paradigm) was impaired in old snails, but not in young snails[477]. Other studies have produced similar findings and interestingly Hermann *et al.* (2007) showed that whilst LTM consolidation is impaired, acquisition (or learning) is not compromised in old snails[174].

With regards to age-related changes to feeding behaviour, Arundell *et al.* (2005) demonstrated in old snails that there was a significant decrease in the number of sucrose-evoked bites as well as an increase in bite duration when compared to young snails[21]. They also found that the increase in bite duration was due to an increase in the protraction phase, but not rasp phase, and that the lower bite frequency was mainly caused by an increase to the swallow phase of the feeding cycle[21].

A subsequent investigation from the same group utilised semi-intact preparations to record spontaneous action potential activity from the CGCs following the application of sucrose to the lips[336]. It was observed that CGC firing rates in response to sucrose stimulation increased significantly in young snails, but failed to do so in old snails[240]. It was also shown that the RMP of the B1 and B4 motor neurons was significantly hyperpolarised in the old snails, which is likely due to the decrease in CGC firing frequency[336]. Furthermore, this study as well as Yeoman *et al.* (2008) study showed that the amplitude of CGC evoked EPSPs was enhanced and attenuated in B1 and B4, respectively, in old snails[336,507]. This is consistent with the behavioural observations, in which both the protraction (mediated by B1) and the swallow phases (mediated by B4) are longer with age. This increase of the EPSP amplitude in B1 contradicts the RMP data, but is likely a compensatory mechanism to minimise the effects of reduced CGC excitability with age[507].

1.6.3 The electrophysiological properties of ageing CGCs

The age-related changes to behaviours associated with the CGCs have largely been attributed to a decline in CGC firing frequency and alterations to the action potential waveform[393,392,336]. Some of the reported changes include, for example, action potential

narrowing, hyperpolarisation of the RMP, increase of the fAHP amplitude and increases of the mAHP and sAHP durations[393,392,336].

In the ageing CGCs, the role of the sAHP in the decline of neuronal firing frequency has been of particular interest[392]. The reason for this is that the sAHP is a critical regulator of the inter-spike interval and is largely mediated by a Ca^{2+}-activated K^+ current- a conductance heavily implicated in the ageing of mammalian neurons[352,48,102,324,364].

Scutt (2012) provided evidence for the existence of Ca^{2+}-activated K^+ currents in the *Lymnaea* CGCs[392]. It was initially identified during two-electrode voltage clamp (TEVC) experiments, that a proportion of the total outward K^+ current in the CGCs was dependent on Ca^{2+} due to its sensitivity to cadmium (Cd^{2+}; a non-specific blocker of high-voltage activated Ca^{2+} channels)[392]. Current clamp experiments in this investigation also demonstrated that a proportion of each AHP component was sensitive to Cd^{2+}, with the largest observed in the sAHP where there was approximately a 40% decrease in duration[392]. Subsequent examination of sAHP evoked tail currents in TEVC (measured 100 ms- 1s post repolarisation) confirmed that this current was conducted by K^+ ions, as determined by its reversal potential, and showed that Cd^{2+} reduced the magnitude of these tail currents[392]. These findings revealed that the sAHP in CGCs is partly mediated by an unknown Ca^{2+}-activated K^+ current(s), referred to as the I_{sAHP}[392]. Interestingly, it was also observed that the increase in the sAHP duration in old CGCs was accompanied by an increase in the underlying I_{sAHP}[392].

Whilst it is undisputed that changes to the I_{sAHP} has an important role in the age-related decline in CGC firing frequency, it known that this current is not responsible for all the alterations observed to the CGC action potential waveform with age (Scutt G, personal communication). This suggests that other ionic conductances involved in regulating the CGC action potential, particularly voltage-gated Na^+, Ca^{2+} and K^+ currents, could also be critically involved in these changes with age[416,316,392]. Interestingly, the effects of age have been explored in relation to some of these currents in the CGCs.

1.6.3.1 Voltage-gated Na⁺ currents in the ageing CGCs

Staras *et al.* (2002) conducted a detailed investigation of the voltage-gated currents present in the *Lymnaea* CGCs utilising TEVC[416]. The CGCs possess two types of voltage-gated Na^+ currents: a transient Na^+ current ($I_{Na(T)}$) and a persistent Na^+ current ($I_{Na(P)}$)[416].

It is likely that both these currents are conducted from the same class of channels, $Na_v1^{[136]}$. This particular class is highly selective for Na^+ ions, unlike Na_v2 (found only in invertebrates) that is permeable to Ca^{2+} as well as Na^+ ions[516,136]. In mammals, it has been identified that there are at least nine Na_v1 channel subtypes ($Na_v1.1$-$Na_v1.9$), each encoded by a different subtype of the vertebrate *SCN* gene family[136]. Invertebrates do not express subtypes of the Na_v1 channel, which is only encoded by a single gene[136]. It is thought that alternative splicing of the single Na_v1 gene in invertebrates is responsible for the distinct functional conductances of $I_{Na(T)}$ and $I_{Na(P)}^{[136]}$.

In the CGCs, $I_{Na(T)}$ was shown to be a large inward current that rapidly activated between -65 mV to -50 mV and also rapidly inactivated[416]. Such characteristics are also defining features of $I_{Na(T)}$ in most mammalian and other invertebrate species[66,286,511,68,147]. $I_{Na(T)}$ in the *Lymnaea* CGCs displayed some sensitivity to tetrodotoxin (TTX), but could not be completely abolished by the high concentration utilised despite this being sufficient in mammalian models[261,179,416]. It is thought that this may be a general feature of many pulmonate gastropods, which suggests that there may be slight structural differences to the channel pore (perhaps an evolutionarily adaptation) that prevents it from being fully occluded by TTX when compared to other species[2,416]. Regardless, perfusion of a zero-Na^+ saline completely abolished $I_{Na(T)}$ and this confirmed that the current was conducted by Na^+ ions[416].

Staras *et al.* (2002) had also unveiled that $I_{Na(P)}$ was a low threshold (activated between -90 mV to -60 mV) small inward current, which was thought to be responsible for the hyperpolarisation of the CGC RMP when in a zero Na^+ saline[416]. Indeed, a subsequent investigation by Nikitin *et al.* (2006) corroborated this finding and demonstrated that $I_{Na(P)}$ significantly contributed to the CGC RMP by ~20 mV[316]. This particular study also revealed that this current was slow to activate and that its persistent nature was due to its ultra-slow inactivation kinetics and very slow deactivation kinetics[316].

Whilst a zero Na^+ saline could block $I_{Na(P)}$, further pharmacological examination revealed that this current was TTX resistant and could not be blocked by common vertebrate blockers such as riluzole and phenytoin[416]. However, a very interesting feature of $I_{Na(P)}$ is that this current can be modulated by cAMP[316]. It was shown that cAMP increased $I_{Na(P)}$ and subsequently depolarised the CGC RMP, which lasted up to 24 hours[316]. This is thought to have a very important role in neuronal plasticity of the CGCs[196,317,316].

What happens to voltage-gated Na^+ currents in the ageing CGCs? To date, there have been no published studies examining the effects of age on the CGC $I_{Na(T)}$. Similarly, in mammalian models such as rats and mice there have been no studies documenting any significant changes to $I_{Na(T)}$ during normal brain ageing. Only under pathological conditions such as AD has it been shown that the expression and activity of voltage-gated Na^+ channels conducting $I_{Na(T)}$ increases[111]. This is thought to contribute to the hyperexcitability and epileptic susceptibility often observed in the early stages of AD[111].

Unlike mammalian models and other invertebrate models, some evidence has been provided in *Lymnaea* demonstrating that $I_{Na(P)}$ is altered during normal ageing[393]. It was revealed by Scutt *et al.* (2015) that the depolarising effect of $I_{Na(P)}$ on the CGC RMP increased with age[393]. This had been ascertained by subtracting the mean change of the CGC RMP in a zero-Na^+ saline (blocks NCX as well as $I_{Na(P)}$) from that observed after switching into a Li^+ saline (Li^+ substitutes Na^+ and blocks only the NCX)[393]. This study postulated that the increase in $I_{Na(P)}$ may be responsible for causing the NCX to operate in reverse mode in ageing CGCs[393]. While reverse-mode NCX would have a hyperpolarising effect on the CGC RMP, the increase in $I_{Na(P)}$ meant that there were no overall changes to the old CGC RMP when compared to young CGCs in this particular study[393].

1.6.3.2 Voltage-gated Ca^{2+} channels in the ageing CGCs

The *Lymnaea* CGCs possess at least two distinct voltage-gated Ca^{2+} currents: a high-voltage activated (HVA) Ca^{2+} current and a low-voltage activated (LVA) Ca^{2+} current[416].

Staras *et al.* (2002) characterised the CGC LVA Ca^{2+} current as a small inward current that activated around -60 mV (near the RMP) and inactivated relatively fast[416]. It was also observed that this current was sensitive to Ni^{2+}, but insensitive to Cd^{2+}[416]. This strongly suggested that this current was conducted by a T-type Ca^{2+} channel (Ca_v3), as these features were remarkably reminiscent of Ca_v3 channels expressed in many vertebrate species[416,179,396]. However, the Ca_v3 subtypes ($Ca_v3.1$-3.3) expressed in the CGCs currently remains unknown[179].

It was also demonstrated by Staras *et al.* (2002) that the CGC HVA Ca^{2+} current was a larger inward current that activated around -40 mV and possessed much slower inactivation kinetics[416]. This current was sensitive to Cd^{2+}, but insensitive to ω-conotoxin and ω-agatoxin suggesting that this current may not be conducted by either an

N-type or P-type channel, respectively, of the HVA class[416,179]. A more recent investigation by Scutt (2012) revealed that a component of the HVA current was sensitive to nifedipine, which strongly indicated that a proportion of this current was being conducted by an L-type Ca^{2+} channel[392]. However, the HVA channel responsible for mediating the nifedipine as well as ω-conotoxin and ω-agatoxin insensitive current has yet to be identified.

LVA currents have been shown to have an important role in providing the initial depolarising drive for neurons to reach the activation threshold of Na^+ from rest[340,396,416]. It is thought that this enables LVA currents to regulate firing rates in neurons[340,396]. HVA currents are involved in regulating the rate of repolarisation and influence the AHP as they can supply Ca^{2+} for Ca^{2+}-activated K^+ channels, which are partly involved in mediating this component of the action potential[416,263,392]. Ca^{2+} influx *via* HVA channels during action potential repolarisation has been shown to have a critical role in mediating neurotransmission[388,444,416].

The effects of age on HVA Ca^{2+} currents has been examined in the CGCs. Scutt (2012) revealed that whilst the peak amplitude of the total HVA current was not altered in old CGCs, it activation, inactivation and deactivation kinetics were slower when compared to the young CGCs[392]. This suggests that the amount of current conducted by the HVA channels is not altered with age, but the current is present for a longer duration. Furthermore, Scutt (2012) observed that the magnitude of current conducted by HVA channels (both nifedipine sensitive and nifedipine insensitive) did increase as the snails became very old (12-14 months old as opposed to 10-12 months old)[392]. It had been postulated that the alterations to the properties of HVA channels with age increases the Ca^{2+} supply to Ca^{2+}-activated K^+ channels, which subsequently enhances its conductance and contributes to the decrease in CGC firing predominately *via* the AHP[392].

Interestingly, it has also been reported in numerous rodent models that ageing in the hippocampus is generally associated with an increase in the L-type current [442,441,321]. This increase has been implicated in AAMI, as utilisation of L-type channel antagonists substantially reverses such behavioural deficits[442,441,321].

With regards to the T-type (or LVA) current, preliminary TEVC experiments in our laboratory have demonstrated that this current is not altered in the ageing CGCs. Conversely, a few studies in other species such as *C. elegans* and rodents have documented that the T-type Ca^{2+} current is subjected to changes with increasing

age[485,117]. It has typically been shown that the T-type current is enhanced with age and that blocking this current helps to prevent Ca^{2+} overload in ageing neurons and thus, is neuroprotective[485,117]. This suggests that the structure of T-type channels may be slightly different in the *Lymnaea* CGCs, which makes them more resilient to the effects of age.

1.6.3.3 Voltage-gated K⁺ currents in the ageing CGCs

The CGCs express at least two types of voltage-gated K^+ currents: an A-type K^+ current (I_A) and a delayed rectifier current (I_{DR})[416]. Across all species, these currents have an integral role in regulating action potential repolarisation and can have an important role in mediating the AHP[209,264,416,457,398]. Their role in the action potential waveform has a significant influence on fundamental neuronal processes such as excitability and synaptic plasticity[209,264,416,457,398,399].

Staras *et al.* (2002) initially characterised I_A in the *Lymnaea* CGCs and demonstrated that this current activated around -55 mV and was a transient current with both rapid activation and inactivation kinetics[416]. This current was also sensitive to the non-specific I_A blocker, 4-aminopyridine (4-AP)[416]. All these features were consistent with observations previously documented in other *Lymnaea* cells such as heart ventricular muscle cells as well as neurons from other invertebrate and mammalian species[504,179,412,133].

In addition, Staras *et al.* (2002) also examined the properties of I_{DR} in the *Lymnaea* CGCs[416]. This current activated at approximately -45 mV, was slow to activate and exhibited very little inactivation[416]. This current was also sensitive to the non-specific I_{DR} blocker, tetraethylammonium (TEA)[416]. These characteristics were similar with previous descriptions in other invertebrates and mammalian species[483,498,264,209].

Currently, it is unknown what A-type K^+ channel or delayed rectifier channel subtypes are present in the CGCs. It also has yet to be identified whether genes such as *Shaker, Shal, Shab or Shaw,* for example, are responsible for encoding these VGKCs in the *Lymnaea* CGCs, as has been observed in neurons from closely related species such as *Aplysia* as well as other invertebrate and mammalian models[514,357,520].

To date, no studies have examined the effects of age on I_A or I_{DR} in the CGCs or any other neurons in the *Lymnaea* CNS. Moreover, findings from rodents and other invertebrate models such as *C.elegans* are extremely limited and have generated differing results with

reports that these currents are either enhanced or are unaltered with increasing age (**section 3.1**)[398,512,11].

Thus, unlike voltage-gated Na^+ or Ca^{2+} currents, the general consensus of the changes typically incurred to VGKCs with age is still very unclear. This is surprising given the knowledge of the critical functions of I_A and I_{DR} in neurons[209,264,416,457,398]. This highlights the need for more investigations to be conducted across all species, including *Lymnaea,* examining the effects of age on I_A and I_{DR}.

1.6.4 VGKCs: An overview of structure, selectivity and gating

VGKCs have a crucial role in various neuronal processes including neuronal excitability and neurotransmitter release[158,279,179,501]. To date, there have been no structural studies conducted in *Lymnaea* investigating VGKCs. However, a plethora of studies over the last 20-30 years have demonstrated that the fundamental basic features of VGKCs are evolutionarily highly conserved[28,327].

1.6.4.1 Structure of VGKCs

VGKCs are formed as tetramers with identical or similar subunits that are symmetrically arranged around the central aqeuous pore through which K^+ ions permeate[179,244]. Each subunit consists of six transmembrane segments (**Figure 1.10**), with the N- and C-termini located on the intracellular side of the membrane[179,300,244,501,312,279,76]. X-ray crystallographic studies of VGKCs have shown that the first four segments, S1-S4, form an antiparallel α-helical bundle at the periphery of the channel known as the voltage sensor domain (VSD)[208,514,244,501,179,106].

The last two segments, S5-S6 α-helices, are connected together *via* the P-loop and comprise the pore-forming domain located at the centre of the channel[158,179,244,502,279]. The pore domain (PD) contains the selectivity filter (SF; **section 1.6.4.3**) and channel gates (**section 1.6.4.4**) and thus, is responsible for mediating the flux of K^+ ions through the channel[158,179,244,502,501,279,76].

The VSD is covalently bound to the pore domain by the intracellular S4-S5 linker, an amphiphilic helix[123,158,244,179]. This assists in coupling VSD movements to conformational changes in the pore domain, which subsequently leads to opening or closing of the channel gates[244,46,521].
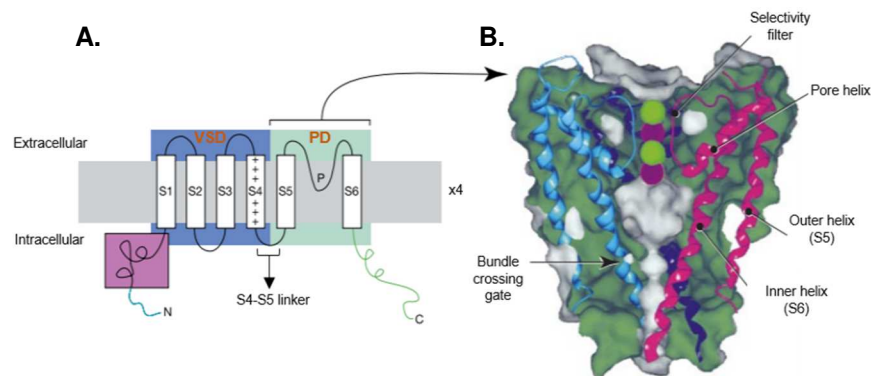
Figure 1.10| Basic structure of VGKCs[501]. (A) Channels are assembled as tetramers. Each monomer is composed of six transmembrane segments with S1-S4 forming the VSD and S5-S6 composing the pore domain, which are connected together *via* the S4-S5 linker. (B) Cross-section of a VGKC reveals the pore domain and its constituents.

1.6.4.2 The important role of the S4 helix in voltage sensing

The positively charged amino acids (arginine and lysine) of the putative S4 helix is thought to be primarily responsible for the electrically sensitive nature of VGKCs[279,5,76,501,179,244,158]. Indeed, studies examining mutant A-type K$^+$ channels have demonstrated that replacing basic residues in the S4 helix with neutral or acidic residues significantly decreases the voltage-dependence of the channel[299,5,332,244].

It has been documented that S4 can each contain up to eight of positively charged residues, which varies between different channels[182,501,179]. These positive charges are often referred to as gating charges and can be observed as the transient capacitive currents that develop prior to the opening of a channel[285,195]. The gating charges on S4 generally move either outwards or inwards through the electric field during depolarisation or hyperpolarisation of the membrane potential, respectively[501,158,244,182,279]. This alters the configuration of other VSD segments and subsequently induces a conformational change to the pore domains that leads to opening or closing of the channel[501,76,279,244,106]. Notably, the precise orientation and movements of S4 has been subjected to a great deal of controversy and has yet to be fully elucidated[330,207,383,229,182,279].

Interestingly, it has been proposed by a few studies that the conserved acidic residues of S2 and/or S3 may also participate in voltage sensing by electrostatically interacting with the basic residues of S4 and moving through the electric field[363,257,158]. To support this, it has been shown that neutralising the S2-S3 acidic residues significantly alters the voltage sensitivity of VGKCs[363,257,158]. Despite this, it is still disputed whether voltage sensing is an intrinsic property of these particular segments.

1.6.4.3 Selectivity of VGKCs

VGKCs are exquisitely selective for K^{+} ions[239,279,312]. The mechanisms of selectivity of VGKCs is highly evolutionarily conserved and has been extensively examined, particularly in KcsA (a simple bacterial K^{+} channel consisting of two transmembrane helices connected to one pore unit) and mammalian Shaker Kv1.2 channels[281,155,299,250,524,267,280,106,501,179]. It has been demonstrated that K^{+} will usually travel from the intracellular side of the membrane into the central water-filled cavity of the channel pore where they become hydrated[524,244,501]. K^{+} ions then pass through the SF where they are dehydrated, before then being rehydrated when they finally approach the extracellular pore entryway[524,244,501]. An unambiguous notion is that this process of ion hydration and its thermodynamics have a central role in governing the selectivity of all ion channels, not just VGKCs[103,155,244,501].

Numerous structural studies, particularly by the Mackinnon group in KcsA, have shown that the architectural framework underpinning this selectivity resides in the conserved signature TVGYG amino acid sequence (with minor variations) on the P-loop, which forms the narrow SF (**Figure 1.11**) located towards the extracellular end of the channel pore[281,525,524,280,501,179,279]. Indeed, mutations of these residues hinders that capacity of VGKCs to distinguish between K^{+} and Na^{+} ions[510,172,408]. The backbone of carbonyl oxygen molecules in this sequence along with the side chain of threonine hydroxyls provide four K^{+} binding sites (denoted S1-S4), which are specifically orientated towards the pore lumen and each contain eight oxygen atoms[501,525,106,312,279]. It has been proposed that the precise geometry and distance of oxygen atoms in the SF mimics the hydration shell of K^{+} and thus, compensates for the energetic cost of dehydration[91,37,106,456,239].

Given the atomic radius of Na^{+} is smaller than that of K^{+}, after it becomes dehydrated it does not fit well in the SF of VGKCs[312,244,525,501]. The Mackinnon group also revealed in KcsA channels that the oxygen atoms are spaced too far apart to adequately mimic the hydration shell of Na^{+} ions and therefore, its permeation through the channel is energetically unfavourable[526,525]. Such crucial findings from crystal structures clarified how VGKCs are highly selective for K^{+} ions and are able to virtually eliminate the flux of Na^{+} ions.

A characteristic feature of VGKCs is its near diffusion-limited rate of conduction[279]. This indicates that K^{+} ions are relieved from the bindings sites and translocated across the membrane very fast. Studies have proposed, based on structural observations, that two K^{+}

ions occupy the SF at any given time, either at the S1/S3 binding sites (1,3 configuration) or S2/S4 binding sites (2,4 configuration)[521,450,368,279]. The remaining two alternate sites are each occupied with a molecule of water[521,450,368,279].

It is very unlikely that K^+ could occupy the adjacent binding sites due to the electrostatic repulsion encountered[450,368,207]. It is this phenomena, however, that propels the movement of K^+ ions along the SF and eventually out of the channel (**Figure 1.11**). This contributes to the high conductance rate, as the energy transfer cost for K^+ to move between the two configurations is very low[521,450,368,279].

Interestingly, studies have also shown that K^+ ions are weakly bound to the S1-S4 binding sites depite the high selectivity of VGKCs[521,450,368,279]. It is believed that this also contributes to the high conduction rate of VGKCs[521,450,368,279].
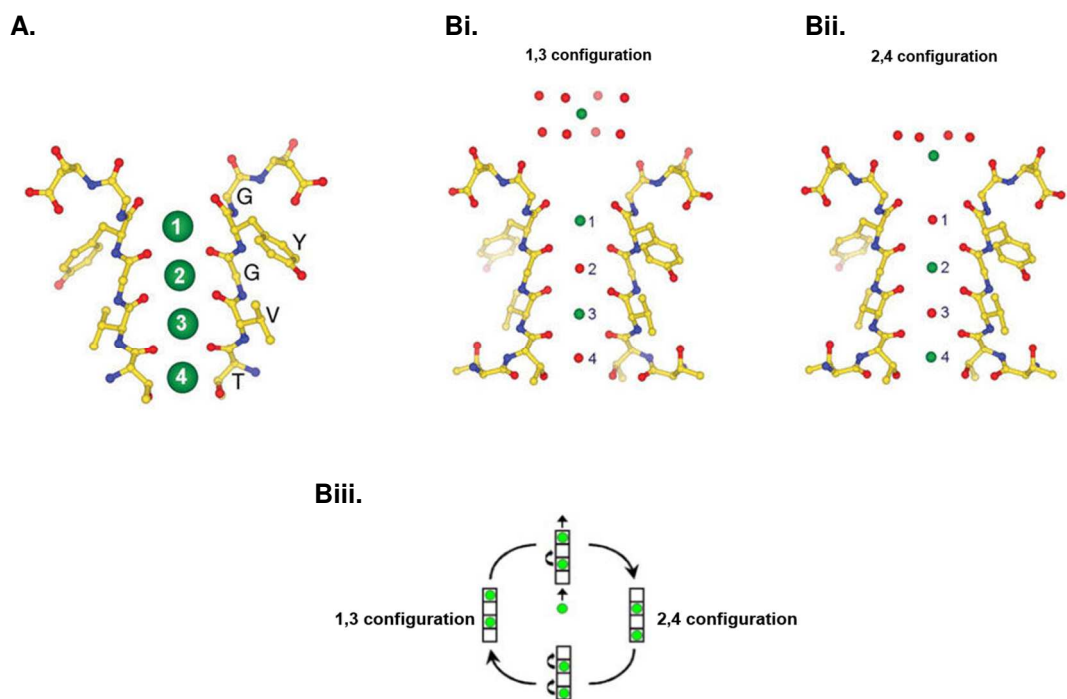
Figure 1.11| The SF of VGKCs[279]. (A) Ball-and-stick representation of the SF in KcsA. This demonstrates the location of the S1-S4 binding sites in the SF that can be occupied by K^+ ions (green balls). The important TVGYG amino acid motif is also shown. (Bi-ii) K^+ ions (green) alternate with water molecules (red) to occupy the SF in the following two congifurations: 1,3 with K^+ ions at the S1/S3 binding sites or 2,4 with K^+ ions at the S2/S4 binding sites. (Biii) Simple cycle illustrating the conduction of K^+ ions (green) through the SF in the 1,3 and 2,4 configurations, which is driven by electrostatic repulsion[521,450,368,279].

1.6.4.4 Gating of VGKCs

VGKCs can be described as having the following four functional states: 1) resting; 2) activated; 3) deactivated, and; 4) inactivated. In the resting state, VGKCs are usually in the closed conformation and cannot conduct K$^+$ ions[179,244,158]. During activation, usually in response to depolarisation, the channels switch to an open conformation to permit the flux of K$^+$ ions[179,244,158]. As neurons repolarise and return to their RMP following activation, channel will begin to deactivate and enter into a non-conductive conformation[514,332,37,502]. If, however, depolarisation of the membrane potential is prolonged following activation, some channels will inactivate and shift into a non-conductive conformation (albeit its kinetic state differs from deactivated channels) [514,332,37,502]. Inactivated channels generally will not conduct again in response to any further activating stimuli until the neuron repolarises, which enables channels to 'deinactivate' (recover from inactivation) and return back to the resting state[502,158].

Gating is the process that controls opening and closing of ion channels. The pore of VGKCs contains two distinguishable gates[179,158,244,279,76]. There is an intracellular gate, otherwise known as the bundle-crossing (BC) gate, formed by the cytoplasmic crossing of C-termini of the S6 helices[501,251,158,244]. This particular gate is considered as the main activation gate of VGKCs[181,250,76,244,158]. X-ray structural studies in combination with mutational studies of eukaryotic VGKCs have implicated the conserved Pro (proline)-Val (valine)-Pro motif in the S6 helix responsible for the bend (or kink) observed in this segment and the generation of a molecular hinge[193,407,443,250,76,279]. It has been suggested that the hinge-bending motions of the S6 helix opens the intracellular gate (moves it away from the central cavity) during activation and then closes it during deactivation[158,244,502].

The second is the extracellular gate, also known as the pore gate (P-gate). This gate is formed by the SF, which undergoes various configurations in response to the status of intracellular gate under different functional states[251,244].

There have been two mechanisms of inactivation described for VGKCs (**Figure 1.12**): N-type and C-type[244,179,502,158]. N-type inactivation is a rapid auto-inhibitory process (typically a few milliseconds) that occurs in some classes of VGKCs[179,244,469,158]. For example, many A-type K$^+$ channels such as Kv1.2 and Kv1.4 undergo this type of inactivation and is responsible for the fast inactivation kinetics typically observed in such channels[118,39]. Notably, N-type inactivation may not be the sole inactivation process for such channels and is dependent on their functions in neurons[39,158,502].

Extensive structural studies involving mammalian and invertebrate A-type K^+ channels have shown that N-type inactivation is mediated by an inactivation peptide assembled into a globule (inactivation ball), which is tethered to either the α-subunit or β-subunit of the N-terminus *via* a hydrophilic chain[469,158,244,179]. When the membrane is depolarised, the chain pushes the inactivation ball into the channel pore to occlude it and cease the conduction of K^+ ions[244,118,39,158]. Hence, this inactivation process is often referred to as the 'ball-and-chain' mechanism[244,118,39,158].

C-type inactivation is a much slower process, but the majority of VGKCs are subjected to this form of inactivation[37,158,244,179]. During this process, conformational changes to the SF closes the extracellular P-gate to prevent the flux of K^+ ions[37,158,244,179,502,501].
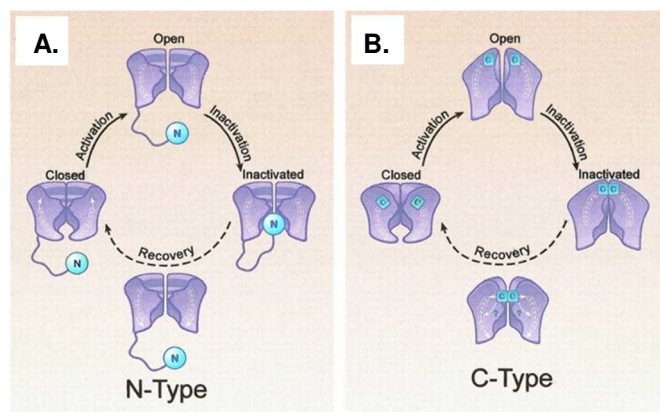
Figure 1.12| Inactivation of VGKCs. (A) N-type inactivation is a very fast process that involves the inactivation peptide entering the channel pore to block it. (B) C-type inactivation is a slower process involving conformational changes to the SF that closes the P-gate and terminates the conduction of K^+ ions. During recovery from inactivation, channels switch back to the closed conformation of the resting state[158,244,502].

1.7   Is OS responsible for altering *Lymnaea* CGC firing properties with age?

To date, much of the work investigating OS in the ageing *Lymnaea* CNS has been conducted on the RPeD1 neuron by the Wildering group in Calgary[478,476]. For example, in their 2012 study they showed that application of 2, 2'-Azobis (2-amidinopropane) dihydrochloride (AAPH), a peroxyl and hydroxyl radical generator, on the young *Lymnaea* CNS significantly reduced RPeD1 firing to rates typically witnessed in old RPeD1 neurons[478]. It was observed that this decrease in firing frequency in the AAPH-treated young RPeD1 neurons was, as in old RPeD1 neurons, accompanied with an increase in the amplitude and duration of the AHP as well as hyperpolarisation of the RMP[478]. Lastly, this particular study also showed that MDA levels were elevated in the

young CNS exposed to AAPH and that this again mimicked what had been observed in old CNS preparations[478]. Based on these findings, it was suggested that OS was involved in the decline of RPeD1 firing with age. Subsequent studies from the same group provided more support for this notion by demonstrating that incubating old RPeD1 neurons and AAPH-treated young RPeD1 neurons with antioxidants, such as glutathione and α-tocopherol, significantly increased RPeD1 firing frequency[476,32].

Interestingly, the Wildering group also suggested that OS was involved in the age-related decrease of CGC firing frequency[477]. This was derived from the observations that treating an old CNS with α-tocopherol significantly increased CGC firing[477]. A major issue of this study was that they simply assumed that α-tocopherol increased CGC firing by reversing the effects of OS[477]. It is not ideal to make such statements as it remains unclear whether α-tocopherol is reversing the effects of OS or whether it is having its effects *via* mechanisms independent of OS.

It is likely that OS is intimately involved in the ageing of the CGCs due to the plethora of studies heavily implicating its role in the ageing of other invertebrate and mammalian neurons[503,445,295,470,87,176,32]. However, more investigations are needed to conclusively establish whether this is a feature of ageing CGCs. Interestingly, many non-ageing studies have often shown that OS has the capacity to directly and indirectly alter ion channels such as VGKCs, VGCCs and Ca^{2+}-activated K^+ channels as well as ionic pumps such as the NCX and Na^+/K^+-ATPase that results in alterations to the electrophysiological properties of neurons[398,399,191,173,272,364]. This is often observed as a decline in neuronal firing[398,399,59]. If OS is involved in the ageing process of the CGCs, the mechanisms by which OS alters the electrophysiological properties of the CGCs will also need to be investigated.

1.8 Summary

The elderly population in the UK is projected to double over the next 30 years, which will increase the prevalence of conditions associated with ageing such as AAMI[4]. This will also increase the burden on health and social care services that are severely understaffed and suffering from financial difficulties[289]. Therefore, it is imperative to conduct more research to understand the mechanisms underlying normal neuronal ageing as this could lead to the development of therapeutics that attenuates detrimental age-related changes in the CNS and potentially even delay the onset of neurodegenerative diseases such as AD.

The use of humans to understand the mechanisms underlying neuronal ageing has proven to be extremely difficult due to the complexity of the human brain[400]. Currently, the majority of neuronal ageing research is conducted on other mammalian models such as rats and mice. The use of these models have identified key changes that occur during ageing such as a decrease in neuronal firing, altered neurotransmission and impaired synaptic plasticity[364,503,445,343]. Problems are also encountered with simpler mammalian models as their brains are still incredibly complex, which has made it difficult for researchers to link alterations in behaviours with age to the properties of individual neurons[355,386]. This top-down approach, however, has been accomplished with invertebrate species. The pond snail, *Lymnaea* stagnalis, has proven to be a very useful animal model to study neuronal ageing because of its relatively simple CNS and the ability to trace behaviours to key neurons[35].

The *Lymnaea* CGCs are particularly interesting as they exhibit several age-related changes often observed in mammalian models. This includes, for example, a decrease in neuronal firing frequency and alterations to neurotransmission[507,21,174,393,478]. These changes to the properties of the CGCs with age have been implicated in hindering important *Lymnaea* behavioural outputs such as feeding and learning and memory[21,478,477].

In *Lymnaea,* OS has been shown to be involved in decreasing RPeD1 firing with age[478]. Whilst it has been suggested that OS may also mediate the age-related decline in CGC firing, no studies to date have produced direct evidence to support this statement[477]. If OS is responsible for reducing CGC firing with age, it would be interesting to further explore the mechanisms *via* which it accomplishes this. In particular, it would be fascinating to examine OS in association with ionic conductances that are not dependent on Ca^{2+}. For example, this includes VGKCs as they are known to have a critical role in regulating the neuronal action potential waveform but their potential involvement in ageing has largely been overshadowed due to the focus on Ca^{2+}-activated K^+ currents[209,264,416,398,318,447].

Thus, the primary hypothesis that will be investigated in the thesis is the following:
OS in Lymnaea stagnalis drives the age-related changes in CGC firing properties and the shape of the action potential waveform by altering voltage-gated ion channels.

Chapter 2: The effects of age and acute oxidative stress on the firing properties of the CGCs

2.1 Introduction

A decrease in neuronal firing frequency is often regarded as a conspicuous hallmark of the ageing CNS. Indeed, across the animal kingdom plentiful studies in vertebrate species including monkeys, rabbits, rats and mice as well as invertebrate species such as *Caenorhabditis elegans*, *Drosophila melanogaster* and *Lymnaea stagnalis* have documented an age-related decrease in neuronal firing and established that this is an evolutionarily conserved change accompanying the ageing of neurons[503].

Alterations to the action potential waveform has been shown to be critically responsible for decreasing neuronal firing with age[393,503,336,292,364]. Many studies in mammalian neurons have demonstrated that the mAHP and sAHP increases significantly with age[422,247,305,322,364]. Certainly, an increase in the duration of both these AHP parameters would have detrimental ramifications on firing frequency as it would increase the inter-spike interval and subsequently delay the generation of successive action potentials. In pyramidal neurons, for example, apamin significantly reverses the age-related decrease in firing frequency by decreasing the mAHP duration *via* the attenuation of SK currents[422,247]. In ageing hippocampal neurons, blocking L-type Ca^{2+} currents with antagonists such as nimodipine significantly increases firing frequency by reducing the sAHP duration *via* depression of the Ca^{2+}-activated K^+ current, I_{sAHP}[247,305,322]. Interestingly, even in invertebrate species such as *C. elegans* and *Lymnaea* an increase in the AHP duration has also been reported and is thought to contribute to the age-related decrease in neuronal firing[392,336,399].

An increase in the mAHP and sAHP are not the only components of the action potential waveform that can influence neuronal firing frequency. Manipulation of the fAHP amplitude, half-width and peak amplitude, for example, have also been shown to significantly vary firing rates[13,409,387,404,293,336,392]. Alterations to such parameters of the action potential waveform, however, have not been as widely investigated with age despite common knowledge that changes to the AHP duration is often not fully accountable for the decrease in neuronal firing. Therefore, it is imperative to conduct a detailed examination of the changes to the action potential waveform with age in order to better understand how the decline in neuronal firing frequency manifests. Importantly, this will also provide an insight into the behaviour of underlying ionic currents and allow

for the utilisation of appropriate pharmacological agents that could potentially reverse these age-related changes.

A plethora of studies have strongly suggested that OS is one of the principle mediators for the age-related changes in neurons[139,470,476,364,59]. So how does OS alter the firing properties of neurons with age? Whilst current knowledge is limited, a study in CA1 hippocampal neurons by Bodhinathan *et al.* (2010), for example, provided some evidence suggesting that OS reduces neuronal firing by hindering Ca^{2+} homeostatic mechanisms[48]. This study found that treating CA1 neurons with the reducing agent, DTT, increased firing by decreasing the age-related increase to the sAHP. However, the effects of DTT could be prevented by thapsigargin (that depletes intracellular Ca^{2+} stores) and ryanodine (used at micromolar concentrations to inhibit ryanodine receptors)[48]. This strongly suggests that oxidative modifications to residues on intracellular Ca^{2+} stores and ryanodine receptors enhances Ca^{2+} release, which leads to the sAHP increase (*via I_{sAHP}*) and subsequent decrease in CA1 neuronal firing with age.

In non-ageing studies, there is ample evidence demonstrating that an increase in OS modifies many ion channels involved in regulating neuronal firing properties. For example, oxidation of cysteine residues on A-type K^+ channels significantly slows inactivation, which causes an increase in the amplitude and duration of the AHP and subsequently decreases neuronal firing[398,59]. In other studies, oxidation of methionine and cysteine residues has been shown to significantly alter the gating properties of Ca^{2+}-activated K^+ channels to enhance their conductance[398,399]. Consequently, this decreases neuronal firing by increasing the AHP duration and hyperpolarising the RMP[398,399]. Thus, there is precedence that OS could alter neuronal firing with age *via* the oxidation of ion channels that shape the action potential waveform.

Most mammalian studies, however, have only provided correlative data for the role of OS in the age-related decrease to neuronal firing frequency[476,32,503,242,144]. Some studies have demonstrated that the decrease in neuronal firing is associated with an increase in OS, but have not investigated a reversal with antioxidants. Alternatively, others have utilised antioxidants to reverse the decrease in neuronal firing, but have not examined whether this is due to a decrease in OS[476,32,503]. Failure to do this means that it cannot be confirmed whether OS is a mechanism responsible for the age-related changes to neuronal firing properties.

Even in simpler organisms such as *Lymnaea stagnalis,* only correlative data linking OS to the age-related decrease in neuronal firing has been provided. In *Lymnaea* neurons including RPeD1 and the CGCs, for example, it has been demonstrated that the decrease in neuronal firing with age can be reversed with antioxidants[478,476,176]. However, it has not been assessed by such studies whether the subsequent increase in firing frequency following antioxidant treatment is due to a decrease in OS. Thus, the aim of experiments in this chapter will be to explore the following questions: '*Is OS responsible for the age-related decline in neuronal firing frequency in the Lymnaea CNS and if so what is its mechanism of action?*'.

The CGCs are of particular interest in this investigation because they have a very important role in regulating feeding behaviour as well as learning and memory in *Lymnaea*[21,336,506,35,427]. It has been well documented that a decrease in CGC firing frequency is involved in impairing these behaviours in ageing *Lymnaea*[21,336,507,392]. To determine the mechanisms by which OS impairs CGC firing properties with age, a comprehensive examination of the action potential waveform needs to be conducted to identify the ionic currents that may potentially be altered. Findings from ageing CGCs will also need to be compared to an experimentally induced OS model to assess whether alterations to CGC firing properties manifest in an analogous manner. This could strengthen the evidence for the role of OS in the age-related decrease to CGC firing. Finally, to provide conclusive and causal affirmation, antioxidants will need to be utilised to examine whether changes to CGC firing properties can be reversed by decreasing OS in the ageing CNS.

The hypothesis of this chapter is as follows: *Age-related changes to the CGC action potential waveform and firing frequency are due to an increase in OS.*

2.2 Methods

2.2.1 Experimental animals

All experiments were conducted on the pond snail, *Lymnaea stagnalis*, which were bred at the University of Brighton. Snails were housed in large tanks that were continually perfused with copper-free water maintained at 18-20°C. Each tank contained up to 100 identically aged snails to maintain a stocking density of one animal per litre of water. Snails were housed on a 12 hour light/dark cycle and fed daily on an alternating diet of round lettuce and vegetable fish flakes (Sera Flora, Germany)[336].

Experiments in *Lymnaea* were conducted on the following two age groups: 3-4 months old (young) and 8-9 months old (old). Young snails were selected at 3-4 months old as this represented the earliest point at which they had reached sexual maturity (adulthood), as noted by the earliest time egg masses were observed in the tanks. The 8-9 months old snails represented old age as survival curves fitted with a Weibull function determined that this was the period when over 80% of the animals in the population had died (**Figure 2.1**)[218].
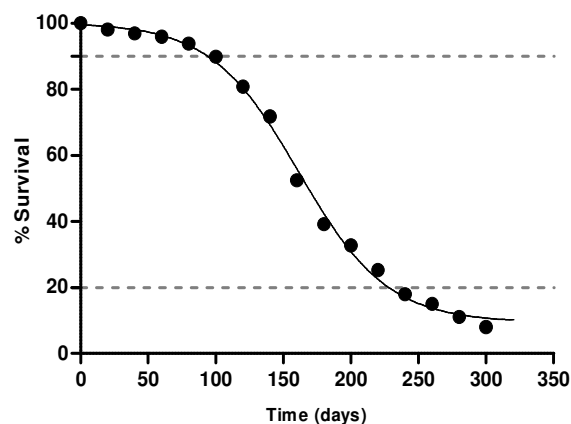
Figure 2.1| *Lymnaea stagnalis* population survival curve. This is a representative plot for one of the *Lymnaea* populations utilised in this thesis. Snails are considered old when over 80% of the population have died (<20% survival) and this typically is the point where the majority of the snails in the population exhibit an ageing phenotype[21,200].

2.2.2 Isolation and preparation of *Lymnaea* CNS

Snails were deshelled gently by hand and transferred to a Sylgard-lined dissecting dish positioned under a light microscope containing 4-(2-hydroxyethyl)-1-piperazineethanesulfonic acid (HEPES)-buffered saline (room temperature). The composition of this control saline was: NaCl 50 mM, KCl 1.7 mM, $CaCl_2$ 4 mM, $MgCl_2$

2 mM, HEPES 10 mM, adjusted to pH 7.9 with NaOH 3 M (Sigma-Aldrich, UK). The snail body was pinned dorsal side-up (foot-down) and an incision was made using micro-scissors through the body wall of the head to reveal the internal organs. All the internal organs- with the exception of the buccal mass- was removed to expose the CNS. The nerve connections between the CNS and the body wall and peripheral organs was severed with micro-scissors to isolate the CNS. However, the dorsal buccal nerves (DBN) attached to the pro-oesophagus was maintained to aid pinning of the preparation.

The isolated CNS was then transferred to an electrophysiological recording chamber and pinned dorsal side-up through the pro-oesophagus and median lip nerves. To record from the CGCs, the cerebral ganglia was inverted as these neurons are located on the ventral surface and a pin was placed over the cerebral commissure to keep the preparation flat and minimise movement (**Figure 2.2A**). The outer ganglion sheath of the cerebral ganglia was removed with fine forceps to expose the surface neurons. The inner connective sheath was then softened by solid protease (Type XIV; Sigma-Aldrich, UK) treatment on the surface of the ganglia for one minute before being washed repeatedly with HEPES-buffered saline. During recordings, the chamber was continuously perfused with saline at a flow rate of 1 ml min^{-1} *via* a gravity feed system and a vacuum pump was used to remove excess solution from the chamber (**Figure 2.2B**).
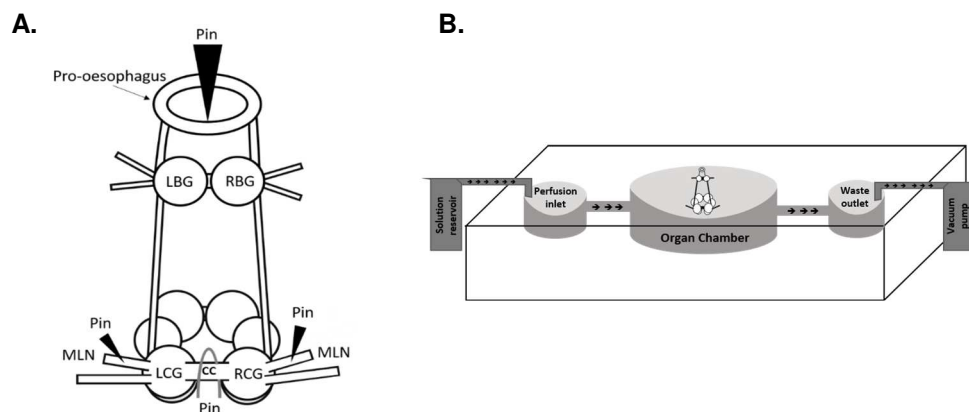
Figure 2.2| Preparation setup. (A) Schematic illustrating the placement of pins in the isolated *Lymnaea* CNS preparation. (B) Diagram of the electrophysiological recording chamber, demonstrating where the isolated CNS was placed and where the extracellular saline entered and exited the bath. Abbreviations: CC- cerebral commissure, LBG – left buccal ganglia, RBG- right buccal ganglia, LCG- left cerebral ganglia, RCG- right cerebral ganglia, MLN- medial lip nerve.

2.2.3 Electrophysiology: Current clamp recordings

Micropipettes for current clamp recordings were made from borosilicate glass capillaries with filaments (OD 1.5 mm, ID 0.6 mm; Harvard Apparatus, UK) and pulled using the P-30 vertical micropipette puller (Sutter Instrument, USA). Micropipettes were backfilled with 4 M potassium acetate solution (Sigma-Aldrich, UK) and the tip was dipped in black indian ink (Windsor and Newton, UK) to aid impalement into neurons. The resistance of microelectrodes were between 10-15 MΩ. In experiments that required the injection of pharmacological agents into the cell, the resistance was lowered to 4-7 MΩ.

Microelectrodes were connected to preamplifier headstages and signals were amplified using the Axoclamp 2B amplifier (AxonInstruments, USA). Prior to impalement of the CGCs, microelectrodes were *bridge balanced* to nullify the voltage drop across the microelectrode. Following impalement, there was a 10 minute acclimatisation period in HEPES-buffed saline for every preparation to allow for the CGC RMP and firing frequency to stabilise.

Amplified analogue signals were digitised using the Digidata 1440A (AxonInstruments, USA) at a sampling frequency of 5 KHz. The data was recorded on a PC running AxoScope® and Clampex® and analysed offline in Clampfit® from the pClamp version 10.5 software package (Molecular Devices, USA).

2.2.3.1 Protocol to evoke CGC action potentials

Current injections during intracellular recordings of the CGCs was performed in Clampex® to assess the properties of evoked action potentials. The protocol involved artificially depolarising CGCs from the RMP with a 5 second 2 nA square wave pulse. This protocol was repeated three times over a 2 minute period and responses were averaged offline in Clampfit®.

2.2.3.2 Protocol for injection of pharmacological agents into CGCs

In experiments involving the administration of pharmacological agents into the intracellular environment of the CGCs, a depolarising pulse protocol was performed in Clampex® to facilitate the influx of agents. This protocol consisted of a series of 1 second 0.5 nA square wave pulse generated every 15 seconds during the 60-90 minute experimental recordings.

2.2.4 Pharmacological agents to examine the role of OS

2.2.4.1 Extracellular OS experiments

This study utilised 2,2'-azobis (2-amidino-propane) dihydrochloride (AAPH; Sigma-Aldrich, UK) to induce OS in the young *Lymnaea* CNS. AAPH is a water-soluble compound containing an azo group (-N=N-) that decomposes to produce peroxyl and hydroxyl radicals[273,243,291]. During recordings of the CGCs, the CNS was perfused with either 1, 3, 10 or 30 mM AAPH (dissolved in HEPES-buffered saline) for 30 minutes following the 10 minute control period (in HEPES-buffered saline only) to assess the acute extracellular effects of AAPH.

In a small sub-set of experiments, 0.1, 0.3, 18 and 20 mM AAPH was also perfused over young CNS preparations.

2.2.4.2 Intracellular OS experiments

The effects of intracellular AAPH on CGC firing properties was examined. In these experiments, 60 mM and 600 mM AAPH (dissolved in 100 mM potassium acetate solution) was backfilled into the current passing microelectrode. Its influx into left CGCs was facilitated by passing a series of depolarising current pulses (**section 2.2.3.2**). Throughout the entire experimental recording (60-90 minutes), the whole CNS was perfused extracellularly with HEPES-buffered saline.

2.2.4.3 Extracellular antioxidant experiments

To examine whether antioxidants could prevent/reverse the effects of OS, preparations were perfused with 0.5 mM vitamin C (dissolved in HEPES-buffered saline; Sigma-Aldrich, UK) and 7 mM vitamin E (dissolved in HEPES-buffered saline containing 0.01% DMSO; Sigma-Aldrich, UK) for 90 minutes in the old snails or 60 minutes before or after treatment with pro-oxidants in young snails.

Note: Control experiments were conducted to assess the effects of DMSO on CGC firing frequency. The inclusion of 0.01% DMSO in the HEPES-buffered saline did not significantly alter young or old spontaneous CGC firing frequency over a 110 minute period when compared to preparations that been perfused in HEPES-buffered saline only ($p>0.05$ for both, *n=6* RCGCs; mixed ANOVA with Bonferroni post-hoc analysis; data not shown).

2.2.5 Biochemical assays

2.2.5.1 Protein quantification assay

The protein concentration in isolated *Lymnaea* cerebral ganglia samples (where the CGCs are located) was measured spectrophotometrically using the Bradford (Coomassie Blue) assay. In this method, protein standards of bovine gamma-globulin (Bio-Rad, U.S.A) in the range of 1.25-25 µg/mL were made up in dH$_2$O. The cerebral ganglia extracts were also prepared in dH$_2$O at a dilution of 1 in 100. The standards and cerebral ganglia samples, as well as the 'blank' (composed only of dH$_2$O and therefore contained no protein), were placed into microplate wells. This was then followed by the addition of an equal volume of the Quick Start Bradford Reagent (Bio-Rad, U.S.A) to these wells.

There was a 5 minute incubation period at room temperature before the absorbance of the wells were measured at the wavelength of 595 nm. Each absorbance value was subtracted from the absorbance of the blank to correct for any background interferences caused, for example, by light scatter from the microplate. A standard curve was generated for each Bradford assay by plotting the absorbance readings *vs.* their protein concentration (µg/mL) to determine the unknown protein concentration in the cerebral ganglia samples (**Figure 2.4A**).

2.2.5.2 Malondialdehyde assay

Malondialdehyde (MDA) is a marker of OS, specifically lipid peroxidation[22]. An MDA assay was performed on the isolated cerebral ganglia samples to measure the extent of lipid peroxidation in this region of the CNS.

Cerebral ganglia samples were homogenised by hand using a pestle in ice-cold KCl solution (1.15%, w/v; Sigma-Aldrich, UK) and then centrifuged for 10 minutes at 12,000 x g at 4°C to yield the supernatant. Standards of MDA (Sigma-Aldrich, UK) were prepared in the range of 0.15-10 nmol/mL in deionised water (dH$_2$O). In test tubes, 40 µL of the supernatant or standard were incubated in the presence of sodium dodecyl sulphate (8.1%, w/v; Sigma-Aldrich, UK), acetic acid (20%, v/v; Sigma-Aldrich, UK) and thiobarbituric acid (0.8%, w/v; Sigma-Aldrich, UK) at 95 °C for 1 hour. An additional test tube referred to as the 'blank' was also prepared and incubated with all these components with the exception of the supernatant or standard so that no MDA was present.

Following the reaction, the samples were centrifuged for 10 minutes at 12,000 x g to produce a clear supernatant. Samples were placed into microplate wells and the absorbance of the wells were measured at a wavelength of 532 nm. Each absorbance value was subtracted from the absorbance of the blank to correct for any background interferences. A standard curve was generated for each MDA assay by plotting the absorbance readings *vs.* their MDA concentration (nmol/mL) to determine the unknown MDA levels in the cerebral ganglia (**Figure 2.3B**).

2.2.5.3 Protein carbonyl ELISA

Protein carbonyls are highly reactive derivatives such as aldehydes and ketones that are generated when ROS oxidises the side chains of proteins and/or cleaves peptide bonds[298]. Thus, protein carbonyl is often utilised in experimental investigations as a marker of OS[164,8,92,353].

In this study, a carbonyl assay was conducted on isolated cerebral ganglia samples. Samples were homogenised in 1% streptomycin sulphate solution (Sigma-Aldrich, UK), using a hand pestle and were left to incubate at room temperature for 30 minutes. Samples were then centrifuged at 4°C for 10 minutes at 6000 g to remove any nucleic acid.

A protein quantification assay (**section 2.2.6.1**) was then conducted on the cerebral ganglia samples. Each sample was diluted to 10 µg/mL protein in 1X PBS saline. Standards of reduced/oxidised BSA (Cell BioLabs, USA) were prepared in test tubes in the range of 0.375-7.5 nmol/mg of protein carbonyl. A 'blank' was also prepared in a test tube containing only dH$_2$O and no protein. The cerebral ganglia samples, standards and blank were added to the 96-well protein binding plate and the protein carbonyl ELISA was performed in accordance to the manufacturer's instructions without any modifications (OxiSelect™ Protein Carbonyl Elisa Kit; Cell BioLabs, USA).

Upon completion of the assay, the absorbance of the wells were measured at a wavelength of 450 nm. The absorbance values were subtracted from the absorbance of the blank to correct for any background interferences. A standard curve was generated for each protein carbonyl assay by plotting the absorbance readings *vs.* their protein carbonyl concentration (nmol/mg) to determine the unknown protein carbonyl levels in the cerebral ganglia (**Figure 2.3C**).
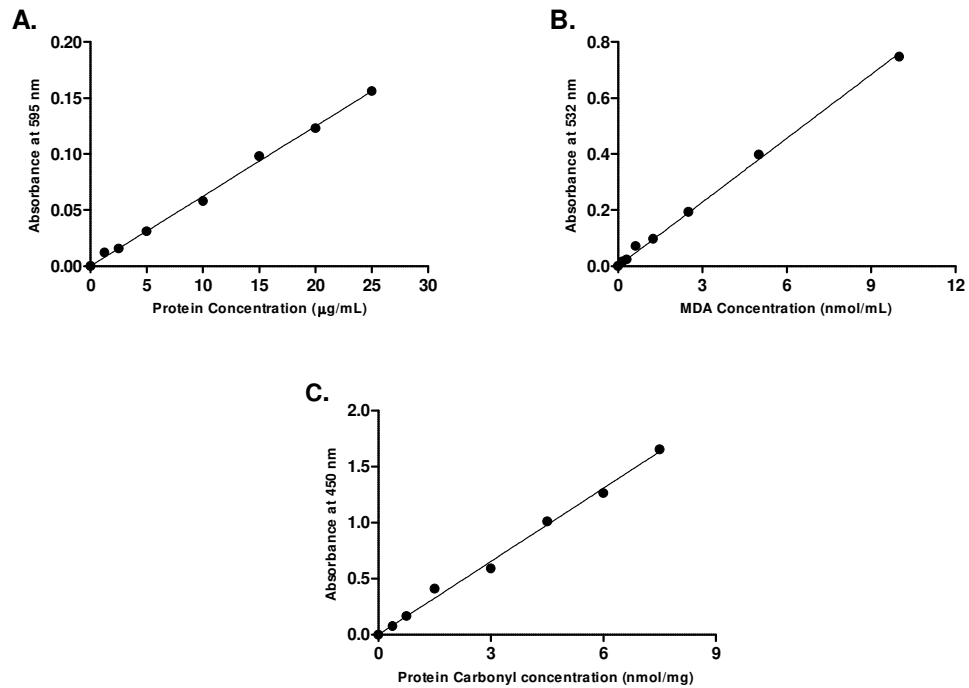
Figure 2.3| Sample standard curves for biochemical assays. (A) Bradford assay standard curve displaying protein concentration (µg/mL) *vs*. absorbance measured at 595 nm. Linear regression analysis of the Bradford standard curve showed that $R^2 = 0.997$. (B) MDA assay standard curve displaying MDA concentration (nmol/mL) *vs*. absorbance measured at 532 nm. Linear regression analysis showed that $R^2 = 0.998$. (C) Protein carbonyl standard curve illustrating protein carbonyl concentration (nmol/mg) *vs*. absorbance measured at 450 nm. Linear regression analysis showed that $R^2 = 0.996$.

2.2.6   Short-term feeding behaviour experiments in *Lymnaea*

Firstly, it is important to note that it would have been preferred to conduct a blinded study when investigating feeding behaviour in *Lymnaea*. However, due to differences in physical appearances between young and old snails (young snails were slightly smaller and their shells were much thinner and darker than old snails) and obvious impairments to feeding motor functions in snails injected with pharmacological agents, it was not possible to perform a blinded study with only a single experimenter in this thesis. In an attempt to reduce bias, all the events recorded within testing periods were measured and video recordings were utilised post-testing to corroborate the acquired results during analysis.

The effects of age and the pro-oxidant, AAPH, on short-term feeding behaviour in *Lymnaea* were investigated using methods previously described by Staras *et al.* (1999) and Arundell *et al.* (2006)[21,419]. In brief, animals were removed from their main tank and housed in smaller tanks containing copper-free water for 3 days in a laboratory maintained

between 20-22°C and set at a 12 hour light/dark cycle. Snails had free access to lettuce in the tanks, but were starved overnight prior to testing.

An hour prior to feeding assessment, young snails were injected with either HEPES-buffered saline (control) or with the AAPH saline to an estimated final concentration of 0.3 mM or 3 mM. Old snails were only injected with the HEPES-buffered saline. Two hundred microliters of the control saline or AAPH saline was injected through the foot of the snail to access the haemolymph. The snail haemolymph volume was estimated to be approximately 1-1.2 mL (young and old, respectively) based on experiments where similarly sized snails were bled by touching the foot with a pair of forceps and encouraging the animals to withdraw into their shells maximally by exuding their haemolymph.

Feeding responses of the snails were then examined by placing them in a 15 cm diameter petri dish containing 90 ml of copper-free water. Initially, the time taken for the snails to emerge (extension of both tentacles) from their shells during the 2 minute period was recorded. Importantly, snails that did not emerge ("non-emergers") were excluded from subsequent stages of the behaviour experiments.

Following this, 5 ml of copper-free water was gently dispersed around the lips of the snails that had emerged and all the number of bites were recorded over the next 2 minutes. At the end of this period, 5 ml of sucrose (0.01 M final bath concentration dissolved in copper-free water; Sigma-Aldrich, UK) was gently pipetted around the lips and the number of bites was recorded for a further 2 minutes. 0.01M sucrose was selected as the stimulus intensity as previous experiments conducted by Kemenes *et al.* (1986) and Arundell *et al.* (2006) demonstrated that 100% of young snails in a population generated feeding responses at this concentration[221,336].

The emergence time, number of bites, bite duration and inter-bite interval were all recorded using the *Lymnaea* feeding software package developed by Staras *et al.* (1998)[420]. Video recordings of all behavioural experiments were conducted to enable offline frame-by-frame analysis. When behavioural experiments had concluded, the number of bites evoked by sucrose was subtracted from the number of bites in water to correct for any contributions the vehicle solution may have had on feeding. The feeding parameters from young, old and AAPH-treated young snails were then entered into Graphpad Prism 7 (GraphPad Software, USA) or SPSS (IBM statistics 24, USA) to determine the population mean value and conduct statistical analysis (**section 2.2.9**).

2.2.7 Current clamp data analysis

2.2.7.1 Analysis of spontaneous action potentials parameters

Analysis of the current clamp recordings was performed offline using Clampfit® from the pClamp version 10.5 software package. Traces were not filtered prior to analysis. The 'Template Search' function in Clampfit® was used to measure at selected intervals (**section 2.2.8.3**), the following parameters: 1) spontaneous firing frequency; 2) RMP; 3) peak amplitude; 4) half-width, and; 5) fAHP amplitude.

The 'Fit' function was used to generate the mAHP time constant by fitting an exponential curve from the peak of the fAHP to the 100 ms time point after the fAHP peak. The sAHP was assessed using the 'Threshold search' function, which measured the duration from the fAHP peak to the RMP. This 'Threshold search' function was also used to determine the CGC action potential threshold. **Figure 2.4** illustrates how the AHP parameters and the RMP potential of the CGC action potentials were measured in Clampfit®.
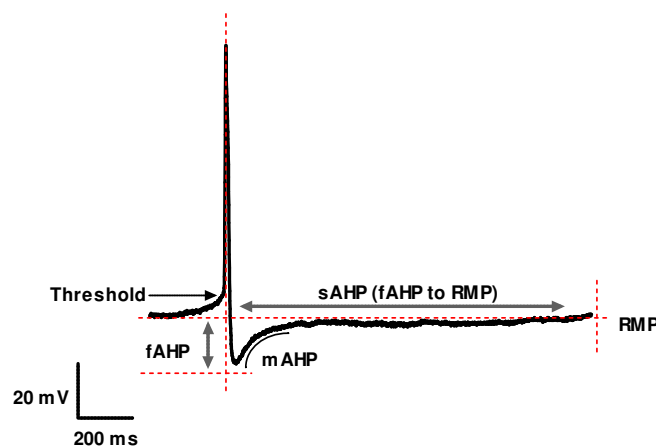
Figure 2.4| Analysis of the AHP and RMP. The fAHP was measured as the amplitude from the action potential threshold to the negative going peak. The mAHP was measured by fitting an exponential curve from the fAHP peak to 100 ms after the fAHP. The sAHP measured as the duration from the end of the fAHP to the RMP. The RMP potential is measured once the CGC has repolarised following the generation of an action potential.

The proportion of snails from each experimental group that demonstrated synchronous activity between the paired CGCs in a CNS preparation was also assessed in Clampfit®. CGC coupling was measured as 1:1 action potentials between the right CGC (RCGC) and left CGC (LCGC) over a 2 minute period at selected times intervals (**section 2.2.8.3**).

The averages for each action potential parameter were calculated and then entered in Graphpad Prism 7 to determine the population mean and conduct statistical analysis (**section 2.2.9**).

2.2.7.2   Analysis of spike frequency adaptation

The 'Template search' function in Clampfit$^®$ was used to measure the number and half-width of the action potentials generated by the CGCs during the 5 second 2 nA depolarising current pulse (**section 2.2.3.1**) at selected intervals (**section 2.2.8.3**). This functionality also measured the instantaneous frequency (Hz) and inter-spike interval (ISI), which was used to construct an '*instantaneous frequency (f) vs. time of spike (t)*' plot to analyse the following SFA parameters: the initial instantaneous firing frequency (f_0), the steady state firing frequency (f_{ss}), the frequency of adaptation (F_{adap}), the time constant of adaptation (τ_{adap}) and the time constant of Ca^{2+} clearance ($\tau_{Calcium}$)[472].

A single exponential curve was fitted to the '*f vs. t*' plot of each data set to yield the τ_{adap} (tau) and f_{ss} (plateau constant). The f_{ss} (Hz) and f_0 (Hz) values was then used to calculate F_{adap} using **equation 2.1**. The $\tau_{Calcium}$ was calculated using the τ_{adap} and F_{adap} values in accordance to **equation 2.2**.[472]

$$\textbf{Equation 2.1} \qquad \textbf{F}_{\textbf{adap}} = (f_0 - f_{ss})/f_0$$

$$\textbf{Equation 2.2} \qquad \tau_{\textbf{Calcium}} = \tau_{\textbf{adap}}/(1 - \textbf{F}_{\textbf{adap}})$$

The calculated values for SFA parameters from each data set were entered in Graphpad Prism 7 to determine the population mean and conduct statistical analysis (**section 2.2.9**).

2.2.7.3   Parameters analysed in each experimental investigation

Analysis was primarily conducted on the RCGCs- except for when examining differences between paired CGCs- as voltage clamp experiments (Chapter 3) were to be performed on this particular CGC and therefore, alterations in ionic currents could be related back to changes in the action potential parameters. This was important because it has been observed that there are slight differences in the ion channel complement mediating the action potential waveform between the RCGC and LCGC (Yeoman MS, personal communication).

Action potential coupling was measured over a 2 minute duration (**section 2.2.7.1**), spontaneous action potential parameters over a 5 minute duration (**section 2.2.7.1**) and evoked action potential parameters over a 2 minute duration (**section 2.2.3.1**) from the trace recordings. Furthermore, the time intervals selected for the measurements of these parameters represented the period by which pharmacological agents had mediated their maximal effects on CGC firing properties (**section 2.2.4**).

2.2.7.3.1 The effects of age and acute extracellular OS on CGC firing properties

In experiments comparing differences between young controls, old and extracellular AAPH-treated young preparations (**section 2.2.4.1**), all spontaneous action potential parameters were measured at 40 minutes and all SFA parameters at 45 minutes from trace recordings of the RCGCs.

Action potential coupling in all these preparations was also measured at 40 minutes from simultaneous recordings of the paired CGCs.

2.2.7.3.2 Reversing alterations to CGC firing with age and acute extracellular OS

To assess whether the effects of extracellular AAPH treatment on young CGC firing could simply be reversed by a HEPES-buffered saline washout period, spontaneous RCGC firing frequency was measured at various intervals. Initially at 5 minutes during the control period, then at 40 minutes following AAPH treatment and finally at 105 minutes after the HEPES-buffered saline wash.

Analysis of reversal with antioxidants involved assessing spontaneous RCGC firing frequency, which was initially measured at 5 minutes during the control period of each experimental study. Then again as follows:

- In the pre-AAPH antioxidant experiments, measurements were conducted at 70 minutes following incubation in the antioxidant saline and then at 105 minutes following perfusion with the AAPH saline.

- In the post-AAPH antioxidant experiments, measurements were conducted at 40 minutes following perfusion in the AAPH saline and then again at 105 minutes following exposure to the antioxidant saline.

- In experiments involving old CNS preparations, measurements were conducted at 100 minutes following perfusion of the antioxidant saline.

2.2.7.3.3 The effects of intracellular OS on CGC firing properties

In the intracellular OS experiments (**section 2.2.4.2**), action potential coupling and all spontaneous action potential parameters were measured at 60 minutes from recordings of the paired CGCs following intracellular injection of the control saline and AAPH saline. In a small sub-set of experiments, these measurements were also taken at 90 minutes.

2.2.7.3.4 The stability of CGC firing frequency during experimental recordings

To assess the stability of spontaneous RCGC firing frequency during an experiment, measurements in a sub-set of young and old control preparations were conducted every 10 minutes over a 110 minute recording period. No electrophysiological experiments exceeded 110 minutes in this thesis. This analysis was performed to ensure that any alterations to CGC firing frequency was caused by the pharmacological agents and not by changes that may inherently occur in the CGCs when recording over time.

Figure 2.5 reveals that RCGC firing frequency did not significantly change in young and old preparations during a 110 minute recording period in HEPES-buffered saline ($p>0.05$ for both, *n=6* RCGCs; repeated-measures ANOVA with Bonferroni post-hoc).
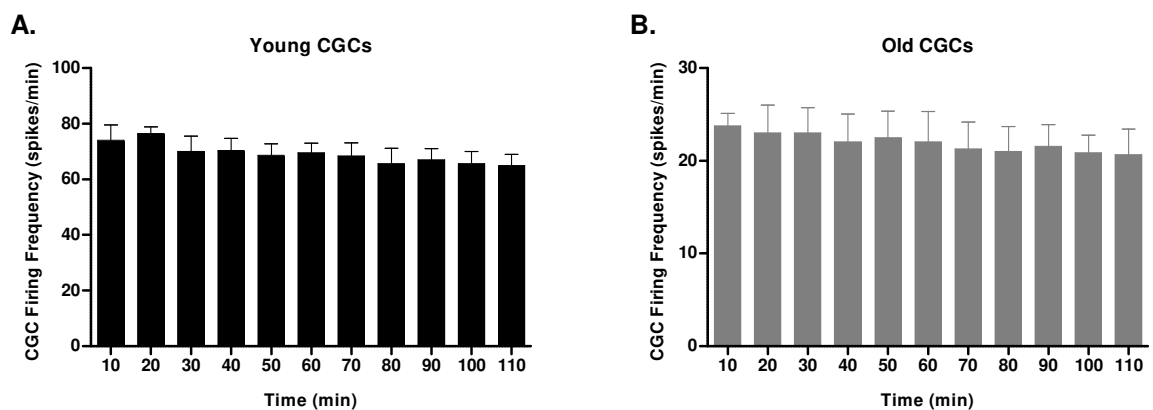
Figure 2.5| Stability of CGC firing frequency. In both (A) young and (B) old control preparations, spontaneous CGC firing frequency did not significantly change during an experimental recording. Data shown as mean ± SEM, *n=6* RCGCs. NS, p>0.05.

2.2.8 Biochemical assay analysis

Standard curves were generated for each assay to determine the unknown MDA concentration (**section 2.2.5.2**) and unknown protein concentration (**section 2.2.5.3**) in the *Lymnaea* cerebral ganglia samples, respectively. Values obtained from the Bradford

assay were multiplied by the amount of volume the cerebral ganglia sample was diluted in to correct for the dilution factor and thus obtain the real protein concentration.

The concentration of MDA in the cerebral ganglia samples was then normalised to protein by dividing by the protein value calculated from the Bradford assay. This was conducted in Microsoft Excel® (Microsoft, USA) and the values generated were entered into GraphPad Prism 7 for statistical analysis (**section 2.9**).

2.2.9 Statistical data analysis

A Pearson's chi-squared test was performed to determine whether the proportion of a categorical variable differed between two independent populations. This analysis was conducted in SPSS statistics 24. An unpaired t-test was performed on data containing two independent groups. A one-way ANOVA for independent groups or a repeated-measures ANOVA for related groups was conducted on data sets containing more than two groups. A two-way ANOVA was performed when data sets had two independent variables. These statistical tests were conducted in GraphPad Prism 7.

When there was a significant difference following an ANOVA test, a Bonferroni multiple comparisons test was conducted in GraphPad Prism 7 to identify where the significant changes had occurred. The Bonferroni method was selected to reduce the likelihood of producing type I errors (incorrect rejection of the null hypothesis in favour of the alternative) when testing multiple hypotheses[80,320,86]. This method accomplishes this by dividing the p-value by the number of comparisons being performed to produce a new lower critical p-value[86]. While the Bonferroni test is regarded as quite conservative because of this, it reduces the possibility of drawing conclusions based on false positive results in this thesis[319].

The following p-values indicated that there was a significant difference: *p<0.05, **p<0.01, and ***p<0.001. For non-significant (NS) values, p>0.05. All data in the results sections are presented as the mean ± standard error of the mean (SEM) and *n* denotes the sample size. Depending on the experimental study, *n* was representative of the following samples: 1) number of RCGCs each from recorded from an individual preparation; 2) number of LCGCs each recorded from an individual preparation; 3) number of paired CGCs (PCGCs) simultaneously recorded from an individual preparation; 4) number of snails utilised during *in vivo* experiments, or; 5) number of cerebral ganglia (CG; both right and left) isolated from an individual CNS preparation.

2.3 Results

2.3.1 Age-related changes to feeding behaviour in *Lymnaea*

Short-term feeding behaviour experiments were conducted to assess whether there were any changes to feeding with increasing age, which would be strongly indicative of changes to CGC firing properties[21,508]. In both the young and old snail population, approximately 11% of the snails did not emerge from their shells when placed in the test arena and thus, there was no significant difference between the two populations (χ^2=0, p>0.05, *n=9* snails; Pearson's chi-squared test; **Figure 2.6A**). Non-emergers were excluded from subsequent testing.

Old snails took significantly longer to emerge than the young snails (p<0.001, *n=8* snails; unpaired t-test; **Figure 2.6B**). In **Figure 2.6C**, the 0.01M sucrose stimulus evoked a significantly lower number of bites in old snails when compared to the young (p<0.05, *n=8* snails; unpaired t-test). Rates decreased from 19 ± 2.3 sucrose bites min^{-1} in the young to 13.2 ± 0.7 sucrose bites min^{-1} in the old. This decrease in old snails was accompanied with a significant increase in the bite duration (p<0.05, *n=8* snails; **Figure 2.6D**) and inter-bite interval (p<0.001, *n=8* snails; **Figure 2.6E**).

Figure 2.6F displays images from the frame-by-frame video analysis demonstrating that the old snails had no issues with opening their mouths wide and protracting their radula out during a sucrose-evoked bite (white arrow) when compared to young snails (visual assessment only, *n=8* snails).
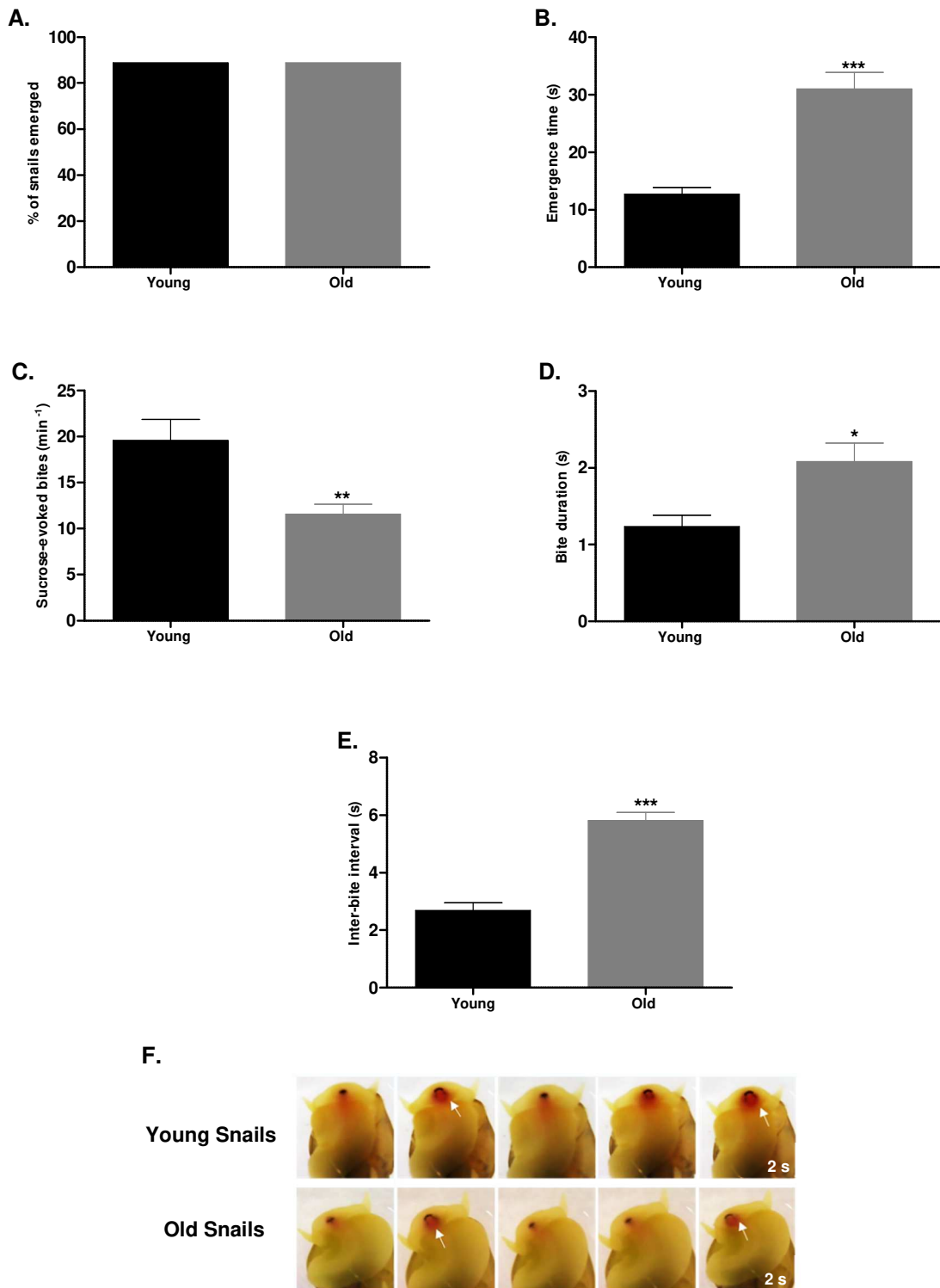
Figure 2.6| Age-related changes to feeding behaviour. (A) Age did not affect the proportion of snails that emerged. However, it (B) increased the time it took for old snails to emerge from their shells, (C) decreased sucrose-evoked bites, and increased both (D) bite duration and (E) the inter-bite interval. (F) Image analysis (every 2 seconds during a 10 second period) shows that mouth opening and radula protrusion during a sucrose-evoked bite (white arrow) was not hindered with age. Data shown as mean ± SEM, *n=8-9* snails per group. *p<0.05 (part D), **p<0.01 (part C) and ***p<0.001 *vs.* young snail (Part B and E).

2.3.2 Spontaneous CGC firing decreases in old snails

In **Figure 2.7A**, sample traces of intracellular recordings from a young and old RCGC illustrates the decrease in firing frequency with increasing age. The reduction in spontaneous firing frequency in old CGCs was significant when compared to the young CGCs (p<0.01, *n=7* RCGCs*; unpaired t-test; **Figure 2.7B**). CGC firing rates decreased by ~70% from 62.8 ± 9.4 spikes min^{-1} in young snails to 20.1 ± 3.1 spikes min^{-1} in the old snails.

The RCGC and LCGC in young and old snails fired in synchronicity in every preparation (χ^2=0, p>0.05, *n=7* PCGCs*; Pearson's chi-squared test; **Figure 2.7C**).
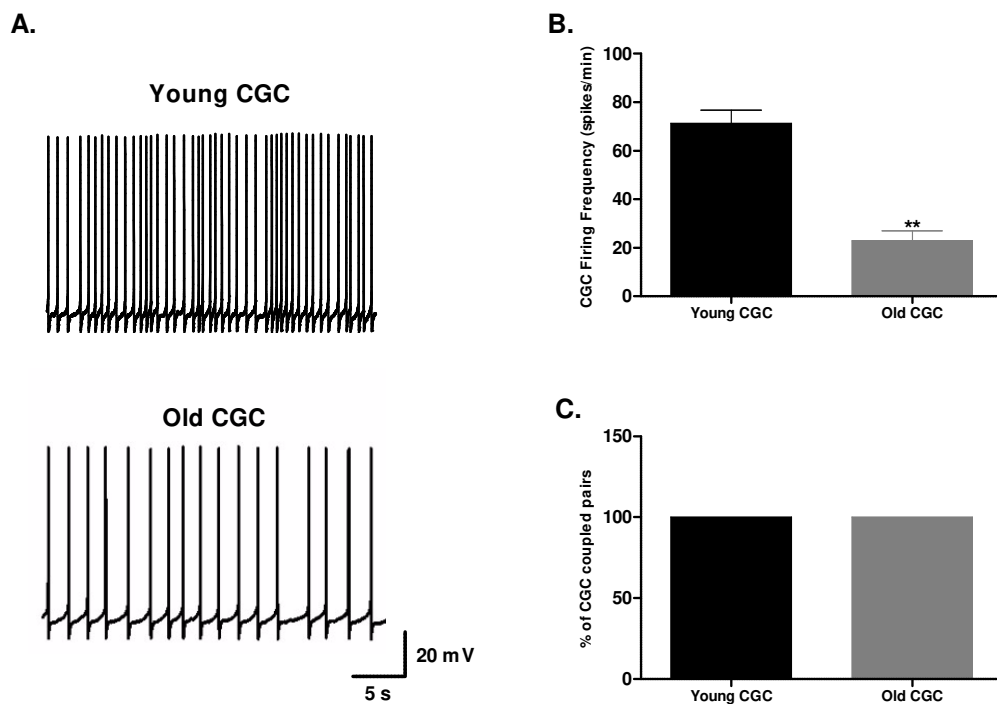
Figure 2.7| Age-related changes in spontaneous CGC firing frequency. (A) Representative sample trace of a young (top) and old (bottom) RCGC spontaneously firing. (B) Firing frequency significantly decreased with age, but there were (C) no alterations to CGC coupling. Data shown as mean ± SEM, *n=7* RCGCs for part B and *n=7* PCGCs for part C. **p<0.01 *vs.* young CGC.

2.3.3 Changes to the CGC AHP and RMP with age

The age-related reduction in firing rates in *Lymnaea* may be due to the CGCs being in a more hyperpolarised state, which could be attributed to changes in the AHP and/or RMP.

In **Figure 2.8Ai**, a representative example of a CGC action potential from a young and old preparation illustrates changes to the AHP with age. The fAHP amplitude increased significantly from -12.6 ± 0.1 mV in the young to -19.8 ± 0.8 mV in the old CGCs ($p<0.001$, *n=7* RCGCs, unpaired t-test; **Figure 2.8Aii**). The sAHP duration also increased significantly from 582.8 ± 141.4 ms in the young CGCs to 2081.2 ± 259.8 ms in the old CGCs ($p<0.05$, *n=7* RCGCs; **Figure 2.8Aiii**). The mAHP duration, however, did not significantly change with advancing age ($p>0.05$, *n=7* RCGCs; data not shown).

Figure 2.8B revealed that the RMP of old CGCs was significantly more hyperpolarised, by ~-16 mV, than that of young CGCs ($p<0.01$, *n=7* RCGCs).
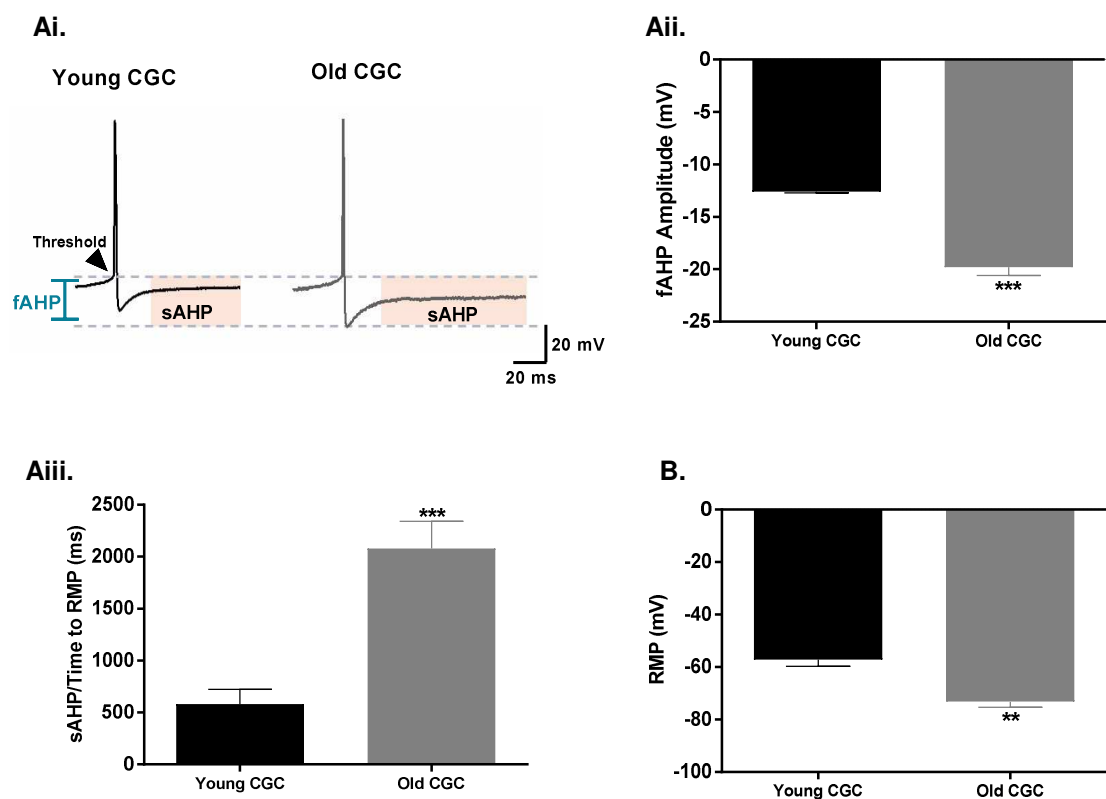
Figure 2.8| Age-related changes to the AHP and RMP. (Ai) Representative RCGC action potential illustrating clear differences to the AHP between the young and old CGC. Both the (Aii) fAHP amplitude and (Aiii) sAHP duration increased significantly with age. (B) Old CGCs also had a significantly more hyperpolarised RMP than young CGCs. Data shown as mean ± SEM, *n=7* RCGCs. **p<0.01 and ***p<0.001 *vs*. young RCGC.

2.3.4 Does the CGC action potential half-width or peak amplitude change with age?

Figure 2.9Ai, a sample trace of RCGC action potential displays clear changes to the half-width with age. The action potentials of old CGCs were significantly narrower, by ~20%, when compared to young CGC action potentials (p<0.01, *n=7* RCGCs; unpaired t-test; **Figure 2.9Aii**).

The peak amplitude of the CGC action potentials, however, did not significantly differ between the young and old CGCs (p>0.05, *n=7* RCGCs; **Figure 2.9B**).
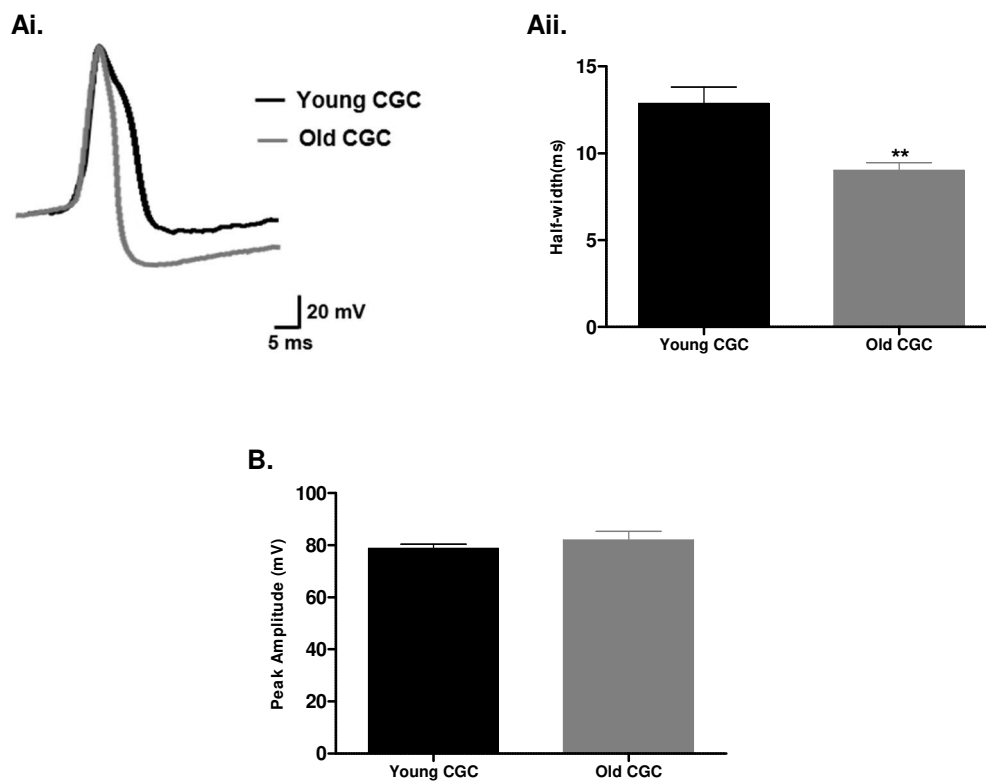
Figure 2.9| Age-related changes to the half-width and peak amplitude. (Ai) Sample traces illustrates that the RCGC action potential narrowed with age and this change (Aii) was statistically significant. (B) The peak amplitude of the CGC action potential was not altered with age. Data shown as mean ± SEM, *n=7* RCGCs. **p<0.01 *vs.* young CGC (part A).

2.3.5 Age-related changes to CGC spike frequency adaptation

Many neurons possess the ability to decrease their firing frequency in response to a constant depolarising input. This phenomenon is known as spike frequency adaptation (SFA). A recent investigation by Scutt (2012) demonstrated for the first time that the CGCs in *Lymnaea* exhibit SFA[393]. Furthermore, that study also showed that the

parameters and dynamics of SFA were altered with increasing age. Thus, the aim of the following section is to assess whether there are any changes to SFA in this ageing *Lymnaea* model.

2.3.5.1 SFA exhibited by the CGCs from young and old *Lymnaea*

Figure 2.10A displays the high frequency action potential bursts generated by a young and old right CGC during the depolarising current pulse evoked from the RMP. Both young and old CGCs exhibited SFA as demonstrated by the exponential decline in the representative '*instantaneous frequency vs. time of spike*' plot in **Figure 2.10B**. Significantly less spikes were evoked in old CGCs when compared to young CGCs (p<0.01, *n=7* RCGCs; unpaired t-test; **Figure 2.10C**). Young CGCs evoked an average of 23 ± 2.4 spikes/5s when depolarised, whereas old CGCs generated only 12 ± 0.8 spikes/5s.
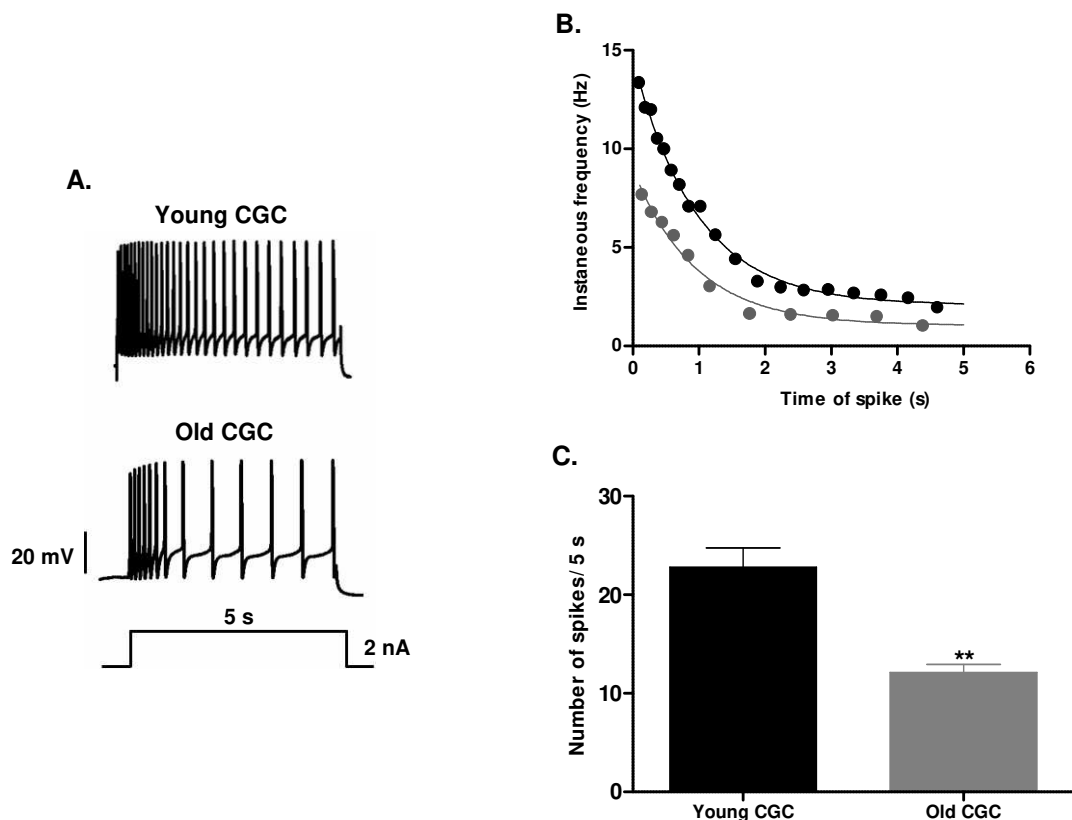
Figure 2.10| Age-related changes to evoked spiking frequency. (A) Sample traces of evoked spikes generated by a young (top) and old (bottom) RCGC. (B) The exponential decline of this plot reveals that both young and old CGCs exhibited SFA. (C) The frequency of evoked spikes during SFA decreased significantly with age. Data shown as mean ± SEM, *n=7* RCGCs. **p<0.01 *vs.* young CGC.

2.3.5.2   Changes to basic SFA parameters in the CGCs with age

Sample traces in **Figure 2.11A** illustrates changes to both initial (f_0) and steady state (f_{ss}) instantaneous firing frequencies during SFA with age. f_0 (Hz) was significantly slower in the old CGCs when compared to young CGCs (p<0.05, *n=7* RCGCs; unpaired t-test; **Figure 2.11B**). The mean f_0 (Hz) value calculated in the young was 12.1 ± 0.5 Hz and this decreased to 8.5 ± 1.1 Hz with age. f_{ss} (Hz) was also significantly lower in the old CGCs when compared to the young (p<0.05, *n=7* RCGCs; **Figure 2.11C**). Values were 3.1 ± 0.6 Hz and 1.2 ± 0.5 Hz for the young and old CGCs, respectively.

In **Figure 2.11D**, the % increase in half-width duration from the spike at f_0 to the spike at f_{ss} did not significantly differ between young and old CGCs (p>0.05, *n=7* RCGCs).
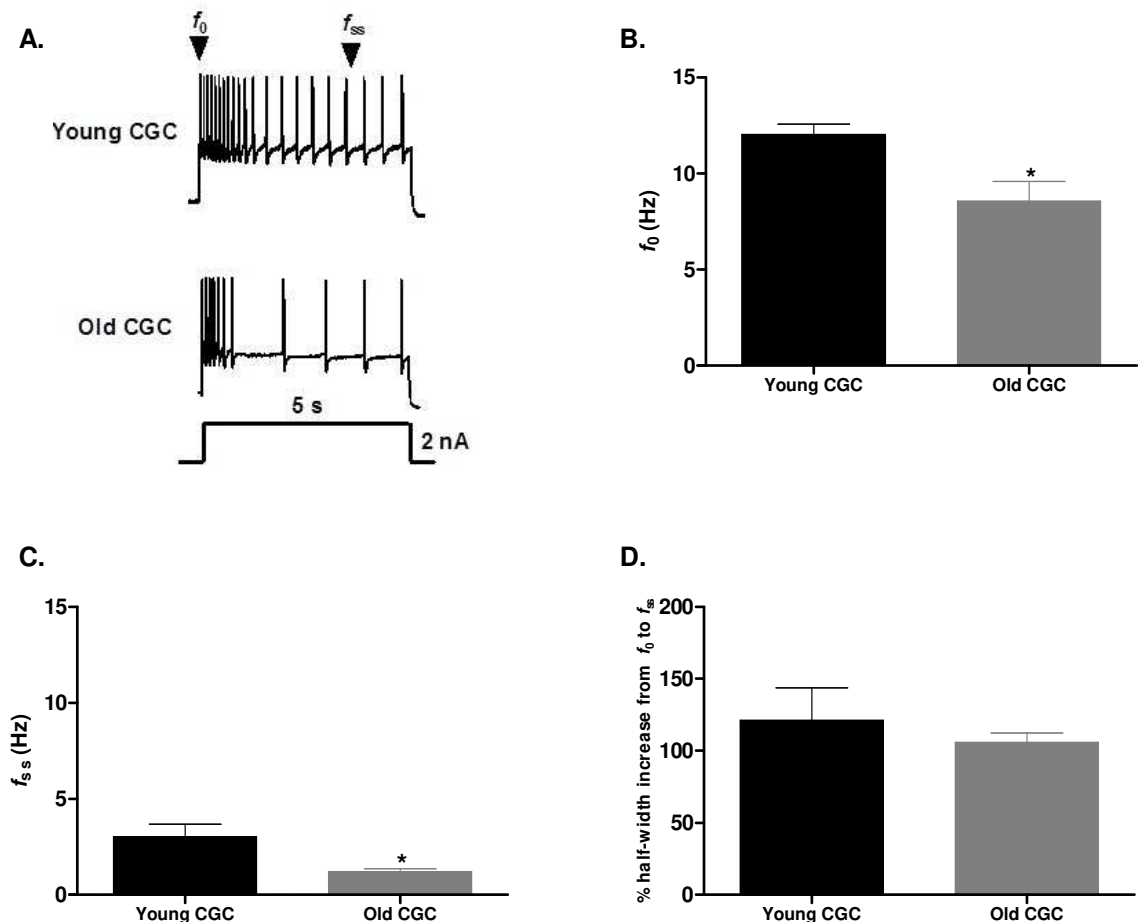
Figure 2.11| Age-related changes to f_0 (Hz) and f_{ss} (Hz). (A) Sample traces of SFA exhibited by a young (top) and old (bottom) RCGC. Both (B) f_0 (Hz) and (C) f_{ss} (Hz) were significantly slower in the old CGCs when compared to young CGCs. (D) The % increase in the half-width duration from f_0 to f_{ss} did not significantly change with age. Data shown as mean ± SEM, *n=7* RCGCs. *p<0.05 *vs.* young CGC.

2.3.5.3 Do the dynamics of SFA change in the CGCs with age?

The strength of adaptation (F_{adap}) and speed of adaptation (τ_{adap}) was assessed to determine whether the dynamics of SFA was altered in ageing CGCs. Analysis of τ_{adap} (**Figure 2.12A**) and F_{adap} (**Figure 2.12B**) revealed no significant changes with age ($p>0.05$, *n=7* RCGCs; unpaired t-test).

F_{adap} and τ_{adap} were subsequently used to calculate the time constant of Ca^{2+} clearance ($\tau_{Calcium}$) in the young and old CGCs in accordance to Equation 2.2. There was no significant difference in $\tau_{Calcium}$ between young and old CGCs ($p>0.05$, *n=7* RCGCs; unpaired t-test; **Figure 2.12C**).
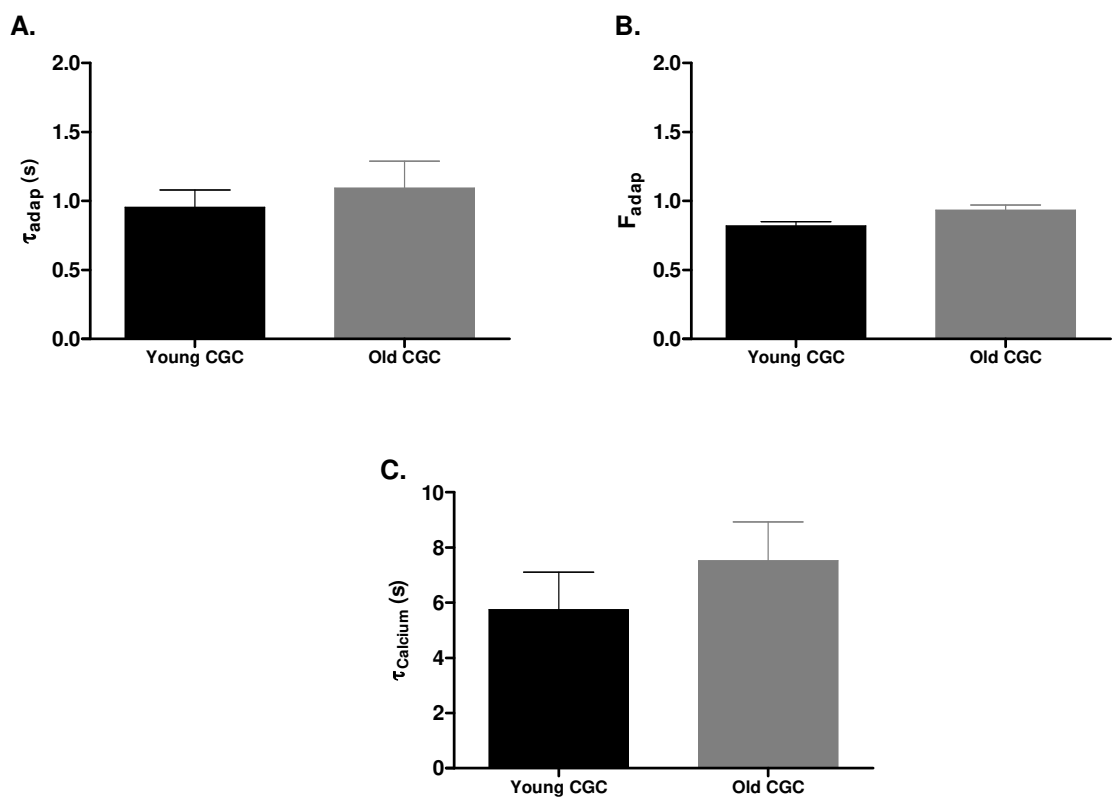
Figure 2.12| Age-related changes to SFA dynamics. (A) τ_{adap}, (B) F_{adap} and (C) $\tau_{Calcium}$ did not significantly change with increasing age in the CGCs. Data shown as mean ± SEM, *n=7* RCGCs. NS, p>0.05 *vs*. young CGC.

2.3.6 Acute extracellular AAPH treatment induces an ageing-like phenotype in young *Lymnaea*

In mammalian CNS studies, it has often been hypothesised that OS plays an instrumental role in the decline of neuronal excitability with age. Work previously on the RPeD1 neuron in the *Lymnaea* CNS has also conclusively shown that experimental OS can mimic

the effects of ageing in this neuron[476,478]. Evidence that OS is a major driver of CGC ageing is at best circumstantial and if OS is causal in CGC ageing there is, to date, no detailing the mechanisms by which OS reduces CGC firing[477]. Thus, the aim experiments in this section was to examine CGC firing properties in the presence of the pro-oxidant generator, AAPH.

2.3.7   The effects of AAPH on young *Lymnaea stagnalis* feeding behaviour

Experiments in this chapter previously demonstrated that ageing in *Lymnaea* was associated with a decrease in the frequency of sucrose-evoked bites. Thus, it was of interest to observe whether acute AAPH treatment in young snails could mimic the ageing feeding behaviour phenotype.

Whilst all the control (HEPES-buffered saline injected) snails and 0.3 mM AAPH injected snails emerged from their shells, approximately 50% of the 3 mM AAPH injected snails did not emerge from their shells within the 2 minute test period (χ^2=9.6, p<0.001 for both groups, *n=8* snails; Pearson's chi-squared test; **Figure 2.13A**). Non-emergers were excluded from participating in subsequent stages of feeding behaviour experiments.

Figure 2.13B reveals that the 3 mM AAPH injected snails took significantly longer to emerge when compared to both the control and 0.3 mM AAPH injected snails (p<0.001 for both groups, *n=4-8* snails*;* one-way ANOVA with Bonferroni post-hoc analysis). The 0.3 mM AAPH injected snails also emerged significantly slower than control snails (p<0.001, *n=8* snails).
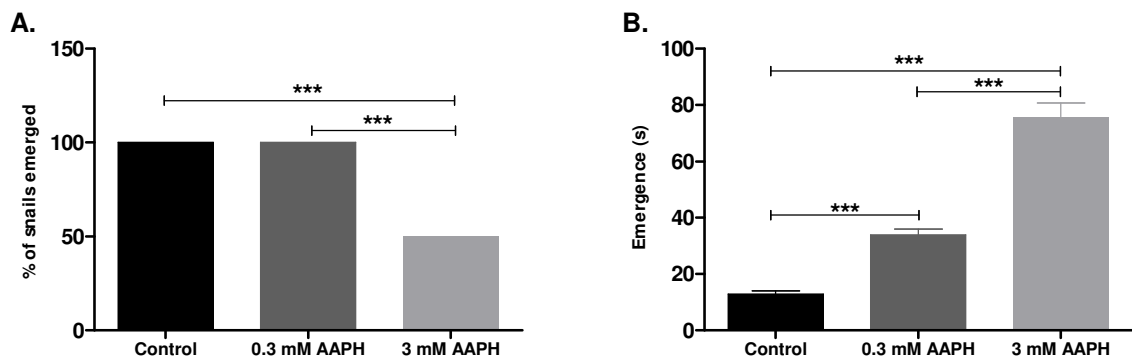
Figure 2.13| AAPH alters the young *Lymnaea* emergence response. (A) Every control and 0.3 mM AAPH injected snails emerged, whilst only 50% of the 3 mM AAPH injected snails emerged. (B) All AAPH injected snails emerged significantly slower from their shells (in a concentration-dependent manner) when compared to control snails. Data shown as mean ± SEM, *n=4-8* snails. ***p<0.001.

The 3 mM AAPH injected young snails that emerged from their shells failed to generate any bites when presented with the 0.01 M sucrose stimulus. These snails appeared to sense the sucrose that had been dispensed around their lips as it was observed that they emerged further out from their shells and that their tentacles became more elongated (visual assessment only; $n=4$ snails; **Figure 2.14A**). The lack of sucrose-evoked bites in these snails meant that other feeding behaviour parameters could not be investigated.

0.3 mM AAPH injected young snails produced significantly fewer sucrose-evoked bites than the controls ($p<0.001$, $n=8$ snails; one-way ANOVA with Bonferroni post-hoc analysis; **Figure 2.14B**). There was a significant decrease in the bite duration ($p<0.01$, $n=8$ snails; **Figure 2.14C**) and a significant increase in the inter-bite interval ($p<0.001$, $n=8$ snails; **Figure 2.14D**) in these snails.

Images from frame-by-frame video analysis in **Figure 2.14Ei-ii** shows that the 0.3 mM AAPH injected young snails also had serious issues with opening their mouths as wide as the controls and struggled to protract their radula out of the open mouth (visual assessment only; $n=8$ snails).

A.

1) In copper-free water   2) 0.01 M sucrose added   3) In sucrose saline

4 s

B. Sucrose-evoked bites (min^{-1}) — Control / 0.3 mM AAPH — ***

C. Bite duration (s) — Control / 0.3 mM AAPH — **

D. Inter-bite interval (s) — Control / 0.3 mM AAPH — ***
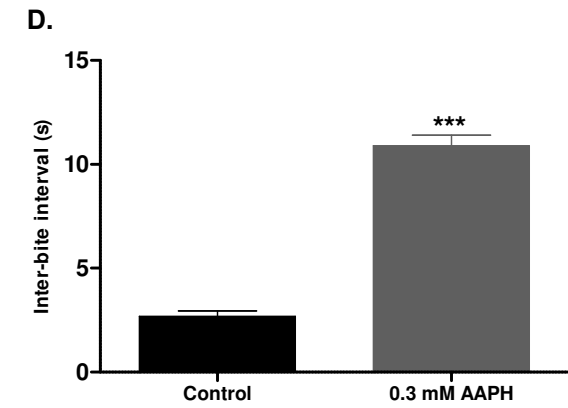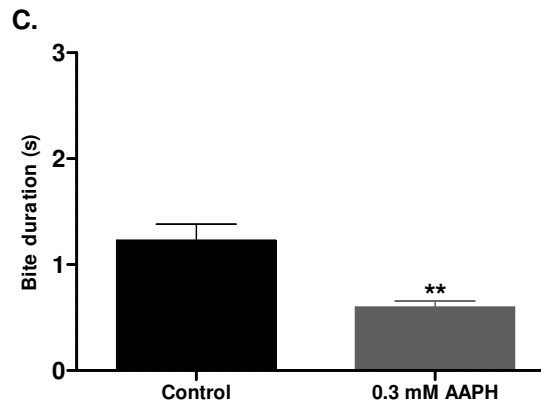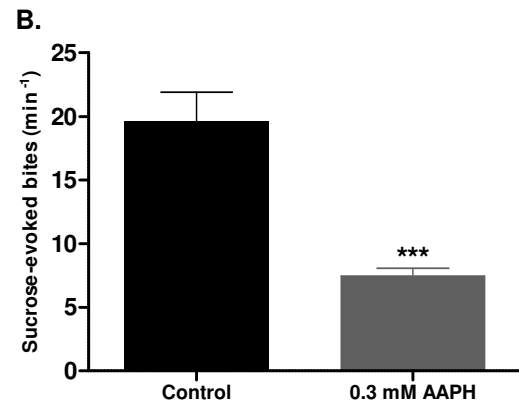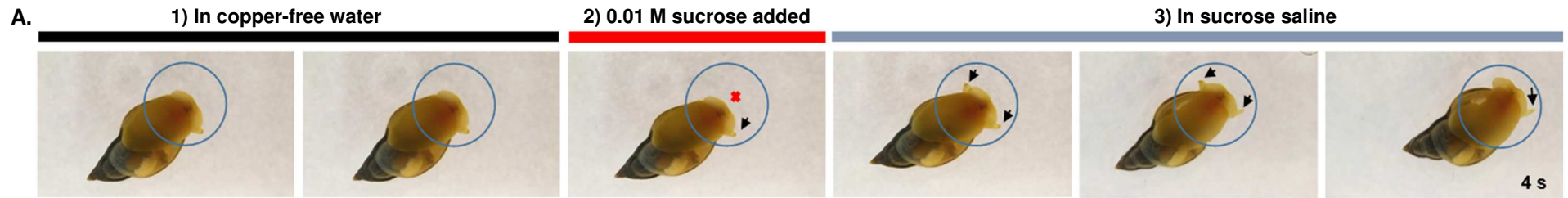
Ei. Control young snails injected with HEPES-buffered saline

2 s

Eii. Young snails injected with 0.3 mM AAPH

2 s

71

Figure 2.14| AAPH alters feeding in young *Lymnaea*. (A) Image analysis (over a 24 s interval) demonstrates that 3 mM AAPH injected snails were able to sense sucrose when it was applied near their lips (red cross), despite not evoking any bites. Snails transitioned from being relatively stationary in the absence of sucrose to more active (black arrows) when presented with the stimulus. **(B)** 0.3 mM AAPH injected snails evoked significantly less bites than control snails. This decrease was associated with an increase in the **(C)** bite duration and **(D)** inter-bite interval. **(Ei-Eii)** Frame-by-frame analysis illustrates that the 0.3 mM AAPH injected snails were unable to open their mouths wide and protract their radula out (red arrow) during a sucrose-evoked bite. Data shown as mean ± SEM, *n=4-8* snails. **p<0.01 and ***p<0.001 *vs*. control.

2.3.8 Acute extracellular AAPH decreases spontaneous firing of the young CGCs

To investigate whether the effects of acute extracellular AAPH treatment on CGC firing properties were dose-dependent, 1, 3, 10 and 30 mM AAPH were selected as the concentrations to be utilised, as they all mediated their effects on young CGCs within 30 minutes. It was important for AAPH to have an effect in 30 minutes or less, as this greatly improves the stability required for voltage-clamp recordings (Chapter 3).

Concentrations <1 mM AAPH, including 0.1 mM and 0.3 mM, both failed to significantly reduced CGC firing frequency within 30 minutes ($p > 0.05$ for both, *n=5* RCGCs; one-way ANOVA with Bonferroni post-hoc analysis; data not shown). Even when perfused for a longer duration of 90 minutes, there were no alterations to CGC firing frequency with these lower AAPH concentrations ($p > 0.05$ for both, *n=5* RCGCs; data not shown).

In **Figure 2.15A**, sample traces of intracellular recordings from young preparations demonstrate that there is a reduction and eventual inhibition of CGC firing in response to increasing AAPH concentrations from 1 mM to 30 mM. **Figure 2.15B** revealed the lowest concentration, 1 mM, caused a 41% decrease in firing frequency that was significantly different when compared to the control ($p < 0.05$, *n=8* RCGCs*;* one-way ANOVA with Bonferroni post-hoc analysis). Rates decreased from 62.9 ± 9.5 spikes min^{-1} in the control to 36.1 ± 8.5 spikes min^{-1} with 1 mM AAPH. At the higher concentrations of 3 mM and 10 mM AAPH there was over a 50% reduction in the CGC firing rate. Firing frequency significantly decreased to 26.1 ± 9.2 spikes min^{-1} at 3 mM ($p < 0.001$, *n=8* RCGCs) and 31.9 ± 2.6 spikes min^{-1} at 10 mM AAPH ($p < 0.05$, *n=8* RCGCs). Interestingly, exposure to 30 mM AAPH completely inhibited spontaneous CGC firing ($p < 0.001$, *n=8* RCGCs).

The highlighted light grey area of the curve in **Figure 2.15B** displays the steady decrease in the firing frequency from 1-10 mM AAPH. The area highlighted in dark grey shows the steep decline in CGC firing rate following application of 30 mM AAPH.

Recordings conducted at 18 and 20 mM AAPH (*n=2* RCGCs; data not shown) demonstrated that there was no gradual decline to the inhibition of CGC firing between 10-30 mM AAPH as the firing frequency at 18 mM resembled values seen at 3 and 10 mM, whilst 20 mM resulted in the complete inhibition of CGC firing.
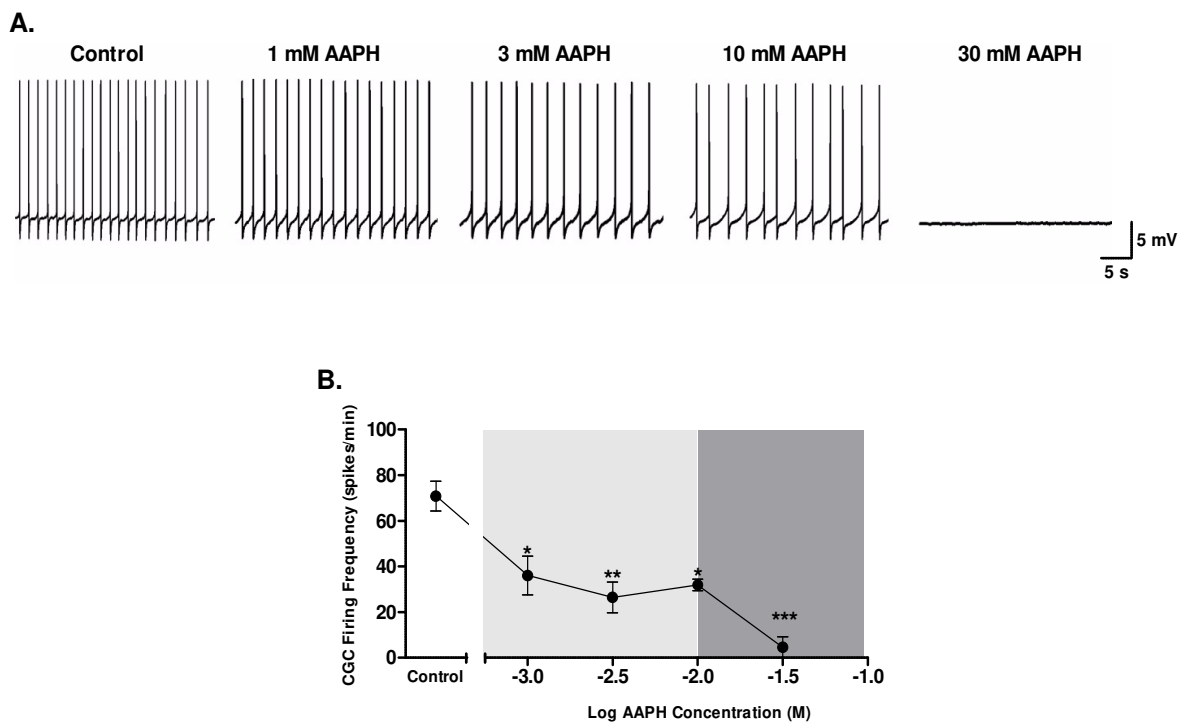
Figure 2.15| Acute extracellular AAPH alters young CGC firing frequency. (A) Sample traces showing firing of RCGCs following exposure to 1-30 mM AAPH. (B) There was a significant reduction in firing frequency with increasing AAPH concentrations (1-10 mM), which was followed by complete suppression of firing with 30 mM AAPH. Data shown as mean ± SEM, *n=8* RCGCs. *p<0.05, **p<0.01, ***p<0.001 *vs*. control.

2.3.9 Effect of acute extracellular AAPH on young CGC action potential synchronicity

Sample traces in **Figure 2.16A** of a paired RCGC and LCGC demonstrates that exposure to the highest concentration of AAPH, 30 mM, alters CGC coupling. Prior to complete cessation of spontaneous CGC firing, 30 mM AAPH significantly impaired CGC synchronicity in approximately 40% of preparations as firing slowed down (χ^2=12.9, p<0.01 *vs*. each group, *n=8* PCGCs; Pearson's chi-squared test; **Figure 2.16B**).

Conversely, CGCs fired in synchronicity in every control and 1-10 mM AAPH-treated preparations (χ^2=0, p>0.05, *n=8* PCGCs; Pearson's chi-squared test).

A.

Control young CGC   30 mM AAPH-treated young CGC

Right CGC

Left CGC

20 mV

2 s

B.

% of young CGC coupled pairs

Log AAPH Concentration (M)
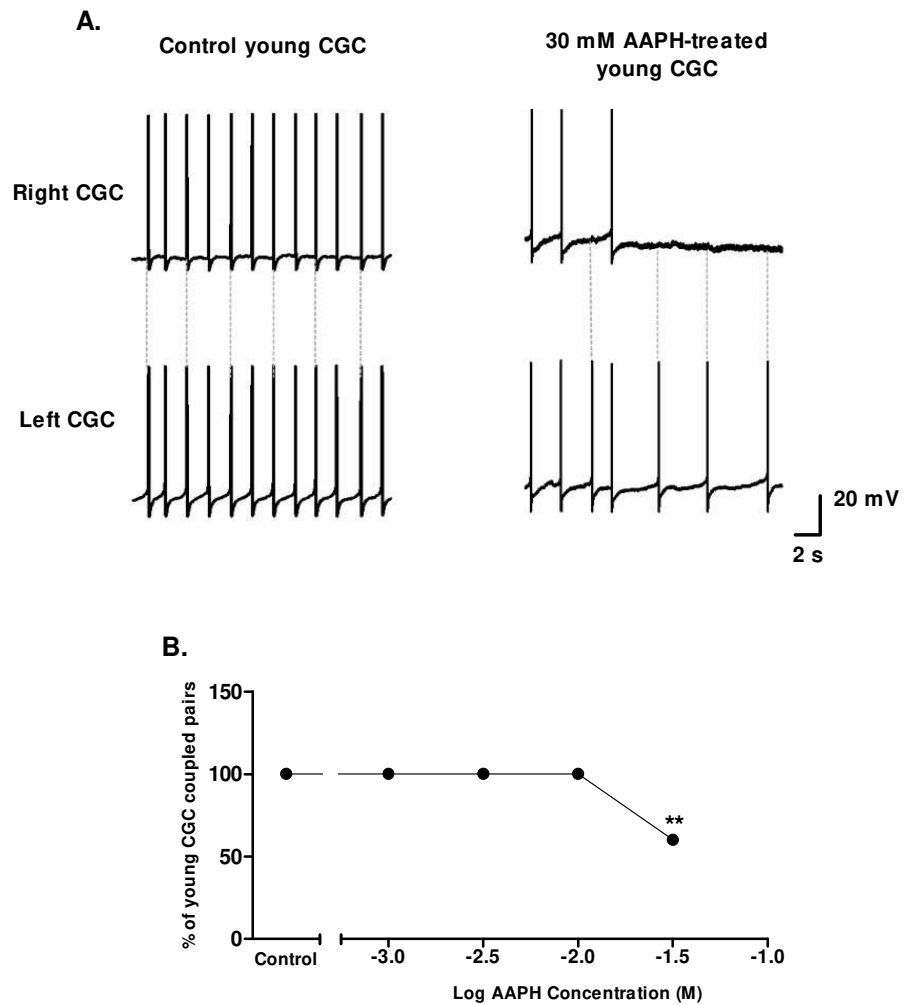
Figure 2.16| CGC coupling following acute extracellular AAPH treatment. (A) Sample traces displaying alterations to synchronicity between the paired RCGC and LCGC following treatment with 30 mM AAPH. (B) The control and 1-10 mM AAPH-treated CGCs were coupled in every preparation, but only 60% of the CGCs were coupled in the 30 mM AAPH preparations. Data shown as mean ± SEM, *n=8* PCGCs. **p<0.01 *vs.* control.

2.3.10 Changes to the RMP and AHP of the young CGC action potential during acute extracellular AAPH treatment

Inhibition of spontaneous CGC firing by 30 mM AAPH meant that it was only possible to analyse the CGC RMP from this group.

In **Figure 2.17A**, sample traces clearly demonstrate that both 3 and 10 mM AAPH altered the AHP amplitude and duration of spontaneously evoked RCGC action potentials in young preparations. Indeed, the fAHP amplitude significantly increased following 3 and 10 mM AAPH treatment (p<0.01, *n=8* RCGCs*;* one-way ANOVA with Bonferroni post-hoc analysis; **Figure 2.17B**). However, 1 mM AAPH did not significantly alter the fAHP amplitude when compared to the control (p>0.05, *n=8* RCGCs).

Treatment with 3 and 10 mM AAPH also significantly increased the sAHP duration when compared with the control (p<0.001 and p<0.05 respectively, *n=8* RCGCs*;* one-way ANOVA with Bonferroni post-hoc analysis; **Figure 2.17C**). 1 mM AAPH only slightly, but not significantly, increased the sAHP (p>0.05, *n=8* RCGCs).

There was no significant difference to the RMP between the 1-30 mM AAPH-treated young CGCs and the young control CGCs (p>0.05, *n=8* RCGCs; one-way ANOVA; **Figure 2.17D**).
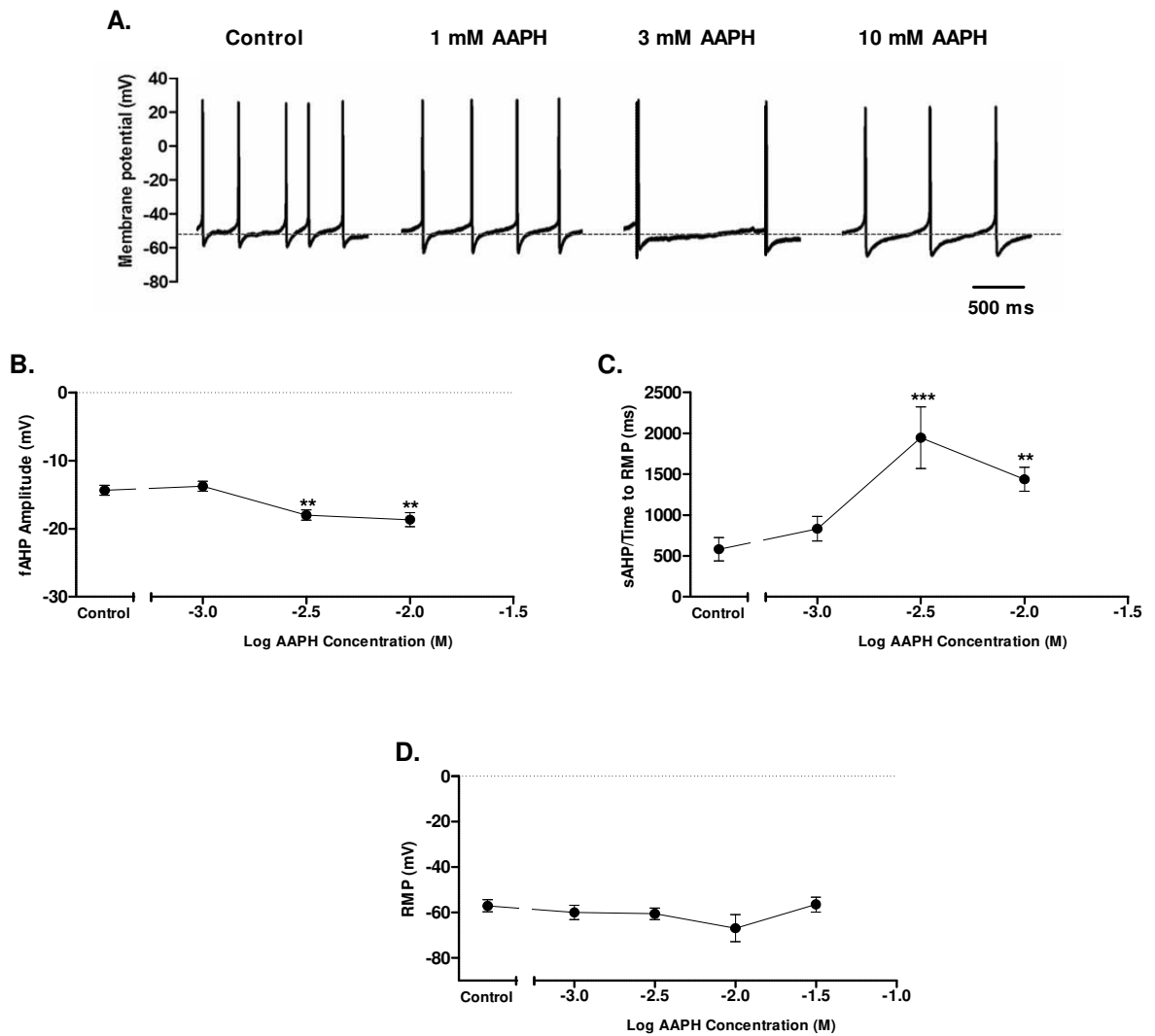
Figure 2.17| Acute extracellular effects of AAPH on the RMP and AHP. (A) Sample traces of young RCGC action potentials illustrate changes to the AHP following treatment with 3 and 10 mM AAPH. There was a significant increase in both the (B) fAHP amplitude and (C) sAHP duration when compared to the control. 1 mM AAPH did not significantly alter AHP parameters. (D) 1-30 mM AAPH treatment did not change the CGC RMP. Data shown as mean ± SEM, *n=8* RCGCs.*p<0.05, **p<0.01, ***p<0.001 *vs.* control.

2.3.11 Does acute extracellular AAPH treatment alter the half-width and peak amplitude of the young CGC action potential?

Perfusion of young CNSs with 1-10 mM AAPH substantially reduced the half-width of the CGC action potentials, although this did not reach statistical significance (p>0.05, *n=8* RCGCs*;* one-way ANOVA; **Figure 2.18A**). **Figure 2.18B** demonstrated that AAPH did not alter the peak amplitude of young CGC action potentials (p>0.05, *n=8* RCGCs).
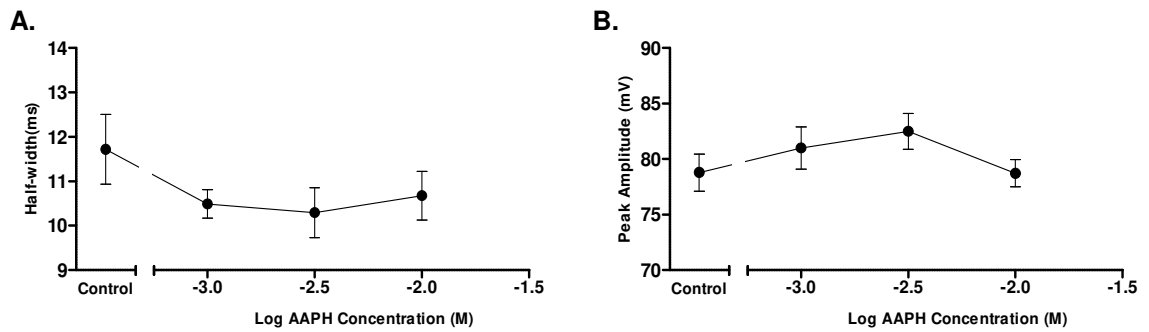
Figure 2.18| Acute extracellular effects of AAPH on the half-width and peak amplitude. 1-10 mM AAPH treatment (A) slightly narrowed young CGC action potentials, but (B) did not alter the peak amplitude. Data shown as mean ± SEM, *n=8* RCGCs. NS, p>0.05.

2.3.12 The extracellular effects of AAPH on young CGC SFA

Results so far have demonstrated that acute treatment with extracellular AAPH can mimic many of the changes observed in the CGC firing properties of old snails. Whilst the dynamics of SFA did not significantly change with age, it was still of interest to examine whether AAPH could affect this property of the CGCs.

2.3.12.1 The acute effects of AAPH on evoked CGC action potentials

In **Figure 2.19A**, sample traces demonstrate changes to the number of young RCGC spikes evoked during a depolarising pulse from the RMP following acute extracellular treatment with 1-30 mM AAPH.

A representative '*instantaneous frequency vs. time of spike*' plot in **Figure 2.19B** reveals that all the control and 1-30 mM AAPH-treated young CGCs exhibited SFA as there was an exponential decay. Young CGCs treated with 3 and 10 mM AAPH evoked significantly fewer action potentials than both control and 1 mM AAPH-treated young CGCs during SFA (p<0.05 and p<0.01, respectively, *n=8* RCGCs*;* one-way ANOVA with Bonferroni post-hoc analysis; **Figure 2.19C**). There was no significant difference between the control and 1 mM AAPH-treated CGCs (p>0.05, *n=8* RCGCs). 30 mM AAPH-treated CGCs evoked significantly fewer spikes than the control and 1-10 mM AAPH-treated CGCs during SFA (p<0.001, *n=8* RCGCs).
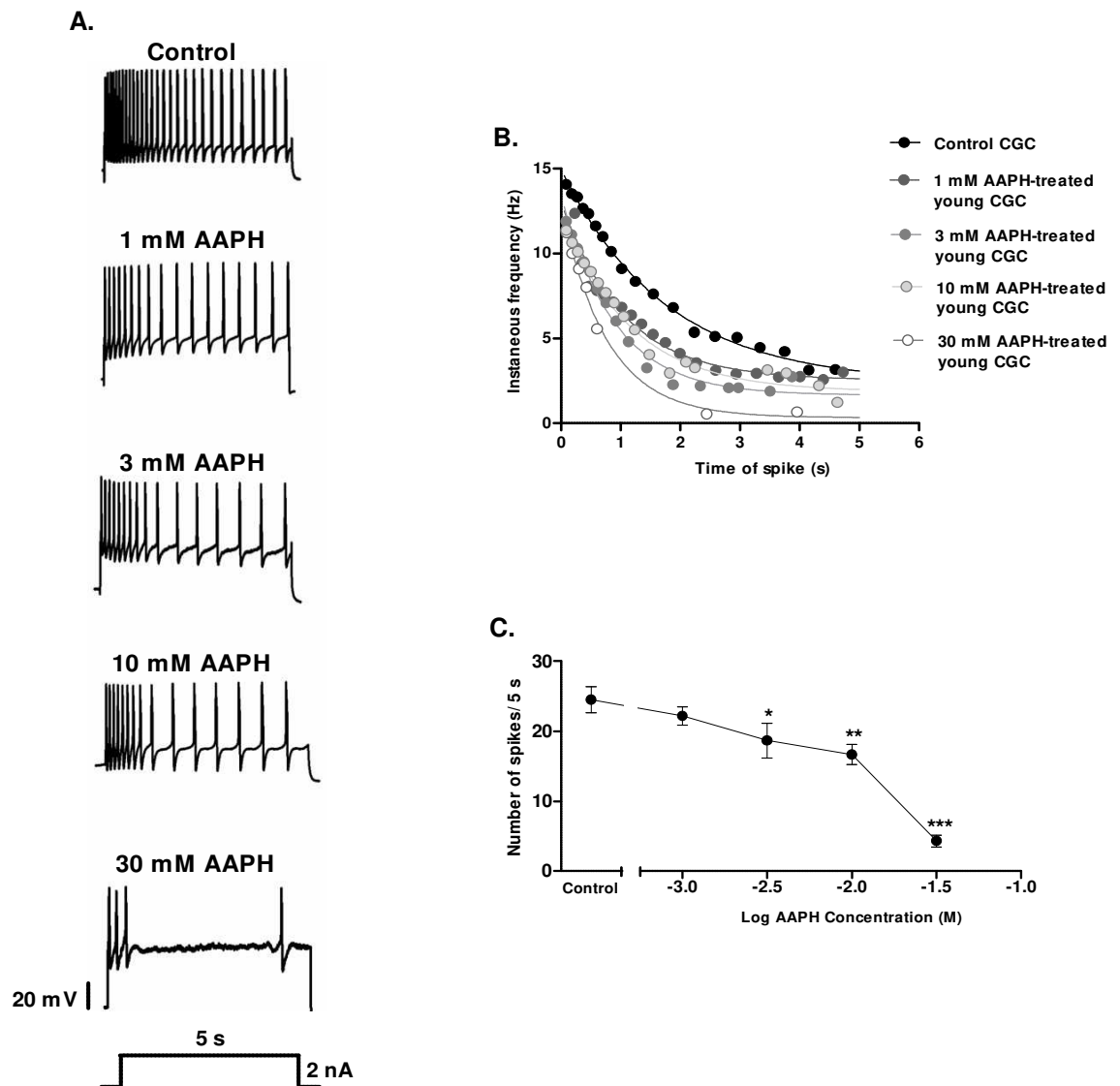
Figure 2.19| Acute extracellular effects of AAPH on SFA. (A) Sample traces of evoked RCGC action potentials in the control and 1-30 mM AAPH-treated preparations. (B) The representative plot shows that each CGC group exhibited SFA, hence the exponential decay. (C) CGCs exposed to 3-30 mM AAPH evoked significantly fewer spikes during SFA than both the control and 1 mM AAPH-treated CGCs. Data shown as mean ± SEM, *n=8* RCGCs. *p<0.05, **p<0.01, ***p<0.001 *vs.* control and 1 mM AAPH.

2.3.12.2 The acute effects of extracellular AAPH treatment on f_0 (Hz) and f_{ss} (Hz) during SFA in young CGCs

f_0 (Hz) in young CGCs treated with 30 mM AAPH was significantly slower than the control and 1-10 mM AAPH-treated CGCs ($p<0.05$, $n=8$ RCGCs; one-way ANOVA with Bonferroni post-hoc analysis; **Figure 2.20A**). 1-10 mM AAPH did not significantly alter f_0 (Hz) ($p>0.05$, $n=8$ RCGCs).

Due to the very low number of CGC spikes evoked in 30 mM AAPH, the mean f_{ss} (Hz) could not be calculated. f_{ss} (Hz) decreased in the 1-10 mM AAPH-treated CGCs, although this was not significant when compared to control CGCs ($p>0.05$, $n=8$ RCGCs; **Figure 2.20B**).

The % increase in half-width duration from f_0 to f_{ss} only significantly differed from the control CGCs following treatment with 30 mM AAPH, which caused a decrease ($p<0.001$, $n=8$ RCGCs; **Figure 2.20C**).
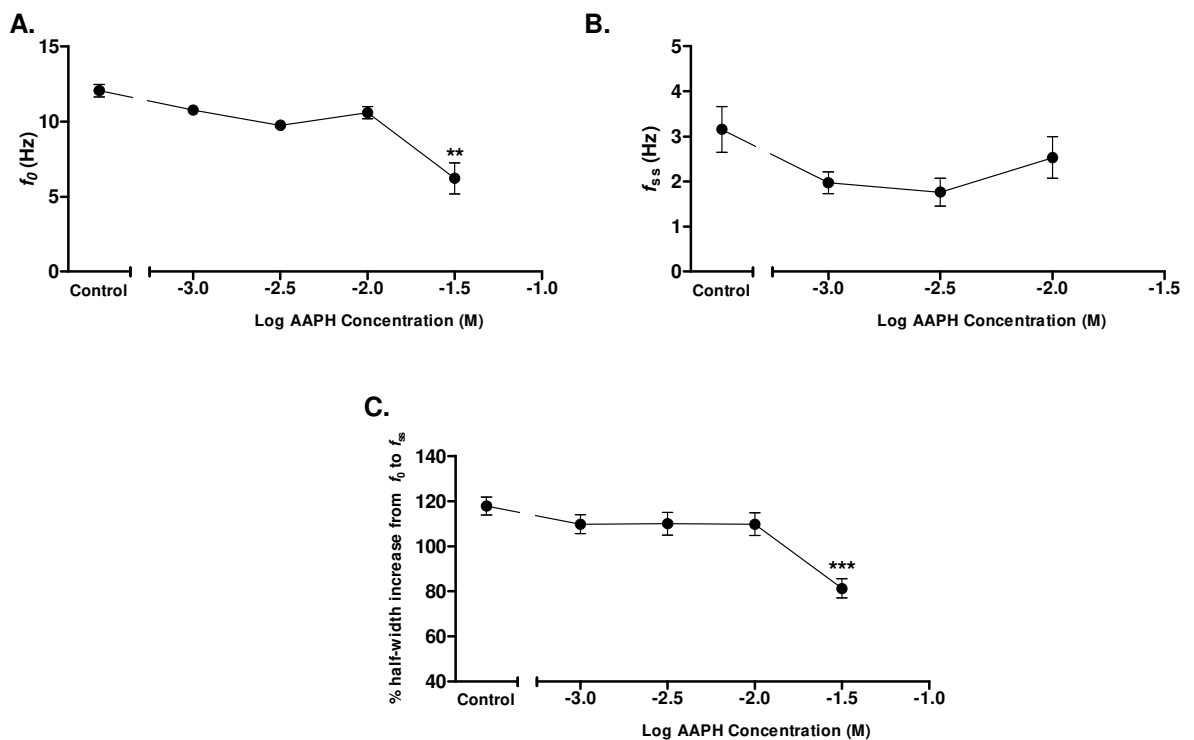
Figure 2.20| Does acute extracellular AAPH alter SFA parameters? (A) 30 mM AAPH significantly decreased f_o (Hz), but 1-10 mM AAPH did not when compared to control CGCs. (B) f_{ss} (Hz) substantially decreased following 1-10 mM AAPH treatment when compared to the control. (C) The % increase in the half-width duration from f_0 to f_{ss} only significantly changed in the 30 mM AAPH-treated CGCs *via* a reduction. Data shown as mean ± SEM, $n=8$ RCGCs. **$p<0.01$ (part A), ***$p<0.001$ (part C) *vs.* control.

2.3.12.3 Does AAPH alter SFA dynamics?

Neither F_{adap} nor τ_{adap} changed significantly between the control and 1-10 mM AAPH preparations (p>0.05, *n=8* RCGCs; one-way ANOVA with Bonferroni post-hoc analysis; **Figure 2.21A and B, respectively**). Due to the lack of action potentials evoked by the CGCs during exposure to 30 mM AAPH (see Figure 2.19A) it was not possible to calculate the values for these SFA parameters.

$\tau_{Calcium}$ also did not significantly differ between the control and 1-10 mM AAPH preparations (p>0.05, *n=8* RCGCs; **Figure 2.21C**).
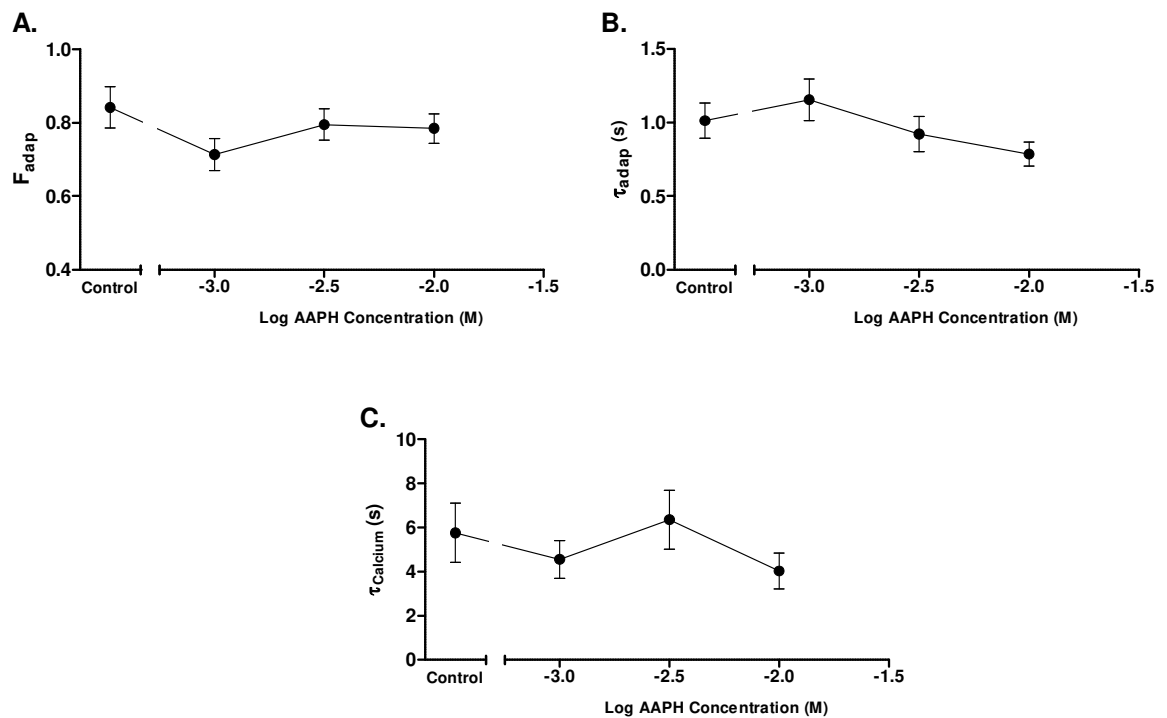
Figure 2.21| Acute extracellular AAPH does not alter SFA dynamics. (A) F_{adap}, (B) τ_{adap} and (C) $\tau_{Calcium}$ did not significantly differ between control and the 1-10 mM AAPH treated CGCs. Data shown as mean ± SEM, *n=8* RCGCs, NS, p>0.05.

2.3.13 Result summary of the changes to the CGC action potential parameters with increasing age and acute extracellular OS

CGC Parameter	Young Control CGC values	Parameter altered in old CGCs?	Parameter altered in 3 mM AAPH-treated young CGCs?
Spontaneous CGC Action Potentials			
Firing Frequency	62.8 ± 9.4 spikes min^{-1}	↓ (red) 20.1 ± 3.1 spikes min^{-1} (**)	↓ (red) 26.1 ± 9.2 spikes min^{-1} (*)
fAHP	-12.6 ± 0.1 mV	↑ (red) -19.8 ± 0.8 mV (***)	↑ (red) -18.7 ± 1.2 mV (**)
sAHP	582.8 ± 141.4 ms	↑ (red) 2081.2 ± 259.8 ms (***)	↑ (red) 1946 ± 378.3 ms (***)
RMP	-57.1 ± 2.6 mV	↑ (red) -70.1 ± 0.3 mV (***)	**No Change** -60.6 ± 2.5 mV (**NS**)
Half-Width	13.4 ± 1.4 ms	↓ (red) 9.3 ± 0.4 ms (**)	↓ (black) 9.9 ± 0.7 ms (**NS**)
Peak Amplitude	78.8 ± 1.7 mV	**No Change** 81.9 ± 3.3 mV (**NS**)	**No Change** 80.9 ± 1.9 mV (**NS**)
Evoked CGC Action Potentials			
Firing Rate	23 ± 2.4 spikes/5s	↓ (red) 12 ± 0.8 spikes/5s (**)	↓ (red) 19.1 ± 0.1 spikes/ 5s (*)
f_0 (Hz)	12.1 ± 0.5 Hz	↓ (red) 8.5 ± 1.1 Hz (*)	↓ (black) 9.37 ± 0.4 Hz (**NS**)
f_{ss} (Hz)	3.1 ± 0.6 Hz	↓ (red) 1.79 ± 0.3 Hz (*)	↓ (black) 2.3 ± 0.6 Hz (**NS**)
F_{adap}	0.79 ± 0.1	**No Change** 1.24 ± 0.3 (**NS**)	**No Change** 0.81 ± 0.1 (**NS**)
τ_{adap}	0.95 ± 0.2 s	**No Change** 1.04 ± 0.4 s (**NS**)	**No Change** 0.92 ± 0.2 s (**NS**)
$\tau_{Calcium}$	5.6 ± 1.5 s	**No Change** 7.74 ± 2.4 s (**NS**)	**No Change** 6.3 ± 1.3 s (**NS**)

Table 2.1| Spontaneous and evoked CGC action potential parameters of old and 3 mM AAPH-treated young CGCs compared to the young control CGCs. Red upward or downward facing arrows indicate a significant increase or decrease of the parameter, respectively. Black upward or downward facing arrows indicate a substantial (>20% change) but not significant increase or decrease of the parameter, respectively. Data shown as mean ± SEM, *n=7-8* RCGCs for parameter. *p<0.05, **p<0.01 and ***p<0.001 *vs*. young CGCs. NS, not statistically significant.

2.3.14 The ability of acute extracellular AAPH treatment to induce OS in the young *Lymnaea* CNS

Given that acute extracellular AAPH treatment caused young CGCs to mimic many age-related changes of CGC firing properties, it was important to determine whether AAPH was inducing OS to elicit these changes. In addition, the possibility of reversing the effects of acute extracellular AAPH as well as age on CGC firing was also examined.

Dose-response analysis of acute extracellular AAPH on spontaneous and evoked CGC firing properties (**section 2.3.8**), showed that 3 mM AAPH was capable of accurately mimicking many of the age-related changes to CGC firing properties. Results from 10 mM AAPH were not significantly different from those observed with 3 mM AAPH and therefore, 3mM AAPH was selected as the only concentration to be used in subsequent experiments in this thesis.

2.3.14.1 Does 3 mM AAPH treatment mimic age-related changes to OS markers?

To determine whether AAPH's ability to induce an ageing phenotype in young CGCs is due to its pro-oxidant capacity, both protein carbonyl and MDA levels were assessed. Protein carbonyl is a protein that has been oxidised forming a carbon-oxygen double bond on the amino acids converting them into reactive aldehydes and ketones[89]. MDA is a reactive aldehyde formed following oxidation of lipids[22]. These common OS markers were measured in the cerebral ganglia (CG) that had been individually isolated from the whole CNS to determine whether this region, where the CGCs are located, is susceptible to OS.

Protein carbonyl levels in old CG samples were significantly higher than young CG samples ($p < 0.05$, *n=6* CGs; one-way ANOVA with Bonferroni post-hoc analysis, **Figure 2.22A**). Protein carbonyl levels in young CG samples treated with 3 mM AAPH were also significantly higher than the young control CG ($p < 0.05$, *n=6* CGs) and thus mimicked old preparations ($p > 0.05$, *n=6* CGs).

Figure 2.22B shows that MDA levels were significantly elevated in both the old CG ($p < 0.01$, *n=7* CGs) and the 3 mM AAPH-treated young CG ($p < 0.001$, *n=7* CGs) when compared to the young control CG. MDA levels did not significantly differ between the old CG and 3 mM AAPH-treated young CG samples ($p > 0.05$, *n=7* CGs).
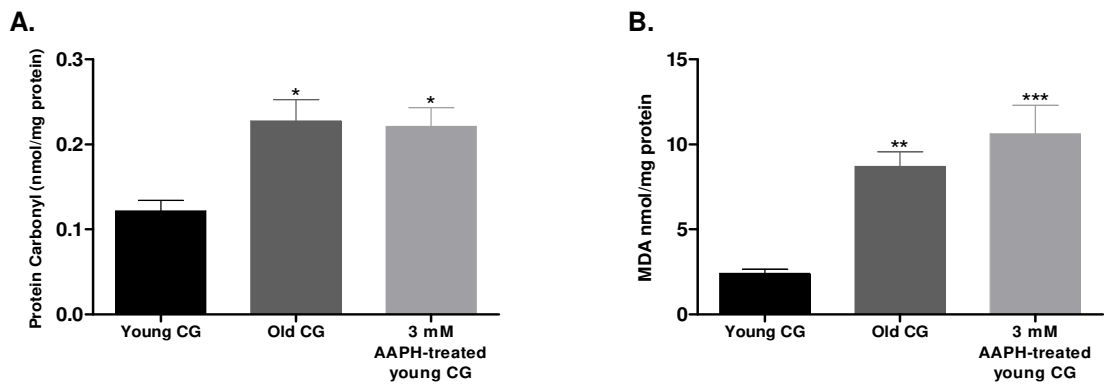
Figure 2.22| Changes to OS markers with age and acute extracellular AAPH treatment. In the old CGs there was a significant increase in both (A) protein carbonyl and (B) MDA levels when compared to the young control CGs. This elevation with age was mimicked by the 3 mM AAPH-treated young CG samples. Data shown as mean ± SEM, *n= 6-7* CGs. *p<0.05, **p<0.01 and ***p<0.001 *vs*. young CG.

2.3.14.2 Can antioxidants reverse the decrease to CGC firing frequency and increase in OS with increasing age?

Treating old preparations with the antioxidant combination saline (0.5 mM vitamin C and 7 mM vitamin E) did not significantly reverse the age-related reduction to spontaneous CGC firing frequency (p>0.05, *n=8* RCGCs; paired t-test; **Figure 2.23A**).

Furthermore, the antioxidant combination saline failed to significantly reverse the age-related increase to MDA levels in old CG samples (p>0.05, *n=8* CGs; unpaired t-test; **Figure 2.23B**).
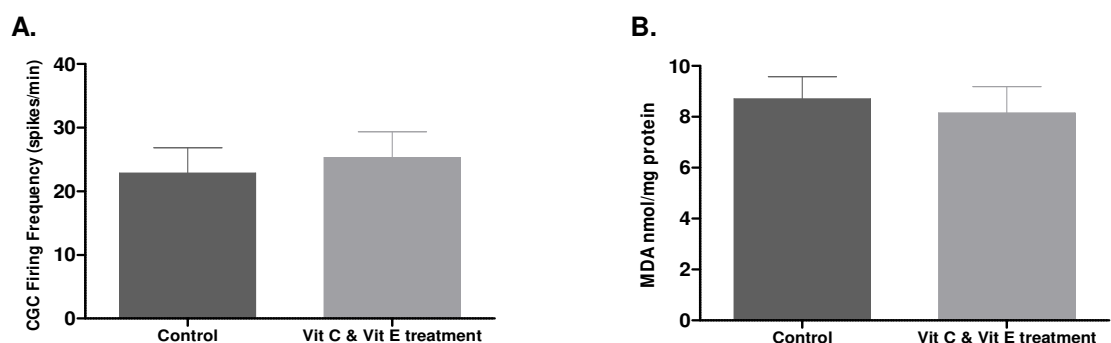
Figure 2.23| Antioxidant treatment in old *Lymnaea*. The antioxidant combination saline failed to significantly (A) increase old CGC firing frequency and (B) decrease MDA levels in the old CG. Data shown as mean ± SEM, *n=8* RCGCs and CGs for part A and part B, respectively. NS, p>0.05.

2.3.14.3 Are the effects of acute extracellular AAPH treatment on young CGC firing frequency reversible?

To assess whether the effects of 3 mM AAPH on CGC spontaneous firing frequency was reversible, AAPH-treated young CNSs were continually washed with HEPES-buffered saline for 1 hour (**section 2.2.7.3**). Sample traces of spontaneous RCGC firing in **Figure 2.24Ai** demonstrates this experiment. CGC firing frequency was significantly reduced by 3 mM AAPH ($p<0.001$, *n=8* RCGCs*;* one-way ANOVA with Bonferroni post-hoc analysis; **Figure 2.24Aii**) and was still significantly lower following the HEPES-buffered saline wash ($p<0.001$, *n=8* RCGCs). There was no significant difference between CGC firing rates during 3 mM AAPH treatment and following the HEPES-buffered wash ($p>0.05$, *n=8* RCGCs).

Bathing young preparations with the antioxidant combination saline (0.5 mM vitamin C and 7 mM vitamin E) following 3 mM AAPH treatment, significantly reversed the effects of AAPH on CGC firing ($p<0.01$, *n=6* RCGCs). Consequently, CGC firing frequency was no longer significantly different from the control ($p>0.05$, *n=6* RCGCs). Furthermore, pre-incubation of young CNSs with the antioxidants prior to extracellular 3 mM AAPH exposure prevented the decrease to CGC firing ($p>0.05$, *n=6* RCGCs*;* **Figure 2.24C**). Both pre- and post-treatment with each individual antioxidant showed a trend to increase CGC firing frequency, but these changes were not significant ($p>0.05$, *n=6* RCGCs; data not shown).

Pre-treatment with the antioxidant combination saline prevented the increase in MDA levels in the young CG that was typically observed following 3 mM AAPH treatment ($p<0.01$, *n=6* CGs; one-way ANOVA with Bonferroni post-hoc analysis; **Figure 2.24D**). Furthermore, post-treatment with the antioxidants significantly decreased MDA levels in the young CG that had been initially elevated by 3 mM AAPH ($p<0.05$, *n=6* CGs). There was no significant difference in the MDA levels between the control CG samples and those in the AAPH-treated CG samples that were pre- or post-treated with the antioxidant combination saline ($p>0.05$, *n=6* CGs).

At present, it has not been explored in this study whether the antioxidant combination saline can also prevent/reverse the increase in protein carbonyl levels in the 3 mM AAPH-treated or old CG samples. Thus, it will be very interesting to examine this in future experiments.
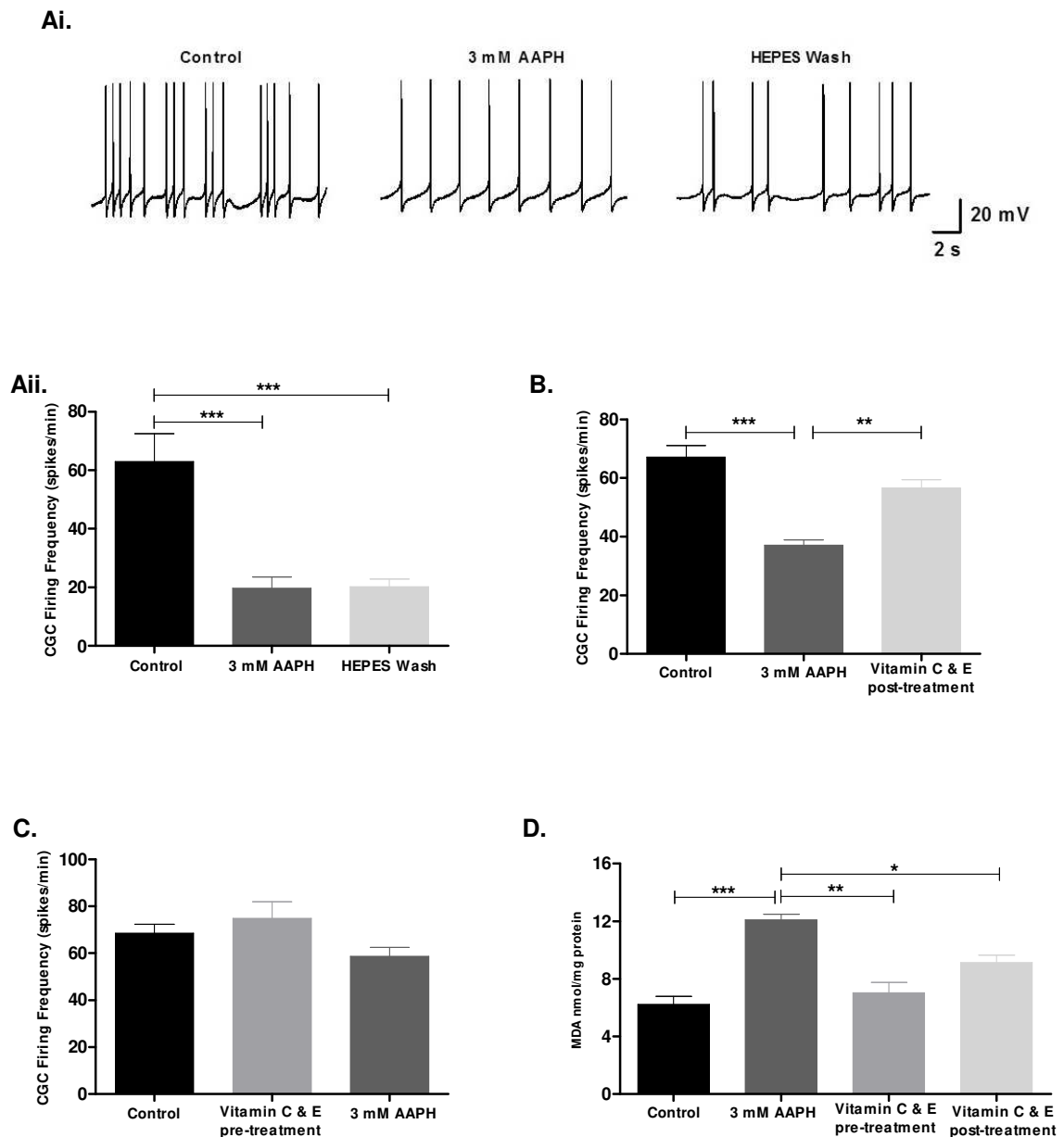
Figure 2.24| Antioxidant treatment in acute extracellular AAPH-treated young *Lymnaea*. (Ai-Aii) Sample traces and the corresponding graph, revealed that the reduction of CGC firing frequency by 3 mM AAPH could not be reversed by a HEPES-buffered saline wash. Post-incubation of the antioxidant combination saline (B) significantly reversed the decrease in CGC firing caused by 3 mM AAPH, whilst pre-incubation (C) prevented its detrimental effects on firing. (D) The significant increase to MDA levels in the young CG by 3 mM AAPH could be prevented and significantly reduced by pre-treatment and post-treatment, respectively, with antioxidants. Data shown as mean ± SEM, *n=8* RCGCs for part A-C and *n=6* CGs for part D. *p<0.05, **p<0.01 and ***p<0.001.

2.3.15 The acute effects of intracellular AAPH on young CGC firing properties

This chapter has shown that acute extracellular AAPH exposure caused young CGCs to mimic many of the age-related changes to CGC firing properties (**Table 2.1**). These changes are believed in part to be due AAPH's pro-oxidative capacity as young preparations exposed to 3 mM AAPH had elevated protein carbonyl and MDA levels and its detrimental effects on firing could be prevented/reversed with antioxidants.

To further explore the mechanisms by which AAPH mediates its effects upon the CGCs, a series of experiments were designed to investigate whether intracellular AAPH treatment could better mimic the effects of age on the CGCs. To test this idea, AAPH was added to the current injecting microelectrode so that it could be applied intracellularly following a series of depolarising pulses (**section 2.2.3.2**).

2.3.15.1 Does intracellular AAPH decrease CGC firing and alter synchronicity?

Figure 2.25A displays sample traces of spontaneous action potentials elicited from the paired young CGCs in each treatment group. LCGCs were impaled with microelectrodes containing AAPH (0-600 mM), while RCGCs (in the same preparation) were impaled with a microelectrode containing 100 mM potassium acetate and thus, acted as the control.

Firing frequency between the AAPH-treated LCGCs (0-600 mM) and the corresponding control RCGCs did not significantly differ (p>0.05, *n=6* PCGCs; two-way ANOVA with Bonferroni post-hoc analysis; **Figure 2.25B**). Furthermore, the firing rates between the AAPH-treated LCGCs and between the control RCGCs did not significantly differ as microelectrode AAPH concentration increased (p>0.05, *n=6* LCGCs and RCGCs).

Intracellular AAPH treatment did not hinder the paired CGCs ability to fire synchronously, regardless of the AAPH concentration present in the microelectrode (χ^2=0, p>0.05, *n=6* PCGCs; Pearson's chi-squared test; **Figure 2.25C**).
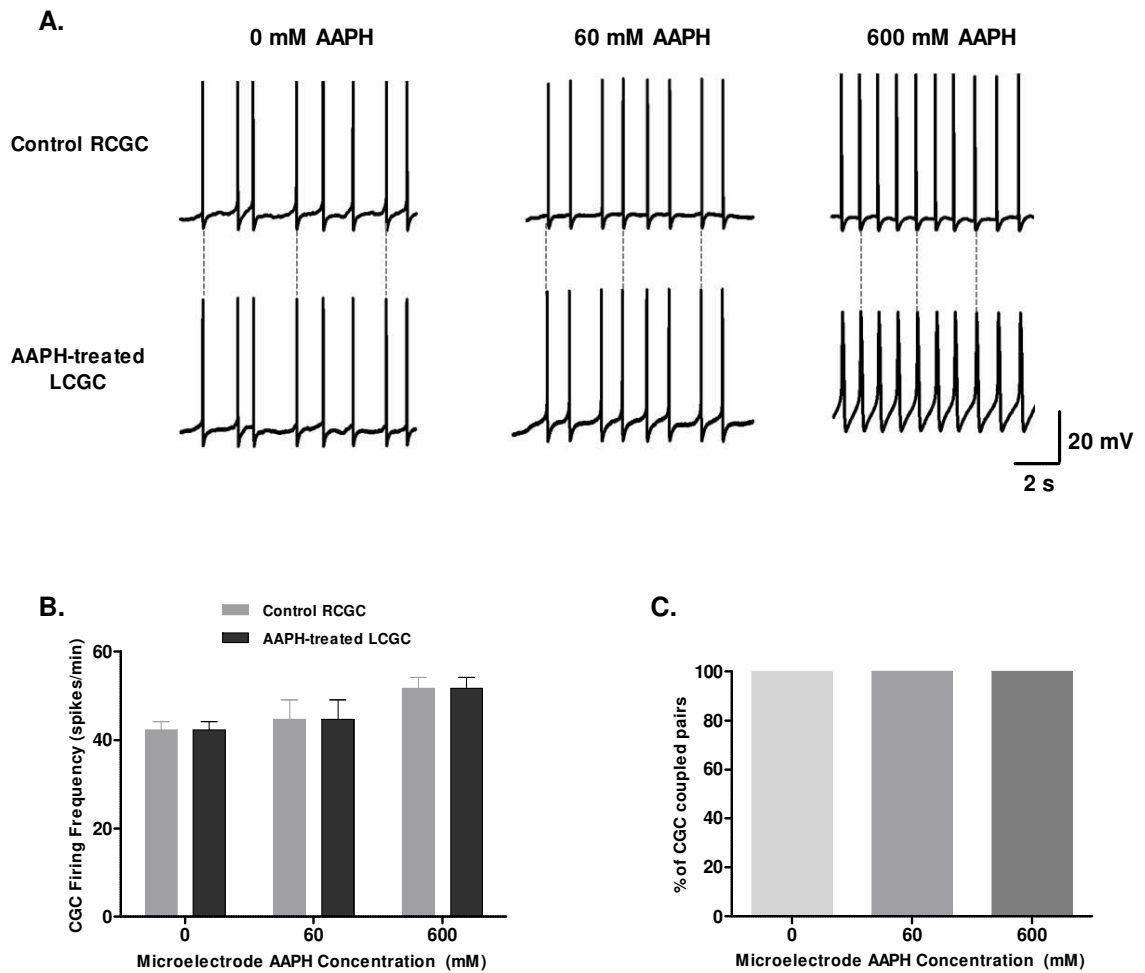
Figure 2.25| Intracellular effects of AAPH on CGC firing frequency. (A) Sample traces of spontaneous firing from the paired CGCs in each group. **(B)** Firing frequency of the AAPH-treated LCGCs did not significantly differ from the corresponding control RCGCs in any group. Additionally, there was no significant change in firing rates between the AAPH-treated LCGCs and between the control RCGCs, as the concentration of AAPH in the microelectrode increased. **(C)** CGC coupling was not impaired in any treatment group. Data shown as mean ± SEM, *n =6* PCGCs, NS p>0.05 *vs*. Control RCGC (part B) or *vs.* 0 mM AAPH (part C).

2.3.15.2 The effects of intracellular AAPH on the peak amplitude and half-width of CGC action potentials

Figure 2.26Ai displays a representative action potential generated by a young LCGC of each treatment group overlapped with an action potential elicited by its contralateral control RCGC. As illustrated, there were profound changes to the peak amplitude and half-width of the LCGC action potential in the 600 mM AAPH group.

The action potential half-width of the LCGCs impaled with 600 mM AAPH in the current injecting microelectrode was significantly broader than its contralateral control RCGC (p<0.01, *n=6* PCGCs; two-way ANOVA with Bonferroni post-hoc; **Figure 2.26Aii**). There was no significant difference in the half-width duration between the AAPH-treated LCGCs and control RCGCs in preparations impaled with 0 mM AAPH or 60 mM AAPH containing microelectrodes (p>0.05 for both, *n=6* PCGCs). Furthermore, the action potential half-width of LCGCs recorded with the 600 mM AAPH microelectrode was significantly larger than that of LCGCs impaled with the 0 mM or 60 mM AAPH microelectrodes (p<0.001 for both, *n=6* LCGCs; one-way ANOVA with Bonferroni post-hoc).

There was no significant change to the action potential peak amplitude between the AAPH-treated LCGCs and the corresponding control RCGCs of the 0 mM and 60 mM AAPH groups (p>0.05, *n=6* PCGCs; two-way ANOVA with Bonferroni post-hoc; **Figure 2.256iii**). Impalement of LCGCs with microelectrodes containing 600 mM AAPH caused a significant reduction to the peak amplitude when compared to the contralateral control RCGC (p<0.001, *n=6* PCGCs) and LCGCs from the 0 mM and 60 mM AAPH groups (p<0.001, *n=6* LCGCs; one-way ANOVA with Bonferroni post-hoc analysis).

In a sub-set of recordings conducted over a longer duration (90 minutes as opposed to 60 minutes), it was observed that the action potential peak amplitude of LCGCs impaled with 600 mM AAPH in the microelectrode became very small, ~2-4 mV (*n=4* LCGCs; data not shown), towards the end of the experiment. This is demonstrated in the sample trace in **Figure 2.26B**. Notably, LCGCs of the 0 mM and 60 mM AAPH group did not exhibit such alterations to the peak amplitude of the CGC action potentials (*n=4* LCGCs; data not shown).
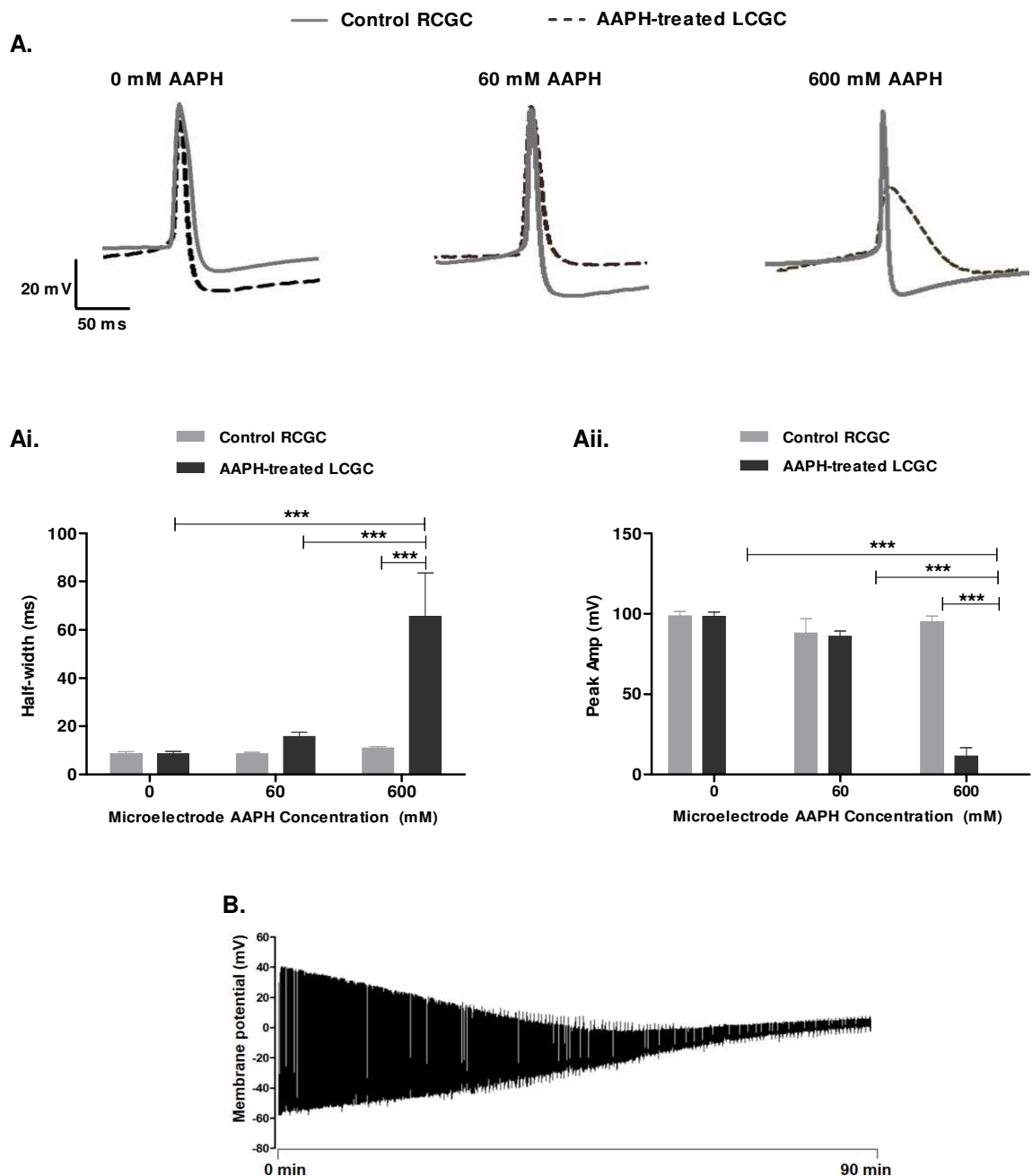
Figure 2.26| Intracellular effects of AAPH on action potential half-width and peak amplitude. (A) Representative action potentials of the control RCGC (solid light grey line) and its corresponding AAPH-treated LCGC (dark grey dotted line) from each group. As illustrated, 600 mM AAPH significantly (Ai) broadened and (Aii) reduced the peak amplitude of LCGC action potentials when compared to its contralateral control RCGC action potentials and those generated by LCGCs impaled with 0 mM and 60 mM AAPH in the microelectrode. (B) The peak amplitude of action potentials generated by LCGCs impaled with 600 mM AAPH dramatically reduced (visual observations) as the experiment progressed. Notably, this was accompanied with substantial depolarisation of the RMP. Data shown as mean ± SEM, *n= 4-6* PCGCs. **p<0.01, ***p<0.001 *vs.* control RCGC.

2.3.15.3 Does intracellular AAPH alter the CGC RMP?

The RMP of LCGCs impaled with 600 mM AAPH in the microelectrode was more depolarised than its contralateral control RCGCs, although this was not significant (p=0.0734, *n=5* PCGCs*; two-way ANOVA with Bonferroni post-hoc analysis; **Figure 2.27**). However, the RMP of LCGCs with 600 mM AAPH was significantly more depolarised than LCGCs recorded with the 60 mM or 0 mM AAPH microelectrode (p<0.01, *n=6* LCGCs; one-way ANOVA with Bonferroni post-hoc analysis). The RMP of the control RCGCs did not significantly vary between the different AAPH groups (p>0.05, *n=6* RCGCs).
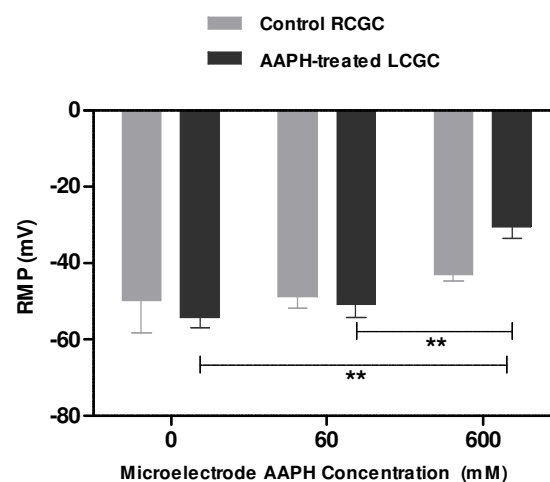
Figure 2.27| Intracellular AAPH alters the RMP. LCGCs impaled with microelectrodes containing 600 mM AAPH were more depolarised than the control RCGCs and significantly more depolarised than LCGCs impaled with 0 or 60 mM AAPH. Data shown as mean ± SEM, *n=6* PCGCs. NS, p>0.05 *vs.* control RCGCs.

2.3.15.4 The effects of intracellular AAPH on the CGC AHP

Figure 2.28Ai displays the fAHP component of the LCGC action potential from each group, which clearly illustrates there are differences in the amplitude. It was revealed in **Figure 2.28Aii**, that the fAHP of the LCGC action potential recorded with 600 mM AAPH in the microelectrode was significantly smaller than its control RCGC (p<0.01, *n=6* PCGCs; two-way ANOVA with Bonferroni post-hoc analysis). There was no significant change to the fAHP amplitude in LCGCs recorded with either 60 mM or 0 mM AAPH in the microelectrode when compared to their contralateral control RCGCs (p>0.05, *n=6* PCGCs). Additionally, the fAHP of LCGCs recorded with 600 mM AAPH

in the electrode was significantly smaller than LCGCs of the 0 mM and 60 mM AAPH groups (p<0.001, *n=6* LCGCs; one-way ANOVA with Bonferroni post-hoc analysis).

The sAHP duration in LCGCs impaled with 0 mM, 60 mM and 600 mM AAPH in the microelectrode did not differ significantly from their contralateral control RCGCs (p>0.05, *n=6* PCGCs; two-way ANOVA; **Figure 2.28B**). There was also no significant difference in the sAHP duration between the LCGCs or the RCGCs from each group (p>0.05 for both, *n=6* LCGCs or RCGCs; one-way ANOVA).
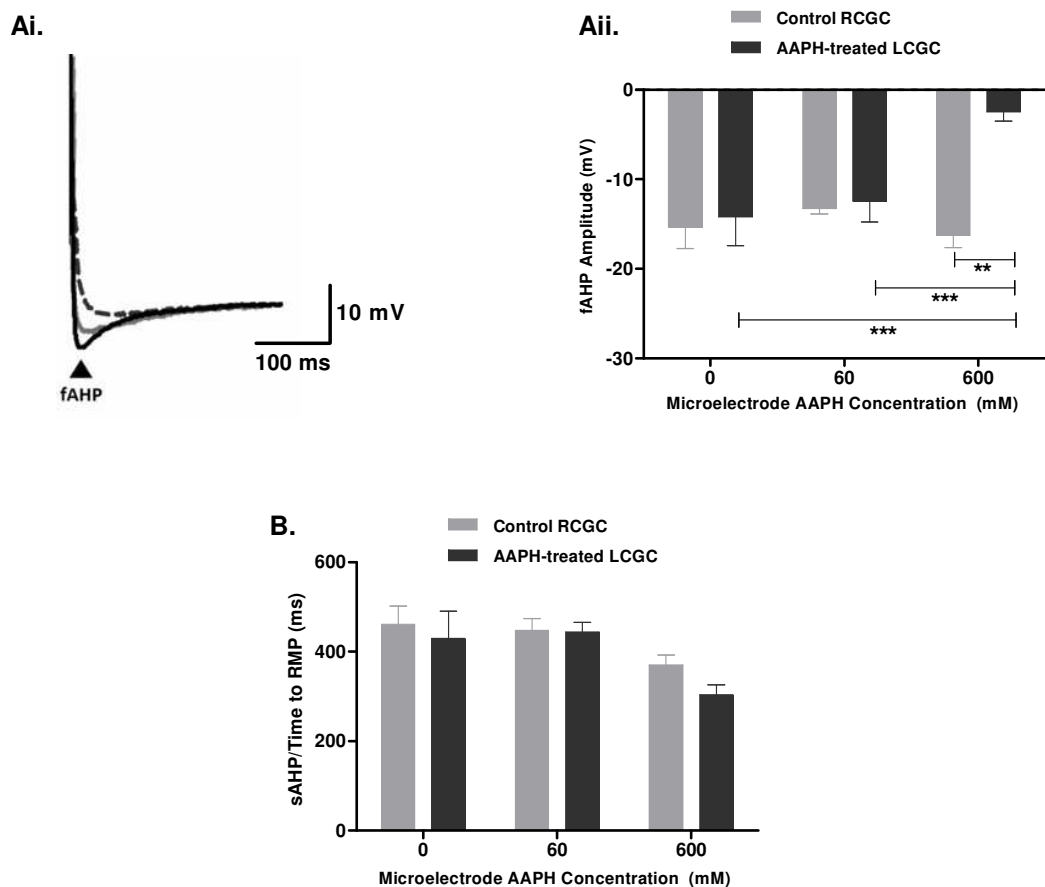
Figure 2.28| Intracellular effects of AAPH on the CGC AHP. (Ai) Representative example of the fAHP component from LCGCs impaled with microelectrodes containing 0 mM (solid black line), 60 mM (solid light grey line) and 600 mM (dotted dark grey line) AAPH demonstrates a decrease in amplitude with increasing concentrations. (Aii) The fAHP was significantly smaller in the 600 mM AAPH-treated LCGCs when compared to LCGCs of the other AAPH groups and to its contralateral control RCGC. (B) Intracellular AAPH did not significantly alter the sAHP at any concentrations. Data shown as mean ± SEM, *n=6* PCGCs. **p<0.01 *vs.* control RCGCs.

2.4 Discussion

The study presented in this chapter investigated the hypothesis that the age-related decrease in CGC firing is caused by OS altering the action potential waveform. In brief, experiments demonstrated that the decrease in CGC firing frequency with age was accompanied with an increase in the amplitude and duration of the AHP, a decrease in the action potential half-width and hyperpolarisation of the RMP. Ageing of *Lymnaea* was also behaviourally associated with a decrease in short-term feeding. This largely corroborated previous findings yielded in ageing *Lymnaea*[393,336,392]. It was also shown in this study that acute experimental OS (induced by AAPH treatment) caused the young CGCs to extensively mimic the ageing electrophysiological phenotype, but had adversely impaired feeding behaviour. The observation that age and AAPH treatment increased markers of OS, and that the effects of AAPH could be prevented/reversed using antioxidants, strongly suggests that OS may be a major driver in the age-related changes to CGC firing properties.

2.4.1 Acute extracellular AAPH treatment induces OS to alter young CGC firing properties

With OS often cited as an instrumental mediator of neuronal ageing, the ability of young preparations to mimic the ageing phenotype following the induction of acute extracellular OS was examined in this chapter[139,143,295,476]. Previous studies in the *Lymnaea* RPeD1 neuron revealed that the age-related decrease in firing frequency could be mimicked in young RPeD1 neurons following exposure to pro-oxidants[478,476]. Whether OS was accountable for the various changes to the action potential waveform with age, such as those described in this study or previously by Scutt *et al.* (2015) and Patel *et al.* (2006), had not been not explored[476,393,336].

Interestingly, this study demonstrated that acute extracellular treatment with the pro-oxidant generator, AAPH, caused young CGCs to mimic many of the changes observed in the old CGCs including reduced firing frequency, an increase in the fAHP and sAHP as well as substantial narrowing of the CGC action potential.

Given that previous investigations have shown that peroxyl radicals generated by dissociation of AAPH damage lipids in the plasma membrane to alter cellular functioning, it was important to establish whether AAPH in this study was altering young CGC firing properties *via* its pro-oxidant capabilities[110,411,326].

Indeed, experiments had demonstrated that changes to young CGC firing properties caused by acute extracellular AAPH treatment was due to its pro-oxidant nature. More specifically, application of 3 mM AAPH extracellularly was associated with increases in both MDA and protein carbonyls in the young cerebral ganglia and its effects on CGC firing properties could be *prevented* by pre-treatment with a mixture of vitamin E and vitamin C and *reversed* by the same combination of antioxidants. Thus, it seems entirely plausible that the ability of AAPH to mimic the effects of age (which had also been associated with a significant increase in MDA and protein carbonyl levels) are due to its pro-oxidant properties and not caused by non-specific effects on ion channels or other membrane proteins.

The observation that neither vitamin E nor vitamin C alone was capable of preventing/reversing the acute extracellular effects of AAPH unless they were combined, suggests that vitamin C may be required to regenerate vitamin E from tocopheryl radicals that are typically formed when oxygen radicals are scavenged within the plasma membrane[436,315]. Hence, studies often using vitamin E will also add vitamin C to the bathing saline to function essentially as a preservative[436]. Alternatively, this finding may be indicative that OS in both the hydrophobic and hydrophilic cellular compartments are important for AAPH to generate the ageing phenotype. This suggests that AAPH may be targeting the hydrophobic membrane to alter ion channel functioning or additionally might be affecting the hydrophilic pore of the ion channel.

Further evidence that AAPH's actions are predominately *via* its effects on the plasma membrane and integral ion channels came from experiments that examined the effects of intracellular AAPH on CGC firing frequency and the action potential waveform.

Administration of AAPH into the CGC intracellular milieu failed to alter spontaneous firing frequency regardless of the concentration present and thus, unlike extracellular AAPH, did not mimic this particular feature of ageing. Whilst exposure to the lowest AAPH concentration in the microelectrode, 60 mM, also did not significantly alter the CGC action potential waveform, the inclusion of 600 mM AAPH in the microelectrode did mediate opposite changes to what had been observed with age. This included significant depolarisation of the RMP, a reduction of the peak amplitude, action potential broadening and a decrease of the fAHP.

Whether these changes are due to AAPH inducing OS intracellularly is currently unknown as experiments utilising, for example, fluorescent probes (such as Amplex Red or Dichlorodihydrofluorescein) or immunoassays to measure intracellular ROS levels have yet to be performed[319]. However, the changes to the action potential waveform likely indicates that the AAPH concentration in the CGCs impaled with 600 mM in the microelectrode might be inducing an extreme form of OS and/or is neurotoxic. This notion stems from observations that the action potential of the young AAPH-treated LCGCs became almost negligible towards the very end of experimental recordings and the highly depolarised RMP was stabilising towards 0 mV. This suggests that AAPH is causing adverse intracellular modifications/damage that may possibly be facilitating the death of the treated LCGCs.

Numerous intracellular targets such as organelles or the domains of ion channels/pumps could be affected by the actions of AAPH, both directly or indirectly, to yield such manifestations to CGC firing properties. AAPH intracellularly, for example, may be damaging the mitochondria and consequently impairing critical processes such as ATP synthesis. Insufficient ATP availability would inhibit pumps such as the Na^+/K^+-ATPase, which would depolarise the RMP and as the Na^+ driving force decreases, reduce the peak amplitude of action potentials and eventually inhibit their generation altogether[272,156,303]. This depolarisation of the RMP also means that the neuron is above the activation threshold for voltage-gated gated Ca^{2+} channels, which would increase Ca^{2+} influx during firing. This would not only further depolarise the membrane potential, but would also broaden action potentials (as observed) and could lead to Ca^{2+} overload. Such severe damage to the mitochondria and subsequent impairment to Ca^{2+} homeostasis, if persistent, would ultimately trigger apoptosis[185,318,495].

Alternatively, the effects of intracellular AAPH may be independent of OS and/or neurotoxicity and instead could be due to the nature of the compound itself. AAPH is a relatively large molecule that is positively charged and thus, entrapment of large concentrations of this molecule in the CGCs may lead to non-specific depolarisation of the RMP. Such significant depolarisation of the RMP would decrease the Na^+ driving force, prolong Ca^{2+} channel activation and decrease the activation of K^+ channels. This would account for the peak amplitude reduction, increase in half-width and decrease in fAHP amplitude observed in LCGCs following impalement with the 600 mM AAPH microelectrode.

Caution is needed when drawing conclusions from these experiments as it does not necessarily suggest that AAPH is causing young CGCs to mimic the ageing phenotype by solely targeting extracellular constituents. It may be that the concentration of AAPH in the intracellular environment is not within the appropriate range to induce changes typically observed in old CGCs. This is reflective, however, of the limitations associated with sharp electrode recordings and not being able to control, and therefore determine, the AAPH concentration present intracellularly. Whole-cell patch clamp may have been a more suitable alternative technique for such experiments as the cell's intracellular content can be dialysed completely with the micropipette solution[272]. This provides a more efficient way of delivering pharmacological agents faster, but importantly the concentration present intracellularly can be more accurately determined.

If AAPH, however, is primarily targeting the extracellular components to mimic the ageing CGC phenotype, it then raises the question as to the source of free radicals attacking the CGCs in the ageing CNS. The likely possibility are glial cells, which outnumber and surround neuronal cells bodies and are the most potent ROS generators in the CNS[187,25]. Studies in mammalian models have shown that glial cells undergo replicative senescence and exhibit the SASP[429,430,277]. These cells are typically larger than their younger counterparts and secrete a range of inflammatory mediators such as IL-6, IL-1β and TNFα and also generate excessive ROS[142].

Interestingly, a few studies in *Lymnaea* have demonstrated a clear link between inflammation and OS with age. Watson *et al.* (2012) revealed that there was an increase in inflammation in the ageing CNS, which increased OS (as determined by MDA levels) and was accompanied with a significant decrease in old RPeD1 firing frequency[476,478]. Such findings strongly allude that glial cells may be an important source of ROS in the ageing *Lymnaea* CNS.

2.4.2 The CGC action potential waveform with age and acute extracellular OS

Whilst acute extracellular AAPH treatment mimicked many of the age-related changes to the CGC action potential waveform, a parameter that had not been altered by AAPH was the RMP. The lack of hyperpolarisation to the RMP suggests that some of the critical mechanisms involved in regulating the CGC RMP may more be resilient to the effects of OS.

K$^+$ currents are often documented as having a pivotal role in regulating the RMP of neurons[130,178,79,488,58]. For example, one of the primary functions of the inward rectifier is to set and stabilise the RMP following the generation of action potentials[178]. Inward rectifiers will generate a large inward current when the membrane potential is negative relative to the E_{rev} for K$^+$ to facilitate K$^+$ influx and depolarise cells back to their RMP. Conversely, when the membrane potential is more positive that E_{rev} for K$^+$, inward rectifiers will produce an outward current to promote K$^+$ efflux and subsequently hyperpolarise neurons back to the RMP[130,178].

A-type K$^+$ channels and delayed rectifiers also have a significant influence on maintaining a negative RMP in neurons. Pharmacological inhibition of these VGKCs with agents such as 4-AP (I_A) and TEA (I_{DR}) in mammalian and invertebrate neurons, as well as VGKC knockout rodent models have shown that the RMP becomes significantly more depolarised[65,412,457,416].

Interestingly, there is evidence that oxidation of VGKCs results in significant hyperpolarisation of the RMP. A study in mammalian enteric neurons, for example, demonstrated that peroxyl radicals (which can also be generated by AAPH) increases the outward conductance of voltage-gated inward rectifiers and subsequently hyperpolarises the RMP[177]. Another study in *C. elegans* found that oxidative modifications to the A-type K$^+$ channel significantly hyperpolarised sensory neurons[59].

So why does AAPH not hyperpolarise the RMP of young CGCs? It could be that OS induced by acute extracellular AAPH treatment is not sufficient, in terms of time course, to alter properties of the ion channels involved in regulating the RMP. It may be that chronic exposure to AAPH in young CGCs could better replicate the ageing CGC phenotype. After all, ageing and its associated changes are manifestations driven by chronic processes.

Such findings does not exclude the possibility that VGKCs are not altered by acute AAPH treatment, especially as it is not known in any great detail which K$^+$ currents are involving in regulating the CGC RMP. The other CGC action potential parameters altered by acute AAPH treatment such as half-width and the AHP are thought to be substantially regulated by K$^+$ currents and this would suggest that AAPH is most likely affecting some VGKCs[457,416]. Therefore, it will be important for future experiments to comprehensively identify all the currents involved in regulating the CGC RMP (as well as other

components of the action potential waveform in general) and to record these currents in voltage clamp to examine if they are altered with acute OS as well as with increasing age.

The ageing-like changes incurred in young CGCs following acute extracellular AAPH treatment was not always demonstrated across the range of concentrations utilised. Exposure to 1-10 mM AAPH caused a substantial decrease to spontaneous firing frequency that mimicked rates observed in old CGCs, but had not differed significantly from each other. However, treatment with 30 mM AAPH drastically reduced and eventually suppressed young CGC firing and thus did not accurately mirror the ageing CGC phenotype of this study.

The effects of 30 mM AAPH on the CGCs suggests that this concentration may be inducing an extreme form of OS that, unlike lower concentrations, is severely enhancing the function of ion channels involved in slowing down neuronal firing such as K^+ channels. These channels can alter the parameters of an action potential in numerous ways to reduce firing including, for example, by increasing the half-width, fAHP amplitude and/or sAHP duration[247,305,322,364]. Indeed, it was noted that the sAHP duration was about 7 seconds in the 30 mM AAPH-treated young CGCs prior to inhibition of firing, whereas with lower concentrations of AAPH and even with age the sAHP lasted for ~2 seconds. This suggests that 30 mM AAPH may be profoundly augmenting K^+ currents. Future experiments assessing OS markers such as MDA or protein carbonyl across all the concentrations of AAPH utilised in this study (not just at 3 mM AAPH) would help ascertain whether 30 mM AAPH is inducing extreme OS in young *Lymnaea*.

Whilst the actions of 30 mM AAPH did not reflect the 8-9 month old ageing phenotype of this study, it may be mimicking an extreme ageing phenotype often witnessed in snails a few days before they die. The uncoupling of the CGCs and stark reduction in spontaneous firing before complete cessation caused by 30 mM AAPH was reminiscent to observations made in a very small population of snails that had reached 12 months old in our laboratory. Interestingly, Patel *et al.* (2006) also documented that the CGCs of very old snails that had reached 11-12 months were also uncoupled[336].

With regards to the other concentrations of AAPH utilised, 1-10 mM, it was generally found that both 3 and 10 mM AAPH in the bathing saline mimicked the ageing phenotype more accurately than 1 mM AAPH. This suggests that the level of free radical production by 1 mM AAPH may not be sufficient to significantly modify ion channels involved in

regulating the CGC action potential waveform. Additionally, antioxidant defence mechanisms in the *Lymnaea* CNS may be able to deal with radicals more effectively at lower concentrations of AAPH and reverse their effects, as they are not being overwhelmed. It would be useful for future investigations to measure ROS activity and antioxidant capacity at each concentration of AAPH in young preparations to comprehensively examine the redox status.

The significant increase in the fAHP amplitude observed with 3 and 10 mM AAPH-treated young CGCs suggests that OS may be involved in increasing the fAHP in ageing CGCs. An increase in the fAHP would decrease firing, as it would prolong neurons from re-establishing their RMP and subsequently delay the depolarisation required for the generation of successive action potentials. Of the currents known to be present in the *Lymnaea* CGCs, it is postulated that modifications to I_A and/or I_{DR} may be responsible for the fAHP increase with age in this study[416,316,392,393,457].

I_A has been shown to have a prominent influence on the fAHP in mammalian and other invertebrate neurons. Disterhoft *et al.* (2015), for example, demonstrated that I_A conducted by Kv4.2/Kv4.3 channels increased with age and that this was responsible increasing the fAHP in ageing CA3 hippocampal neurons[409]. In *C. elegans*, it has also been revealed that enhancement of I_A contributes to the age-related decrease in neuronal firing partly *via* an increase in the fAHP[59].

Inactivation of I_A is redox modulated, which makes this channel very susceptible to unwanted oxidative modifications[398]. Indeed, studies in young cultured cells/animal models have often demonstrated that an increase in experimental OS drastically slows the inactivation kinetics of I_A and consequently decreases neuronal excitability by increasing the fAHP of action potentials[398,399,59].

With regards to I_{DR}, previous investigations by Staras *et al.* (2002) and Vavoulis *et al.* (2010) have shown that this conductance is involved in the mediating the fAHP of CGC action potentials[416,457]. At present, however, no studies have directly examined I_{DR} in relation to the components of the action potential waveform with age or experimental OS.

Intuitively, enhancement of either I_{DR} or I_A in the CGCs would likely lead to an increase in the fAHP duration. Therefore, it would be fascinating to extensively explore the properties of these VGKCs with increasing age and acute OS.

The sAHP, is perhaps, the most widely investigated parameter in neuronal ageing electrophysiological studies and it was interesting to observe the acute extracellular OS could mimic the age-related increase to the sAHP duration[1,292,393,447,318,392]. An increase in the sAHP slows down firing frequency by increasing the inter-spike interval, which subsequently delays the onset of successive action potentials. A plethora of studies in mammalian neurons have shown that the Ca^{2+}-activated K^+ current, I_{sAHP}, underlying the sAHP is enhanced with age due to an increase in $[Ca^{2+}]_i$[1,292,447,398,392]. Even in the *Lymnaea* CGCs (Scutt G, personal communications), an increase in I_{sAHP} has been demonstrated to be involved in augmenting the sAHP duration with age[392].

The voltage-gated K^+ currents, I_A and I_{DR}, can also regulate the sAHP[264,146]. Alterations to the inactivation kinetics of I_A has been shown to significantly increase the duration of the sAHP with age and experimental OS in both invertebrate and mammalian neurons[59,399]. I_{DR} substantially contributes to the sAHP due to the minimal inactivation typically exhibited by this current[264]. Whilst little is known about the effects of age on the functioning of I_{DR}, it is likely that enhancement to this current with age would increase the sAHP duration[11,398]. Thus, it would be very interesting to investigate whether I_A and I_{DR} are also involved in increasing this particular phase of the AHP by examining the properties of these currents in the old and AAPH-treated young CGCs.

The decrease in CGC firing frequency with age and acute OS was also accompanied with narrowing of the CGC action potential. Initially, this may seem unusual as reduction of the half-width would repolarise action potentials faster and should lead to the generation of more action potentials as opposed to less. However, increasing the rate of repolarisation may cause a decrease in firing frequency by enabling neurons to enter the AHP phase sooner. As there is an increase in amplitude and duration of the AHP in old and AAPH-treated young CGCs, this then delays the generation of subsequent action potentials.

The half-width decrease could be indicative of an increase in voltage-gated K^+ currents. Both I_A and I_{DR} are critical regulators of action potential repolarisation and suppression of either one of these currents has previously been shown to significantly broaden action potentials in many mammalian and invertebrate neurons, including the CGCs[234,338,231,104,119]. Therefore, an increase in the conductance of these voltage-gated K^+ currents, perhaps due to oxidative modifications to the channels, would help explain the narrowing observed to the CGC action potentials with age and acute OS.

2.4.3 The effects of age and acute OS on SFA in the CGCs

The CGCs examined in this study all exhibited SFA, as demonstrated by the exponential decline in the *instantaneous frequency vs. time of spike* plots. Given that Scutt *et al.* (2015) had previously revealed that the dynamics of SFA were significantly altered in old CGCs, it was of interest to determine if this was still the case in the old CGCs of this study and to examine whether OS may be involved in any possible alterations to SFA parameters[393].

It was observed that old CGCs evoked significantly fewer spikes than the young CGCs during the depolarising pulse. This was associated with an increase in both initial (f_0) and steady-state (f_{ss}) instantaneous firing frequencies. This result differed slightly from the Scutt *et al.* (2015) study, which had only demonstrated a decrease in f_{ss} (Hz) in the old CGCs[393]. A possible explanation for this is that the expression of channels involved in regulating f_0 (Hz) in the CGCs is different between these two studies and thus, the effects of age on these channels and subsequently on f_0 (Hz) differs.

Interestingly, it has been shown that changes in environmental conditions can alter the expression of ion channels in cells[367,416]. There were differences between the Scutt *et al.* (2015) study and this study in relation to housing conditions (from a large shallow tank in a recirculating water system to small deeper holding tanks in a non-recirculating water system) and feeding regime (from feeding 5 days a week to 7 days a week). These changes had been implemented in our laboratory to improve infection control and survival rates of the snails, but in doing so could have also potentially altered the expression of some ion channels.

Of the known currents present in the *Lymnaea* CGCs and knowledge derived from mammalian investigations, it is postulated that voltage-gated K^+ currents may be involved in the f_0 (Hz) decrease observed with age in this study[141,424,416]. I_A is an important regulator of f_0 (Hz) due to its fast activation kinetics. Studies in hippocampal and amygdala neurons, for example, have demonstrated that suppression of I_A with 4-AP significantly increases f_0 (Hz) by reducing the amplitude of the fAHP and decreasing the inter-spike interval[141,424].

I_{DR} has also been described as the largest conductance responsible for regulating the inter-spike interval during intense repetitive spiking[159]. This coupled with the very little inactivation typically displayed by I_{DR}, means that this current has a strong influence on

f_0 (Hz)[18,152]. Indeed, enhancement of I_{DR} has been shown in mammalian hippocampal and sympathetic neurons to significantly decrease f_0 (Hz)[18,152].

With regards to f_{ss} (Hz), I_{sAHP} has been established in mammalian neurons as having a very prominent role in regulating this phase during SFA because of its slow activation and inactivation properties[382,351,159,393,472,392]. The f_{ss} (Hz) phase is very important since it is where the adaptive response manifests[382,351,159,393,472,392]. I_{sAHP} decreases f_{ss} (Hz) by increasing the sAHP duration of each spike during intense firing. It had previously been observed in our laboratory (Scutt G, personal communications), both theoretically and experimentally, that an increase in I_{sAHP} contributed to the slowing of f_{ss} (Hz) in ageing CGCs. However, this may not be the case for the old CGCs of this study based on the analysis of SFA dynamics (F_{adap}, τ_{adap} and $\tau_{calcium}$) using Wang's mathematical model (**section 2.2.7.2**).

τ_{adap} is the time constant for adaptation- essentially how long it takes for adaptation to occur[472]. As described by the model, τ_{adap} is linked to intracellular Ca^{2+} kinetics of a neuron. In brief, intense repetitive spiking opens VGCCs that facilitates Ca^{2+} influx and leads to the activation of Ca^{2+}-activated K^+ currents (particularly I_{sAHP})[472]. These currents slow down firing by hyperpolarising the RMP and increasing the duration of the sAHP, which consequently reduces Ca^{2+} influx. However, if calcium homeostatic mechanisms are unable to reduce $[Ca^{2+}]_i$ then τ_{adap} increases[472,392]. Thus, τ_{adap} is related to the time course of Ca^{2+} clearance, denoted as $\tau_{calcium}$[472]. F_{adap} is the strength of adaptation and is determined, as detailed in the model, by the conductance of Ca^{2+}-activated K^+ currents and Ca^{2+} influx with each spike[472]. The greater the Ca^{2+} influx and increased conductance of Ca^{2+}-activated K^+ currents, the larger the F_{adap}.

As τ_{adap}, F_{adap} and $\tau_{calcium}$ did not significantly change in this study, according to Wang's model this suggests that Ca^{2+} influx *via* VGCCs and the conductance of Ca^{2+}-activated K^+ currents are not significantly altered in these old CGCs.

Changes to I_A or I_{DR}, however, may be responsible for the age-related decrease in f_{ss} (Hz). Numerous investigations in hippocampal and cortical neurons have demonstrated that suppressing either one of these voltage-gated K^+ currents causes a significant decrease in f_{ss} (Hz) because of their critical role in regulating the inter-spike interval during repetitive firing[141,424,159]. It would be interesting to examine the properties of I_A and I_{DR} in old CGCs as alterations to these currents may not only be accountable for the decrease in f_{ss}

(Hz) and/or f_0 (Hz), but could also explain many of the changes observed to spontaneously generated CGC action potentials with age (**section 2.4.2**).

When investigating SFA in this thesis, the CGCs during experiments were left at their RMPs and not held at a defined holding potential when eliciting the depolarising current pulse. As a result of this experimental design limitation, the observed decrease in evoked spiking frequency with age may simply be due to the RMP of the old CGCs being significantly more hyperpolarised than that of young CGCs as opposed to changes in intrinsic excitability. Future experiments should be modified so that both young and old CGCs are held at a defined holding potential to enable for a more direct comparison of intrinsic excitability.

This experimental limitation may also explain why SFA parameters- a measure of the dynamics of intrinsic excitability- were found to be unaltered with increasing age. Given that age-related changes to spontaneous CGC action potential parameters were largely consistent between this study and the Scutt *et al.* (2015) study, this limitation may also account for the differences between the two investigations with regards to intrinsic excitability where the latter had observed significant changes to SFA dynamics[393]. Thus, caution is needed with the current interpretations of these findings.

Applications of concentrations ≥3 mM AAPH reduced the number of evoked spikes in young preparations. Despite AAPH-treated CGCs not being stimulated from a defined holding potential, their RMP had not significantly differed from young controls and this suggests that acute OS has the capacity to decrease intrinsic excitability. As 3 and 10 mM AAPH mimicked age-related changes to spontaneous CGC parameters remarkably well, the decrease in evoked firing in old CGCs may be reflective of some alterations to intrinsic excitability irrespective of having been stimulated from a more hyperpolarised RMP.

Acute OS, however, did not alter SFA dynamics (F_{adap}, $\tau_{\alpha dap}$ and $\tau_{calcium}$) when compared to young control CGCs. This suggests, at least with respect to Scutt *et al.* (2015) study, where the young and old CGCs were stimulated from a defined holding potential, that OS may not be responsible mediating changes to SFA with age[393].

It may be that acute OS is not sufficient to alter the dynamics of SFA, but chronic exposure to pro-oxidants that more accurately reflects the ageing process could induce some of the changes observed previously in old CGCs[393,392]. Thus, it may be interesting

for future experiments to develop a chronic model of OS induced by AAPH in young *Lymnaea* to assess whether there are any changes to SFA dynamics.

Alternatively, it could be that changes in SFA manifests due to alterations in intracellular components and is not specifically linked to membrane effects. It may be found that treating young CGCs intracellularly with AAPH could alter the dynamics of SFA to a similar manner that had been documented previously in old CGCs[393,392].

2.4.4 Deficits to feeding behaviour in *Lymnaea* with age and acute OS

Given the crucial role of the CGCs in gating and modulating the feeding rhythm, it was important to determine whether the alterations to CGC firing properties with age and acute OS in this study was associated with any functional changes to feeding behaviour[35,506,507,336].

Analysis of short-term feeding behaviour revealed that old snails took longer to emerge from their shells and evoked significantly fewer bites than young snails due to an increase in the bite duration and inter-bite interval. This corroborated previous findings by Arundell *et al.* (2006)[21]. Acute AAPH exposure in young snails mimicked ageing by decreasing feeding frequency, but did so in a manner that was relatively inconsistent with the ageing *Lymnaea* phenotype.

Injection with 3 mM AAPH caused a whole-body withdrawal in up to 60% of young snails and completely impeded the ability of these snails to re-emerge from their shells when placed in the test arena. The remaining slower emergent snails (~40% of the population) failed to generate any bites in response to the sucrose stimulus. The observations that 3 mM AAPH had more marked effects *in vivo* than *ex vivo* suggests that other components in snails such as the feeding apparatus and withdrawal reflex muscles are also susceptible, in addition to the CNS, to the actions of AAPH.

It is unlikely that 3 mM AAPH *in vivo* is hindering the properties of chemosensory neurons to inhibit sucrose-evoked feeding. This stems from observations that the emergent snails extended further out of their shells, maximally elongated their tentacles and glided around following sucrose application near the lips. Interestingly, this was reminiscent to findings document by Arundell *et al.* (2006) where it had been observed that the ability of old snails to sense sucrose was not impaired as there were no changes to median lip nerve activity in semi-intact preparations[21]. This suggests that peripheral

processing of chemosensory information may inherently be more resilient to the effects of OS with age.

There was a significant decrease in sucrose-evoked bites in the 0.3 mM AAPH injected young snails. Unlike the old snails, however, this was accompanied with a significant decrease in bite duration and extreme lengthening of the inter-bite interval (approximately twice as long than in old snails). It appeared that these deficits to feeding behaviour in the 0.3 mM AAPH injected snails was primarily due to their inability to open their mouth wide and protrude their radula out, which had not been observed in the old snails. This suggests that there may be significant issues with the cellular and structural components involved in feeding (section 1.5), particularly in the protraction phase.

Contrary to the old snails, it is dubious whether 0.3 mM AAPH is affecting the gating and modulatory functions of the CGCs to alter feeding behaviour in young snails. This is based on preliminary *in vitro* experiments where it was observed that 0.3 mM AAPH treatment failed to significantly alter CGC firing frequency. This strongly suggests that 0.3 mM AAPH *in vivo* may be targeting many other neurons or constituents of the feeding apparatus, perhaps those specifically involved protraction, to adversely hinder feeding behaviour. Hence, its effects *in vivo* appeared more profound than *in vitro*. Both the *in vivo* and *in vitro* findings with 0.3 mM AAPH treatment strongly suggests that the decrease in feeding frequency is predominately occurring *via* mechanisms that is not largely consistent with the ageing process.

Overall, the data gathered from these short-term feeding behaviour experiments demonstrates that feeding decreases with both increasing age and acute experimental OS. However, the mechanisms by which this occurs clearly differs and strongly suggests that the increase in OS with age may not be fully responsible for mediating the changes to feeding behaviour.

2.4.5 Reversing age-related changes to the CGC firing properties

Unlike the effects of acute AAPH treatment on young CGCs, the age-related changes to CGC firing frequency could not be reversed with the use of antioxidants. At first this may suggest that OS is not responsible for mediating the changes to the CGC firing properties with age, however, this may not necessarily be the case.

It could be that the duration of antioxidant treatment in the old preparations or the concentration of antioxidants utilised was insufficient to reverse the untold modifications that have occurred to the cellular components of the CGCs over the last several months (remember ageing is driven by chronic processes). Whilst MDA and protein carbonyl levels were relatively similar between the old and AAPH-treated young CGCs, it may be found that other OS markers such as protein nitration or 4-HNE are higher in the old CGCs. This would indicated that OS is actually greater in the old CGCs and consequently that there is more oxidative modifications/damage.

Utilising antioxidants for a longer duration (hours to a few days) and/or at a higher concentration may provide sufficient time and drive for the antioxidants to effectively reverse oxidative modifications in old CGCs. Only then may a reversal to the age-related decrease in CGC firing and alterations to the action potential waveform be observed.

At present, it can neither be confirmed nor excluded whether OS is responsible for the age-related changes to the CGCs. However, the observations that acute OS in young CGCs closely mimicked many of the age-related electrophysiological changes strongly suggests that OS is an important mechanism involved in altering the CGCs with increasing age.

2.5 Conclusion

In conclusion, the data gathered in this chapter demonstrates that the age-related decrease in CGC firing frequency is associated with hyperpolarisation of the RMP, action potential narrowing and an increase in the amplitude and duration of the AHP. These changes to the CGCs were accompanied with a decrease in sucrose-evoked feeding in the old *Lymnaea.* The age-related alterations to CGC firing properties were largely mirrored in young *Lymnaea* treated with acute extracellular, but not intracellular, AAPH. However, age-related changes to feeding behaviour were not accurately mimicked by acute AAPH treatment in young snails. The data from this study also strongly suggests that OS, which increased significantly in the cerebral ganglia with age and acute AAPH treatment in the young, may be responsible for driving the alterations to CGC firing properties. Interestingly, many of the changes to CGC action potential waveform with age and acute OS greatly implicate the involvement of voltage-gated K^+ currents.

Chapter 3: The properties of voltage-gated outward currents in the *Lymnaea* CGCs with increasing age and acute oxidative stress

3.1 Introduction

Neuronal firing frequency has been a well explored feature due to its important role in encoding and transferring information between neurons[60,214]. The action potential waveform has a critical influence on neuronal firing frequency as well as neurotransmitter release, but surprisingly is not often discussed in the literature. Experiments in Chapter 2, for example, demonstrated that an increase in the amplitude and duration of the CGC AHP contributed to the decrease in firing frequency with age and acute OS. Other studies have shown that action potential broadening can lead to greater Ca^{2+} influx, which stimulates the release of more neurotransmitters that can either increase or decrease the firing of post-synaptic neurons[180,307]. Thus, the shape of an action potential in neurons and its firing frequency can ultimately dictate behavioural outputs of an organism such as feeding and learning and memory.

The aim of investigating the parameters of the CGC action potential in the previous chapter had been to acquire an insight into the ionic currents that may potentially be altered with age and acute OS. This is possible because different ionic currents regulate different components of an action potential and thus, determine its shape. It was observed in the old and 3 mM AAPH-treated young CGCs that there were profound changes to the amplitude and duration of the AHP, narrowing of the action potential and hyperpolarisation of the RMP.

Ca^{2+}-activated K^+ currents have been heavily implicated as mediators for such changes to the neuronal action potential with age as it has often been observed that their conductance is altered due to OS and impaired Ca^{2+} homeostasis[246,440,151,447,393,294]. Indeed, similar findings have been demonstrated previously in our laboratory where an increase in $[Ca^{2+}]_i$ in old CGCs, caused by reversal of the NCX (**section 1.6.3.1**), enhanced I_{sAHP} and consequently contributed to a decrease in firing frequency *via* an increase in the sAHP duration[392]. However, an increase in Ca^{2+}-activated K^+ currents in the old CGCs was not fully accountable for the reduction in firing frequency (Scutt G, personal communication) and could not explain many changes typically observed to the ageing CGC action potential waveform, such as the decrease in half-width or increase in the fAHP amplitude[392,336]. This finding strongly challenges the notion often made in the neuronal ageing field, particularly in mammalian models, that Ca^{2+}-activated K^+ currents are the

main instigators for changes to neuronal firing properties, especially as such studies have not fully examined the action potential waveform in relation to these currents[246,440,151,447,294].

Voltage-gated K⁺ currents, however, are recognised as having an instrumental role in regulating various action potential parameters including the half-width, RMP and AHP in neurons across all species[26,404,190,31]. Therefore, the possible involvement of these currents in changes to neuronal firing properties with age should not be disregarded. The seminal paper by Staras *et al.* (2002), identifying the ionic currents expressed by young CGCs, had described the presence of VGKCs in these neurons (**section 1.6.3.3**). It was found that the CGCs had an A-type K⁺ current and a delayed rectifier that principally contributed to the total early and sustained voltage-gated outward current, respectively[416]. This strongly suggested that these currents may have a very important role in regulating CGC firing properties[416]. It was also noted by Staras *et al.* (2002) that the CGCs did not appear to express a voltage-dependent inward rectifier current[416].

I_A, with its distinctive fast activation and relatively fast inactivation kinetics, is heavily involved in regulating action potential repolarisation and can cause neurons to fire at lower frequencies by increasing the inter-spike interval[231,133]. To date, the effects of age on I_A have produced differing results. It has been demonstrated during normal ageing in *C. elegans* that aberrant ROS activity increases the I_A conductance in neurons, which leads to a decrease in excitability and subsequent impairment of sensory functions[398]. Conversely, healthy ageing of CA1 hippocampal rat neurons has been shown to decrease I_A when compared to the young[11]. Pathological ageing studies such as those involving AD have also produced contradictory results, with reports in CA3 hippocampal neurons of either an increase or decrease in the amplitude of I_A[387,409].

Determining whether an increase or decrease in I_A conductance is a characteristic feature of neuronal ageing is not yet known, as the effects of increasing age on this current has not yet been explored in many different organisms. It is well known, however, that the A-type K⁺ channel is susceptible to oxidative modifications[398,186]. For example, an increase in the I_A conductance has been shown to be caused by oxidation of cysteine and methionine residues on the VSD and gate domains[374,399]. This slows down activation and inactivation of the A-type K⁺ channels[374,398]. Considering this vulnerability to oxidative modifications, it will be particularly interesting in this study to investigate the CGC I_A

and assess how it changes with increasing age, especially as OS has been implicated as a causative factor for the alterations observed to CGC firing properties.

I_{DR}, with its very slow activation kinetics and very little inactivation, has been recognised as the major conduit for K^+ efflux in most neurons[512,26]. It is activated following depolarisation to repolarise action potentials[512,26]. It does this to regulate repetitive firing in neurons by increasing the interval between action potentials[9]. Evidence of changes to I_{DR} during normal and even pathological ageing is extremely limited. Primarily studies have reported an increase in the expression of delayed rectifier channels in mammalian neurons such as neocortical and hippocampal neurons with age, but have not examined the electrophysiological consequences of these changes[115,398].

The delayed rectifier channel has also been shown to be susceptible to oxidative modifications, but these changes are extremely detrimental[398,512]. In *C. elegans,* for example, oxidation of the delayed rectifier channel results in the formation of oligomers that are held together by disulphide bridges between cysteine residues[398]. This renders the channel non-conductive and promotes neuronal death[398]. Due to the very important role of I_{DR} in action potential repolarisation, it is important to examine the properties of this current with age and acute OS to increase knowledge in this very limited field.

The aim of experiments in this chapter will be to investigate how outward VGKCs change in the CGCs with increasing age and acute OS. TEVC is the optimal technique for this because, unlike patch clamp, it is able to sufficiently clamp large cells at desired potentials more accurately as well as the record large currents generated by such cells[160,29]. The basic principle of the TEVC technique is that two microelectrodes penetrate a cell (**Figure 3.1**). One records the membrane potential (V_m) and the other is a current injecting microelectrode that adjusts the V_m to the command potential set by the user[160].
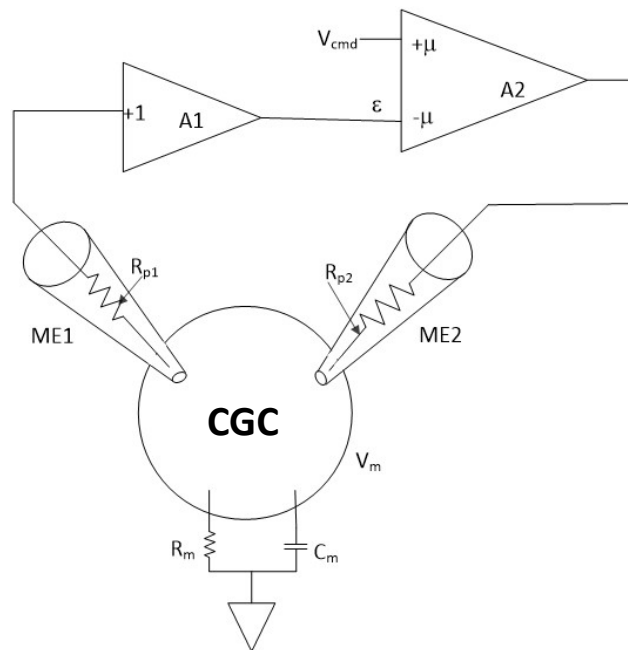
Figure 3.1| Overview of the TEVC circuit[97]. Neurons of interest are impaled with two microelectrodes. The voltage-sensing microelectrode (ME1) connected to the unity-gain buffer records the membrane potential (V_m). This is then compared to the voltage command potential (V_{cmd}) in the high-gain differential amplified (A2), which will inject a current *via* the current-passing microelectrode (ME2). The current injected is proportional to the difference between V_m and V_{cmd} and therefore, clamps the neuron at the desired command potential.

This chapter will test the following hypothesis: *Changes to the CGC action potential waveform and the decrease in firing frequency with increasing age and acute OS involve alterations to the conductive properties of voltage-gated outward K^+ currents.*

3.2 Methods

3.2.1 Preparation of isolated *Lymnaea* CNS for TEVC

Isolation of the *Lymnaea* CNS from young (3-4 month old) and old (8-9 month old) snails and preparation in the electrophysiological recording chamber containing HEPES-buffered saline was performed as detailed in Chapter 2 (**section 2.3**).

To conduct voltage-clamp recordings of RCGCs (**section 2.2.7.3**), the right cerebral-buccal connective and the cerebral commissure were also gently crushed using fine forceps to improve space clamp (red lines; **Figure 3.2**).
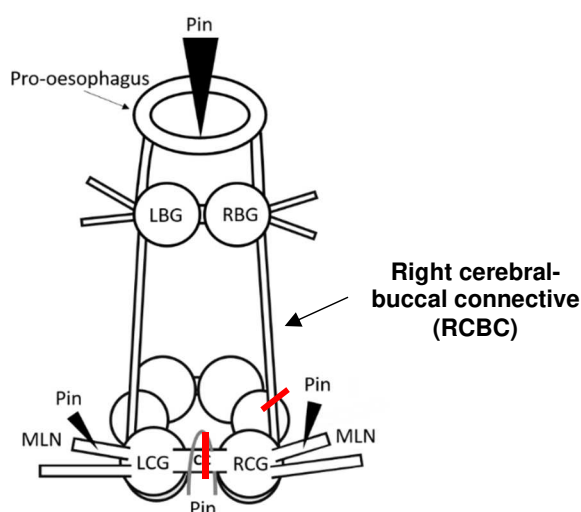
Figure 3.2| Modifications to the *Lymnaea* CNS preparation for TEVC recordings. Prior to recording of the RCGC, the right cerebral-buccal connection (RCBC) as well as the cerebral commissure (CC) were gently crushed (red lines) to reduce space clamping issues. Abbreviations: RCG (right cerebral ganglia), LCG (left cerebral ganglia), MLN (medial lateral nerves), RBG (right buccal ganglia) and LBG (left buccal ganglia).

3.2.1.1 Preparation of AAPH-treated young CNSs

To investigate the effects of acute OS on CGC ionic conductances, a subset of young preparations were incubated in a HEPES-buffered saline containing 3 mM AAPH for 30 minutes (**section 2.2.4.1**) prior to TEVC recordings. Experiments in Chapter 2 had demonstrated that this concentration of AAPH and duration of treatment was sufficient to induce OS in the cerebral ganglia and accurately mimic many age-related changes to CGC firing properties.

In addition, all the buffers utilised to isolate various ionic currents (**section 3.2.3**) in this chapter also contained the addition of 3 mM AAPH to maintain a consistent state of OS in the preparation throughout recordings.

3.2.2 The TEVC Setup

For TEVC recordings, micropipettes were made from borosilicate glass capillaries with filaments (OD 1.5 mm, ID 0.6 mm; Harvard Apparatus, UK) and pulled using the P-30 vertical micropipette puller (Sutter Instrument, USA). Micropipettes were backfilled with 3 M potassium acetate/0.5 mM potassium chloride solution (Sigma-Aldrich, UK) and the tips were dipped in black Indian ink (Windsor & Newton, UK) to facilitate impalement of the microelectrodes into the RCGC.

In all experiments, the current passing microelectrode attached to high gain differential headstage had a resistance between 4-7 MΩ, whilst the voltage sensing electrode attached to the unity-gain headstage had a resistance between 10-15 MΩ. Prior to impalement, both microelectrodes were *bridge balanced* to eliminate the voltage drop across the microelectrode. Following impalement of the RCGC, preparations were perfused in HEPES-buffered saline for a 10 minute acclimatisation period under current clamp mode to allow for firing frequency and the membrane potential to stabilise. CGCs were only accepted as suitable if their RMP was below -50 mV and the voltage recordings from both electrodes showed values that were within 2 mV of each other. During this period an aluminium (foil) sheet was also slowly positioned between the current injecting and voltage sensing microelectrodes to minimise capacitive coupling during recordings.

CGC signals derived from the microelectrodes were amplified using the Axoclamp 2B amplifier (AxonInstruments, USA) and analogue signals were digitised using the Digidata 1440A (AxonInstruments, USA). The signals sampled at 5 kHz were recorded on a PC running Axoscope and Clampex® and analysed offline in Clampfit®, all part of the pClamp version 10.5 software package (Molecular Devices, USA).

In TEVC experiments, measurements were made relative to the bath electrode. A Ag/AgCl pellet was used as a bath electrode in most experiments because of its extremely low resistance[415].

In experiments examining outward Cl⁻ currents, an agar salt bridge was utilised to prevent the voltage offset encountered with the Ag/AgCl ground when the extracellular chloride

concentration is altered during recordings[415]. Agar salt bridges were constructed in the laboratory by filling bent borosilicate capillary tubes (no filament, OD 1.5 mm, ID 0.6 mm; Harvard Apparatus, UK) with a 1% agarose/3 M KCl solution, which set into a gel immediately.

3.2.3   Chemicals and salines

All the salines utilised in TEVC experiments contained $CaCl_2$ despite the presence of Ca^{2+} channel blockers to maintain the stability of the CGC membrane during recordings.

3.2.3.1   HEPES-buffered saline

Composition as detailed in Chapter 2 (**section 2.3**).

3.2.3.2   Zero-Na⁺/CdCl₂ saline

The zero-Na^+/$CdCl_2$ saline was used to block Na^+, high-voltage activated (HVA) Ca^{2+} and Ca^{2+}-activated K^+ currents during the isolation of the total voltage-gated outward currents in the *Lymnaea* CGCs. The saline composition was: N-methyl-D-glucamine 50 mM, $CdCl_2$ 100 µM, KCl 1.7 mM, $CaCl_2$ 4 mM, $MgCl_2$ 2 mM, HEPES 10 mM, adjusted to pH 7.9 with HCl 1M (Sigma-Aldrich, UK)[416,393]. Preparations were incubated in this saline for 10 minutes as this ensured all targeted currents were completely blocked and no CGC action potentials were generated.

3.2.3.3   Zero-Na⁺/4-AP/CdCl₂ saline

This saline was utilised to block the A-type K^+, Na^+, HVA Ca^{2+} and Ca^{2+}-activated K^+ currents during experiments examining the sensitivity of I_A in the *Lymnaea* CGCs. The saline composition was N-methyl-D-glucamine 50 mM, $CdCl_2$ 100 µM, 4-AP 4 mM, KCl 1.6 mM, $CaCl_2$ 4 mM, $MgCl_2$ 2 mM, HEPES 10 mM, adjusted to pH 7.9 with HCl 1 M (Sigma-Aldrich, UK)[393]. Preparations were incubated in this saline for 15 minutes to completely suppress I_A.

3.2.3.4   TEA/4-AP/CdCl₂ saline

The tetraethylammonium (TEA)/4-AP/$CdCl_2$ saline was used block the delayed rectifier, A-type K^+, Na^+, HVA Ca^{2+} and Ca^{2+}-activated K^+ currents during experiments examining

the sensitivity of I_{DR} in the *Lymnaea* CGCs. The saline composition was: TEA 50 mM, 4-AP 4 mM, $CdCl_2$ 100 µM, KCl 1.7 mM, $CaCl_2$ 4 mM, $MgCl_2$ 2 mM, HEPES 10 mM, adjusted to pH 7.9 with TEA hydroxide 3M (Sigma-Aldrich, UK). Preparations were incubated in this saline for 15 minutes as this provided sufficient time to completely inhibit I_{DR}.

3.2.3.5 High K⁺ saline

This saline was used to block Na^+, HVA Ca^{2+} and Ca^{2+}activated K^+ currents during examination of the ion selectivity of channels in the *Lymnaea* CGC. The saline composition was: N-methyl-D-glucamine 50 mM, $CdCl_2$ 100 µM, potassium acetate 16 mM, $CaCl_2$ 4 mM, $MgCl_2$ 2 mM, HEPES 10 mM, adjusted to pH 7.9 with HCl 1M (Sigma-Aldrich, UK). Preparations were incubated in this saline for 10 minutes.

3.2.3.6 Zero Cl⁻ saline

This saline substituted chloride-based salts with other anionic salts to block voltage-gated outward Cl^- currents in the *Lymnaea* CGCs. To prevent contamination from other currents when examining the sensitivity of Cl^- currents, this saline also inhibited Na^+, HVA Ca^{2+}, Ca^{2+}-activated K^+ and voltage-gated K^+ currents. The saline composition was: TEA acetate 50 mM, cadmium sulphate 100 µM, 4-AP 4 mM, potassium acetate 1.6 mM, calcium acetate 4 mM, magnesium acetate 2 mM, HEPES 10 mM, adjusted to pH 7.9 with TEA hydroxide 3 M (Sigma-Aldrich, UK). Preparations were incubated in this saline for 10 minutes as this allowed for I_{Cl} to be completely suppressed in the CGCs.

3.2.3.7 Pharmacological agents

To isolate Cl^- currents, blockers including 5-Nitro-2-(3-phenulpropylamino) benzoic acid (NPPB, 100 µM; Tocris Biosciences, UK), 4,4′-diisothiocyanatostilbene-2,2′-disulfonate (DIDS, 100 µM; Sigma-Aldrich, UK) and niflumic acid (NFA, 1 mM; Sigma-Aldrich, UK) were utilised during recordings.

Experiments characterising the inward rectifier (I_R) involved using the non-specific blockers, barium chloride (Ba^{2+}, 4 mM; Sigma-Aldrich, UK) and caesium chloride (Cs^{2+}, 2 mM; Sigma-Aldrich, UK).

CNS preparations were incubated with each chloride channel blocker or inward rectifier blocker for 15 minutes before eliciting voltage clamp protocols to provide sufficient time for the blockers to mediate their effects.

3.2.4   TEVC protocols utilised to investigate properties of ionic currents

To study voltage-gated currents from young, old and 3 mM AAPH-treated young CGCs, various voltage clamp protocols were evoked in this investigation. Clampex® was used to design and execute these protocols as well as record the current response elicited by the CGCs. **Table 3.1 and 3.2** describes the voltage protocols utilised.

Each particular voltage protocol was repeated three times (responses were averaged offline in Clampfit®) within a 2 minute period. Once the protocol had concluded, the amplifier was switched back to current clamp mode from TEVC mode until the next protocol was ready to be conducted. This was a 3 minute rest interval when in the same saline or the incubation time detailed in **section 3.2.3** when switching to another saline. The rest period was crucial as it relieved the stress upon the CGCs, which occurs when clamping the potential of cells for long durations[415].

3.2.4.1 Voltage step protocols

In TEVC experiments of this study step protocol were utilised to measure steady-state currents at a desired voltage as well as examine inactivation, deactivation, reversal potential and the kinetic properties of voltage-gated outward currents in the *Lymnaea* CGC.

Voltage Protocol	Step Illustration	Description
VP1: Activation protocol from -90 mV holding potential.	+30 mV / 100 ms / -90 mV / 50 ms	This protocol was designed to elicit the voltage-gated outward currents of the *Lymnaea* CGCs during TEVC recordings. The CGCs were held at -90 mV for 50 ms to remove inactivation before stepping to a series of potentials from -90 mV to +30 mV in 10 mV increments for 100 ms each to active the voltage-gated outward currents[416,375].
VP2: Activation protocol from -40 mV holding potential.	+30 mV / -40 mV / 50 ms / -90 mV / 100 ms	This protocol is an adaptation of VP1 in which the holding potential was altered from -90 mV to -40 mV[416]. The purpose of this was to inactivate I_A and allow for its isolation *via* subtraction from the total outward current evoked in response to VP1. In this protocol, the CGCs were held at -40 mV for 50 ms to inactivate A-type K+ channels before stepping to a series of potentials from -90 mV to +30 mV in 10 mV increments for 100 ms to activate the remaining voltage-gated outward currents[416].
VP3: The reversal potential protocol for voltage-gated outward currents.	+30 mV / 100 ms / +20 mV / -90 mV / 50 ms / 500 ms	This protocol was used to evoke tail currents from the CGCs to determine the reversal potential for the conducting ion of interest. The CGCs were held at -90 mV for 50 ms to remove inactivation, which was followed by a +30 mV step for 100 ms to activate the voltage-gated outward currents before stepping to a series of potentials from -90 mV to +20 mV in 10 mV increments for 500 ms each to generate the tail currents[504,375].
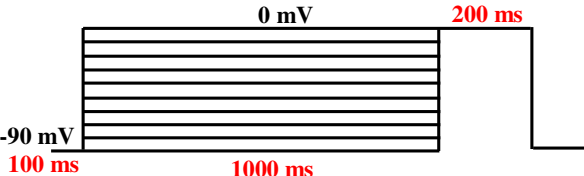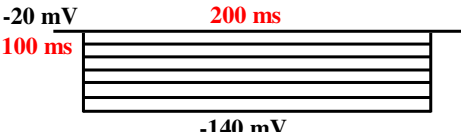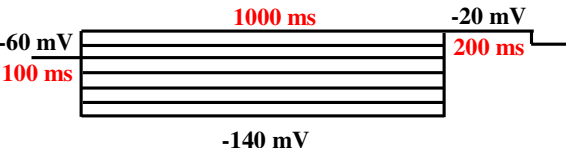
Voltage Protocol	Step Illustration	Description
VP4: Steady-state inactivation protocol for voltage-gated outward currents.		This protocol was designed to study the steady-state inactivation properties of the voltage-gated outward currents in young, old and 3 mM AAPH-treated young CGCs. The CGCs were held at -90 mV for 100 ms to remove inactivation, followed by a 1s pre-pulse to a range of voltages between -90 mV to 0 mV in 10 mV increments to activate the voltage-gated outward currents before the 200 ms test pulse at 0 mV, to examine the amplitude of the remaining current[101,375].
VP5: Activation of the inward rectifier from -20 mV holding potential.		The purpose of this protocol was to explore the presence of an inward rectifier current in CGCs of young, old and 3 mM AAPH-treated young preparations. The CGCs were held at -20 mV for 100 ms before stepping to a series of potentials from -20 mV to -140 mV in 20 mV increments for 200 ms[416].
VP6: Steady-state inactivation protocol for the inward rectifier current.		This protocol was implemented to study the steady-state inactivation properties of the inward rectifier current of the young, old and 3 mM AAPH-treated young CGCs. The CGCs were held at -60 mV for 100 ms, followed then by a 1 s pre-pulse from -20 mV to -140 mV in 20 mV increments to activate the inward rectifier before the 200 ms test pulse at -20 mV, to observe the remaining current.

Table 3.1| The TEVC protocols. This table details the voltage protocols that were designed in Clampex® and utilised in this study to examine the ionic currents of young, old and 3 mM AAPH-treated young RCGCs.

3.2.4.2 Action potential waveforms protocols

In a subset of experiments in this study, a refinement of the conventional TEVC method known as the "action potential (AP)-clamp" technique was utilised. Instead of the traditional voltage step protocols (Table 3.1), a pre-recorded single young CGC action potential (acquired in current clamp mode; **section 2.2.3**) was imported into Clampex® and used as the voltage command. The rationale for this approach was to profile the behaviour of voltage-gated outward currents during a more physiological stimulus, the young CGC action potential.[70,451]
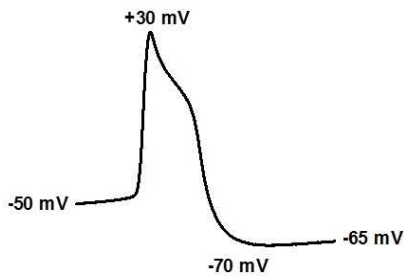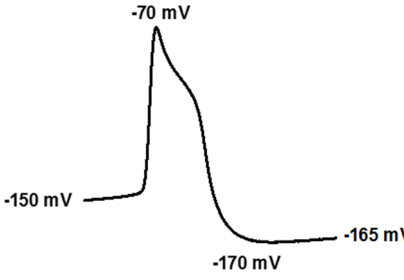
Voltage Protocol	AP Waveform Illustration	Description
AP1: Young CGC action potential from -50 mV holding potential.		The purpose of this protocol was to study the behaviour of voltage-gated outward currents during the firing of a young CGC action potential. The CGCs were held at -50 mV as this represented the typical RMP of young preparations.
AP2: Young CGC action potential from -150 mV holding potential.		The purpose of this protocol was to remove (*via* subtraction) passive responses evoked by the CGCs during AP1 that were not mediated by voltage-gated ion channels. Holding the CGCs at -150 mV, where no voltage-gated currents were active, revealed only the passive responses generated by the CGCs during the AP waveform command protocol.

Table 3.2| AP-clamp protocols. This table describes the action potential waveform protocols that were evoked in Clampex®.

3.2.6 Data analysis

3.2.6.1 Filtering and leak subtraction of voltage clamp recordings

Traces were filtered offline prior to the analysis of currents that had been acquired during experimental recordings. This was accomplished using the 'Filter' function in Clampfit® and selecting a low-pass Gaussian filter to filter the traces at 1 KHz, a 1/5 of the sampling frequency (5 kHz). The 'Leak subtraction' function in Clampfit® was then employed to remove the voltage-independent leak current.

3.2.6.2 Subtraction of voltage-gated ionic currents

A digital subtraction needed to be performed for the isolation of certain voltage-gated currents in this study. To do this, the 'Subtract Control' function in Clampex® was utilised on the selected trace recordings.

3.2.6.3 Analysis of current amplitude

Measurements of the peak amplitude of currents were conducted offline using Clampfit®. The data generated was entered in GraphPad Prism 7 to calculate the population mean and subsequently utilised in the construction of I-V plots, activation curves, steady-state inactivation curves as well as calculating % block (by pharmacological agents) of a current.

The amplitude of all currents were measured at the early component between 5-25 ms and at the sustained component between 70-90 ms during the 100 ms step of the activation voltage protocols. The currents generated from the steady-state inactivation protocol were measured between 150 ms-170 ms at the 0 mV test pulse. For the inward rectifier current the peak amplitude was measured at 10-15 ms during the 200 ms voltage step of the activation protocol as well as between 150 -170 ms during the -40 mV test pulse of its steady-state inactivation protocol.

3.2.6.3 Analysis of current area

Assessment of the area of a current from AP-clamp experiments were conducted offline in Clampfit®. Two cursors were placed on traces from where the measurements were to be taken from each current and the 'Template search' function in Clampfit® was the utilised to determine the area under the current. The data generated was entered in GraphPad Prism 7 for further analysis.

3.2.6.4 Analysis of the activation and inactivation rates of I_A

The activation rate for I_A was measured offline in Clampfit® on filtered and leak subtracted traces. The 'Template Search' function was utilised to measure the time to peak from 0 ms of the protocol at +30 mV in the young, old and 3 mM AAPH-treated young CGCs. Note, the time to peak was selected as the measure for activation rate as it avoided any interferences from transient capacitive artefacts may be present at the very

start of a voltage trace. This would not have been the case if an exponential was used to fit the activation.

The I_A inactivation rate was calculated by fitting a single exponential function (**Equation 3.1**[415]) from the peak to the trough of the current in the young, old and 3 mM AAPH-treated young CGCs. The inactivation time constant for I_A from -30 mV to +30 mV were calculated using the 'Fit' function in Clampfit® and selecting the Chebyshev method.

$$f(t) = A_i e^{-t/\tau} + C$$

Equation 3.1| Exponential function fitted to currents to calculate inactivation rates and the reversal potential[415]. For each component (*i*), this function solves for the amplitude (A), tau (τ), and the constant *y*-offset (C)[415].

3.2.6.5   Analysis of the reversal potential and deactivation rates

The reversal potential (E_{rev}) of a current and its deactivation rate were determined by fitting an exponential function to the tail currents across the entire voltage range of the protocol (**VP3 and VP6**). This was performed offline by utilising the 'Fit' function in Clampfit® and selecting the Chebyshev method (**Equation 3.1**[415]). The number of fits required to best fit the tail currents was determined by conducting a sum-of-squares *F*-test, which compared different exponential models.

The tail current amplitude data generated from the exponential fits were entered into GraphPad Prism 7 to generate a population mean that was then plotted as a function of voltage. A linear regression (**Equation 3.2**) were fitted to tail currents and the reversal potential of the current determined from the point where the regression line crossed the zero current axis. Reversal potentials for each current were calculated using this method and then the mean ± SEM determined.

$$f(x) = mx + c$$

Equation 3.2| Linear regression function where *m* is the slope of the line and *c* is the *y*-intercept. This was fitted to the data sets on the tail current amplitude *vs.* voltage plots to calculate the mean reversal potential of an ionic current[415].

3.2.6.6 Activation Curves

To construct an activation curve for a particular current, its reversal potential (**section 3.6.4**) and amplitude across the full range of voltages (**section 3.6.3**) was initially ascertained for each current. These values were then used to calculate the conductance at each step of the voltage protocol in accordance to **Equation 3.3**.

$$G = I / (V_m - E_{rev})$$

Equation 3.3| This equation was used to calculate conductance of the current, whereby G is conductance (nS), *I* is current amplitude (nA), V_m is the voltage of the protocol steps (mV) and E_{rev} is the reversal potential of the conducting ion (mV).

The G values for each step were normalised to maximum conductance (G/G_{max}). The normalised conductance values for each preparation were then entered into GraphPad Prism 7 and plotted as a function of voltage, which was then fitted with a single Boltzmann sigmoidal function (**Equation 3.4**). The "Top" and "Bottom" parameters of the Boltzmann curve were constrained to 1 and 0, respectively. Notably, the conductance values when $V_m=E_{rev}$ had to be excluded to enable the successful fitting of the Boltzmann function. The reason for this is that when V_m is around the reversal potential of the conducting ion, the difference between V_m and E_{rev} is extremely small and subsequently produces a very large error when calculating G.

Individual Boltzmann fits generated the V_{50} (potential to activate 50% of available channels) and slope factor (voltage-dependence of channel opening) values before the mean ± SEM were determined for each CGC group in Graphpad Prism 7. When there was no differences in the mean V_{50} and/or slope factor values between the data sets of the three CGC groups, a global (shared) fit of the Boltzmann sigmoidal function was fitted to the population mean of the normalised conductance values from all three groups.

$$G/G_{max} = 1/(1+\exp[(V_{50}-V_m)/k])$$

Equation 3.4| The Boltzmann sigmoidal equation fitted to activation curves. G/G_{max} is normalised conductance, V_{50} is the threshold potential for half-maximal conductance (in mV), V_m is the membrane potential (mV) and *k* (or slope factor) is the voltage dependence (in mV/e-fold change).

3.2.6.7 Steady-state inactivation curves

To construct steady-state inactivation curves, the measured peak current amplitude (*I*) for each voltage step was normalised to the maximal current (I_{max}). The normalised current values for every preparation was then entered into GraphPad Prism 7 and plotted as a function of voltage, which was then fitted with a single Boltzmann sigmoidal function in accordance to **Equation 3.5**. The "Top" and "Bottom" parameters of the Boltzmann curve were constrained to 1 and 0, respectively.

The V_{50} (potential to inactivate 50% of available channels) and slope factor (voltage-dependence of inactivation) values were derived from individual Boltzmann fits for each preparation before determining the population mean ± SEM in GraphPad Prism 7. When there was no significant difference in the mean V_{50} and/or slope factor values between the data sets of the three CGC groups, a global (shared) fit of the Boltzmann sigmoidal function to the mean *I/I_{max}* values was performed for some currents.

$$I/I_{max} = 1/(1+\exp[(V_m-V_{50})/k])$$

Equation 3.5| The Boltzmann sigmoidal equation fitted to activation curves. G/G_{max} is normalised conductance, V_{50} is the threshold potential for half-maximal conductance (in mV), V_m is the membrane potential (mV) and *k* (or slope factor) is the voltage dependence (in mV/e-fold change).

3.2.6.8 Nernst Equation

The Nernst equation (**Equation 3.6**) was utilised to predict the reversal potential of a conducting ion based on its valence and concentration across the CGC membrane.

$$E_{rev} = \frac{RT}{zF} \ln\left[\frac{[X]_o}{[X]_{in}}\right]$$

Equation 3.6| The Nernst equation used to calculate the reversal potential of a conducting ion, where E_{rev} is the reversal potential, R is the universal gas constant (equal to 8.3145 J K^{-1} mol^{-1}), T is temperature in Kelvin (293.2 K), z is the charge of the ion, *F* is Faraday's constant (96485 C mol^{-1}), [*X*]$_{out}$ is the extracellular concentration of the ion and [*X*]$_{in}$ is the intracellular concentration.

3.2.7 Statistical data analysis

Experimental data was analysed for statistical significance in GraphPad Prism 7. In addition to the statistical tests described in Chapter 2 (**section 2.10**), the following were also conducted in this chapter:

- A mixed ANOVA was performed when comparing the population means between two or more groups that were split on two factors[51]. The first was the within-subjects (or repeated-measures) factor that represented either voltage (mV) or time (ms) in this chapter. The second was the between-subjects factor that represented either the different CGC groups or different ionic currents.

- A paired t-test was performed to compare two population means from the same data set.

- A one-sample t-test for independent samples was performed when determining whether the population mean was significantly different from the hypothesised mean.

- An extra sum-of-squares *F-test* had been conducted on the data to compare the goodness-of-fit of two different mathematical models.

- A Grubb's (extreme studentized deviate) test was conducted to detect a single outlier at a particular voltage step within each treatment group. This method accomplishes this by calculating the difference between a potential outlier and the population mean divided by the SD[268]. If the Z-ratio generated from this calculation is larger than the critical Z-ratio, then the deviation is considered to be statistically significant and the outlier can be excluded[268].

The following p-values indicated that there was a significant difference: *$p<0.05$, **$p<0.01$, and ***$p<0.001$. For non-significant (NS) values, $p>0.05$. All data in the results sections are presented as the mean ± standard error of the mean (SEM) and n represents the number of RCGCs each recorded from an individual preparation.

3.3 Results

3.3.1 The total voltage-gated outward current in young, old and 3 mM AAPH-treated young CGCs

To challenge the notion often made in the literature that Ca^{2+}-activated K^+ currents are principally responsible for age-related changes to neuronal firing properties (**section 3.1**), all experiments in this study inhibited these currents in the *Lymnaea* CGCs. The main focus was then shifted to the potential involvement of voltage-gated K^+ currents in the changes to CGC firing properties with age, especially as it is well recognised that these currents have an important role in regulating many parameters of the action potential waveform[26,404,190,31].

Initial experiments in this chapter examined age-related changes to the total voltage-gated outward current. CGCs were perfused in a zero-Na^+/$CdCl_2$ saline to block all inward currents and inhibit the activation of outward Ca^{2+}-dependent K^+ currents.

Currents were evoked from a holding potential of -90 mV (VP1) and depolarised to voltages between -90 mV and +30 mV (**Figure 3.3A**). A representative sample trace of the total outward current elicited by a young RCGC in response to this protocol is also shown. As demonstrated, the total outward current rapidly activates and peaks ~20 ms into the depolarising steps (arrow 1). At more depolarised potentials and following a brief inactivation period, a sustained current (arrow 2) was observed that did not appear to show any signs of inactivation over the 100 ms voltage step.

I-V curves of the total early outward current did not significantly differ between young, old and 3 mM AAPH-treated young CGCs (p>0.05, *n=8* RCGCs*;* mixed ANOVA with Bonferroni post-hoc analysis; **Figure 3.3Bi**). Similarly, there was no significant difference in the amplitude of the total sustained current between the three groups (p>0.05, *n=8* RCGCs*;* **Figure 3.3Bii**).
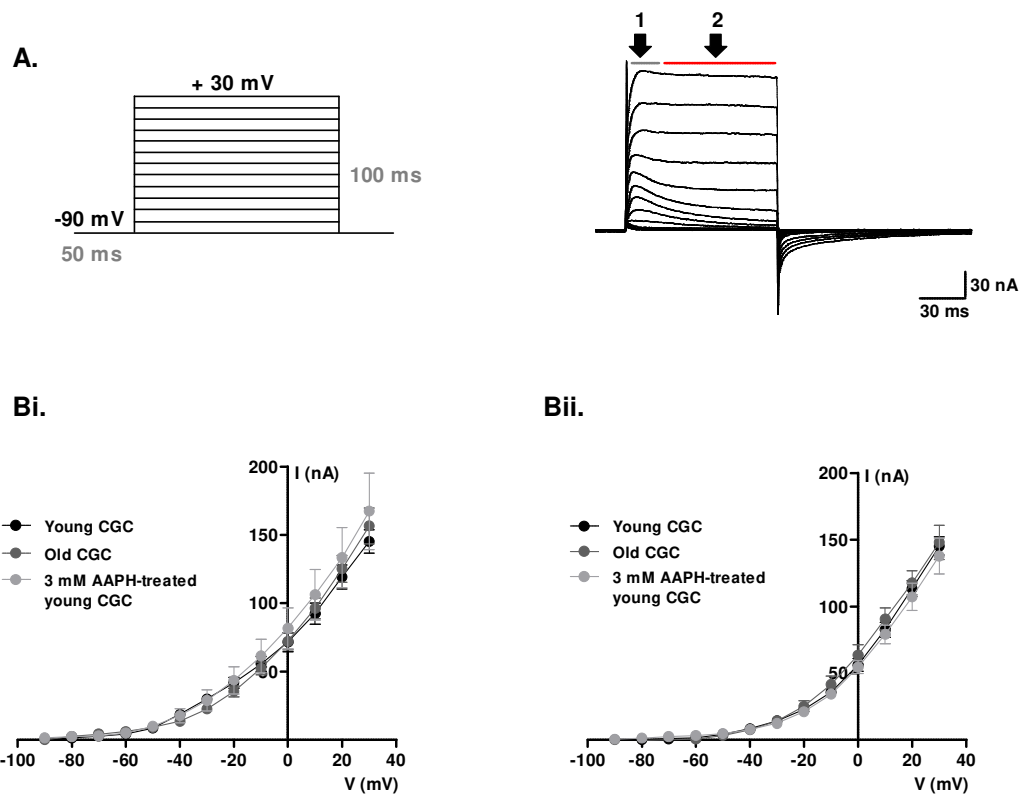
Figure 3.3| Total voltage-gated outward current. (A) Sample trace of total outward current generated by a young RCGC in response to VP1. Arrow 1 highlights the early transient current and arrow 2 shows the sustained non-inactivating current that follows. (B) The amplitude of the total (Bi) early and (Bii) sustained current did not differ between the three CGC groups. Data shown as mean ± SEM, *n=8* RCGCs. NS, p>0.05.

3.3.2   Voltage-gated outward K$^+$ currents of the *Lymnaea* CGC

Despite no significant difference in the amplitude of the total outward ionic current, it is possible that ageing and acute OS may alter the activation/inactivation kinetics of the constituent currents or the proportion that each individual current contributes toward the total outward CGC current.

3.3.2.1   The K$^+$ reversal potential

Preparations were bathed in a zero-Na$^+$/CdCl$_2$ saline containing the Cl$^-$ channel blocker, NPPB. In **Figure 3.4A**, a representative sample trace from a young RCGC recording illustrates tail currents that were elicited in response to VP3 and used to assess the E$_{rev}$ of K$^+$. All CGC tail currents were fitted with a double exponential function. A comparison of a single and double exponential fit to the tail currents in a young RCGC is shown in **Figure 3.4B**. A single exponential function (top) resulted in a poor fit particularly to the

fast component of the tail currents (black arrow), which deviated from the fitted (red) curve. With a double exponential fit (bottom), the tail currents, particularly the fast component, did not deviate from the fitted (red) curve. A sum-of-squares F-test comparing the two exponential models confirmed that a double exponential fit was the most suitable for the CGC tail currents (p>0.05, $n=8$ RCGCs). This fitting of a double exponential suggests that either the total K^+ current has two deactivation processes or is contaminated with another current, each with a single (different) deactivation process.

Figure 3.4C revealed that the estimated E_{rev} for K^+ did not significantly differ between the three CGC groups (p>0.05, $n=8$ RCGCs; one-way ANOVA with Bonferroni post-hoc analysis). The K^+ reversal potential was estimated as follows: 1) -59.4 ± 1.25 mV for young CGCs; 2) -59.3 ± 2.32 mV for old CGCs, and; 3) -57.6 ± 2.15 mV for 3 mM AAPH-treated young CGCs.
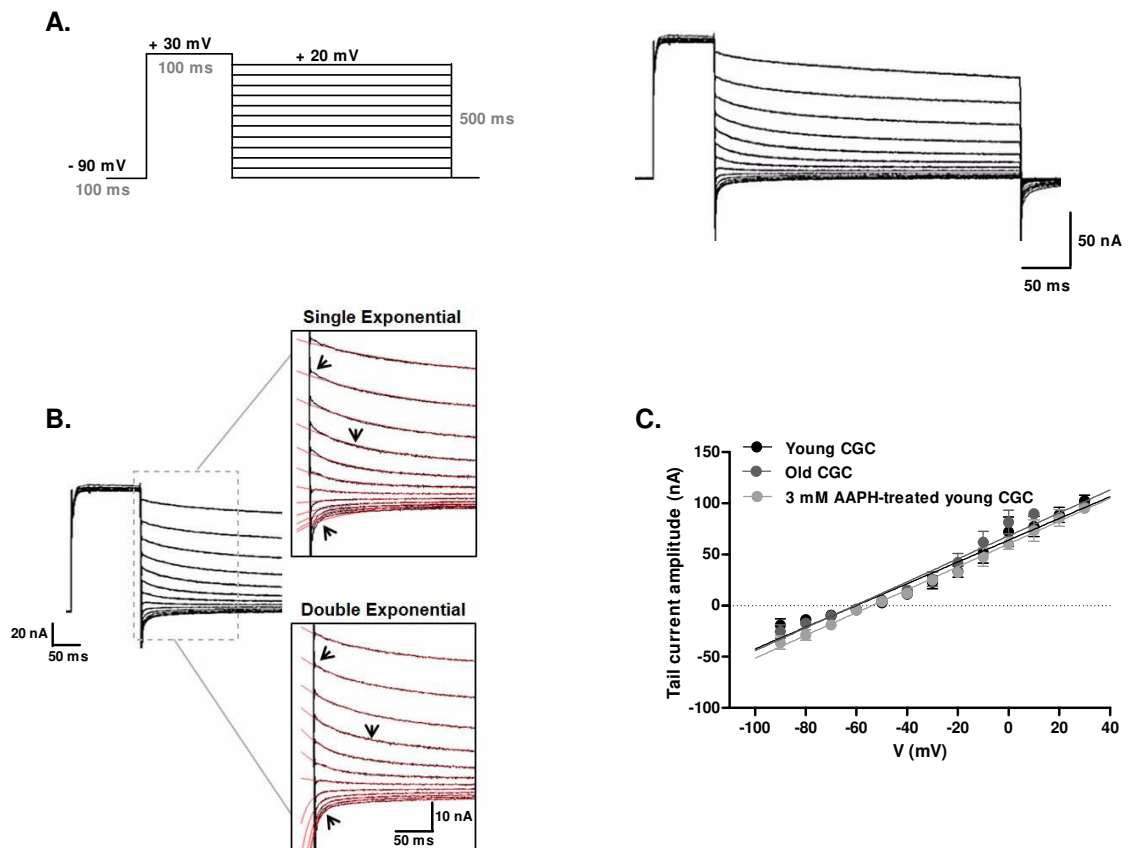
Figure 3.4| Estimated E_{rev} of K^+ in the CGCs. (A) Sample trace of tail currents evoked from a young control RCGC. (B) Illustrates that tail currents fitted with a single (top) exponential function resulted in a poor fit (black arrows highlight the deviation from the fitted red curve) when compared to the fit with a double (bottom) exponential function. (C) The estimated E_{rev} for K^+, ~-60 mV, did not significantly differ between the three CGC groups. Data shown as mean ± SEM, $n=8$ RCGCs. NS, p>0.05 (part C).

3.3.3 Characterisation of I_A

The total voltage-gated early outward current in the CGCs had been previously described as being predominately mediated by I_A[416]. Thus, it was of interest to isolate and characterise this current in the CGCs of this study and subsequently examine the effects of age and acute OS on its properties.

In **Figure 3.5A**, voltage steps from -90 mV to +30 mV (VP1) in the zero-Na^+/$CdCl_2$ saline evoked a series of currents that consisted of an early fast transient (arrow 1) component and a slower sustained component (arrow 2). This early fast transient current was abolished (arrow 3; **Fig 3.5Bi**) following the addition of 4 mM 4-AP (a non-specific I_A blocker) to the bathing saline. The residual 4-AP insensitive current (**Figure 3.5Bi**) was then digitally subtracted from the total outward current (**Figure 3.5A**) to isolate the 4-AP sensitive I_A (**Figure 3.5Bii**).

Another technique routinely utilised to isolate I_A involves manipulating the holding potential of the CGCs in a zero-Na^+/$CdCl_2$ saline. VP2 (Table 3.1) makes use of the fact that I_A rapidly inactivates when held at depolarised potentials[416]. Indeed, altering the holding potential of the protocol from -90 mV to -40 mV (VP2) and stepping from -90 mV to +30 mV, caused inactivation of the A-type current (arrow 4; **Figure 3.5Ci**). The outward current from -40 mV holding potential was then subtracted from the total outward current (**Figure 3.5A**) evoked from -90 mV holding potential (*via* VP1) to isolate I_A (**Figure 3.5Cii**).

Figure 3.5D showed that I_A yielded from both pharmacological and voltage subtractions, activated around -60 mV ($p<0.05$, *n=8* RCGCs*;* one-sample t-test, current > hypothetical value of 0 nA) and that the peak amplitude of the current did not significantly differ between the two isolation methods ($p>0.05$, *n=8* RCGCs; mixed ANOVA with Bonferroni post-hoc analysis). The amplitude of both these currents, however, were significantly smaller than the total early current, indicating that other currents are also substantially active in this region ($p<0.001$, *n=8* RCGCs).

A.
Total outward current

Bi.
4-AP insensitive current

Ci.
-40 mV HP evoked current

30 nA
30 ms

30 nA
30 ms

Bii.
4-AP sensitive I_A

Cii.
Voltage subtracted I_A

30 nA
30 ms

30 nA
30 ms

D.
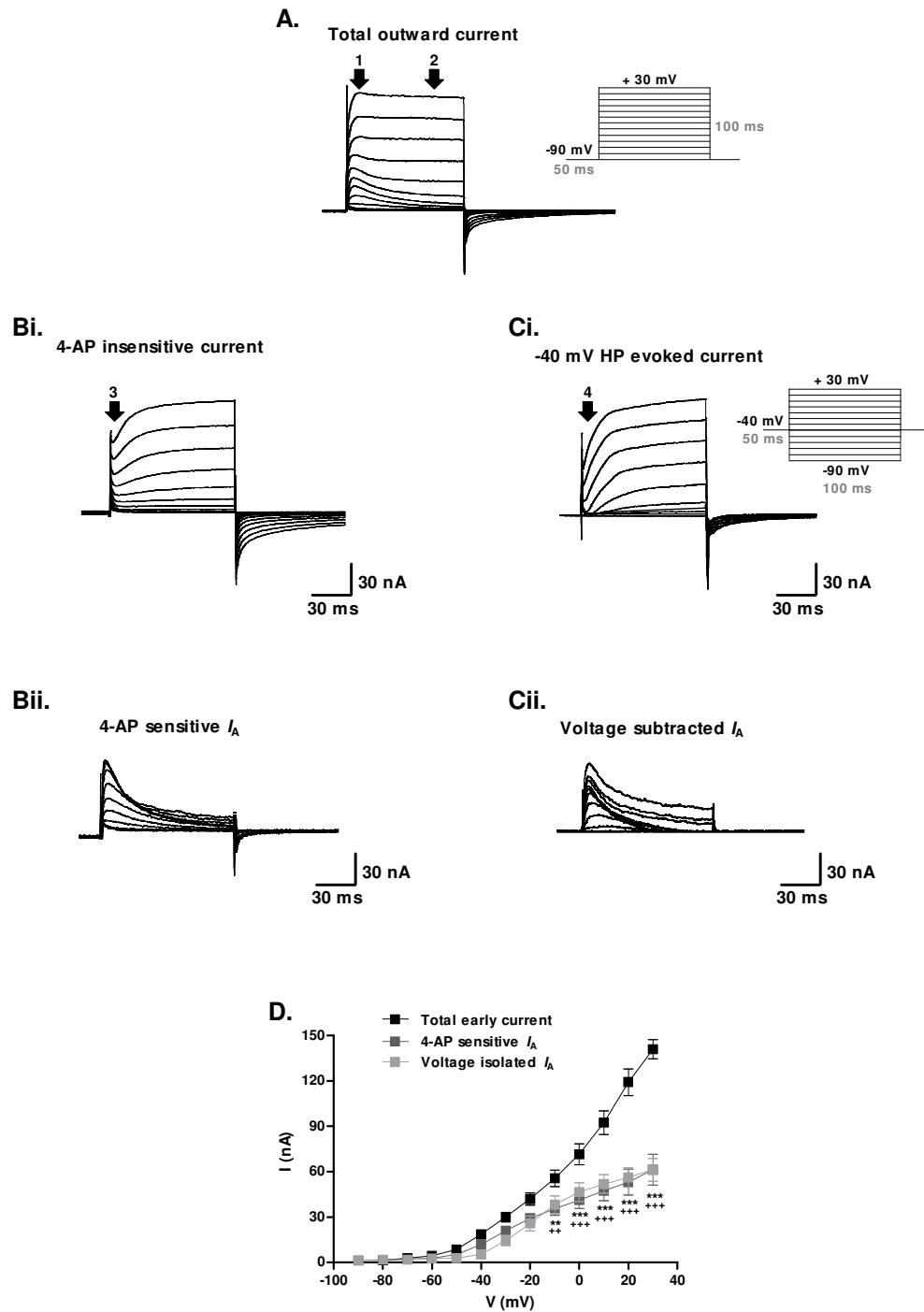
Figure 3.5| Isolation of I_A in young CGCs. (A) Total voltage-gated outward current with arrow 1 pointing at the early transient component and arrow 2 at the sustained component. (Bi) 4-AP blocked the early current (arrow 3), leaving a 4-AP insensitive sustained current. (Bii) Subtraction of (Bi) from (A) isolated I_A. (Ci) The sustained current, but not early current (arrow 4) was evoked from the -40 mV holding potential. (Cii) Subtraction of (Ci) from (A) also isolated I_A. (D) I_A isolated (Bii) pharmacologically or by (Cii) altering the holding potential did not differ from each other, but were significantly smaller than the total early current. Data shown as mean ± SEM, $n=8$ RCGCs, [++]/**p<0.01,[+++]/***p<0.001 vs. total early current (part D). Graph symbols: asterisk (*) designated for 4-AP sensitive I_A and plus ([+]) for Voltage isolated I_A.

127

3.3.3.1 Activation properties of I_A with age and acute OS

As the 4-AP sensitive I_A and voltage-isolated I_A were not significantly different from one another, the remaining experiments in this chapter will utilise 4-AP in the process of isolating I_A.

I-V plots in **Figure 3.6A** exhibited a noticeable decrease in the voltage sensitivity (rightward shift) of I_A with both age and acute OS. However, the peak amplitude of I_A did not significantly differ between the three CGC groups across the potential range of VP1 (p>0.05, $n=8$ RCGCs; mixed ANOVA with Bonferroni post-hoc analysis). Additionally, as in the young CGCs, it was observed that I_A activated around -60 mV in both the old and 3 mM AAPH-treated young CGCs (p<0.05, $n=8$ RCGCs; one-sample t-test, current > hypothetical value of 0 nA) and thus, did not significantly differ from one another (p<0.05, $n=8$ RCGCs; one-way ANOVA with Bonferroni post-hoc analysis).

Given that a large proportion of the amplitude of I_A in the I-V plot is dependent on the voltage across the membrane, a more informative way to analyse these data sets is to plot activation curves that looks specifically at the proportion of channels open in the membrane and how these change with increasing voltage. To study this, the peak I_A data (**Figure 3.6A**) as well as the estimated E_{rev} for K^+ (**Figure 3.4C**) was used to generate activation curves (G/G_{max} $vs.$ voltage).

I_A activation curves for young, old and 3 mM AAPH-treated young CGCs in **Figure 3.6B** were fitted well with the Boltzmann sigmoidal function. However, there was a significant rightward shift in the curves with both age and acute AAPH-treatment (p<0.001, $n=8$ RCGCs; mixed ANOVA with Bonferroni post-hoc analysis). Independent Boltzmann fits for each *Lymnaea* preparation revealed that this was due to changes in both V_{50} and the slope factor.

The V_{50} shifted to a more positive potential from -54.6 ± 3.6 mV in young CGCs to -31.7 ± 3.3 mV and -36.2 ± 4.1 mV in the old and 3 mM AAPH-treated young CGCs, respectively (p<0.05, $n=8$ RCGCs; one-way ANOVA with Bonferroni post-hoc analysis; **Figure 3.6Ci**). The slope factor was less steep with values becoming more positive from 4.37 ± 1.3 mV in young CGCs to 24.5 ± 5.2 mV in old CGCs and 27.6 ± 4.5 mV in 3 mM AAPH-treated young CGCs (p<0.05, $n=8$ RCGCs; **Figure 3.6Cii**).

Sample traces of the 4-AP sensitive I_A (evoked at -30 mV command potential from the -90 mV holding potential of VP1) demonstrates that in both old and 3 mM AAPH-treated

young CGCs it takes longer to reach the peak of this current when compared to young CGCs (**Figure 3.6Di**). This difference was statistically significant (p<0.05, *n=8* RCGCs; **Figure 3.6Dii**).
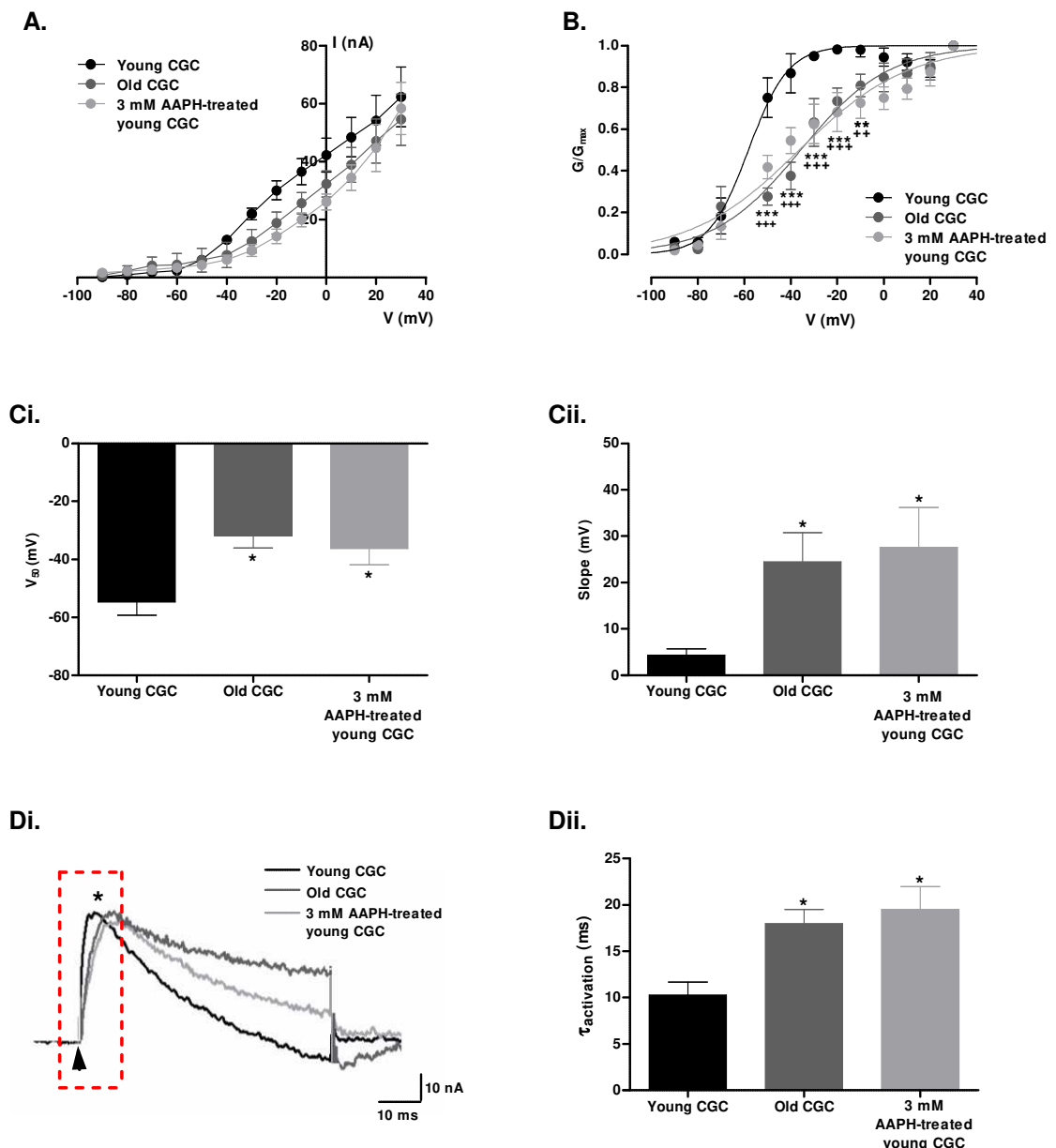
Figure 3.6| Activation properties of I_A with age and acute OS. (A) Peak amplitude of I_A did not differ between the three CGC groups. (B) I_A activation curves exhibited a significant rightward shift with age and acute OS due to a significant increase in (Ci) V_{50} and the (Cii) slope factor. (Di) Representative current traces, evoked at -30 mV command potential, illustrates that old and AAPH-treated young CGCs reach the I_A peak (asterisk) much slower than young CGCs. (Dii) Indeed, this slowing of the I_A activation rate was significant. Data shown as mean ± SEM, *n=8* RCGCs. [+]/[*]p<0.05, [++]/[**]p<0.01, [+++]/[***]p<0.001, *vs.* young CGCs (part B-D). Graph symbols: asterisk (*) designated for Old CGCs and plus (+) for 3 mM AAPH-treated young CGCs (part B).

3.3.3.2 Inactivation of I_A changes with age and acute OS

Steady-state inactivation of I_A was examined by conducting the voltage protocol (VP4) illustrated in **Figure 3.7Ai**. This figure also displays a representative sample trace of the current response elicited by a young RCGC during this protocol.

The steady-state inactivation curve (I/I_{max} *vs.* voltage) in **Figure 3.7Aii**, fitted successfully with a Boltzmann function, demonstrated that I_A in young, old and 3 mM AAPH-treated young CGCs all exhibited pronounced steady-state inactivation. A global fit of the Boltzmann function to the inactivation data was rejected due to slight differences in either the V_{50} and/or slope factor. However, individual fittings of the Boltzmann function to each preparation found that these changes in V_{50} and the slope factor between the three CGC groups were not significant (p>0.05 for both, *n=8* RCGCs; one-way ANOVA with Bonferroni post-hoc analysis; data not shown). This indicates that the threshold and voltage-dependence of I_A inactivation is not altered with age or acute OS.

Sample traces of I_A from its peak, evoked at -30 mV command potential from the -90 mV holding potential of VP1, illustrates that ageing and acute OS altered its inactivation kinetics (**Figure 3.7Bi**). The time constant of I_A inactivation was measured by successfully fitting a single exponential function from the peak (asterisk) to the trough (arrow) of the current. **Figure 3.7Bii** showed that inactivation of I_A in both the old and 3 mM AAPH-treated young CGCs was significant slower (from -30 mV to + 30 mV) than in young CGCs (p<0.01, *n=8* RCGCs*;* mixed ANOVA with Bonferroni post-hoc analysis). There was no significant differences in the I_A inactivation time constants between old and 3 mM AAPH CGCs (p>0.05, *n=8* RCGCs).

Ai.

0 mV

200 ms

-90 mV

100 ms 1000 ms

15 mV
100 ms

Aii.

- Young CGC
- Old CGC
- 3 mM AAPH-treated young CGC

I/I_{max}

V (mV)

Bi.

— Young CGC
— Old CGC
— 3 mM AAPH-treated young CGC

*

10 nA
10 ms

Bii.

- Young CGC
- Old CGC
- 3 mM AAPH-treated young CGC

$\tau_{inactivation}$ (ms)

*** ** * * * * *

V (mV)
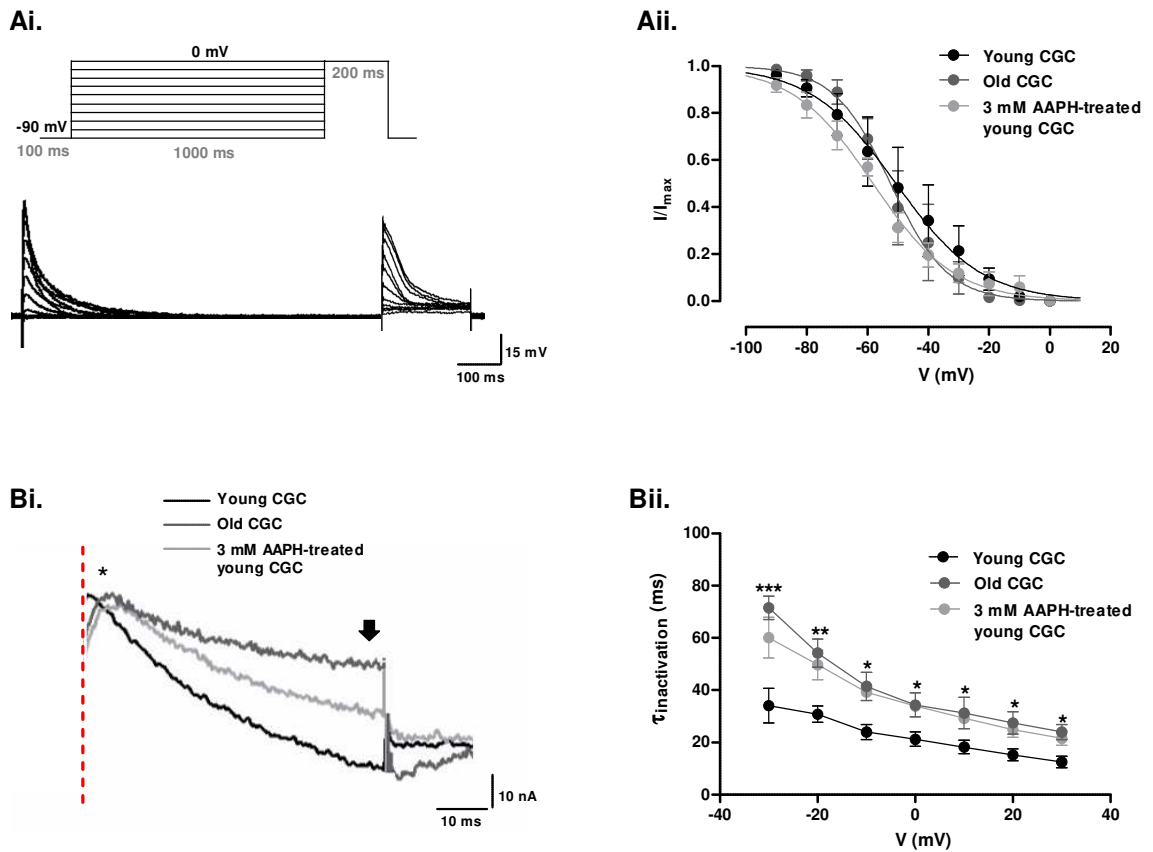
Figure 3.7| Inactivation of I_A with age and acute OS. (Ai) Sample trace of the current response generated by a young RCGC, which was used to construct (Aii) steady-state inactivation plots. These curves exhibited pronounced steady-state inactivation and did not significantly differ between the three CGC groups. (B) I_A inactivation kinetics did change. (Bi) Sample traces of I_A, evoked at -30 mV command potential, demonstrates that inactivation is much slower (from asterisk to arrow) in old and AAPH-treated young CGCs when compared to young CGCs and that this (Bii) is statistically significantly from -30 mV to + 30 mV. Data shown as mean ± SEM, *n=8* RCGCs, ***p<0.001, ++/**p<0.01, +/*p<0.05 *vs*. young CGCs (part Bii). Graph symbols: asterisk (*) designated for Old CGCs and plus (+) for 3 mM AAPH-treated young CGCs.

3.3.3.3 The I_A window current

I_A analysed from young, old and 3 mM AAPH-treated young CGCs all exhibited a window current when the activation and steady-state inactivation curves were superimposed (**Figure 3.8Ai-iii**). This feature represents the period where I_A channels are available for activation, but inactivation of the current is submaximal.

I_A opened at physiologically relevant potentials in all three CGC groups, but the magnitude (area) of the window currents did significantly decrease with age and acute OS (p<0.05, *n=8* RCGCs; one-way ANOVA with Bonferroni post-hoc analysis).

At the peak of the window current, in all three CGC groups, up to ~60% (calculated as a proportion of G_{max}) of the available channels were active in the young CGCs, ~35% in the old CGCs and ~40% in the 3 mM AAPH-treated young CGCs.

In relation to the RMP of the CGCs, -57.6 mV for young CGCs, -73.2 mV for old CGCs and -60.3 mV for 3 mM AAPH-treated young CGCs (Chapter 2), there were significant differences in the proportion of I_A active between each of the CGC groups (p<0.01, *n=8* RCGCs; **Figure 3.8B**). At their respective RMPs (calculated as a proportion of G_{max}), ~35% of the I_A channels were open in the young, ~20% in the 3 mM AAPH-treated young CGCs and, ~10% in the old CGCs.
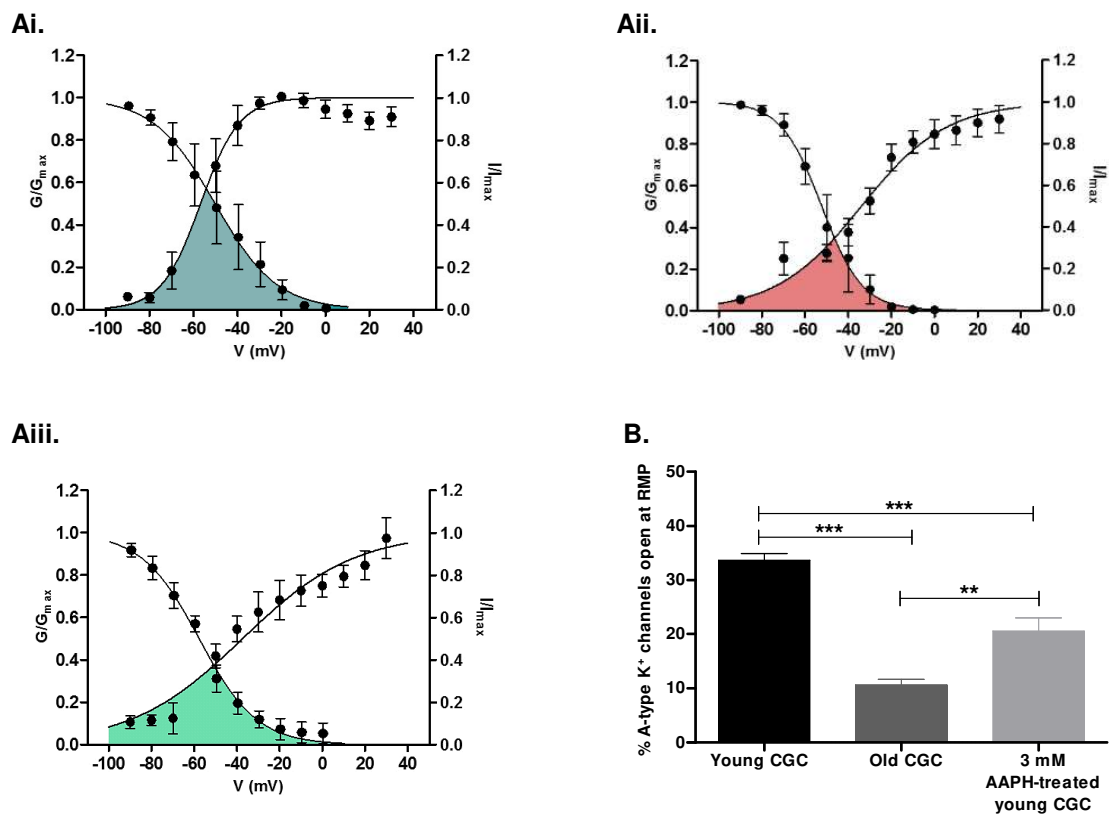
Figure 3.8| I_A **window current. (A) The window current in (Ai) young CGCs is larger than that of (Aii) old and (Aiii) 3 mM AAPH-treated young CGCs. (B) A significantly smaller proportion of A-type K⁺ channels were open at the RMP of old CGCs when compared to both young and 3 mM AAPH-treated young CGCs at their respective RMPs. Young CGCs had the greatest proportion of A-type K⁺ channels open at their RMP. **p<0.01 *vs.* Old CGC and ***p<0.001 *vs.* Young CGC (part B).**

3.3.4 Characterisation of I_{DR}

To isolate I_{DR} from the total outward current, I_A (arrow 1; **Figure 3.9Ai**) was first blocked (arrow 2; **Figure 3.9Aii**) by bathing young CGCs in a zero-Na$^+$/CdCl$_2$/4-AP saline.

Figure 3.9Aiii, displays I-V curves for the sustained currents before and after the addition of 4-AP to the bathing saline. The amplitude of the 4-AP insensitive sustained current was smaller than the total sustained outward current, which reached significance at very depolarised potentials ($p < 0.05$, $n=8$ RCGCs*; mixed ANOVA with Bonferroni post-hoc analysis*). Interestingly, this indicates that a small proportion of I_A also contributes to the sustained component of the total voltage-gated outward CGC current.

A substantial proportion of the 4-AP insensitive sustained current was identified as I_{DR}, as its amplitude reduced following the extracellular application of 50 mM TEA. **Figure 3.9B** illustrates a representative trace of the TEA/4-AP insensitive current (+TEA) overlaid on the 4-AP insensitive current (control), both evoked at the +10 mV command potential of VP1. The difference between these two currents is reflective of the amplitude of the TEA sensitive I_{DR}. The accompanying bar graph in this panel reveals that I_{DR} accounted for ~80% of the 4-AP insensitive sustained current.

Figure 3.9Ci displays a typical example of the TEA sensitive I_{DR} isolated by subtraction of the TEA/4-AP insensitive current from the 4-AP insensitive current. The TEA sensitive I_{DR} demonstrated the characteristic features of a 'classical' I_{DR}, such as being slow to activate and undergoing very little inactivation[504,375,416]. I-V curves of the sustained currents in **Figure 3.9Cii** reveals that the reduction of the control 4-AP insensitive sustained current by TEA was significant ($p < 0.05$, $n=8$ RCGCs). The amplitude of the TEA sensitive I_{DR} was significantly larger than the sustained TEA/4-AP insensitive current ($p > 0.001$, $n=8$ RCGCs), indicating that I_{DR} is the principal contributor to the total outward sustained current in young CGCs.

A.

Ai.

Total outward current

Aii.

4-AP insensitive current

+30 mV

100 ms

-90 mV

50 ms

20 nA

30 ms

Aiii.

I (nA)

- Total sustained current
- 4-AP insensitive sustained current

V (mV)

B.

+ 10 mV

-90 mV

Control

+ TEA

20 nA

10 ms

% reduction

50 mM TEA

Ci.

TEA sensitive I_{DR}

20 nA

30 ms

Cii.

I(nA)

- 4-AP insensitive sustained current
- TEA/4-AP insensitive sustained current
- Subtracted (I_{DR})

V (mV)
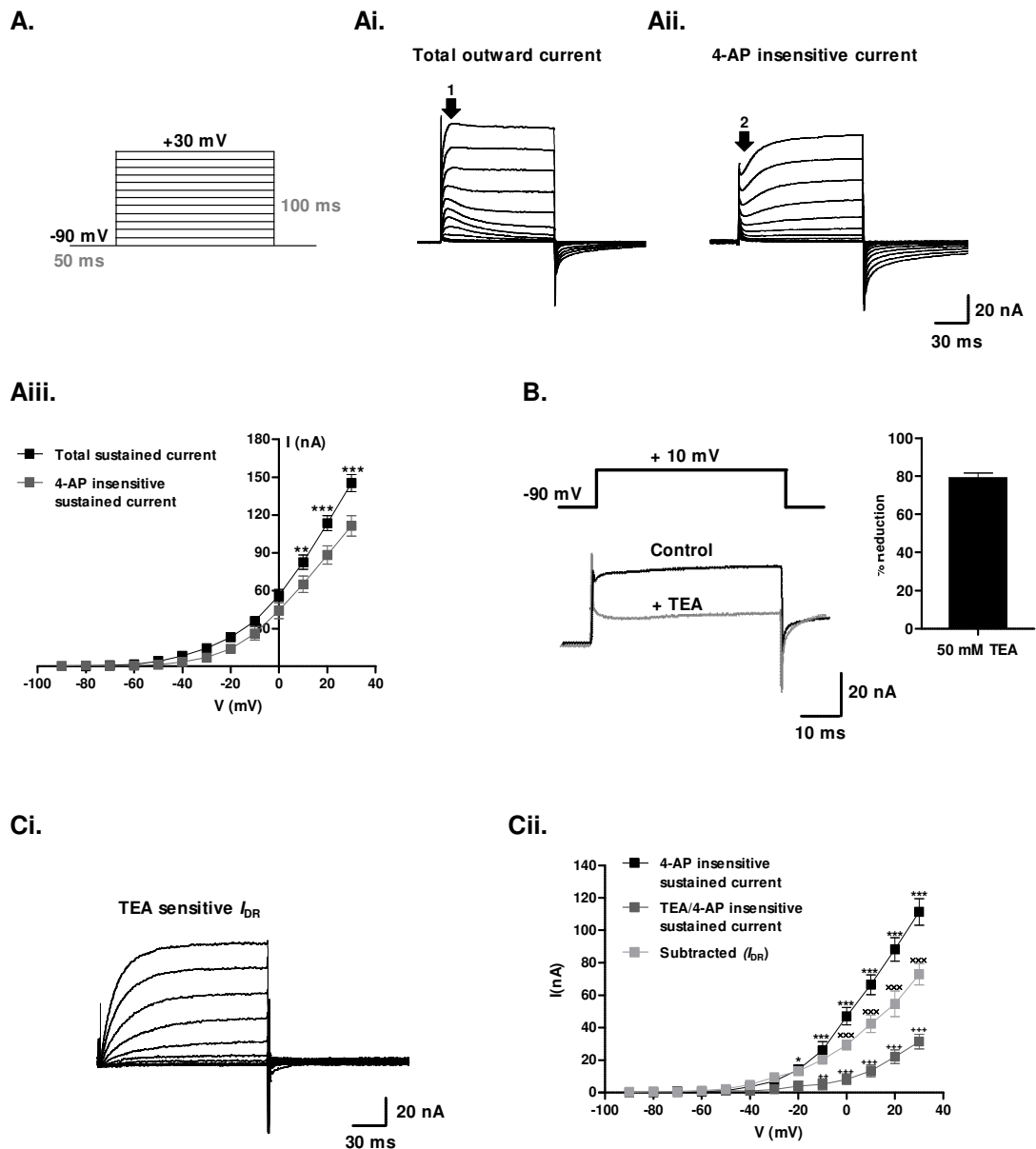
Figure 3.9| I_{DR} **isolation in young CGCs. (A) VP1 evoked voltage-gated currents. (Ai) To isolate** I_{DR}, I_A **(arrow 1) was first blocked (Aii) with 4-AP (arrow 2), as shown in this sample trace. (Aiii)** I_A **significantly contributes to the total sustained outward current. (B) Sample trace illustrates that TEA reduced the 4-AP insensitive (control) current by ~80%. (Ci) The TEA sensitive** I_{DR} **(isolated** *via* **subtraction) activates slowly and undergoes minimal inactivation. (Cii)** I_{DR} **is the largest component of the 4-AP insensitive sustained current. Data shown as mean ± SEM,** *n=8* **RCGCs.** ^{x}**p<0.05,** $^{++}$**p<0.01,**$^{xxx/+++/***}$**p<0.001. Graph symbols for Part Cii: asterisk (*) designated for sustained 4-AP insensitive current (**vs. **sustained TEA/4-AP insensitive current), plus (**$^{+}$**) for sustained TEA/4-AP insensitive current (**vs. I_{DR}**) and cross (**^{x}**) for** I_{DR} **(**vs. **sustained 4-AP insensitive current).**

3.3.4.1 I_{DR} properties with age and acute OS

Figure 3.10A revealed that the amplitude of the TEA sensitive I_{DR} did not significantly differ between young, old and 3 mM AAPH-treated CGCs (p>0.05, *n=8;* mixed ANOVA with Bonferroni post-hoc analysis). I_{DR} in all 3 groups activated at approximately -50 mV (p<0.05; *n=8* RCGCs*;* one-sample t-test, current > hypothetical value of 0 nA) and reached a maximal magnitude of approximately 60 nA at the +30 mV command potential.

I_{DR} activation curves generated for young, old and 3 mM AAPH-treated young CGCs were successfully fitted with a global Boltzmann sigmoidal function (p>0.05; *n=8;* extra sum-of-squares *F*-test; **Figure 3.10B**). This indicates that V_{50} and slope factor is not significantly altered with age and acute OS.

A particularly interesting feature of the I_{DR} global activation curve was that it was very shallow. This strongly suggests that the voltage-dependence of activation is weak in the delayed rectifiers of the *Lymnaea* CGCs.

Notably, mean conductance values from the 3 mM AAPH-treated young CGC group did not fit particularly well to the Boltzmann curve between -40 mV to -70 mV where there was an unusual upward deflection. One data set was principally responsible for this deviation as it consistently (protocols repeated 3 times; **section 3.2.4**) evoked a larger current, predominantly at these voltages, when compared to other data sets in the AAPH group. This yielded a larger conductance value during calculations and subsequently increased the population mean substantially at these voltages. The conductance values between -40 mV to -70 mV from this one data set could not be excluded as its deviation from the population mean was not deemed to be a significant outlier (p>0.05 for -40 mV, -50 mV and -70 mV, *n=8* RCGCs*;* Grubbs' test; data not shown).

Steady-state inactivation properties of I_{DR} in the three CGC groups was then examined using VP4 (Figure **3.10Ci**). The accompanying sample trace of a typical response evoked by this protocol in a young RCGC illustrates that I_{DR} undergoes very little inactivation. The steady-state inactivation curve in **Figure 3.10Cii** was successfully fitted with a global Boltzmann function (p>0.05, *n=8;* extra sum-of-squares *F*-test; **Figure 3.10Cii**), indicating no significant changes in the V_{50} and slope factor with age or acute OS. This shallow curve also shows that inactivation of I_{DR} is weakly voltage-dependent in the three CGCs groups. The incomplete inactivation over the 1000 ms test period duration of the voltage protocol is considered to be a characteristic feature of I_{DR}[375,504,416].
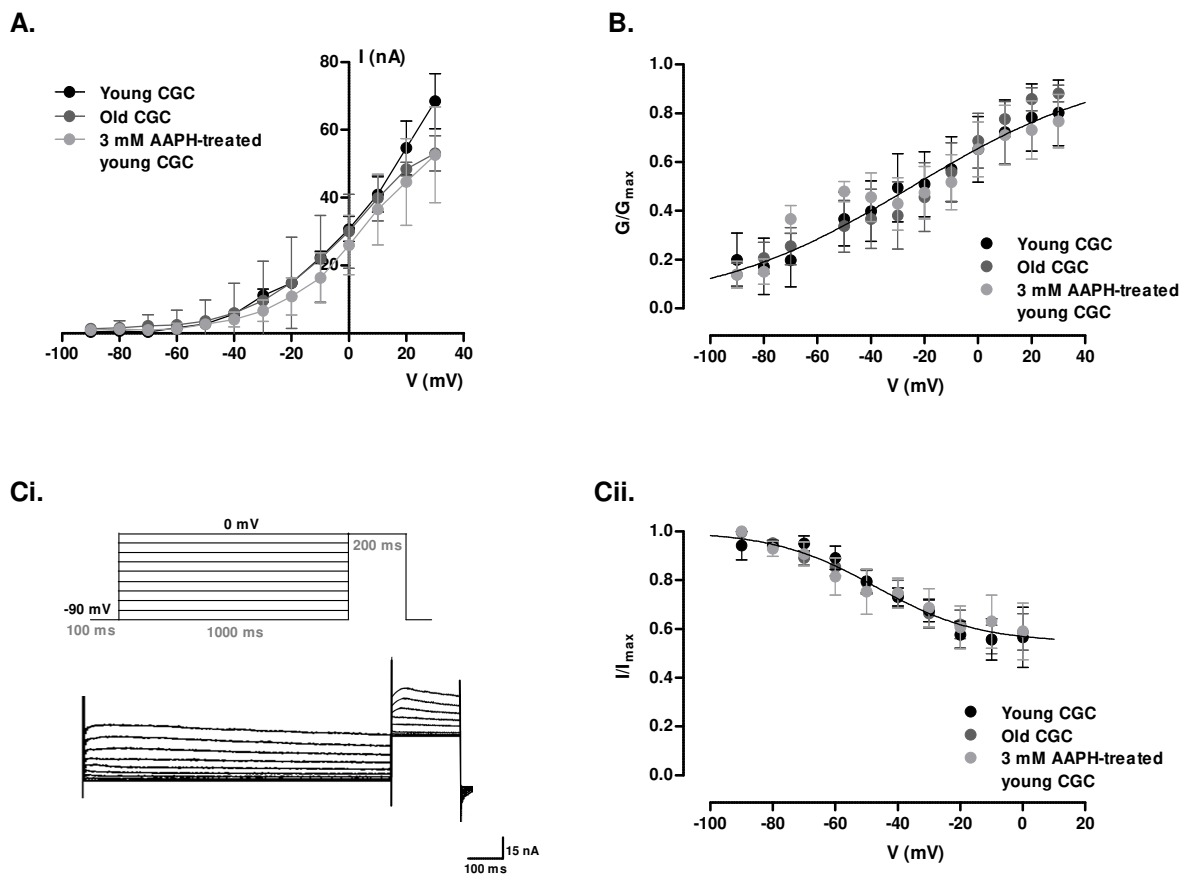
Figure 3.10| I_{DR} **properties with age and acute OS. (A) The amplitude and activation threshold (~-50 mV) of the TEA sensitive** I_{DR} **did not significantly change between the three CGC groups. (B) There was also no significant differences between the** I_{DR} **activation curves. (Ci) Sample trace of the steady-state inactivation current response evoked by a young RCGC in response to VP4, reveals that** I_{DR} **exhibits very little inactivation. (Cii)** I_{DR} **inactivation properties did not significant alter with age or acute OS. Data shown as mean ± SEM,** *n* =8 **RCGCs. NS, p>0.05.**

3.3.5 The TEA/4-AP insensitive outward current

Experiments in section **3.3.4.1**, unveiled the presence of a voltage-gated outward current in the CGCs that had not been previously reported in the *Lymnaea* literature. This current was insensitive to 50 mM TEA and 4 mM 4-AP and did not display the typical features of a 'classical' I_{DR}. Sample traces from a young RCGC in **Figure 3.11A** demonstrates that the TEA/4-AP insensitive current has a 'biphasic' phenotype with a fast transient activation component followed by a smaller slower sustained component, whereas the TEA sensitive I_{DR} has a very slow activation phase that is followed by a larger sustained component.

The activation threshold of these two currents also significantly differed ($p < 0.01$, $n = 8$ RCGCs; unpaired t-test; **Figure 3.11B**). The TEA/4-AP insensitive current activated at approximately -30 mV, while the TEA sensitive I_{DR} activated around -50 mV ($p < 0.05$, $n = 8$; one-sample t-test, current > hypothetical value of 0 nA).

Sample traces in **Figure 3.11Ci** from a young RCGC demonstrates that tail currents (evoked *via* VP3) of the TEA/4-AP insensitive current (isolated in the TEA/4-AP/CdCl$_2$ saline) were larger, slower and more persistent than the TEA sensitive I_{DR} tail currents (isolated *via* subtraction of the TEA/4-AP insensitive current from the 4-AP insensitive current). All tail currents were fitted with a double exponential function ($p < 0.01$, $n = 8$ RCGCs; sum-of-squares *F-test*). **Figure 3.11Cii** confirmed that the TEA/4-AP insensitive current generated significantly larger tail currents than the TEA sensitive I_{DR} ($p < 0.01$, $n = 8$ RCGCs; mixed ANOVA with Bonferroni post-hoc). This plot also showed that the E_{rev} of the TEA/4-AP insensitive current (-31.1 ± 1.09 mV) was significantly more depolarised that the estimated E_{rev} for I_{DR} (-61.2 ± 1.37 mV) ($p < 0.01$, $n = 8$ RCGCs; unpaired t-test). This indicates that the TEA/4-AP insensitive current is not principally conducted by K$^+$ ions.

Figure 3.11Ciii showed that the slower deactivation rate of the TEA/4-AP insensitive current was significant when compared the TEA sensitive I_{DR} ($p < 0.01$, $n = 8$ RCGCs; mixed ANOVA with Bonferroni post-hoc analysis). The tail currents of the TEA/4-AP insensitive current were persistent as deactivation was incomplete 1 s after the +30 mV step had concluded and returned back to the -90 mV holding potential ($p < 0.05$, $n = 8$ RCGCs; one-sample t-test, current > hypothetical value of 0 nA). I_{DR} tail currents had completely deactivated by this point ($p > 0.05$, $n = 8$ RCGCs; one-sample t-test, current > hypothetical value of 0 nA) and thus differed significantly from the TEA/4-AP insensitive sustained current ($p < 0.001$, $n = 8$ RCGCs; unpaired t-test; **Figure 3. 11Civ**).
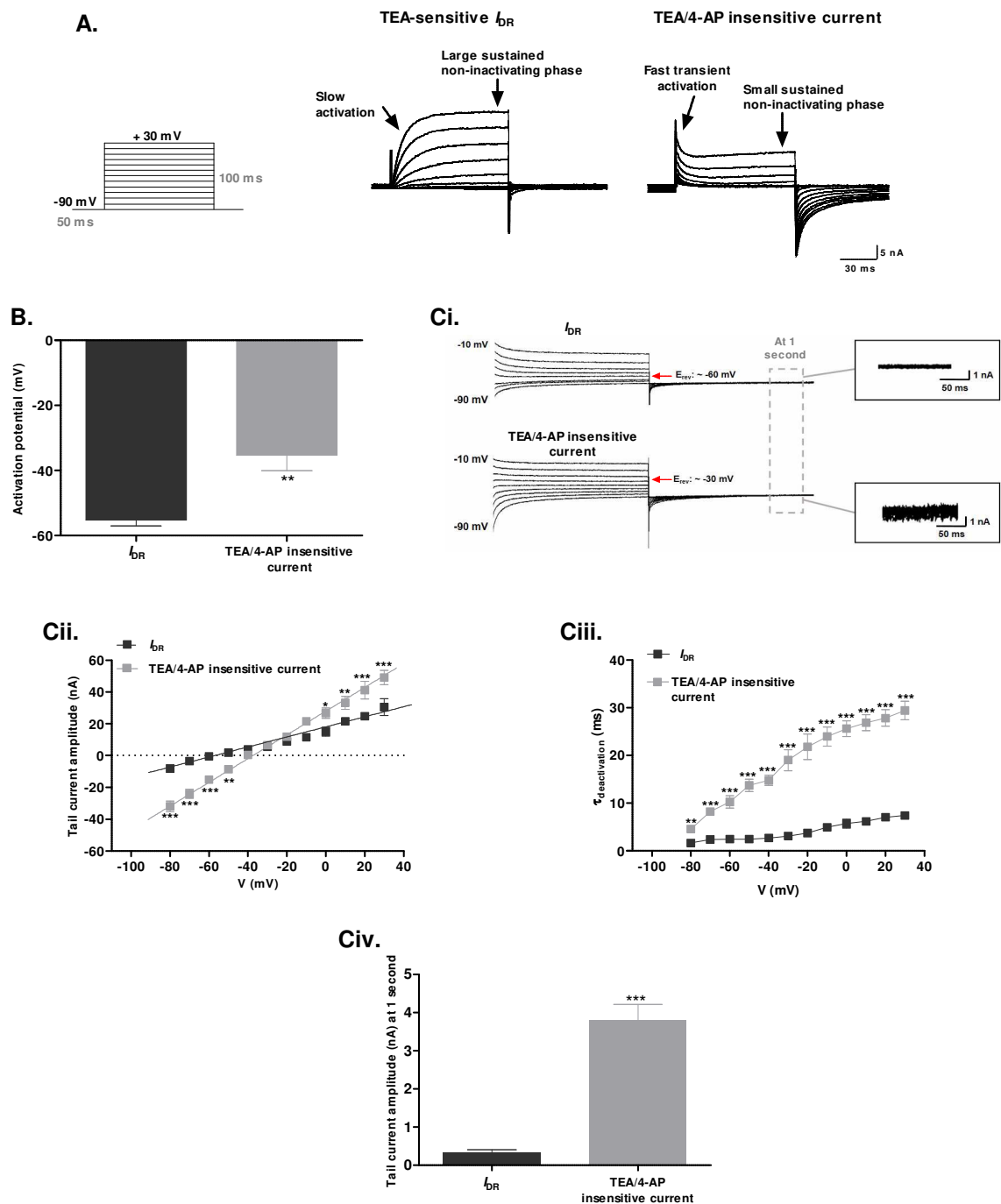
Figure 3.11| TEA sensitive I_{DR} *vs*. TEA/4-AP insensitive current in young CGCs. (A) Sample trace of I_{DR} (right) and the TEA/4-AP insensitive current (left). (B) The sustained TEA/4-AP insensitive current activated ~-30 mV and I_{DR} activated at ~-50 mV. (Ci) Sample traces illustrating differences in the amplitude and decay of tail currents generated by I_{DR} (top) and the TEA/4-AP insensitive current (bottom). (Cii) I_{DR} tail currents were significantly smaller and its estimated E_{rev} is more hyperpolarised than the TEA/4-AP insensitive current. When compared to I_{DR}, the TEA/4-AP insensitive current (Ciii) deactivated significantly slower and a (Civ) significant proportion of this current had still not deactivated 1 second after the +30 mV step of VP3 had concluded. Data shown as mean ± SEM, *n=8* RCGCs. **p<0.01 and***p<0.001 and *vs*. I_{DR}.

3.3.6 Is the TEA/4-AP insensitive current a single current or a mixture of currents?

Figure 3.12A displays a sample trace of the TEA/4-AP insensitive current evoked from a young RCGC in response to VP1 in the TEA/4-AP/$CdCl_2$ saline. This 'biphasic' current consists of an early transient component followed by a sustained non-inactivating component.

Activation thresholds of both the early and sustained component of the TEA/4-AP insensitive current in young CGCs were determined from I-V plots (see **Figures 3.13** and **3.14**, respectively). **Figure 3.12B** revealed that the activation threshold of the early component was significantly more negative than the sustained component ($p < 0.01$, *n=8* RCGCs; unpaired t-test). The early TEA/4-AP insensitive current activated ~-50 mV and the sustained TEA/4-AP insensitive current at ~-30 mV ($p < 0.05$ for both currents, *n=8* RCGCs; one-sample t-test, current > hypothetical value of 0 nA), which strongly indicates that the TEA/4-AP insensitive current is composed of at least two different conductances.
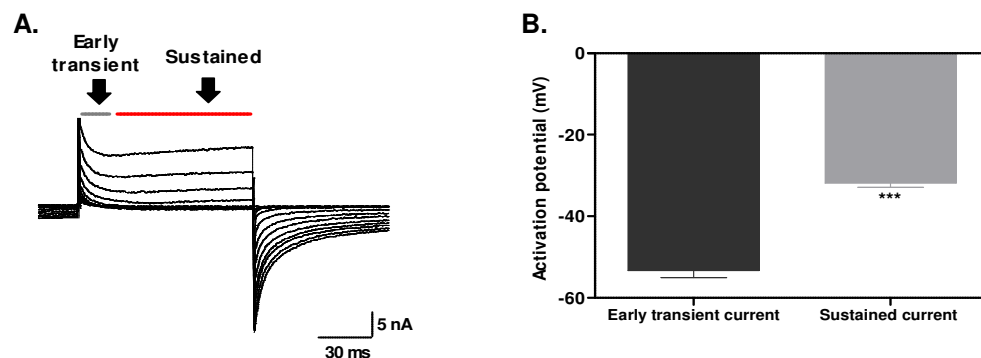
Figure 3.12| Activation threshold of the TEA/4-AP insensitive current. (A) Sample trace of the TEA/4-AP insensitive current evoked by a young RCGC. (B) The early transient component activates at a significantly more hyperpolarised potential (~-50 mV) than the sustained component (~-30 mV). Data shown as mean ± SEM, *n=8* RCGCs. **p<0.01 *vs*. Early transient current.

3.3.6.1 The effects of age and acute OS on the early transient TEA/4-AP insensitive current

Sample traces of the total TEA/4-AP insensitive current in **Figure 3.13A** and the I-V relationship in **Figure 3.13B**, demonstrate that the early transient component of the this current enhanced with age and acute OS ($p < 0.01$, *n=8* RCGCs; mixed ANOVA with Bonferroni post-hoc analysis). There were no significant differences between the old and 3 mM AAPH-treated young CGCs ($p > 0.05$, *n=8* RCGCs).

The activation potential of the early transient TEA/4-AP insensitive current, derived from the I-V curve, was ~-50 mV in all three CGC groups (one-sample t-test, current > hypothetical value of 0 nA) and thus, had not significantly differed from each other ($p > 0.05$, $n=8$ RCGCs; one-way ANOVA with Bonferroni post-hoc analysis).

Activation curves in **Figure 3.13Ci**, showed that old and 3 mM AAPH-treated young CGCs significantly differed from young CGCs ($p < 0.01$, $n=8$ RCGCs; mixed ANOVA), which was due to a rightward shift in V_{50} ($p < 0.01$, $n=8$ RCGCs; one-way ANOVA; **Figure 3.13Cii**).
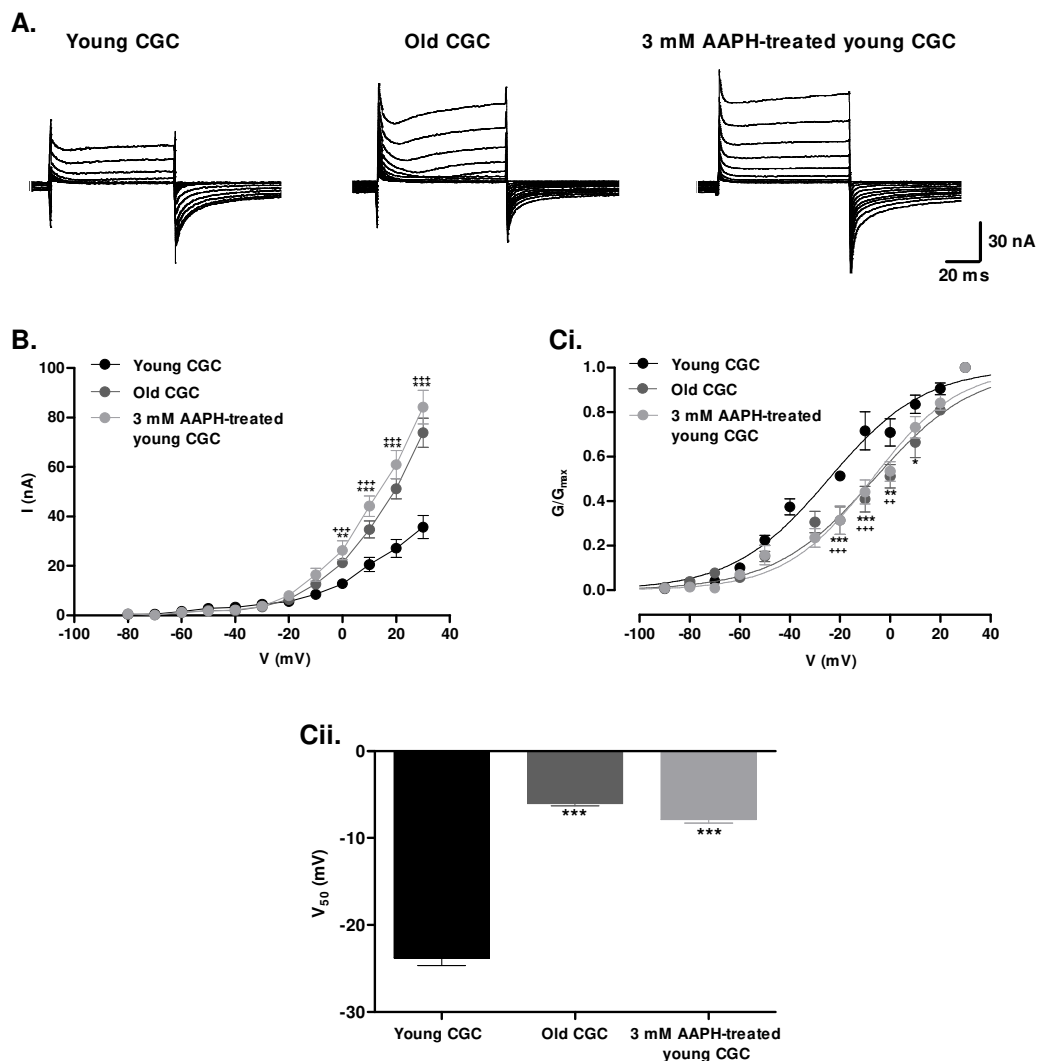
Figure 3.13| Age and acute OS alters the early transient TEA/4-AP insensitive current. (A) Sample traces illustrate that the TEA/4-AP insensitive current is larger in both old and 3 mM AAPH-treated young CGCs. (B) The increase of the early current was significant. (Ci) There was a significant rightward shift in the activation curves with age and acute OS due to a (Cii) decrease in V_{50}. Data shown as mean ± SEM, $n=8$ RCGCs. $^{+/*}p < 0.05$, $^{++/**}p < 0.01$, $^{+++/***}p < 0.001$ vs. young CGCs. Graph symbols: asterisk (*) designated for Old CGCs and plus (+) for 3 mM AAPH-treated young CGCs.

3.3.6.2 The sustained TEA/4-AP insensitive current

The sustained TEA/4-AP insensitive current increased significantly with age and acute OS ($p<0.01$, *n=8* RCGCs*;* mixed ANOVA with Bonferroni post-hoc analysis; **Figure 3.14A**). The amplitude of the sustained current did not differ between old and 3 mM AAPH-treated young CGCs ($p>0.05$, *n=8* RCGCs). Additionally, the activation threshold of the sustained (~-30 mV; one-sample t-test, current > hypothetical value of 0 nA) was not significantly different between the three CGC groups ($p>0.05$, *n=8* RCGCs; one-way ANOVA with Bonferroni post-hoc analysis).

Activation curves for the sustained TEA/4-AP insensitive current from all three CGC groups were well fitted with a global Boltzmann sigmoidal function ($p>0.05$, *n=8* RCGCs*;* extra sum-of-squares *F*-test; **Figure 3.14B**), signifying no significant changes to V_{50} and the slope factor with age or acute OS.

Steady-state inactivation curves in **Figure 3.14Ci** showed that the sustained TEA/4-AP insensitive current exhibited minimal inactivation (*~10%*) in all three CGC groups during 1000 ms step of VP4. A global Boltzmann fit to the steady-state inactivation data was unsuccessful ($p<0.05$, *n=8* RCGCs*;* extra sum-of-squares *F*-test). Individual Boltzmann fits to each preparation revealed that this was due to a significant increase in the slope factor with both age and acute OS ($p<0.05$, *n=8* RCGCs*;* one-way ANOVA; **Figure 3.14Cii**). This indicates that voltage-dependent inactivation of the sustained TEA/4-AP insensitive current is weaker in the old and 3 mM AAPH-treated young CGCs.
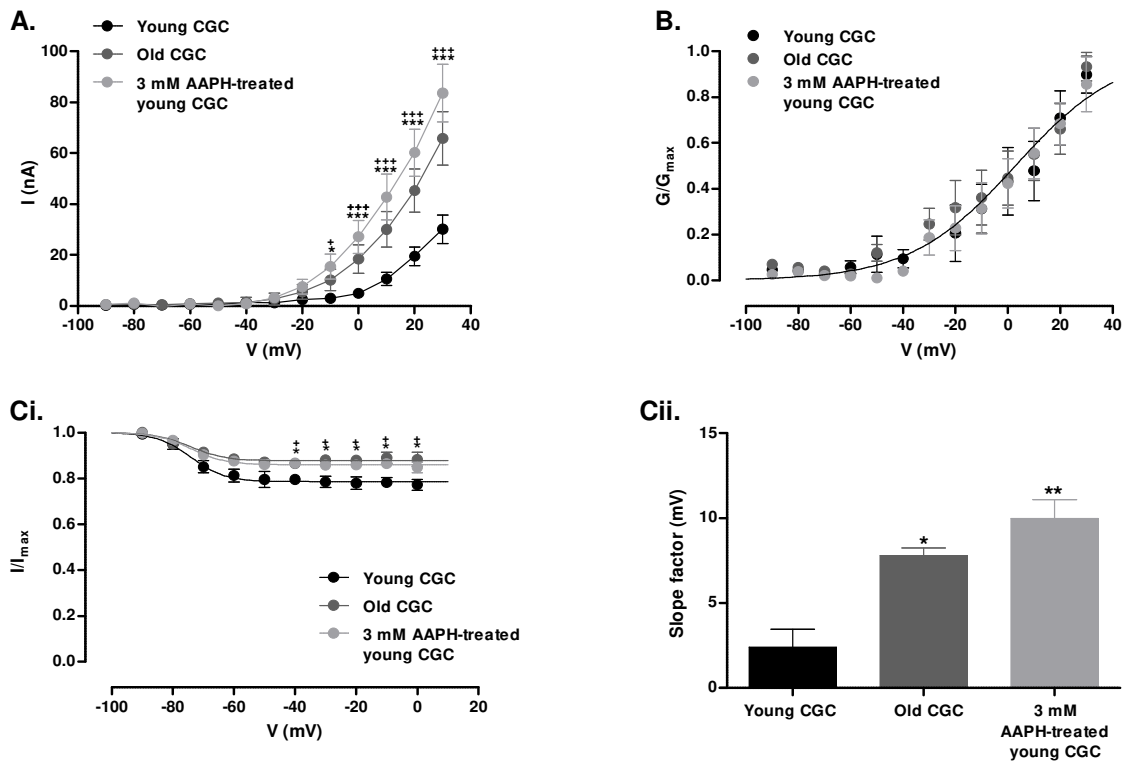
Figure 3.14| Age and acute OS alters the sustained TEA/4-AP insensitive current. (A) This current, which activated around -30 mV, was significant larger in both the old and 3 mM AAPH-treated young CGCs. (B) Activation curves did not significantly change with age or acute OS. (Ci) Steady-state inactivation curves revealed that this conductance undergoes very little inactivation in all three CGC groups. However, curves were less steep in both the old and 3 mM AAPH-treated young CGCs due to (Cii) a significant increase in slope factor. Data shown as mean ± SEM, *n=8* RCGCs. +/*p<0.05, **p<0.01, +++/***p<0.001 *vs.* young CGCs. Graph symbols: asterisk (*) designated for Old CGCs and plus (+) for 3 mM AAPH-treated young CGCs.

3.3.6.3 Age and acute OS alters the TEA/4-AP insensitive current reversal potential

The E_{rev} of the TEA/4-AP insensitive current in the CGCs was examined from tail currents evoked by VP3 in the TEA/4-AP/CdCl₂ saline (**Figure 3.15A**). Tail currents were fitted with a double exponential function in each CGC group (p<0.01, *n=8* RCGCs; sum-of-squares *F-test*).

Figure 3.15B showed that the E_{rev} of the young TEA/4-AP insensitive current (-31.1 ± 1.09 mV) was significantly different from both old (-40.1 ± 0.45 mV) and 3 mM AAPH-treated young CGCs (-41.2 ± 1.84 mV) (p<0.001, *n=8* RCGCs; one-way ANOVA with Bonferroni post-hoc analysis).
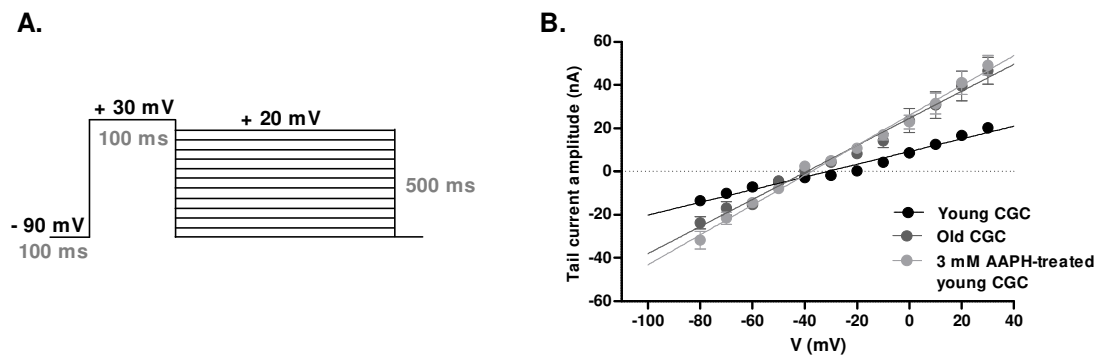
Figure 3.15| Age and acute OS on the E_{rev} of the TEA/4-AP insensitive current. (A) VP3 was utilised to generate the tail currents required for reversal potential analysis. **(B)** The E_{rev} of the TEA/4-AP insensitive current was significantly more hyperpolarised in both old and 3 mM AAPH-treated young CGCs, by ~-10 mV, when compared to young CGCs. Data shown as mean ± SEM, *n=8* RCGCs. ***p<0.001 *vs.* young CGC (part B).

3.3.7   Characterisation of the CGC sustained TEA/4-AP insensitive current

Notably, pharmacological approaches implemented in this study were unable to block the early transient TEA/4-AP insensitive current and at present this current could not be explored further. Thus, this section will characterise the sustained TEA/4-AP insensitive current and examine whether this current changes with age and acute OS.

3.3.7.1   Is the sustained TEA/4-AP insensitive current conducted by chloride ions?

Given that the E_{rev} of the total TEA/4-AP insensitive current was significantly more positive than the estimated E_{rev} for K^+ (**Figure 3.12C**), it was possible that the sustained TEA/4-AP insensitive current was carried by Cl^- ions as its E_{rev} resembled previous descriptions of voltage-gated outward Cl^- currents in vertebrate and other invertebrate neurons[460,490,220].

In **Figure 3.16Ai-ii**, bathing young preparations in a zero Cl^- saline reduced the amplitude of the sustained TEA/4-AP insensitive current, leaving a residual sustained TEA/4-AP/zero Cl^- insensitive current. **Figure 3.16Aii**, showed that subtraction of this residual current from the control sustained TEA/4-AP insensitive current isolated a voltage-gated outward Cl^- current (I_{Cl}).

Figure 3.16B showed that I_{Cl} activated around -35 mV (p<0.05, *n=7* RCGCs; one-sample t-test, current > hypothetical value of 0 nA). Additionally, the amplitude of I_{Cl} was both significantly smaller than the control sustained TEA/4-AP insensitive current and larger

than the TEA/4-AP/zero Cl$^-$ insensitive current at more depolarised potentials (p<0.01 for both, *n=7* RCGCs; mixed ANOVA with Bonferroni post-hoc analysis). This indicates I_{Cl} is the principle contributor of the sustained TEA/4-AP insensitive current in young CGCs.

The effects of established voltage-gated Cl$^-$ channel blockers on the sustained TEA/4-AP insensitive current was also assessed. 100 µM NPPB mimicked the effects of the zero Cl$^-$ saline by reducing the sustained TEA/4-AP insensitive current by ~60% (p>0.05, *n=7* RCGCs; unpaired t-test; **Figure 3.16C**). However, 100 µM DIDS and 1 mM niflumic acid did not alter the sustained TEA/4-AP insensitive current (p>0.05, *n=4* RCGCs; mixed ANOVA; data not shown).
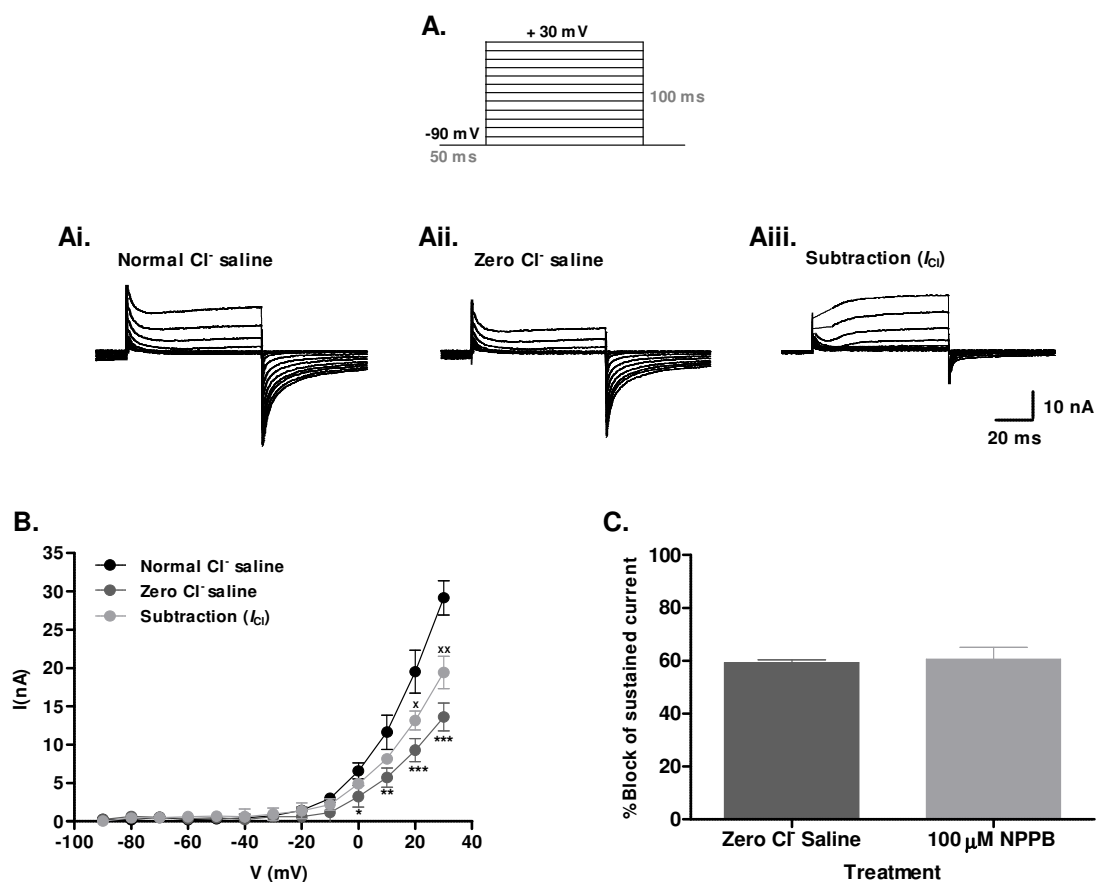
Figure 3.16| I_{Cl} **in young CGCs. (A) Sample traces show that the (Ai) TEA/4-AP insensitive current substantially (Aii) reduced in the zero Cl$^-$ saline, leaving a residual TEA/4-AP/zero Cl$^-$ insensitive current. (Aiii) Subtraction of (Aii) from (Ai) isolated I_{Cl}. (B) The sustained TEA/4-AP insensitive current is predominately conducted by Cl$^-$, as I_{Cl} was significantly larger than the sustained TEA/4-AP/zero Cl$^-$ insensitive current. (C) NPPB mimicked the zero Cl$^-$ saline by reducing the sustained TEA/4-AP insensitive current by ~60%. Data shown as mean ± SEM, *n=7* RCGCs. $^{x/*}$p<0.05, $^{xx/**}$p<0.01 and ***p<0.001. Graph symbols: asterisk (*) designated for zero Cl$^-$ saline and cross (^{x}) for I_{Cl}.**

3.3.7.2 The contribution of I_{Cl} to the large slow persistent tail currents of the sustained TEA/4-AP insensitive current

Figure 3.17A displays sample traces of young CGC tail currents (evoked *via* VP3) of the TEA/4-AP insensitive current, the TEA/4-AP/zero Cl⁻ insensitive current and I_{Cl}. These traces show that I_{Cl} exhibited faster deactivation kinetics than the other two currents and analysis confirmed this following the successful double exponential fit to the tail currents of each conductance ($p < 0.01$, *n=7* RCGCs; sum-of-squares *F-test*).

Tail currents of both the TEA/4-AP insensitive current and the TEA/4-AP/zero Cl⁻ insensitive current were significantly larger in amplitude than I_{Cl} tail currents ($p < 0.01$, *n=7* RCGCs; mixed ANOVA with Bonferroni post-hoc analysis; **Figure 3.17B**). There was no significant difference between the TEA/4-AP insensitive current and the TEA/4-AP/zero Cl⁻ insensitive current ($p > 0.05$, *n=7* RCGCs). This indicates that the large tail currents of the TEA/4-AP insensitive current are not principle mediated by the deactivation of I_{Cl}.

In **Figure 3.17C**, the slow decaying tail currents of the sustained TEA/4-AP insensitive current was due to the deactivation properties of the sustained TEA/4-AP/zero Cl⁻ insensitive current as the deactivation time constant did not significantly differ between these two conductances ($p < 0.001$, *n=7* RCGCs). I_{Cl} did not contribute towards the slow deactivation kinetics of the sustained TEA/4-AP insensitive current as its tail currents decayed significantly faster ($p < 0.01$, *n=7* RCGCs).

The persistent nature of the sustained TEA/4-AP insensitive tail currents was also due to the TEA/4-AP/zero Cl⁻ insensitive current, as tail current amplitudes did not significantly differ between these conductances when measured at the -90 mV holding potential 1 s after the +30 mV step had concluded ($p > 0.05$, *n=7* RCGCs; one-way ANOVA with Bonferroni post-hoc analysis; **Figure 3.17D**). Conversely, I_{Cl} tail currents significantly deactivated by this time point ($p < 0.001$ *vs.* both currents, *n=7* RCGCs).
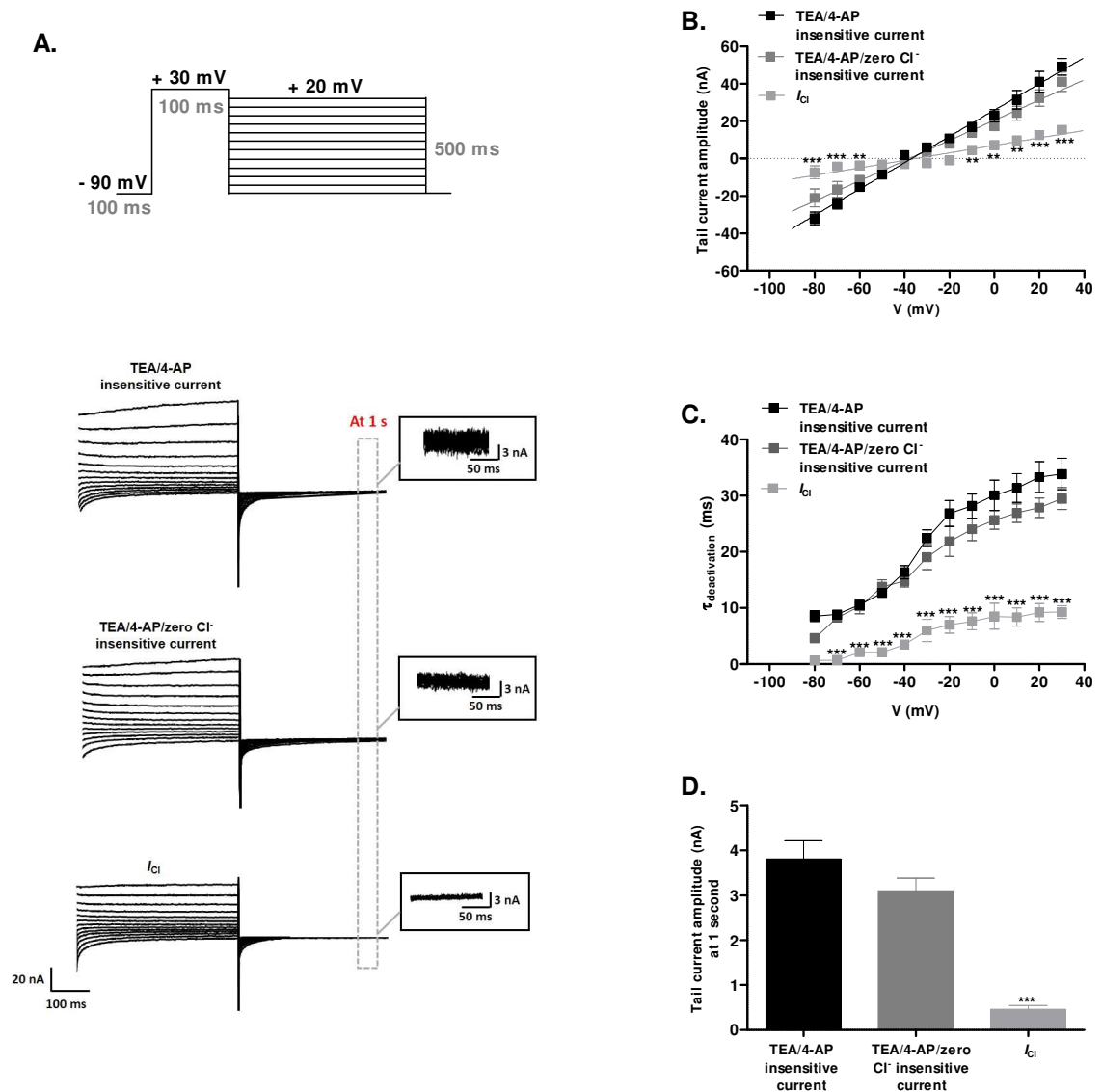
Figure 3.17| Comparison of deactivation properties. (A) Sample traces of deactivating tail currents evoked (*via* VP3) by the sustained TEA/4-AP insensitive current, sustained TEA/4-AP/zero Cl⁻ insensitive current and *I*Cl in young RCGCs. The deactivating *I*Cl tail currents were significantly (B) smaller in amplitude, (C) decayed faster, and (D) were not persistent when compared to tail currents of the TEA/4-AP insensitive current and TEA/4-AP/zero Cl⁻ insensitive current. (B-D) The deactivation kinetics of the TEA/4-AP/zero Cl⁻ insensitive current did not differ significantly from the TEA/4-AP insensitive current. Data shown as mean ± SEM, *n=7* RCGCs. **p<0.01, ***p<0.001 *vs.* sustained TEA/4-AP insensitive current and sustained TEA/4-AP/zero Cl⁻ insensitive current.

3.3.7.3 Does I_{Cl} change with age and acute OS?

In contrast to the young CGCs (see **Figure 3.16C**), 100 µM NPPB did not alter the amplitude of the sustained TEA/4-AP insensitive current in both old (**Figure 3.18Ai**) and 3 mM AAPH-treated young CGCs (**Figure 3.18Aii**) (p>0.05, *n=7* RCGCs; mixed ANOVA Bonferroni post-hoc analysis).

This was not due to changes in the sensitivity of the voltage-gated chloride channels to NPPB, as the perfusion with a zero Cl⁻ saline also failed to significantly reduce the TEA/4-AP insensitive current in the old CGCs (**Figure 3.18Bi**) and 3 mM AAPH-treated young CGCs (**Figure 3.18Bii**) (p>0.05, *n=3* RCGCs). This suggests that I_{Cl} is suppressed with age and acute OS.

The residual sustained TEA/4-AP/NPPB insensitive current was significantly larger in both the old and 3 mM AAPH-treated young CGCs when compared to young control CGCs (p<0.001, *n=7* RCGCs; **Figure 3.18C**).
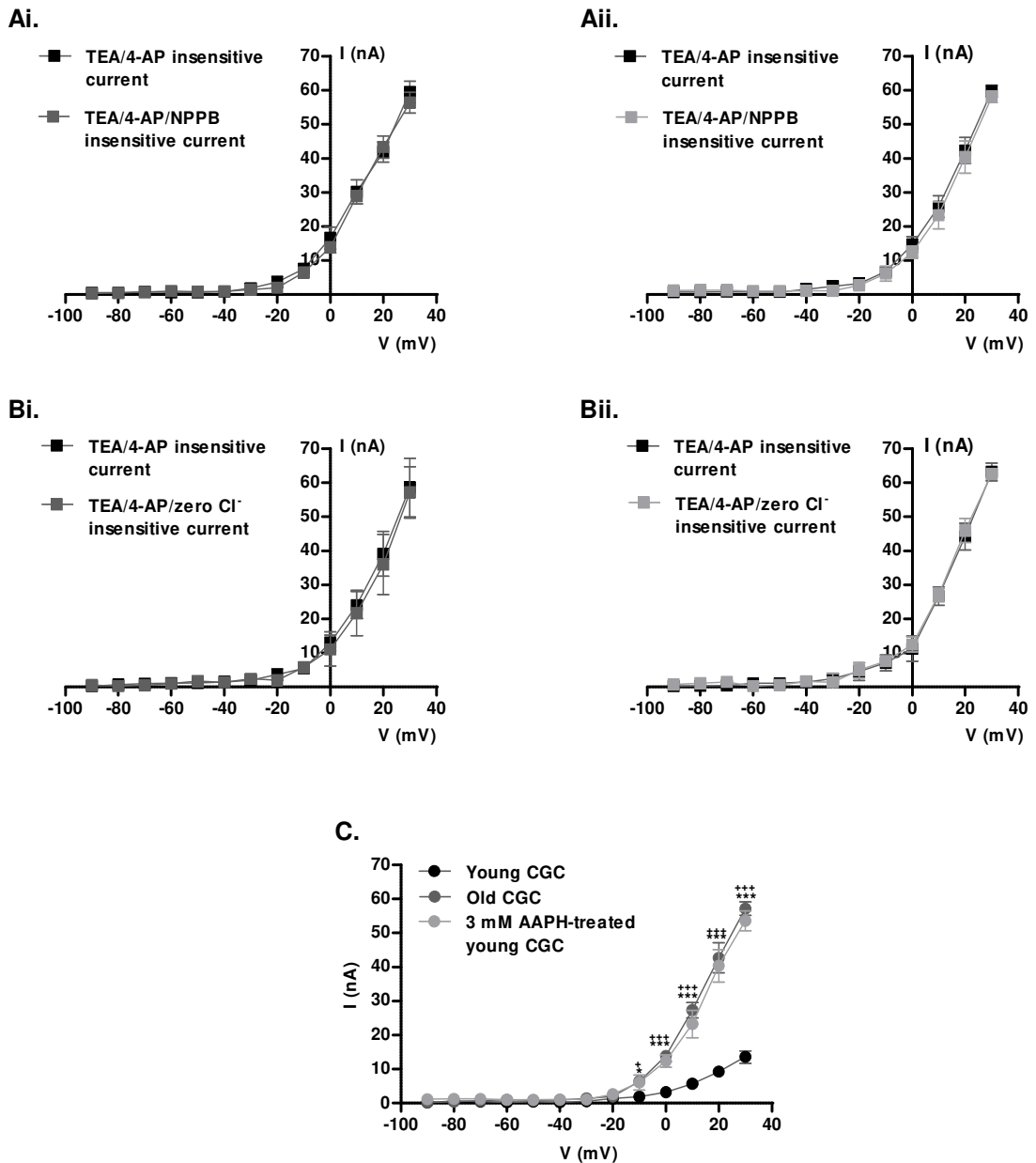
Figure 3.18| I_{Cl} **is altered with age and acute OS. (A) NPPB did not decrease the sustained TEA/4-AP insensitive current in (Ai) old or (Aii) 3 mM AAPH-treated young CGCs. The zero Cl⁻ saline also did not alter this current in (Bi) old or (Bii) 3 mM AAPH-treated young CGCs. (C) The residual sustained TEA/4-AP/NPPB insensitive current increased significantly with age and acute OS. Data shown as mean ± SEM,** *n=3-7* **RCGCs.** $^{+++}$**/*** **p<0.001** *vs.* **young CGCs. Graph symbols: asterisk (*) designated for Old CGC and cross (ˣ) for 3 mM AAPH-treated young CGC.**

3.3.8   Reversal potential and deactivation of the sustained TEA/4-AP/zero Cl⁻ insensitive current

An initial question raised was whether suppression of I_{Cl} with age and acute OS was responsible for the hyperpolarising shift to the E_{rev} of the TEA/4-AP insensitive current (see **Figure 3.12A**).

Figure 3.19A, tail currents recorded in the TEA/4-AP/zero Cl⁻ saline and fitted with a double exponential function ($p > 0.05$, *n=7* RCGCs*; sum-of-squares *F-test*) showed a leftward shift in the E_{rev} when compared to that of the TEA/4-AP insensitive current in the young CGCs. This hyperpolarising shift to the E_{rev} from -31.1 ± 1.09 mV in the TEA/4-AP saline to -46.2 ± 3.82 mV following perfusion in the zero Cl⁻ saline was significant ($p < 0.05$, *n=7* RCGCs; paired t-test). This indicates that suppression of I_{Cl} with age and acute OS is responsible for the hyperpolarised E_{rev} of the TEA/4-AP insensitive current.

Figure 3.19B revealed that E_{rev} for the TEA/4-AP/zero Cl⁻ insensitive current in young CGCs did not significantly differ from that of the old (-40.1 ± 0.45mV) and 3 mM AAPH-treated young CGCs (-41.2 ± 1.84 mV) ($p > 0.05$, *n=7* RCGCs; one-way ANOVA with Bonferroni post-hoc analysis). Notably, the E_{rev} of the sustained TEA/4-AP insensitive current did not significantly change when Cl⁻ ions were removed from the extracellular saline in both old and 3 mM AAPH-treated young CGCs ($p > 0.05$ for both, *n=7* RCGCs*, paired t-test; data not shown). This demonstrates that in addition to I_{Cl} there is another previously unreported current, the sustained TEA/4-AP/zero Cl⁻ insensitive current, conducted by the CGCs.

Figure 3.19B also showed that the tail current amplitude of the sustained TEA/4-AP/zero Cl⁻ insensitive current increased significantly in old and 3 mM AAPH-treated young CGCs when compared to young CGCs ($p < 0.001$, *n=7* RCGCs*; mixed ANOVA with Bonferroni post-hoc analysis).

The rate of deactivation of the TEA/4-AP/zero Cl⁻ insensitive current was significantly slower with age and acute OS ($p < 0.001$ for both, *n=7* RCGCs; **Figure 3.19C**). Lastly, the persistent TEA/4-AP/zero Cl⁻ insensitive tail currents were also significantly larger (measured 1 second following the voltage drop from +30 mV command potential to the -90 mV holding potential) in both old and 3 mM AAPH-treated young CGCs when compared to young CGCs ($p < 0.001$, *n=7* RCGCs; one-way ANOVA with Bonferroni post-hoc analysis; **Figure 3.19D**).
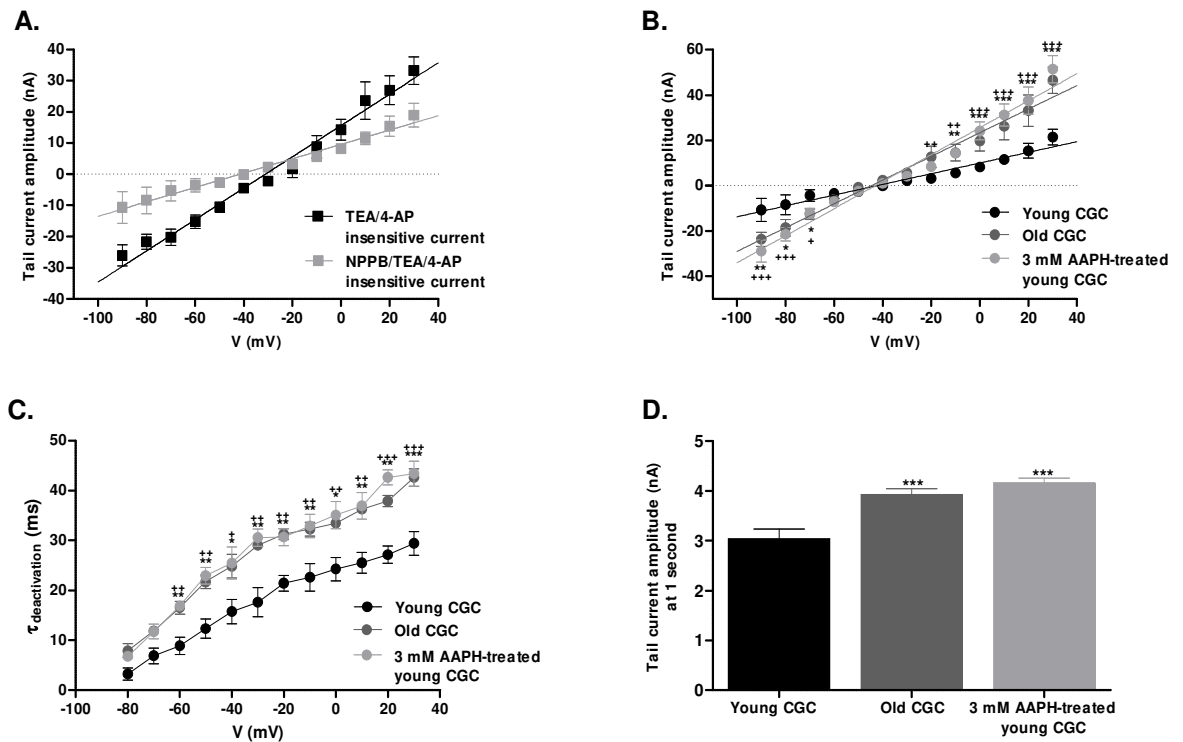
Figure 3.19| The sustained TEA/4-AP/zero Cl⁻ insensitive current with age and acute OS. (A) Inhibition of I_{Cl} in young CGCs caused a significant leftward shift in the E_{rev} of the sustained TEA/4-AP/zero Cl⁻ insensitive current. **(B)** The E_{rev} of the TEA/4-AP/zero Cl⁻ insensitive current did not significantly differ between the three CGC groups. However, the amplitude of the deactivating tail currents increased significantly with age and acute OS. Additionally, deactivation of the sustained TEA/4-AP/zero Cl⁻ insensitive current was significantly **(C)** slower and **(D)** more persistent in these CGCs. Data shown as mean ± SEM, *n=7* RCGCs. $^{+/*}p<0.05$, $^{++/**}p<0.01$, $^{+++/***}p<0.001$ *vs.* young CGC. Graph symbols: asterisk (*) designated for Old CGC and plus (⁺) for 3 mM AAPH-treated young CGC (part B-C).

3.3.9   What is the sustained TEA/4-AP/zero Cl⁻ insensitive current?

The lack of I_{Cl} in both old and 3 mM AAPH-treated young CGCs was a surprising revelation as it was being masked by the significant increase in the TEA/4-AP/zero Cl⁻ insensitive current. Thus, this section will examine this residual current with the aim of developing a better understanding of the nature of this current.

3.3.9.1   Sustained TEA/4-AP/zero Cl⁻ insensitive current *vs.* I_{Cl}

Figure 3.20Ai displays sample current traces (evoked *via* VP1) from a young RCGC. The TEA/4-AP/zero Cl⁻ insensitive current exhibits a biphasic phenotype with its fast activation followed by a small sustained component. This differs from I_{Cl}, which activates slower into a larger sustained component (**Figure 3.16B** for comparison of current amplitudes). The activation threshold of the two currents also significantly differed (p<0.05, *n=7* RCGCs; paired t-test; Figure **3.20Aii**). I_{Cl} activated at around -35 mV, whilst the sustained TEA/4-AP/zero Cl⁻ insensitive current activated around -20 mV (p<0.05 for both, *n=7* RCGCs*;* one-sample t-test, current > hypothetical value of 0 nA). Findings from **Figure 3.20A**, along with the differences in the deactivation kinetics between these two currents (see **Figure 3.17**) suggests that these currents may be mediated by different channels.

Comparisons of the activation and inactivation properties of these two sustained currents, however, suggests otherwise. The activation curve in **Figure 3.20B** was fitted successfully with a global Boltzmann sigmoidal function, indicating no significant shift in V_{50} or slope factor between the two currents (p>0.05, *n=7* RCGCs; mixed ANOVA with Bonferroni post-hoc analysis). Steady-state inactivation curves in **Figure 3.20C**, showed that both these currents exhibited very little inactivation. Despite a global Boltzmann fit between the currents being unsuccessful, there were no significant changes to V_{50} or slope factor (p>0.05 for both, *n=7* RCGCs*;* unpaired t-test; data not shown).
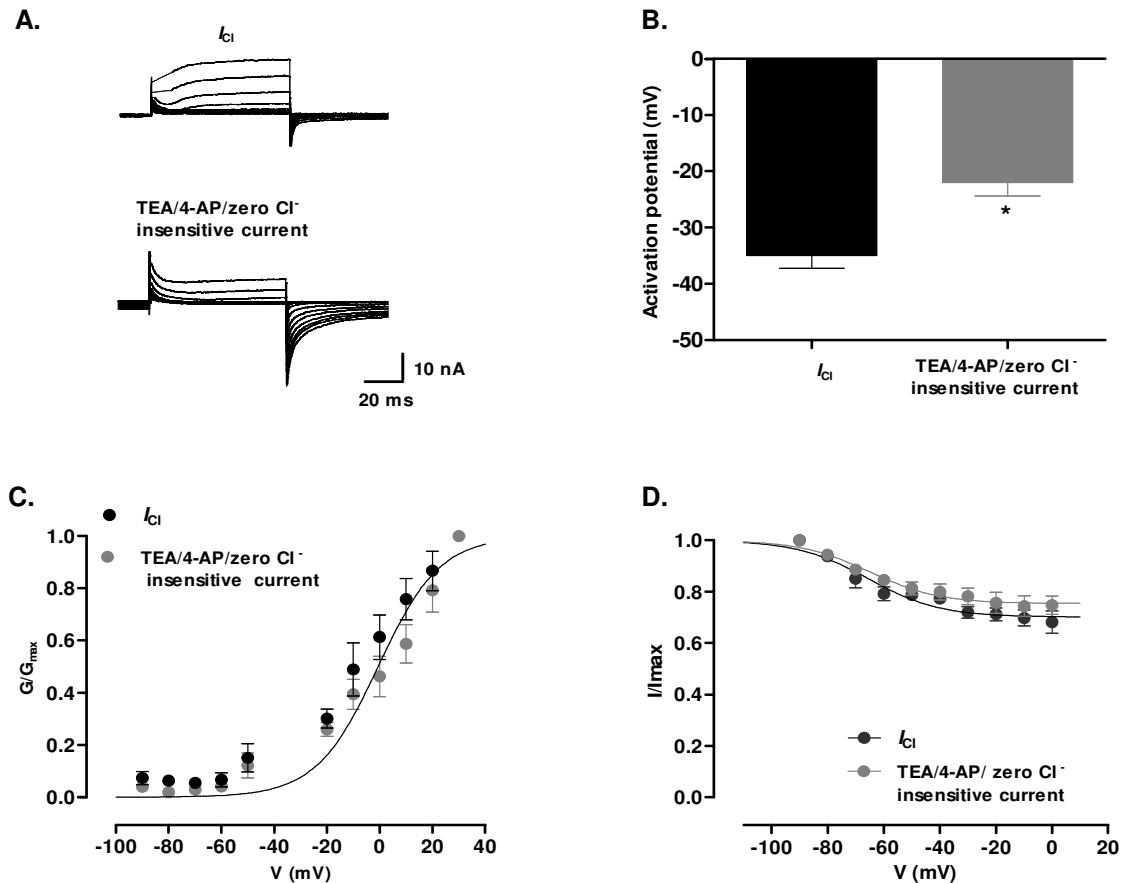
Figure 3.20| TEA/4-AP/zero Cl- insensitive current and I_{Cl} in young CGCs. (A) Sample traces illustrate that the TEA/4-AP/ zero Cl- insensitive current activates fast and is followed by a small sustained component. I_{Cl} activates slowly into a larger sustained component. (B) The activation threshold of the TEA/4-AP/zero Cl- insensitive current (~-20 mV) was significantly more depolarised than I_{Cl} (~-35 mV). The (C) activation and (D) steady-state inactivation properties between the two currents did not significantly differ. Data shown as mean ± SEM, *n=7* RCGCs. *p<0.05, **p<0.01 *vs*. I_{Cl}.

3.3.9.2 Is the sustained TEA/4-AP/zero Cl⁻ insensitive current a proton current?

In **Figure 3.21Ai**, the I-V relationship of the sustained TEA/4-AP/zero Cl⁻ insensitive current in young CGCs revealed that altering the extracellular proton concentration (10-fold from pH 7.9 to pH 6.9) did not alter the amplitude of the current (p>0.05, *n=3* RCGCs; mixed ANOVA with Bonferroni post-hoc analysis). The E_{rev} of the TEA/4-AP/zero Cl⁻ insensitive current also did not change in response to altering the extracellular pH (p>0.05, *n=3* RCGCs; **Figure 3.21Aii**) and therefore, demonstrated that young CGCs do not conduct a voltage-gated outward proton current.

Despite this, it was still possible that the increase in the sustained TEA/4-AP/zero Cl⁻ insensitive current with age and acute OS could be due to a proton current. However, as

with young CGCs, altering the extracellular pH did not significantly change the amplitude or shift the E_{rev} of the current in the old CGCs (p>0.05, *n=3* RCGCs; **Figure 3.21Bi-Bii**) and 3 mM AAPH-treated young CGCs (p>0.05, *n=3* RCGCs; **Figure 3.21Ci-Cii**).
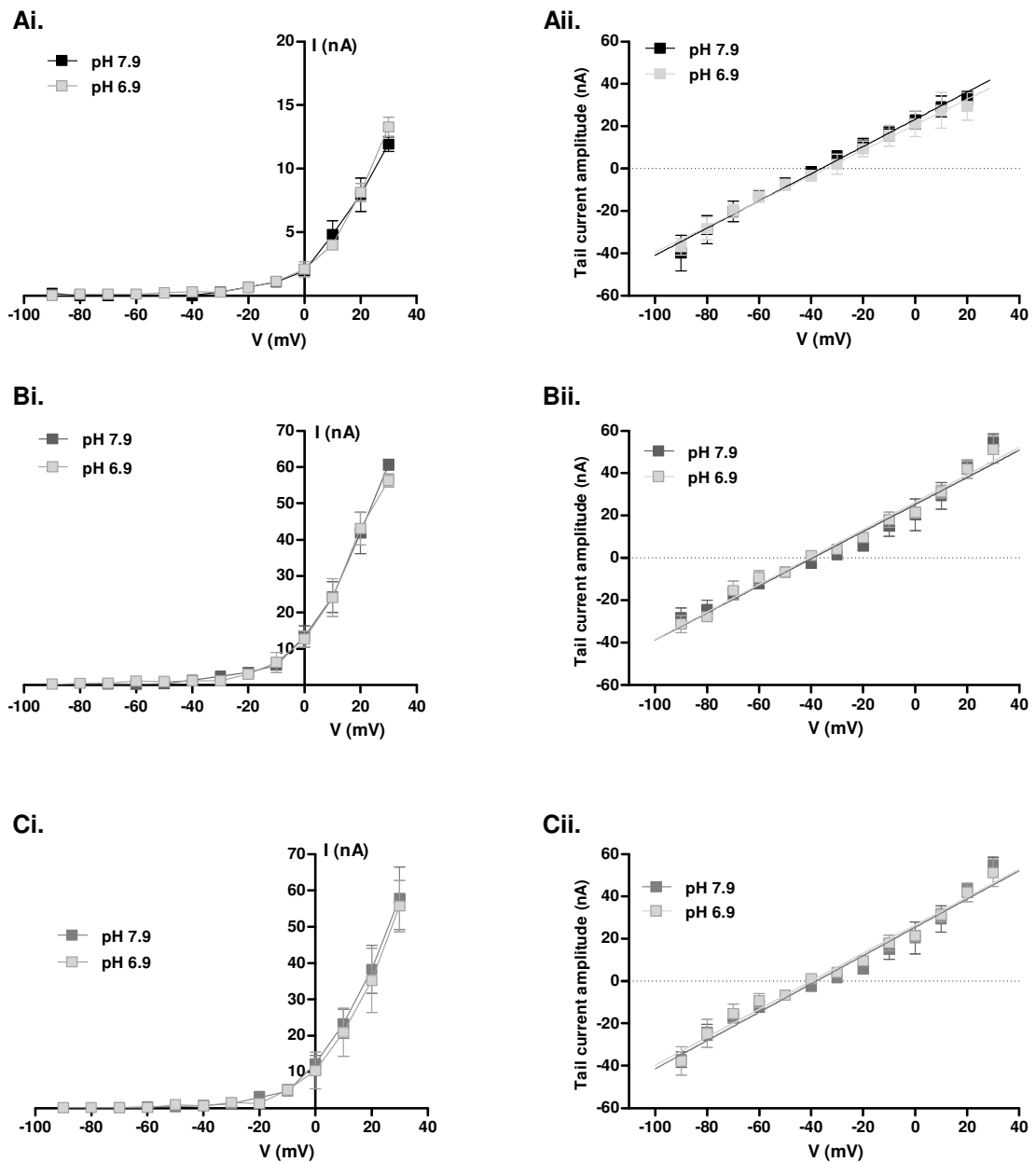
Figure 3.21| Do the CGCs conduct a voltage-gated outward proton current? Increasing the extracellular proton concentration (from pH 7.9 to pH 6.9) did not alter the (Ai-Ci) amplitude of the sustained TEA/4-AP/zero Cl⁻ insensitive current or (Aii-Ciii) shift its E_{rev} in the young, old and 3 mM AAPH-treated young CGCs, respectively. Data shown as mean ± SEM, *n=3* RCGCs. NS, p>0.05.

3.3.10   The action potential waveform of the *Lymnaea* CGCs

To better understand the role of voltage-gated outward currents in shaping the CGC action potential, a young RCGC action potential waveform was used as the voltage clamp

command during AP-clamp experimental recordings. I_A, I_{DR}, I_{Cl} and the TEA/4-AP/NPPB insensitive currents were isolated in young CGCs in the same manner (in terms of saline solutions utilised and digital subtractions) as when performing voltage step protocols (**section 3.3.3-3.3.7**).

In **Figure 3.22A**, AP1 (protocol from -50 mV holding potential) evoked currents in young CGCs revealed that the 4-AP sensitive isolated I_A activated around the RMP and was the only current active until the membrane potential had surpassed the CGC action potential threshold (~-45 mV). During the rising phase of the young CGC action potential, I_A continued to rapidly increase. This phase of the CGC action potential command then sequentially activated I_{DR} (~ -40 mV), I_{Cl} (~ -35 mV) and TEA/4-AP/NPPB insensitive current (~-20 mV).

The peak of the CGC action potential corresponded with the establishment of the I_A peak. From the start of repolarisation, I_A decreased as it started to inactivate, while I_{DR}, I_{Cl} and TEA/4-AP/NPPB insensitive currents increased further to reach their maximal amplitude slightly later at the "shoulder" of the CGC action potential command (~0 mV).

Before the occurrence of the fAHP, both I_{Cl} and TEA/4-AP/NPPB insensitive current amplitudes returned to zero. Conversely, both I_A and I_{DR} currents were still active at this point and contributed a similar proportion to the fAHP. However, both these currents were no longer active when the sAHP developed.

Figure 3.22B, reveals the contribution each conductance makes to the total outward current mediating a single young CGC action potential. I_A was the predominant contributor (49%) as its magnitude (area under the curve) was substantially larger than I_{DR} (p>0.05, $n=6$ RCGCs; one-way ANOVA with Bonferroni post-hoc analysis) and significantly larger than both I_{Cl} (p<0.05, $n=6$ RCGCs) and the TEA/4-AP/ NPPB insensitive current (p<0.01, $n=6$ RCGCs). I_{DR} was the second major contributor (35%) to the total voltage-gated outward current as it was significantly larger than both I_{Cl} (p<0.05, $n=6$ RCGCs) and the TEA/4-AP/NPPB insensitive current (p<0.05, $n=6$ RCGCs). I_{Cl} represented 9% of the total outward current of a young CGC action potential while the TEA/4-AP/NPPB insensitive current made up 7%. This very slight difference in magnitude between these two conductances was not significant (p>0.05, $n=6$ RCGCs).
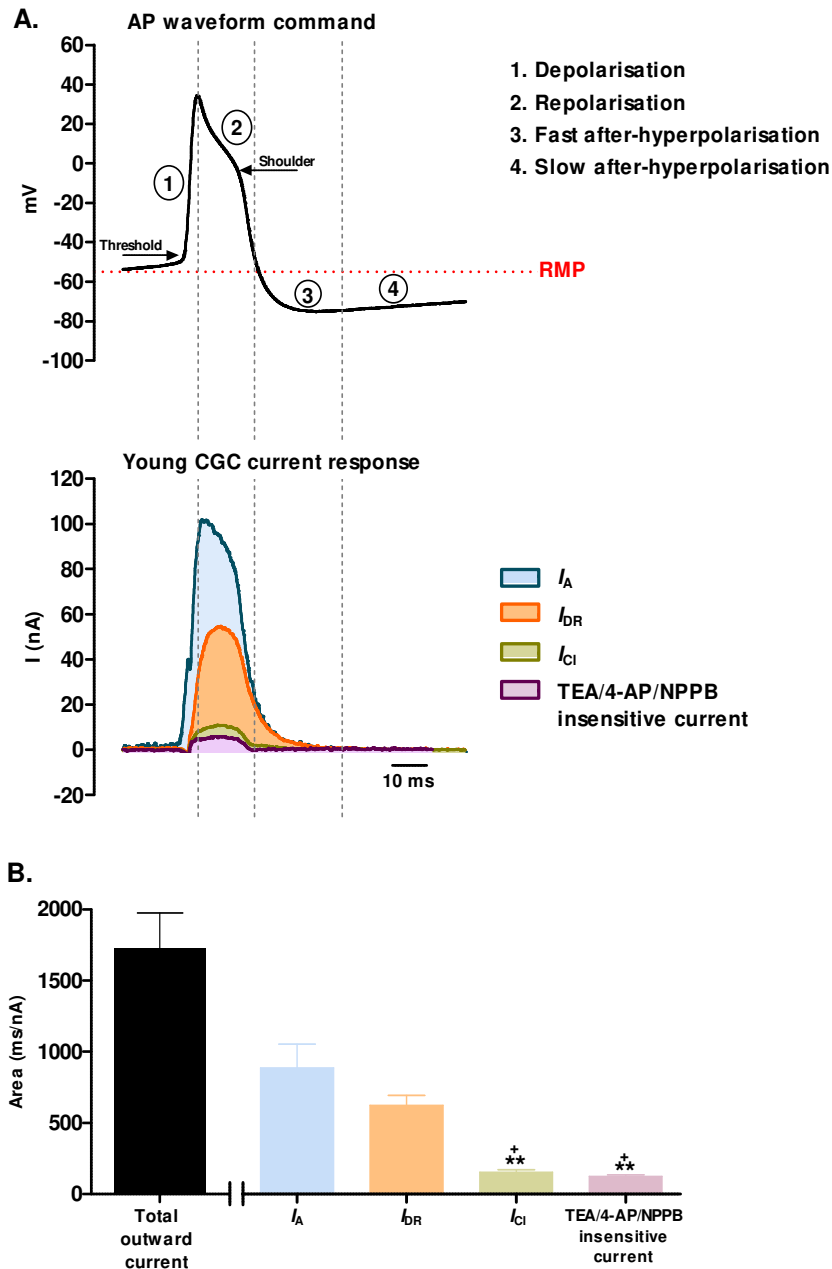
Figure 3.22| Profiling voltage-gated outward currents in a young CGC action potential.
(A) I_A, during the AP-waveform command, activated near the RMP (-50 mV), reached
maximal conductance at the action potential peak and inactivated prior to the onset of
the sAHP. I_{DR} activated during the rising phase of the action potential, reached maximal
conductance at the shoulder of the repolarising action potential and deactivated before
the sAHP commenced. Both I_{Cl} and the TEA/4-AP/NPPB insensitive current activated
during depolarisation, reached maximal conductance at the shoulder of the repolarising
action potential, and appeared to have completely deactivated prior the onset of the
fAHP. (B) I_A is the largest voltage-gated outward current active during the action
potential, closely followed by I_{DR}, then I_{Cl} and finally the TEA/4-AP/NPPB insensitive
current. Data shown as mean ± SEM, *n=6* RCGCs. [+]p<0.05 *vs.* I_{DR} and **p<0.01 *vs.* I_A
(part B).

3.3.11 The inward rectifier K$^+$ current of *Lymnaea* CGCs

An additional voltage-gated K$^+$ current of interest in this thesis was the inward rectifier (I_R). As the name suggests, unlike the other voltage-gated K$^+$ currents, this current is an inward K$^+$ conductance. It has previously been shown in other organisms that this current has an important role in regulating neuronal firing and the RMP, but little is known about its contribution to the age-related decrease in neuronal firing[130,162].

3.3.11.1 Characterisation of I_R

Initial characterisation of I_R was performed on young RCGCs perfused in a zero-Na$^+$/CdCl$_2$ saline. To elicit I_R, CGCs were held at -20 mV before conducting hyperpolarising steps from -20 mV to -140 mV (VP5; **Figure 3.23Ai**). **Figure 3.23Aii** shows a typical trace of the evoked current and reveals that I_R is a fast activating and fast inactivating current.

The sample trace in **Figure 3.23Bi** of I_R evoked at -140 mV command potential from -20 mV holding potential of VP5, illustrates that increasing the extracellular K$^+$ concentration 10-fold from 1.6 mM to 16 mM greatly increases the amplitude of the current. Indeed, this increase was statistically significant (p<0.001, *n=6* RCGCs; mixed ANOVA with Bonferroni post-hoc analysis **Figure 3.23Bii**).

Figure 3.23Bii also revealed that the estimated E$_{rev}$ of I_R shifted from ~-60 mV in normal K$^+$ saline to ~-20 mV in the high K$^+$ saline. This shift was approximately 40 mV and deviated slightly from the 58 mV shift prediction calculated in accordance to the Nernst equation if K$^+$ was the sole conducting ion through this channel.

The sensitivity of the CGC I_R to extracellular blockers was then explored (**Figure 3.23C**). The addition of 4 mM barium chloride or 2 mM caesium chloride to the zero-Na$^+$/CdCl$_2$ saline both failed to alter the amplitude of I_R when compared to the control recorded in the zero-Na$^+$/CdCl$_2$ saline (p>0.05, *n=4-6* RCGCs*;* mixed ANOVA with Bonferroni post-hoc analysis). Perfusion of preparations in a 50 mM TEA/CdCl$_2$ saline also did not significantly alter the amplitude of the CGC I_R when compared to the control (p>0.05, *n=4-6* RCGCs).
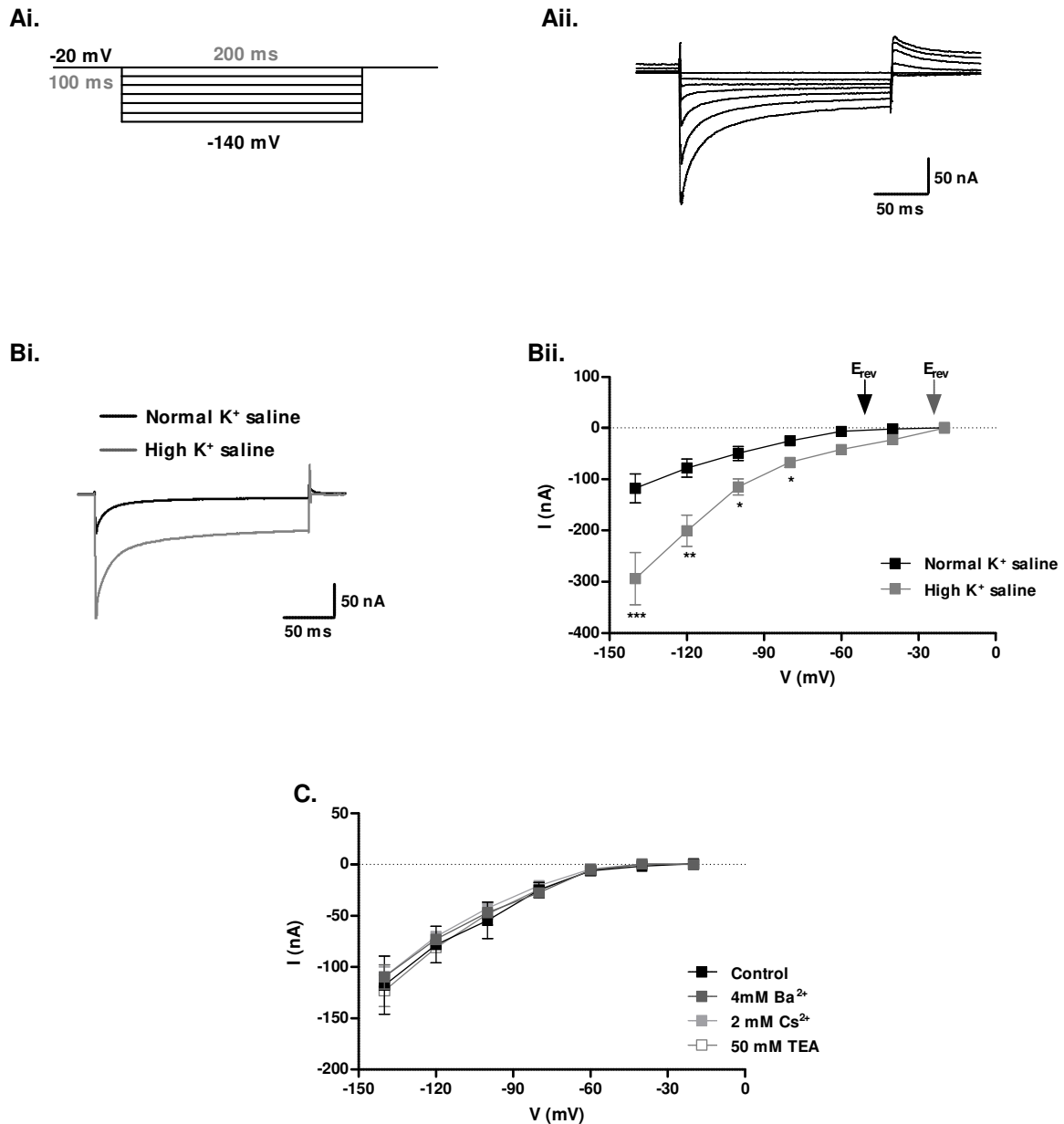
Figure 3.23| I_R in the CGCs. (Ai) VP5 evoked I_R in young RCGCs bathed in the zero-Na$^+$/CdCl$_2$ saline. (Aii) Sample trace of I_R illustrates that this current activates and inactivates relatively fast. (Bi) Sample trace of I_R evoked from -140 mV command potential demonstrates that this current substantially increased following the increase in the extracellular K$^+$ concentration from 1.6 mM to 16 mM. (Bii) This increase was significant and was accompanied with a rightward shift in the estimated E$_{rev}$ of K$^+$, from ~-60 mV in the normal K$^+$ saline (black arrow) to ~-20 mV in the high K$^+$ saline (grey arrow). (C) The CGC I_R is Ba^{2+}, Cs^{2+} and TEA insensitive. Data shown as mean ± SEM, n=4-6 RCGCs. *p<0.05, ***p<0.001 vs. normal K$^+$ saline (part Bii).

3.3.11.2 Do the properties of I_R change with age and acute OS?

The I-V relationship for I_R in **Figure 3.24A** showed that there was no significant change to the amplitude of this current between young, old and 3 mM AAPH-treated young CGCs (p>0.05, *n=6* RCGCs*;* mixed ANOVA with Bonferroni post-hoc analysis).

In **Figure 3.24B**, I_R activation curves (G/G$_{max}$ *vs.* voltage) could be fitted with a global Boltzmann sigmoidal function (p>0.05, *n=6;* extra sum-of-squares *F-test*), indicating that there were no significant changes to the V$_{50}$ or slope factor parameters between the three CGC groups (p>0.05, *n=6* RCGCs; mixed ANOVA with Bonferroni post-hoc analysis).

Given that the CGC I_R is fast inactivating, it was of interest to observe whether there were changes to the rate of inactivation with age or acute OS. The time constant for I_R inactivation was measured by successfully fitting a single exponential function from the peak to the trough of the current. **Figure 3.24C** shows that while the I_R time constants of inactivation appeared faster in both the old and 3 mM AAPH-treated young CGCs when compared to the young CGCs, this difference did not reach statistical significance (p>0.05, *n=6* RCGCs; mixed ANOVA with Bonferroni post-hoc analysis).

The steady-state inactivation properties of I_R were also investigated to determine if there were any changes to the voltage-dependence of inactivation. Using the protocol (VP6) shown in **Figure 3.24D**, I_R in young, old and 3 mM AAPH-treated young CGCs did not fully inactivate (~20% of the current was still active). A global Boltzmann sigmoidal function could be fitted to the data and this indicated that there was no significant difference to the V$_{50}$ or slope factor parameters between the three CGC groups (p>0.05, *n=6* RCGCs*;* extra sum-of-squares *F-test*).
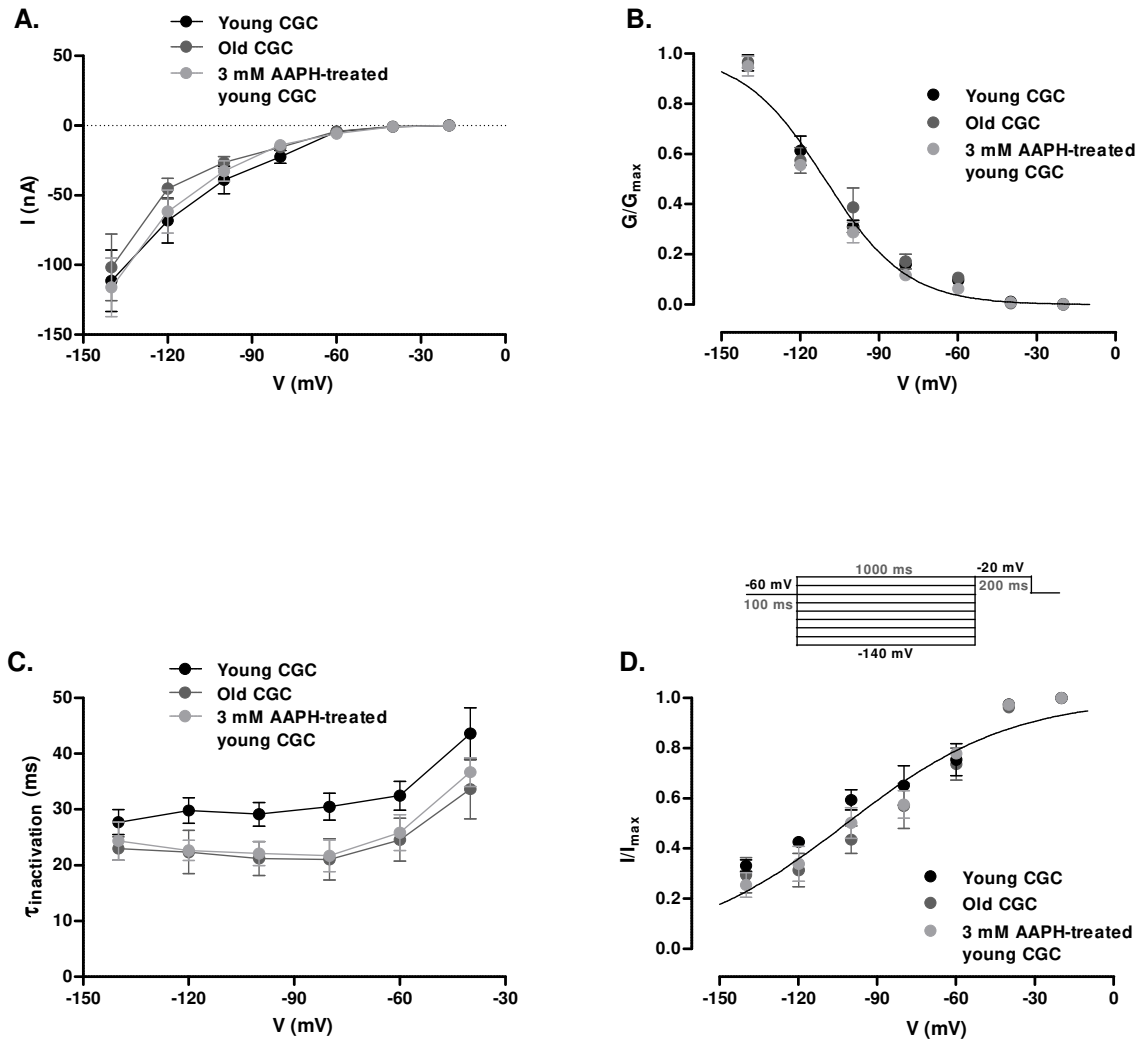
Figure 3.24| The effects of age and acute OS on I_R. (A) The peak amplitude and (B) activation properties (V_{50} and slope factor) of I_R did not significantly differ between the three CGC groups. (C) I_R in old and 3 mM AAPH-treated young CGCs inactivated slightly faster than the young CGCs, however, this was not significant. (D) VP6 was executed to examine the inactivation properties of the CGC I_R. The accompanying plot, fitted with a global Boltzmann sigmoidal function, reveals that there were no significant changes to inactivation properties with age or acute OS. Data shown as mean ± SEM, *n=6* RCGCs. NS, p>0.05.

3.3.14 Results summary of the changes to voltage-gated outward currents of the CGCs with age and acute OS

Current	Parameter	Young CGCs	Parameter altered in old CGCs?		Parameter altered in 3 mM AAPH-treated young CGCs?	
I_A	Activation threshold (mV)	~-60 mV	No Change	~-60 mV (NS)	No Change	~-60 mV (NS)
	Peak Amplitude (nA)	62.34 ± 7.13 nA	No Change	57.1 ± 5.84 nA (NS)	No Change	54.5 ± 6.51 nA (NS)
	Activation V_{50} (mV)	-54.6 ± 4.58 mV	↓	-38.4 ± 4.32 mV (***)	↓	-36.2 ± 5.67 mV (***)
	Activation slope factor (mV)	4.37 ± 1.34 mV	↑	24.4 ± 6.25 mV (***)	↑	27.6 ± 6.57 mV (***)
	$\tau_{activation}$ (ms)	10.3 ± 1.40 ms	↑	-18.1 ± 2.64 ms (*)	↑	-19.5 ± 4.25 ms (*)
	Inactivation V_{50} (mV)	-50.9 ± 2.33 mV	No Change	-52.8 ± 5.16 mV (NS)	No Change	-58.8 ± 1.87 mV (NS)
	Inactivation slope (mV)	10.4 ± 2.57 mV	No Change	6.39 ± 1.37 mV (NS)	No Change	9.52 ± 1.08 mV (NS)
	$\tau_{inactivation}$ (ms)	12.5 ± 2.2 ms	↑	-23.9 ± 2.91 ms (*)	↑	-21.5 ± 2.72 ms (*)
I_{Cl}	Peak Amplitude (nA)	19.4 ± 2.2 mV	↑	0 nA (***)	↑	0 nA (***)
TEA/4-AP/zero Cl⁻ insensitive current	Activation threshold (mV)	~-30 mV	No Change	~-30 mV (NS)	No Change	~-30 mV (NS)
	Peak Amplitude (nA)	13.59 ± 1.84 nA	↑	62.5 ± 1.98 nA (***)	↑	59.5 ± 1.98 nA (***)
	Activation V_{50} (mV)	-3.47 ± 2.34 mV	No Change	-4.64 ± 0.57 mV (NS)	No Change	-4.23 ± 1.93 mV (NS)
	Activation slope factor (mV)	11.3 ± 2.61 mV	No Change	22.5 ± 3.16 mV (NS)	No Change	19.5 ± 2.06 mV (NS)
	Inactivation V_{50} (mV)	-66.9 ± 3.51 mV	No Change	-76.3 ± 2.51 mV (NS)	No Change	-73.9 ± 2.01 mV (NS)
	Inactivation slope factor (mV)	12.21 ± 3.6 mV	↑	7.80 ± 0.43 (*)	↑	9.98 ± 1.11 (*)
	Deactivating tail current (nA)	21.4 ± 3.52 nA	↑	46.5 ± 5.68 nA (***)	↑	51.4 ± 5.93nA (***)
	$\tau_{deactivation}$ (ms)	29.41 ± 2.39 ms	↑	42.6 ± 1.77 ms (***)	↑	43.4 ± 2.48 ms (***)
I_{DR} and I_R	All Parameters	-	No Changes (NS)		No Changes (NS)	

Table 3.3| The voltage-gated outward currents of the CGCs. This table summarises the voltage-gated outward currents that changed with age and acute OS and indicates what properties were specifically altered for each current. Red upward or downward facing arrows indicate a significant increase or decrease of the parameter, respectively. Data shown as mean ± SEM, *n=6-9* RCGCs. *p<0.05, **p<0.01 and ***p<0.001 *vs.* young CGCs. NS, not statistically significant.

3.4   Discussion

This study is the first comprehensive account detailing changes to the voltage-gated outward ionic currents with increasing age and acute OS in the CGCs of *Lymnaea stagnalis*. Experiments in this chapter revealed that the total voltage-gated outward current did not change in the old and 3 mM AAPH-treated young CGCs, but the properties of the underlying constituent currents were altered. Specifically, there was a decrease in the rate of activation and inactivation of I_A, suppression of a newly identified voltage gated Cl^- current, and an increase in a previously undocumented TEA/4-AP/zero Cl^- insensitive current. These changes may be responsible for the alterations to the CGC action potential waveform and the subsequent decrease in firing frequency that was previously described in Chapter 2. It was also observed, however, that the properties of I_{DR} and the recently discovered I_R were not compromised with age or acute OS.

3.4.1   The total voltage-gated outward current of the *Lymnaea* CGCs

An important finding from experiments in this chapter was that while there were no changes to the amplitude of the total voltage-gated outward current of the CGCs with age and acute OS, the constituent currents and their kinetics were altered.

A number of previous studies examining both normal and pathological ageing of the CNS have proposed the idea that alterations to the properties of certain ionic currents may be masked by compensatory changes in others[288,84,216]. This may occur in an attempt to reduce age-related hindrances to key neuronal processes such as excitability and/or neurotransmission. Additionally, these compensatory changes may arise to maintain important homeostatic mechanisms such as those involved in regulating intracellular Ca^{2+} levels[288,84,216]. It has been demonstrated, for example, that an increase in I_A can be compensated by an increase in I_R, which may potentially occur to impede action potential narrowing and the consequential decrease in neurotransmitter release[288].

Thus, it appears that current compensation may be happening in the CGCs with age and acute OS to possibly hamper extreme alterations to the action potential waveform and firing frequency, and consequently limit adverse changes to behavioural outputs such as feeding.

3.4.2   The A-type K$^+$ current of the *Lymnaea* CGCs

Experiments conducted in this chapter confirmed the presence of I_A in the CGCs, which had initially been reported by Staras *et al.* (2002)[416]. It was found that the amplitude of the 4-AP sensitive I_A isolated in this study was much smaller than that documented by Staras *et al.* (2002) and represented only 60% of the total outward early current compared to the 80% in the Staras *et al.* (2002) study. This difference could possibly be due to the reduced expression of A-type K$^+$ channels in the CGCs of this study. There is some evidence that changes in environmental factors such as temperature or food can alter ion channel expression in cells and it is possible such differences may be accountable for this finding[367]. Alternatively, the observed differences may be because Staras *et al.* (2002) did not inhibit Ca^{2+}-activated K$^+$ channels[416]. This is important as some Ca^{2+}-activated K$^+$ channels have exhibited sensitivity to 4-AP and thus, may contribute to the amplitude of I_A when isolated[344,17].

Consistent with Staras *et al*. (2002) study and findings in some mammalian neurons, I_A activated at approximately -60 mV, which was around the CGC RMP[198,13,375,416]. Previous studies have shown that the low activation threshold of I_A is important in enabling neurons to fire at lower frequencies by regulating the rate of action potential repolarisation and maintaining a more negative RMP[12,370,311].

Both age and acute OS failed to alter the peak amplitude of I_A. Whether this is a reflection of what typically occurs during healthy neuronal ageing is difficult to know as the limited studies published to date have produced conflicting results (**section 3.1**). Whilst there were no changes to the amplitude of I_A in this study, both age and acute OS caused a significant rightward shift in the activation curves. This shift was due to a change in both V_{50} and slope factor, which suggested that A-type K$^+$ channels were less sensitive to voltage. These findings demonstrate that channel activation is slower in response to depolarisation of the CGC membrane potential with age and acute OS, but once opened the amount of K$^+$ ions conducted from the channels is not significantly compromised.

The rightward shift in the I_A activation curve with acute OS is consistent with previous studies that have shown that oxidative modifications to the voltage sensor and/or the gate domains can alter the activation properties of I_A[398,374,58]. To date, however, the effects of age on I_A conductance properties have not been described elsewhere. Interestingly, the kinetics of I_A activation was also significantly slower in both old CGCs and young CGCs treated with 3 mM AAPH. This strongly implies that opening of the activation gate

(C→O) of the A-type K$^+$ channel is impaired in some manner by oxidative modifications occurring during CGC ageing.

As with mammalian neurons and other invertebrate neurons, I_A in each CGC group characteristically exhibited pronounced steady-state inactivation[17,13,504]. Boltzmann fits to the data revealed that the voltage-dependence of inactivation was not altered with age or acute OS. However, the rate of inactivation was significantly slower.

I_A is thought to largely undergo N-type inactivation (**section 1.6.4.4**)[469,398]. It has been well established that N-type inactivation is regulated by redox agents, which makes this mechanism susceptible to unwanted oxidative modifications[58,374,398]. Indeed, aberrant ROS activity has been shown to oxidise cysteine and methionine residues of the inactivation ball domain to diminish its hydrophobic interactions with residues in the channel pore and consequently slow channel inactivation[184,58,374,398]. This may be occurring in the old and AAPH-treated young CGCs to slow I_A inactivation.

Could the changes observed to the properties of I_A with age and acute OS account for the decrease in CGC firing and alterations to the action potential waveform? AP-clamp experiments established that I_A is the major contributor to the total voltage-gated outward current (representing 49%) underlying young CGC action potentials. Thus, it would be predicted that alterations to I_A would have a profound impact on the firing properties of the CGCs.

In young CGCs I_A is activated near the RMP (~-60 mV), which based on previous studies is thought to allow I_A to dampen excitability and control repetitive firing[349]. Whilst some A-type K$^+$ channels activated around the RMP in old and 3 mM AAPH-treated young CGCs, the alterations to the voltage sensitivity and kinetics of I_A activation will reduce the proportion of channels open at any given voltage. With it taking ~20 ms for I_A to fully activate in the old and 3 mM AAPH-treated young CGCs, this current will not reach maximal conductance until after the peak of the action potential (as it takes ~17 ms to reach the peak) and the process of repolarisation has begun. In young CGCs, I_A fully activates in ~15 ms and this closely coincides with the establishment of the action potential peak, as demonstrated in AP-clamp experiments.

Importantly, A-type K$^+$ channels in the young, old and 3 mM AAPH-treated young CGCs will all be involved in repolarising action potentials, which corroborates previous studies identifying this as one of the main functions of I_A[349]. However, I_A in young CGCs due

to its faster inactivation kinetics will not have such a profound impact on the rate of repolarisation when compared to the old and 3 mM AAPH-treated young CGCs. This notion was supported by the finding that CGC action potentials were narrower with age and acute OS.

The slower inactivation kinetics of I_A in the old and 3 mM AAPH-treated young CGCs also means that this current will have a greater contribution to the fAHP when compared to young CGCs. This may help explain the increase in the fAHP and early sAHP (~70 ms) observed with age and acute OS. However, this also suggests that other currents in the CGCs such as I_{DR} or even Ca^{2+}-activated K^+ currents may be predominately responsible for the increase to the sAHP with age and acute OS[392,416].

Regardless, the possible increase in the fAHP and slight increase in the early sAHP caused by slower inactivation of I_A with age and acute OS would be expected to decrease CGC firing frequency.

3.4.3 The delayed rectifier of the *Lymnaea* CGCs

I_{DR} isolated in this chapter exhibited similar properties to what had been described previously by Staras *et al.* (2002) in the CGCs as well as in mammalian neurons, with regards to its slow activation from a threshold of ~-50 mV, very little inactivation and sensitivity to TEA[256,434,452,375,416]. The TEA sensitive I_{DR} contributed ~35% of the total outward current underlying a young CGC action potential and was predominately involved in regulating the rate of repolarisation.

As with I_A, the amplitude of I_{DR} in this study was substantially smaller than what had been documented by Staras *et al.* (2002), despite the amplitude of the total outward sustained current being very similar between these two studies[416]. Some studies have shown that alterations to housing conditions or feeding may alter the expression of certain ion channels, although as of yet this has not been demonstrated with I_{DR}[230,416]. Alternatively, there are some Ca^{2+}-activated K^+ currents sensitive to TEA. Thus, I_{DR} isolated in the Staras *et al.* (2002) study may be contaminated as no blockers for Ca^{2+}-activated K^+ currents were utilised[489,157].

It has been documented that the activation of some mammalian delayed rectifiers such as Kv1.2, for example, have a relatively weak voltage-dependence[44,468,192,309,167]. The activation I_{DR} in the CGCs, however, was very weakly voltage-dependent as reflected by

the extreme shallow activation curves. This suggests that the structure and/or molecular mechanisms involved in voltage sensing (**section 1.6.4.2**) may differ slightly in the delayed rectifier channels of the *Lymnaea* CGCs.

This very weak voltage-dependence of the CGC I_{DR} may arise due to a smaller number of effective gating charges moving through the electric field upon activation. This could be caused by each voltage-sensing residue contributing less to the gating charge and/or a decrease in the number of residues present[278,480]. Alternatively, it may be that coupling of VSD movements to gate opening is weaker in the CGG delayed rectifiers. In channels where activation is strongly voltage-dependent such as the A-type K^+ channel, for example, it has been reported that this coupling is extremely tight and yields a steeper activation curve[194,195]. It has also been recognised in mammalian models that this coupling is not strong in weak voltage sensitive channels such as BK, which have been heavily investigated with regards to this matter[195,183,194,480].

At present, the mechanisms responsible for weaker coupling between VSD movements and gate opening in weak voltage sensitive channels have yet to be fully elucidated. It may be that the molecular interactions between S4-S5 linker to the S6 helices, that is necessary for this coupling, differs in weak voltage-dependent channels when compared strong voltage-dependent channels[455].

The overall weak voltage sensitivity of the CGC I_{DR} (extremely shallow steady-state inactivation curves were also exhibited in all CGC groups) is likely responsible for the slow activation of this current as well as the minimal inactivation it undergoes. This would also enable I_{DR} to operate over a wider voltage range and may allow it to fine-tune numerous action potential parameters such as repolarisation, the AHP and the RMP[480,194].

The shallow CGC I_{DR} activation curve may not actually be indicative of weaker voltage-dependence, but rather could be reflective of the presence of more than one channel subtype in the CGCs. Each delayed rectifier channel subtype could possess different V_{50} and slope factor parameters, which consequently may alter the overall shape of the total I_{DR} activation curve. Currently, it is not known whether different delayed rectifier channel subtypes are expressed in the CGCs.

The lack of change to I_{DR} activation and inactivation properties with age and acute OS was very interesting considering the important role this current has in neurons. Delayed

rectifiers provide one of the major routes for K^+ efflux in neurons and are instrumental in action potential repolarisation[401,349]. Previous studies have also shown that I_{DR} is a large contributor to the fAHP and sAHP due to the minimal inactivation exhibited by this current[403,264,416]. Indeed, this was observed by Staras *et al.* (2002) who showed that blocking I_{DR} significantly broadened CGC action potentials and reduced the amplitude and duration of the AHP[416]. With the activation threshold of I_{DR} near the RMP of neurons, this current is also involved in regulating a negative RMP[237,79,349]. As there were no significant changes to this current with age and acute OS, this strongly suggests that other currents such as I_A may be responsible (at least partially) for the changes to the CGC RMP, half-width and AHP with age and acute OS.

Whether the lack of change to I_{DR} properties observed in this study was unusual is currently not known as the literature examining the effects of age on I_{DR} is extremely limited (**section 3.1**)[115,398]. Experimental OS models have consistently shown that ROS can increase the conductance of I_{DR}, but only under pathological conditions such as AD where ROS activity is greater than in healthy neuronal ageing[484,513,374,398]. This may explain why the AAPH model of acute OS in this study did not alter I_{DR} as ROS activity may have not been sufficiently high enough in the young cerebral ganglia.

Given that the application of 3 mM AAPH in this study mimics the normal ageing CGC phenotype remarkably well, strongly suggests that I_{DR} is not sensitive to OS during healthy ageing. It is most likely that delayed rectifiers are particularly resilient to the effects of age in order to protect neurons, as pathological conditions have shown that increasing K^+ efflux *via* I_{DR} activates caspases and triggers neuronal apoptosis[513,401,512].

3.4.4   The inward rectifier of the *Lymnaea* CGC

I_R prefers to facilitate K^+ influx, but physiologically is still an outward K^+ current. Contrary to Staras *et al.* (2002), this study showed for the first time that the *Lymnaea* CGCs exhibit a voltage-activated inward rectifier K^+ current. It is currently unknown why these two studies differed with regards to the finding of this current. This could be due to differences in the *Lymnaea* feeding conditions and/or feeding regime between these two studies, as it has been shown that the expression of some ion channels are sensitive to environmental changes[230,416].

I_R characterised in this study activated in response to a hyperpolarising protocol and had an estimated E_{rev} ~-60 mV, which strongly suggested the principal conducting ion was K^+. This was confirmed by increasing the extracellular potassium concentration 10-fold from 1.6 mM to 16 mM, which significantly increased the amplitude of I_R and caused the E_{rev} to shift from ~-60 mV to ~-20 mV. This depolarising shift was by ~40 mV, which deviated slightly from the 58 mV shift predicted from the Nernst equation if K^+ was the only conducting ion. Taken together, the electrophysiological characteristics and the reversal potential data established that this current was an inward rectifier K^+ current.

A fascinating feature observed with the CGC inward rectifier was its relatively fast inactivation kinetics. Whilst most inward rectifiers tend to be very slow to inactivate, there have been some reports of ultrafast inactivating inward rectifiers[413,125]. It is thought that fast inactivating inward rectifiers are specifically involved in rapidly repolarising action potentials[413,125].

Another interesting feature of the CGC inward rectifier was that it could not be blocked by conventional extracellular blockers such as Ba^{2+}, Cs^{2+} and TEA. In mammalian models, it has been shown that inward rectifiers are generally not insensitive to the effects of all three of these extracellular blockers[241,88,347]. It could be that the binding sites required to block the inward rectifier are located purely intracellularly in the *Lymnaea* CGC and therefore, channels have to be blocked in this manner. It is often observed in the literature that Ba^{2+} and Cs^{2+}, as well as other high affinity I_R blockers such as Mg^{2+}, are placed in a patch pipette so that they can diffuse into the cell in order to attenuate I_R[178,162]. Thus, future TEVC experiments in the CGCs could involve including I_R blockers into the current injecting microelectrode to assess whether this current could be blocked *via* an intracellular manner.

Experiments in this chapter revealed that the amplitude of I_R as well as its activation and inactivation properties did not significantly alter with increasing age or acute OS. To date, this is the first study to show that the properties of I_R are not altered by OS during normal neuronal ageing.

Whilst the role of I_R in the CGCs has yet to be determined, it is predicted (based on previous mammalian and other invertebrate studies) that this current will be important in stabilising the CGC RMP and regulating excitability[178,130]. As I_R is active around the CGC RMP, it will be involved in regulating the inter-spike interval and preventing the

unwanted generation of action potentials caused by weak depolarising stimuli[130,178,162]. Only when the depolarising stimulus is sufficiently large enough, will I_R permit the firing of action potentials[130,178,162].

3.4.5 The E_{rev} of K^+ in the *Lymnaea* CGCs

Examining the activation properties of voltage-gated K^+ currents in this study had required the E_{rev} of K^+ during calculations. Analysis of tail currents elicited by the CGCs had approximated the E_{rev} of K^+ to be around -60 mV. The AHP of the CGC action potential, which is thought to be largely driven by K^+ currents, was considerably more negative than -60 mV. Thus, it is expected that the true E_{rev} of K^+ in the CGCs will be below the AHP peak at a value more negative than -60 mV.

It is also clear that the E_{rev} for K^+ estimated in this study was substantially more depolarised to what has typically been reported in the literature. In mammalian neurons, the E_{rev} of K^+ has often been shown be around -70 mV to -90 mV [165,410,404]. Even previous studies involving the *Lymnaea* CGCs have documented similar findings that the E_{rev} of K^+ is between -75 mV to -90 mV[457,416,392].

This discrepancy has arisen due to contamination of the tail currents elicited by outward voltage-gated K^+ currents in the zero-Na^+/$CdCl_2$/NPPB saline. Tail currents were not completely selective for voltage-gated K^+ currents because the TEA/4-AP/NPPB insensitive current, with its significantly more depolarised E_{rev} and slower deactivation kinetics, could not be blocked and thus raised the reversal potential. Hence, the E_{rev} of K^+ could only be estimated rather than conclusively determined from the tail current analysis in this study. The presence of the TEA/4-AP/NPPB insensitive current most likely explains why tail currents had to be fitted with a double exponential function as it suggested, prior to discovery of this current, that the total voltage-gated outward K^+ current may have been contaminated with another current, each with a single (different) deactivation process.

Unlike this study, Staras *et al.* (2002) and Scutt (2012) had previously been able to generate a more accurate value for the E_{rev} of K^+ as analysis had been conducted on tail currents generated by the deactivation of both voltage-gated and Ca^{2+}-activated K^+ currents[392,416]. This greater presence of K^+ currents is likely to have substantially minimised any positive shift to the reversal potential caused by contamination from the

(previously unidentified) TEA/4-AP/NPPB insensitive current. Another study by Vavoulis *et al.* (2010), had also accurately estimated that the E_{rev} of K^+ was between -75 mV to -90 mV, as values confined within this range permitted the successful reproduction of the CGC action potential in the Hodgkin-Huxley-type computational model[457]. However, the benefit of this last experimental approach is that the reversal potential of an ion can be accurately estimated given the lack of contamination from other ionic currents.

Experiments in this chapter had also assessed tail currents that had been elicited by the TEA sensitive I_{DR} in an attempt to yield a more accurate estimation of the E_{rev} of K^+. This also generated a more positive value than expected (~-60 mV), which was surprising given that TEA sensitive I_{DR} tail currents had been isolated *via* subtraction and should have removed any potential contamination from the TEA/4-AP/NPPB insensitive current.

A possible explanation for this is that TEA may be blocking other voltage-gated currents that are not mediated by K^+ ions. A few studies have previously demonstrated that TEA can suppress inward chloride currents[380,381]. This is not a possibility in this thesis as all inward currents were inhibited. However, interesting preliminary experiments in *Xenopus laevis* CNS neurons (Li W, personal communications) have also shown this in relation to voltage-gated outward anion currents (which are primarily mediated by Cl^- ions). Indeed, the double exponential fit to I_{DR} tail currents in this study may be due to the presence of another current with a different deactivation process rather than I_{DR} consisting of two deactivation processes.

There are several methods that could be conducted by future experiments to more accurately estimate the CGC E_{rev} of K^+ and minimise issues caused by contamination from other ionic currents. First, if tail currents generated by VGKCs are to be used for this analysis, then it is important to identify the channel(s) conducting the TEA/4-AP/NPPB insensitive current and find an appropriate blocker. Second, the Staras *et al.* (2002) and Scutt (2012) approach could be utilised, whereby Ca^{2+}-activated K^+ currents are not inhibited to enhance the total outward K^+ current of the CGCs and consequently minimise any positive shift to the reversal potential caused by the TEA/4-AP/NPPB insensitive current[392,416]. Third, the intracellular K^+ concentration could be determined (perhaps *via* the use of a K^+ fluorescent indicator such as PBFI-AM) and used in the Nernst equation along with the known extracellular K^+ concentration to more accurately estimate the E_{rev} of K^+ in the CGCs. Fourth, I_{DR} tail currents could be isolated in a zero Cl^- saline to prevent the possibility that TEA may be blocking voltage-gated Cl^- currents.

Lastly, all experiments examining the activation properties of voltage-gated K^+ currents could be conducted in a high K^+ saline. This would enhance the amplitude of K^+ currents and substantially reduce contamination from other currents, which would enable for the calculation of a more accurate E_{rev} value. However, values generated from analysis in the high K^+ saline, such as V_{50} and slope factor, would not be in a physiologically relevant range.

It is very important to note that the changes to the activation properties of voltage-gated K^+ currents with age and acute OS, such as the rightward shift to I_A activation curves (**section 3.3.3**), are still observed even when the E_{rev} of K^+ is theoretically set to a more hyperpolarised value. Manipulation of the E_{rev} of K^+ (not shown in this thesis) from approximately -60 mV to -80 mV (derived from previous *Lymnaea* studies[392,416,457]) caused a small (non-significant) rightward shift in all the voltage-gated K^+ current activation curves (I_A, I_{DR} and I_R) in young, old and 3 mM AAPH-treated young CGCs, by ~ 5 mV to V_{50} and ~3 mV to the slope factor. Thus, interpretations made with regards to the activation properties of voltage-gated K^+ current in this study are valid despite the discrepancies surrounding the E_{rev} of K^+.

3.4.6 The TEA/4-AP insensitive currents of the *Lymnaea* CGCs

This study has characterised an exciting novel TEA/4-AP insensitive current in the young, old and 3 mM AAPH-treated young CGCs. Several lines of evidence presented in this chapter suggests that this current is not an unblocked component of I_{DR}. First, this novel current has a 'biphasic' phenotype with a fast transient activation phase followed by a smaller sustained component, whereas I_{DR} activated slowly into a larger sustained component. Second, the TEA/4-AP insensitive current (measured at the sustained component) activated at a significantly more depolarised potential (~-30 mV) than I_{DR} (~-50 mV). Third, the TEA/4-AP insensitive current represented ~30% of the total sustained current, whereas I_{DR} made up ~70% in the young CGCs. This signified that I_{DR} was the dominant voltage-gated sustained outward current, which corroborated previous findings in mammalian and other invertebrate neurons[264,416,152]. Fourth, the E_{rev} for the TEA/4-AP insensitive current was significantly more depolarised (-30 mV) than the estimated E_{rev} for I_{DR} (-60 mV), indicating that the TEA/4-AP insensitive current is not primarily conducted by K^+ ions. Finally, analysis of deactivation kinetics demonstrated that tail currents generated by the TEA/4-AP insensitive current were significantly larger in amplitude and slower to deactivate than I_{DR} tail currents. Interestingly, the very slow

deactivation kinetics of the TEA/4-AP insensitive current and the observation that its tail currents were inward at voltages below the RMP suggests that this conductance may have a possible role in CGC pacemaking activity.

The 'biphasic' phenotype exhibited by the TEA/4-AP insensitive current alluded to the possibility that this current may be a mixed conductance. Analysis of the activation threshold revealed that the early transient component activated at a significantly more hyperpolarised potential (-50 mV) than the sustained component (-30 mV), which confirmed this suspicion. Although, it is possible that different ions conducted from the same channel may alter the activation potential[230,416]. If they are two distinct currents, then this may also explain why it was necessary to fit a double exponential function to the deactivating tail currents of the TEA/4-AP insensitive current.

Interestingly, both the early and sustained TEA/4-AP insensitive currents increased significantly, by ~40%, with age and acute OS. The increase in the magnitude of these currents meant that I_A and I_{DR} were no longer the principle voltage-gated outward currents contributing to the total outward current of the CGCs. This indicates that the channels mediating the TEA/4-AP insensitive currents are particularly vulnerable to oxidative modifications with age.

Neuronal ageing studies have provided a wealth of evidence showing that OS can increase the conductance of an ion channel in numerous ways including oxidation of amino acids on the voltage sensor, activation/inactivation gates and/or channel pore[469,184,374,398]. Hydroxyl and peroxyl radicals, both of which are generated by AAPH, have also been shown to alter the properties of ion channels[173,398]. At present, however, the molecular mechanisms by which OS in the CGCs increases the conductance of the early and sustained TEA/4-AP insensitive current is unknown.

The increase in the early transient TEA/4-AP insensitive current with age and acute OS was associated with a significant rightward shift in the activation curves due to a change in V_{50} for the current. This suggests that the voltage sensor domains of the channel are being oxidised, which is subsequently slowing the transmission of the voltage-driven conformational change required to open the channel pore. Whether the inactivation properties of this current changes with age or acute OS is not known as this conductance could not be isolated due to the difficulties in finding a suitable pharmacological blocker.

However, experiments did establish that this current was not a voltage-gated chloride or proton current.

The fast transient nature of the early TEA/4-AP insensitive current as well as its -50 mV activation potential and rightward shift in the activation curve with age and acute OS was remarkably reminiscent to the 4-AP sensitive I_A conductance. Thus, this current could be a 4-AP insensitive I_A. While no studies have reported the existence of such a current, it has been shown in mesencephalic neurons that there is a fast activating transient current that shares very similar properties to I_A, but is insensitive to 4-AP[314]. Alternatively, it may be that the early TEA/4-AP insensitive current is not sensitive to the concentration of 4-AP utilised in this study. Increasing the concentration of 4-AP, however, may not necessarily resolve this problem as higher concentrations have been shown to inhibit other voltage-gated K^+ currents[393,416,13,50].

The early TEA/4-AP insensitive current and its tail currents could not be isolated *via* subtraction due to the lack of blockers for this current. It was also not possible to isolate the early current by removing contamination from the sustained TEA/4-AP insensitive current as the latter current could not be completely blocked. This meant that the E_{rev} of the early TEA/4-AP insensitive current could not be determined to provide information about its conducting ion. Thus, simple experiments in the future manipulating the K^+ concentration of the bathing saline may provide insight as to whether the early TEA/4-AP insensitive of the CGCs is conducted by K^+ ions. If this current is then found to be a 4-AP insensitive I_A, then it would probably decrease CGC firing frequency with age and acute OS in a similar manner that had been postulated for the 4-AP sensitive I_A (**section 3.4.2**).

The increase in the sustained TEA/4-AP insensitive current with age and acute OS was not due to changes in the activation properties of the channel, as both V_{50} and the slope factor were unaltered. Whilst this current displayed little inactivation across the three CGCs groups, a rightward shift in the steady-state inactivation curve was observed with age and acute OS due to a change in the slope factor. This meant that the current inactivated less when compared to young CGCs, as voltage-dependence was weaker. This coupled with slower deactivation kinetics of the sustained TEA/4-AP insensitive current in the old and 3 mM AAPH-treated young CGCs suggests that a greater proportion of channels remains open for much longer, potentially explaining the increased magnitude of this current in these CGCs. The altered deactivation kinetics of the sustained TEA/4-

AP insensitive current with age and acute OS also suggests that the possible role of this current in pacemaking activity is augmented and thus, may be accountable for some of the changes observed in the CGC firing properties.

3.4.7 The discovery of a voltage-gated outward chloride current in the CGCs

Given that the sustained TEA/4-AP insensitive current was deemed not to be a voltage-gated K^+ current due to its significantly depolarised reversal potential, experiments investigated whether this sustained current was I_{Cl}. Previous studies in mammalian and other invertebrate cells have demonstrated voltage-gated outward Cl^- currents can have an E_{rev} of $\sim$-30 mV and activate around -35 mV, which is very similar to the properties exhibited by the sustained TEA/4-AP insensitive current of the *Lymnaea* CGCs[460,490,220]. A study in the invertebrate *Tritonia diomedea* also showed that voltage-gated outward Cl^- currents possess extremely slow and large persistent tail currents, which further fuelled speculation that the CGC sustained TEA/4-AP insensitive conductance may be I_{Cl}[490].

Perfusion of preparations in a zero Cl^- saline or in the presence of the Cl^- channel blocker, NPPB, caused a significant reduction ($\sim$60%) to the sustained TEA/4-AP insensitive current in the young CGCs. This confirmed for the first time that a voltage-gated outward Cl^- current is present in the *Lymnaea* CGCs. Notably, other chloride channel blockers including DIDS and niflumic acid did not reduce the sustained TEA/4-AP insensitive current. This is likely a reflection of the channel sub-type(s) present in the *Lymnaea* CGC, as each sub-type tends to exhibit different sensitivities toward various blockers.

To date, nine voltage-gated chloride channels (CLC 1-9) have been identified in vertebrates and invertebrate species. CLC-1 and 2 are expressed on the plasma membrane, CLC 3-7 (typically regarded as Cl^-/H^+ antiporters as opposed to a classical chloride channels) are generally located intracellularly and finally both CLC-Ka and CLC-Kb are predominately expressed on the plasma membrane of renal and inner ear epithelial cells[301,423,462]. Currently, it is not known what subtypes are expressed by the *Lymnaea* CGC, but CLC1-2 can be ruled out as both these channels are inward rectifying chloride channels[462].

Isolation of I_{Cl} showed that its tail currents were small and channels were fast to deactivate, which indicated that this current was unlikely to be involved in pacemaking. However, the reduction of the sustained TEA/4-AP insensitive current by NPPB and the

zero Cl⁻ saline demonstrated that the residual unblocked current still possessed large slow persistent tail currents. Thus, this current may contribute to pacemaking activity in the CGCs.

In contrast to young CGCs, I_{Cl} appeared to be absent in the old and 3 mM AAPH-treated young CGCs as the zero Cl⁻ saline and NPPB both failed to alter the amplitude of the sustained TEA/4-AP insensitive current. This suppression of I_{Cl} with age and acute OS was masked by a significant increase in the residual sustained TEA/4-AP/zero Cl⁻ insensitive current. At present, it is not known why I_{Cl} is completely attenuated with age or acute OS. Interestingly, a non-neuronal ageing study showed that hydroxyl radicals can suppress outwardly rectifying I_{Cl} of bronchial cells[205]. This provides some precedence for the findings of this current study, especially as AAPH can produce hydroxyl radicals[273,243,291].

E_{rev} analysis revealed that the presence of I_{Cl} was responsible for significantly depolarising the E_{rev} of the TEA/4-AP insensitive current in young CGCs when compared to the old and 3 mM AAPH-treated young CGCs, where I_{Cl} was suppressed. However, the residual TEA/4-AP/zero Cl⁻ insensitive current between the three CGC groups shared a similar E_{rev} and this strongly suggested that this current was being conducted by the same ion(s) in each group.

What is the role of I_{Cl} in the CGCs and how would suppression of this current with age and acute OS alter CGC firing? AP-clamp experiments demonstrated that I_{Cl} activates during depolarisation of the action potential (activation threshold is ~-35 mV). With the activation threshold of voltage-gated Cl⁻ channels only slightly more positive that the E_{rev} for Cl⁻, I_{Cl} will be small (in magnitude) due to the weak driving force. At this stage, the activated channels will initially slow down the rate of depolarisation of the CGCs as Cl⁻ move into the cell. As the CGC action potential continues to depolarise and deviate further away from the E_{rev} of Cl⁻, the influx of Cl⁻ increases and the current will start contributing toward repolarising the CGC action potential. When the membrane potential then falls below E_{rev} of Cl⁻ during the repolarisation phase, channels will begin to conduct an inward current. This efflux of Cl⁻ ions will act to depolarise the CGCs and therefore, slow the rate of repolarisation.

It is unlikely that the depolarising effect of I_{Cl} will be profound as this current only constituted 9% of the total voltage-gated outward current evoked during a young CGC

action potential. Additionally, it appeared from AP-clamp experiments that the amplitude of I_{Cl} was close to zero by the time the cell had reach the E_{rev} of Cl^-. This is probably due to the extremely fast deactivation rate of the current, which strengthens the notion that I_{Cl} may only have a small depolarising effect in the CGCs.

Overall, it appears that the main role of I_{Cl} in young CGCs is to make them less excitable. This would suggest that suppression of the hyperpolarising I_{Cl} current with age and acute OS may be a compensatory change that occurs to potentially reduce the decrease to CGC firing.

3.4.8 Is the sustained TEA/4-AP/zero Cl⁻ insensitive current a proton current?

The possibility that the residual TEA/4-AP/zero Cl⁻ insensitive current (or at least a proportion of it) was conducted by a voltage-gated proton channel was explored in this study. Some voltage-gated proton currents are outwardly rectifying currents that have an activation threshold in the range of +10 to -40 mV, depending on the neuron[57,94,189,490]. Why there is such a big variation in the activation threshold of proton currents is unknown, but as with other currents it is probably a reflection of the functions they perform in the neuron. Interestingly, voltage-gated outward proton currents have been demonstrated to increase in neurodegenerative diseases such as AD and in young mammalian models of OS[57,493,492,189]. Whether there are changes to these voltage-gated outward proton currents during normal neuronal ageing is currently not known.

In *Lymnaea,* visceral and parietal neurons have been shown to conduct an outward proton current that activates around -30 mV, which is not too dissimilar from the activation potential of the sustained TEA/4-AP/zero Cl⁻ insensitive current in the CGCs of this study[57]. However, altering the pH of the zero Cl⁻ saline from pH 7.9 to pH 6.9 did not alter the conductance or reversal potential of the TEA/4-AP/zero Cl⁻ insensitive current in the young, old and 3 mM AAPH-treated young CGCs. This established for the first time that the *Lymnaea* CGCs do not conduct a voltage-gated outward proton current.

3.4.9 The sustained TEA/4-AP/zero Cl⁻ insensitive current of the *Lymnaea* CGC

Given that the sustained TEA/4-AP/zero Cl⁻ insensitive current increased with age and acute OS and presumably has an important role in regulating CGC firing and the action

potential waveform, it was important to identify the conducting channel mediating this current in order to gain a better understanding of its functions.

Experiments had established that this conductance was not a proton current and the use of zero Cl^- saline during recordings excluded the possibility that this residual current was conducted by Cl^- ions. However, this does not mean that voltage-gated chloride channels are not conducting the sustained TEA/4-AP/zero Cl^- insensitive current as blocking the conductance of voltage-gated chloride channels is notoriously difficult even when a zero Cl^- saline or classical antagonists such as NPPB are being utilised[462,301].

There are two possible explanations for this situation. First, most chloride channels are not actually selective for chloride ions but instead display a general selectivity toward all anions[356,531,301]. Second, chloride channels possess large pores that are difficult to occlude and hence, many I_{Cl} blockers have been described as either redundant or weak because they struggle to prevent the permeation by anions including chloride itself[356,531,462,301]. So, if a weak blocker is used Cl^- ions may still pass through the channel and in the presence of a zero Cl^- saline the substitution anion(s) may also permeate the channel. Thus, a residual current will be elicited as had been demonstrated in this study.

As the efficacy of the NPPB block on voltage-gated Cl^- channels in the CGCs is not known, it was not entirely surprising that a residual current was still present when NPPB was added to the zero Cl^- saline as an additive measure to block any potential permeation from other anions. Some of the anions that have been shown to permeate Cl^- channels includes negatively charged amino acids, nitrates, bicarbonate, bromide, phosphates and even acetate[462,301]. The zero Cl^- saline used in this study was composed mostly of acetate-based salts to replace chloride-based salts and therefore, there is a possibility that the residual sustained current could be mediated by acetate anions.

Whilst such a scenario could be conceivable in the young CGCs, it is less so in the old and 3 mM AAPH-treated young CGCs. The reason for this is that suppression of I_{Cl} would strongly suggest that voltage-gated Cl^- channels are being blocked in some manner and therefore, it would be unexpected if anything could be conducted by the channel. Unless, for example, residues on the SF are altered by oxidative modifications during ageing that increases the channel's affinity for other anions over Cl^-. However, this has not been observed in Cl^- channels or any other ion channels for that matter. While this is probably unlikely, residues such threonine and cysteine found in the SF of voltage-gated ion

channels are known to be susceptible to oxidative modifications and this could provide a possible explanation for these findings[398].

Determining whether the sustained TEA/4-AP/zero Cl⁻ insensitive current is conducted by voltage-gated Cl⁻ channels is challenging, particularly as evidence presented in this chapter produced some confounding results. First, the conductance and steady-state inactivation properties between the isolated I_{Cl} and the sustained TEA/4-AP/zero Cl⁻ insensitive current were indistinguishable suggesting that both these currents may be conducted by the same channel. Although, it could be that there are two channels conducting currents with very similar properties. Second, the sustained TEA/4-AP/zero Cl⁻ insensitive current with its hyperpolarised activation threshold and slower deactivation kinetics than I_{Cl} suggests that these currents may be mediated by different channels. However, these particular changes could be reflective of the fact that in isolating this current the natural conducting ion has been removed from the saline and as such this may have altered the properties of the channel. Currently, the precise nature of this current and its conducting channel is unknown.

To examine whether the sustained TEA/4-AP/zero Cl⁻ insensitive current is conducted by voltage-gated Cl⁻ channels, a few different electrophysiological approaches could be implemented in future investigations. Using the TEVC setup, the extracellular anion concentration of the zero Cl⁻ saline could be altered to examine if there are any changes to the amplitude of this residual current and whether any shifts to the reversal potential occur in accordance to predictions derived from the Nernst equation. As acetate-based salts were predominately used to compose the zero Cl⁻ saline, the concentration of this particular anion could be altered. Any changes observed in response to altering the extracellular anion concentration would strongly indicate that the TEA/4-AP/zero Cl⁻ insensitive current is conducted by a voltage-gated Cl⁻ channel because of their relatively poor selectivity among different anions[462,301].

Another technique that could be utilised to provide more conclusive evidence that the TEA/4-AP/zero Cl⁻ insensitive current is being conducted by a voltage-gated chloride channel is to perform single channel recordings in the *Lymnaea* CGCs. This technique provides a direct approach to examine the microscopic properties of individual ion channels such as their kinetics and the nature of the conducting ions[323,377].

Different patch clamp configurations could be implemented to record single-channel activity in the CGCs. The first is cell-attached patch clamp, which involves the pipette forming a seal onto the membrane, but not rupturing it. Here, the patch of membrane's extracellular surface is exposed to the pipette solution that represent the extracellular milieu. The second configuration is inside-out patch clamp, which involves excising a patch of membrane from the cell with the intracellular surface of the membrane exposed to the bathing saline. The last method is outside-out patch clamp, where the extracellular surface of an excised patch of the membrane is exposed to the bathing saline.

Outside-out patch clamp would be the ideal method, albeit the most challenging, to study the question of interest. The reason for this is that the membrane patch can be exposed successively to different extracellular solutions, which means that the single channel current can be repeatedly measured under varying extracellular conditions[415]. Thus, the distribution of anions can be altered across the same CGC patch (containing only one or a few voltage-gated chloride channels, as other channels will be blocked) during recordings[415]. In such experiments, if the chloride single channel current is not abolished following extracellular perfusion of the CGC patch with a zero Cl⁻ saline, this would directly show that the channel is conducting the remaining TEA/4-AP/zero Cl⁻ current. Following this, if a zero Cl⁻ saline with a modified anion concentration (such as higher/lower acetate concentration) altered the single channel conductance and shifted the reversal potential in line with calculations derived from the Nernst equation, this would provide strong evidence demonstrating that the TEA/4-AP/zero Cl⁻ current is mediated by other anions conducted *via* voltage-gated chloride channels.

3.5   Conclusion

In conclusion, this chapter extensively examined the properties of voltage-gated outward currents that regulate the CGC action potential waveform with age and acute OS. The changes incurred to the properties of these currents with age were accurately mimicked by young CGCs following acute extracellular AAPH treatment, which strongly suggests that OS is involved in the age-related changes in CGCs. Whilst the amplitude of total voltage-gated outward current did not change, the composition of its underlying constituent currents did, with alterations observed specifically in I_A and the newly discovered I_{Cl} and TEA/4-AP/zero Cl⁻ insensitive current. The delayed activation and inactivation exhibited by I_A may explain the decrease in CGC firing frequency and the

altered action potential waveform with age and acute OS. The properties of I_{DR} and I_R, the other voltage-gated K$^+$ currents examined, were not altered with age or acute OS. However, it is predicted that the suppression of I_{Cl} in the old and AAPH-treated young CGCs as well as an increase in the amplitude and delayed inactivation of the sustained TEA/4-AP/zero Cl$^-$ insensitive current may also be involved in the alterations to the action potential waveform and firing frequency in these CGCs.

Chapter 4: The role of voltage-gated outward currents on the firing properties of the CGCs

4.1 Introduction

A challenging issue has emerged in understanding how changes to the properties of voltage-gated outward currents (observed in Chapter 3) alters the firing properties of the CGCs with age and acute OS. This stems from the relatively limited knowledge regarding the role of voltage-gated outward currents in mediating CGC action potentials.

Initial experiments by Staras *et al.* (2002) in the young CGCs as well as by Vavoulis *et al.* (2012) in a Hodgkin-Huxley type computational CGC model, demonstrated that blocking I_{DR} with TEA broadened action potentials, decreased the AHP amplitude and depolarised the RMP[58,53]. This suggests that I_{DR} regulates the rate of repolarisation during an action potential, contributes to the development of the fAHP and is involved in maintaining a negative RMP in the young CGCs. Vavoulis *et al.* (2012) also noted that suppression of I_A broadened the model CGC action potential, which suggested this current has an important role in repolarising the CGCs[58]. However, whether the inhibition of these voltage-gated K^+ currents altered other parameters such as the sAHP or those associated with SFA and consequently how these changes influence CGC firing frequency has not yet been investigated. Thus, at present many of the ionic currents in the CGCs have often been assumed to have a similar function to those observed previously in mammalian and other invertebrate neurons. This may not necessarily be the situation due to differences, for example, in ion channel structure or subtype expression.

The aim of experiments in this chapter will be to investigate the role of voltage-gated outward currents in regulating the young CGC action potential. Currently, the role of the TEA/4-AP/zero Cl⁻ insensitive current and I_R in the CGCs cannot be investigated due to the lack of specific antagonists. Therefore, this study will focus on the role of I_A, I_{DR} and the newly identified I_{Cl} in the young CGCs. While I_{DR} did not change with age or acute OS, it was still imperative to fully understand the role of this current in the CGCs as it may shed an insight as to why delayed rectifiers appear to be more resilient to the effects of age and acute OS. Additionally, it is important to establish whether the functions of I_{DR} matched previous descriptions documented in *Lymnaea*[58,53]. This is particularly important as it appears that the ionic current complement of the CGCs from snails in this study differed slightly from what had been detailed by Staras *et al.* (2002)[58,53].

Based on the AP-clamp experimental findings of Chapter 3, where I_A, I_{DR} and I_{Cl} were activated during the rising phase of the young CGC action potential and had reached their maximum conductance during the repolarisation phase, it is predicted that these voltage-gated outward currents will have an important role in repolarising the CGCs. Additionally, it was observed that both I_A and I_{DR} had not fully inactivated/deactivated by the onset of the fAHP and thus, it is also predicted these currents may have an important role in modulating the CGC fAHP.

The hypothesis of this chapter is as follows: *I_A, I_{DR} and I_{Cl} are involved in reducing CGC firing in young Lymnaea by regulating the repolarisation and the after-hyperpolarisation phases of the action potential.*

4.2 Methods

4.2.1 Experimental animals

All experiments in this chapter were carried out on *Lymnaea stagnalis* aged 3-4 months old that had been housed in accordance to descriptions in Chapter 2 (**section 2.2.1**).

4.2.2 Preparation of the isolated *Lymnaea* CNS

Isolation of the CNS from young *Lymnaea* and preparation in the electrophysiological recording chamber containing HEPES-buffered saline was conducted as detailed in Chapter 2 (**section 2.2.2**).

4.2.3 Electrophysiological recordings

4.2.3.1 Current clamp setup

The electrophysiological setup to conduct current clamp recordings of the RCGCs was performed as detailed in Chapter 2 (**section 2.2.3**).

4.2.3.2 Current clamp protocols

A depolarising step protocol, evoked from the RMP of the CGCs, was performed as previously described in Chapter 2 (**section 2.2.4.1**) to assess SFA in young control RCGCs and young RCGCs treated with the voltage-gated outward current blockers.

4.2.4 Chemicals and salines

4.2.4.1 Control saline

Composition of the HEPES-buffered saline as described in Chapter 2 (**section 2.3**).

4.2.4.2 4-AP saline

To block I_A in the *Lymnaea* CGCs, a HEPES-buffered saline containing the addition of 4-AP was utilised during recordings. The composition of this saline was: 4-AP 4 mM, NaCl 50 mM, KCl 1.7 mM, CaCl$_2$ 4 mM, MgCl$_2$ 2 mM, HEPES 10 mM, adjusted to pH 7.9 with NaOH 3 M (Sigma-Aldrich, UK).

4.2.4.3 TEA saline

To block I_{DR} in the *Lymnaea* CGCs, a HEPES-buffered saline containing the addition of TEA was utilised during recordings. The composition of this saline was: TEA 50 mM, KCl 1.7 mM, CaCl$_2$ 4 mM, MgCl$_2$ 2 mM, HEPES 10 mM, adjusted to pH 7.9 with NaOH 3 M (Sigma-Aldrich, UK).

Note: The extracellular concentration of Na$^+$ ions in this saline *via* the addition of NaOH was approximately 6 mM. Whilst this was substantially lower than what was present in the control HEPES-buffered saline, 50 mM *via* NaCl, the concentration in the TEA saline was still sufficient to evoke CGC action potentials.

As 50 mM TEA extracellularly was required to completely block I_{DR} in the CGCs (**section 3.3.4**), the inclusion of NaCl in the saline was not an option as this would have had an osmotic effect and subsequently compromised the functioning of all neurons in the *Lymnaea* CNS.

4.2.4.4 NPPB saline

To block I_{Cl} in the *Lymnaea* CGCs, a HEPES-buffered saline containing the addition of NPPB was utilised during recordings. The composition of this saline was: NPPB 100 µM (Tocris Biosciences, UK), NaCl 50 mM, KCl 1.7 mM, CaCl$_2$ 4 mM, MgCl$_2$ 2 mM, HEPES 10 mM, adjusted to pH 7.9 with NaOH 3 M (Sigma-Aldrich, UK).

4.2.5 Setup of experimental conditions during intracellular recordings

Current clamp recordings in every preparation preceded with a 10 minute acclimatisation period in HEPES-buffered saline to allow for the RMP and firing frequency of the RCGCs to stabilise following impalement.

Following this, preparations were perfused with either the control saline (HEPES-buffered saline), 4-AP saline, TEA saline or NPPB saline. Preparations were bathed in each saline for 15 minutes before conducting protocols. This provided sufficient time for pharmacological agents to block the voltage-gated channels of interest (**section 3.2.2**).

As preparations were perfused in each saline for the same duration, RCGC firing properties were measured at the same time intervals across the four condition groups (**section 4.2.6**) during analysis.

4.2.6 Current clamp data analysis

Analysis of current clamp recordings was performed offline in Clampfit® from the pClamp version 10.5 software package. The following parameters (**section 2.2.7.1**) were assessed on unfiltered traces of spontaneously generated action potentials: 1) Firing frequency; 2) RMP; 3) action potential threshold; 4) amplitude of fAHP; 5) duration of sAHP, and; 6) action potential half-width.

With regards to analysis of SFA in the young CGCs (**section 2.2.7.2**), the frequency and half-width of evoked spikes were measured. In addition, instantaneous frequency and the inter-spike interval were measured to construct an '*instantaneous frequency (f) vs. time of spike (t)*' plot in order to determine the initial instantaneous firing frequency (f_0) and the steady state firing frequency (f_{ss}).

In each condition group, all spontaneous action potential parameters were measured at 25 minutes from the experimental trace recordings over a 5 minute duration. Measurements of SFA parameters were conducted at 30 minutes over a 2 minute period (depolarising protocol had been repeated three times within this duration and responses were average offline in Clampfit®; **section 2.2.3.1**).

4.2.7 Statistical Analysis

Experimental data was analysed for statistical significance in GraphPad Prism 7. A one-way ANOVA for independent samples was performed throughout this chapter as every data set contained more than two groups. When there was a significant difference, a Bonferroni multiple comparisons test was performed to identify where the significant change occurred.

The following p-values indicated that there was a significant difference: $*p < 0.05$, $**p < 0.01$, and $***p < 0.001$. For non-significant (NS) values, $p > 0.05$. All data in the results sections are presented as the mean $\pm$ standard error of the mean (SEM) and *n* represents the number of RCGCs each recorded from an individual preparation.

4.3 Results

4.3.1 The effects of blocking I_A, I_{DR} and I_{Cl} on CGC firing frequency

Figure 4.1A displays sample traces of spontaneously evoked CGC action potentials following inhibition of I_A, I_{DR} and I_{Cl}. Notably, it was observed in ~30-40% of young preparations from each drug treatment group that there were periods (or 'bursts') in which the inter-spike interval exhibited variability. These periods were not observed throughout most of the experimental recordings, although their frequency and duration in each treatment has yet to be examined in any further detail in this study.

Figure 4.1B reveals that TEA significantly decreased CGC firing frequency when compared to the control (p<0.001, *n=6* RCGCs; one-way ANOVA with Bonferroni post-hoc analysis) and preparations perfused with either 4-AP (p<0.01, *n=6* RCGCs) or NPPB (p<0.001, *n=6* RCGCs). Firing rates decreased by ~75% from 70.2 ± 2.8 spikes min^{-1} in the control to 22 ± 3.2 spikes min^{-1} in the TEA saline. Neither 4-AP nor NPPB significantly altered young CGC firing frequency when compared to the control (p>0.05 for both, *n=6* RCGCs) or each other (p>0.05, *n=6* RCGCs).
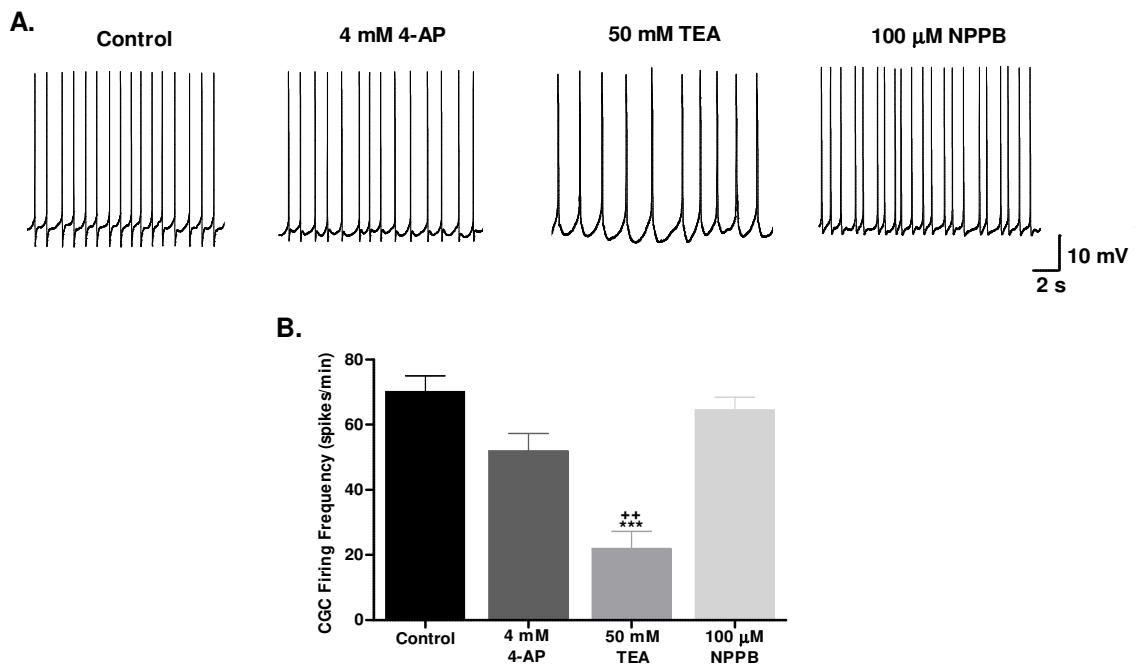
Figure 4.1| Young CGC firing frequency following inhibition of I_A, I_{DR} and I_{Cl}. (A) Sample traces illustrating the effects of blocking I_A, I_{DR} and I_{Cl} on spontaneous CGC firing. (B) Only TEA significantly altered CGC firing frequency, *via* a decrease, when compared to the control as well as 4-AP and NPPB-treated CGCs. Data shown as mean ± SEM, *n=6* RCGCs. ++p<0.01 *vs.* 4 mM 4-AP and ***p<0.001 *vs.* Control and 100 μM NPPB.

4.3.2 The effects of blocking I_A, I_{DR} and I_{Cl} on the CGC AHP and RMP

Sample traces in **Figure 4.2Ai** illustrates that 4-AP, TEA and NPPB all reduced the fAHP amplitude. This decrease to the fAHP of the young CGC action potential was significant when compared to the control (p<0.001 for each treatment, *n=6* RCGCs; one-way ANOVA with Bonferroni post-hoc analysis; **Figure 4.2Aii**). The fAHP amplitude did not significantly differ between the three treatment groups (p>0.05, *n=6* RCGCs).

Figure 4.2B revealed that TEA increased the sAHP duration by ~1000 ms when compared to the control (p<0.001, *n=6* RCGCs) and preparations perfused with either 4-AP (p<0.001, *n=6* RCGCs) or NPPB (p<0.001, *n=6* RCGCs). Interestingly, the RMP of the young CGCs became significantly more depolarised following treatment with either 4-AP (p<0.01, *n=6* RCGCs), TEA (p<0.001, *n=6* RCGCs) or NPPB (p<0.05, *n=6* RCGCs). The RMP did not significantly differ between the three treatment groups (p>0.05, *n=6* RCGCs).
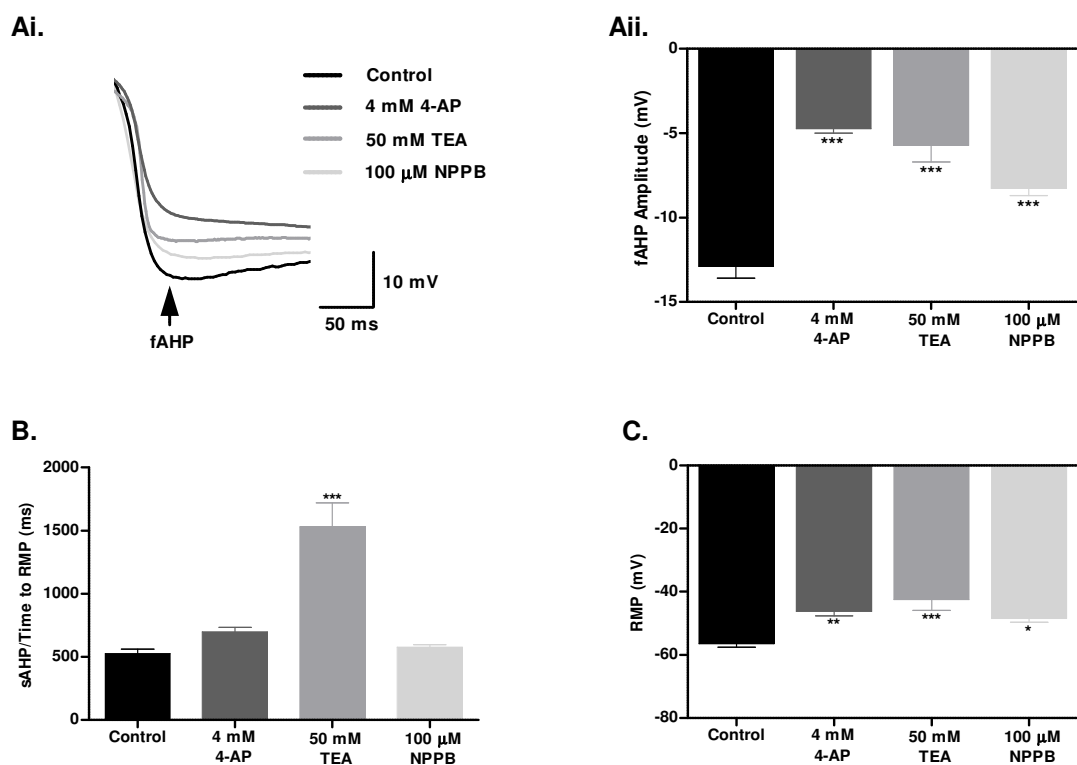
Figure 4.2| CGC AHP and RMP following inhibition of I_A, I_{DR} and I_{Cl}. (Ai) Sample traces of the fAHP demonstrates that this component decreases in each blocker. (Aii) This decrease was significant for each treatment when compared to the control. (B) Only TEA significantly altered the sAHP duration *via* an increase. (C) Each blocker significantly depolarised the RMP. Data shown as mean ± SEM, *n=6* RCGCs. *p<0.05, **p<0.01, ***p<0.001 *vs.* Control (Part A and C); ***p<0.001 *vs.* each group (Part B).

4.3.3 The effects of blocking I_A, I_{DR} and I_{Cl} on the CGC action potential half-width

Sample traces in **Figure 4.3A** displayed the dramatic alterations to the young RCGC action potential half-width following the addition of either 4-AP or TEA to the bathing saline. Both 4-AP and TEA significantly increased the half-width of the CGC action potential ($p < 0.01$ and $p < 0.001$, respectively, *n=6* RCGCs; one-way ANOVA with Bonferroni post-hoc analysis; **Figure 4.3B**) when compared to control and NPPB preparations. The TEA-treated CGC action potential was also significantly broader than the 4-AP-treated young CGC action potential ($p < 0.01$, *n=6* RCGCs). Conversely, NPPB treatment did not significantly alter the action potential half-width when compared to the control ($p > 0.05$, *n=6* RCGCs).

Notably, NPPB appeared to reduce the shoulder of the CGC action potential (arrowhead; **Figure 4.3A**) in every preparation (visual assessment only, *n=6;* data not shown).
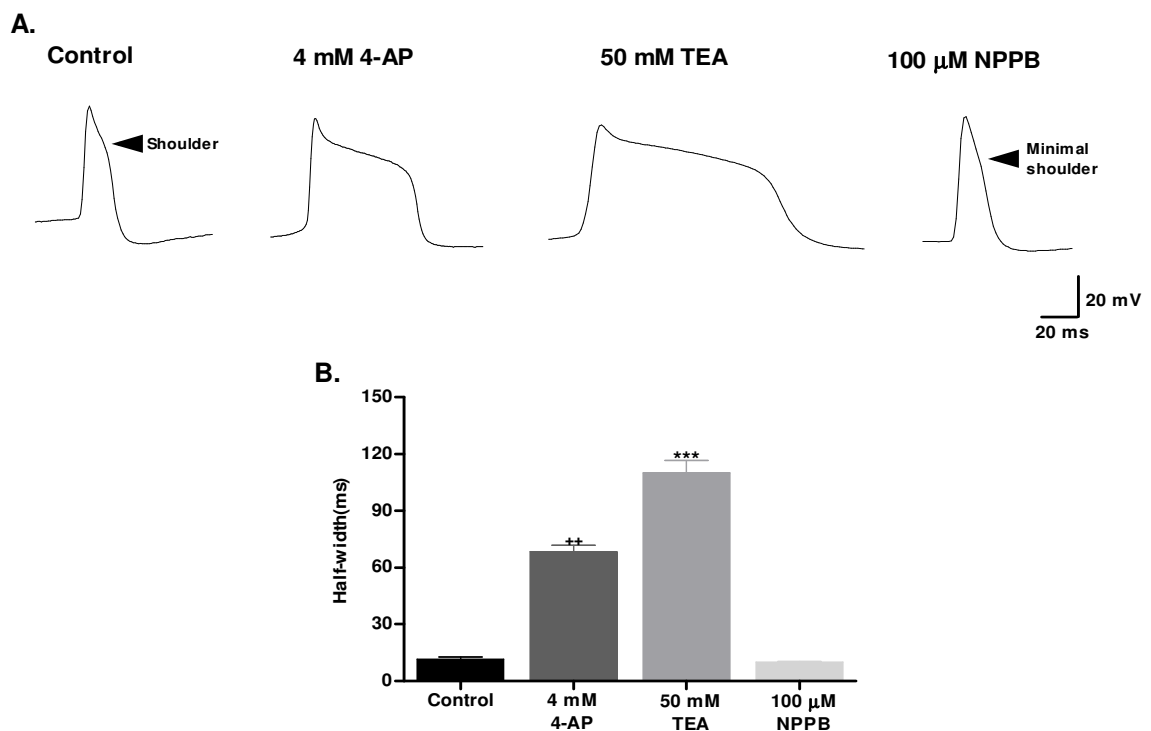
Figure 4.3| Action potential half-width following inhibition of I_A, I_{DR} and I_{Cl}. (A) Sample traces illustrate that TEA and 4-AP broaden the CGC action potential. NPPB reduced the shoulder of the repolarising action potential. (B) Whilst TEA had a more prominent effect on the action potential half-width than 4-AP, both significantly increased this parameter when compared to the control and NPPB-treated CGCs. Data shown as mean ± SEM, *n=6* RCGCs. ++p<0.01, +++/*p<0.001 *vs.* each CGC group. Graph symbols: asterisk (*) designated for 50 mM TEA and plus (+) for 4 mM 4-AP.**

4.3.4 The effects of blocking I_A, I_{DR} and I_{Cl} on evoked CGC firing frequency

4-AP significantly increased the number of CGC spikes (**Figure 4.4A**), evoked from the RMP during the 5 second 2 nA depolarising pulse, when compared to the control, NPPB-treated CGCs (p<0.01, *n=6* RCGCs for both*;* one-way ANOVA with Bonferroni post-hoc analysis) and TEA-treated CGCs (p<0.001, *n=6* RCGCs). Conversely, TEA significantly reduced the number of evoked spikes when compared to the control and NPPB-treated young CGCs (p<0.001 for both, *n=6* RCGCs). There was no significant difference between control and NPPB preparations (p>0.05, *n=6* RCGCs).

In **Figure 4.4B**, TEA significantly increased the half-width of evoked spikes when compared to the other CGC groups (p<0.001 for each group, *n=6* RCGCs). Evoked CGC spikes in 4-AP were significantly broader than the control and NPPB-treated young CGCs (p<0.05 for both, *n=6* RCGCs). NPPB did not alter the evoked action potential half-width when compared to the control (p>0.05, *n=6* RCGCs).
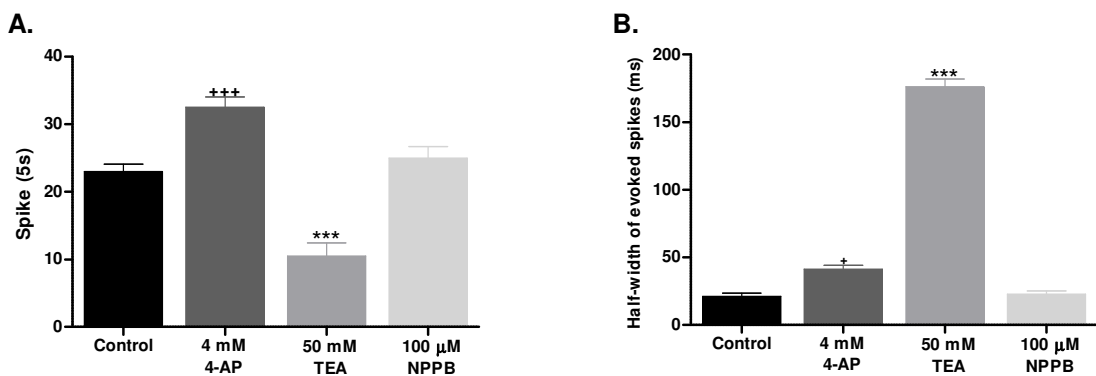
Figure 4.4| Evoked action potentials following inhibition of I_A, I_{DR} and I_{Cl}. (A) 4-AP and TEA significantly increased and decreased, respectively, the number of evoked CGC spikes. (B) 4-AP and TEA, but not NPPB, significantly increased evoked action potential half-width when compared to control CGCs. Data shown as mean ± SEM, *n=6* RCGCs. ⁺p<0.05, ⁺⁺⁺/*p<0.001 *vs.* each CGC group. Graph symbols: asterisk (*) designated for 50 mM TEA and plus (⁺) for 4 mM 4-AP.**

4.3.5 The effects of blocking I_A, I_{DR} and I_{Cl} on basic SFA parameters

Figure 4.5A illustrates a typical action potential burst generated by each treatment group during the 5 second 2 nA depolarising pulse evoked from the CGC RMP. **Figure 4.5B** displays a sample representative '*instantaneous frequency vs. time of spike*' plot from a single preparation in each treatment group. Both TEA and 4-AP appeared to slow SFA, as reflected by the shallow exponential decay, when compared to the control and NPPB-treated young CGCs.

Both f_0 (Hz) in **Figure 4.5Ci** and f_{ss} (Hz) in **Figure 4.5Cii** were significantly higher in CGCs treated with 4-AP when compared to control ($p<0.05$, *n=6* RCGCs; one-way ANOVA with Bonferroni post-hoc analysis), TEA ($p<0.001$, *n=6* RCGCs) and NPPB-treated CGCs ($p<0.01$, *n=6* RCGCs). TEA reduced f_0 (Hz) and f_{ss} (Hz) when compared to control and NPPB-treated CGCs ($p<0.001$ for both, *n=6* RCGCs). These parameters did not differ between control and NPPB-treated CGCs ($p>0.05$, *n=6* RCGCs).
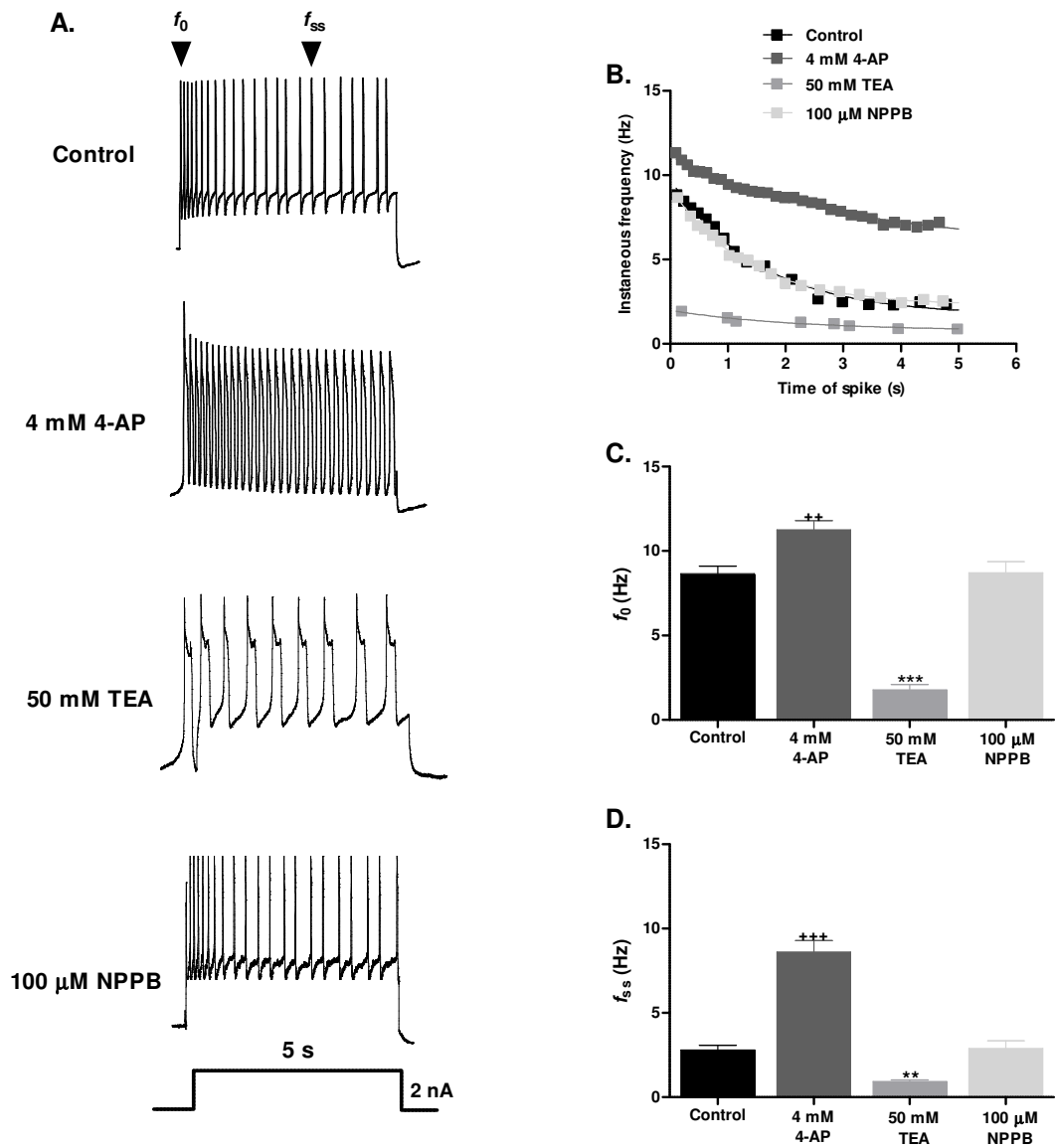
Figure 4.5| SFA parameters following inhibition of I_A, I_{DR} and I_{Cl}. (A) Sample traces of evoked young CGC spikes from each treatment group. (B) This representative plot revealed that SFA increased with 4-AP, decreased with TEA and was unaltered following NPPB treatment. Both (C)f_0 (Hz) and (D)f_{ss} (Hz) during SFA was significantly faster with 4-AP and slower in TEA when to compared to the control and NPPB-treated CGCs. Data shown as mean ± SEM, $n=6$ RCGCs. $^{++/**}$p<0.01, $^{+++/***}$p<0.001 $vs.$ each CGC group. Graph symbols: asterisk (*) designated for 50 mM TEA and plus ($^+$) for 4 mM 4-AP.

4.3.6 Result summary of the changes to the young CGC action potential parameters following the inhibition of I_A, I_{DR} and I_{Cl}

CGC Parameter	Young control CGC parameter values	Parameter altered by blocking I_A with 4 mM 4-AP?	Parameter altered by blocking I_{DR} with 50 mM TEA?	Parameter altered by blocking I_{Cl} with 100 µM NPPB?
Spontaneous CGC Action Potentials				
Firing frequency	70.1 ± 4.8 spikes min^{-1}	⬇ 50.2 ± 2.1 spikes min^{-1} **(NS)**	⬇ 22.3 ± 3.2 spikes min^{-1} **(***)**	**No Change** 64.7 ± 3.8 spikes min^{-1} **(NS)**
fAHP	-11.89 ± 0.6 mV	⬇ -4.72 ± 0.3 mV **(***)**	⬇ -6.72 ± 0.9 mV **(***)**	⬇ -8.26 ± 0.4 mV **(***)**
sAHP	523.4 ± 39.7 ms	⬆ 697.6 ± 34.7 ms **(NS)**	⬆ 1530.3 ± 180.2 ms **(***)**	**No Change** 578.2 ± 21.5 ms **(NS)**
RMP	-56.5 ± 1.1 mV	⬆ -46.4 ± 1.5 mV **(**)**	⬆ -42.1 ± 2.5 mV **(***)**	⬆ -48.1 ± 1.6 mV **(*)**
Half-Width	11.5 ± 1.2 ms	⬆ 65.7 ± 3.2 ms **(**)**	⬆ 110.1 ± 10.4 ms **(***)**	**No Change** 10.1 ± 0.9 ms **(NS)**
Evoked CGC Action Potentials				
Firing rate	23.1 ± 1.2 spikes/5s	⬆ 32.5 ± 1.5 spikes/5s **(***)**	⬇ 10.5 ± 1.9 spikes/5s **(***)**	**No Change** 25.1 ± 1.7 spikes/5s **(NS)**
Half-width	21.30 ± 2.5 ms	⬆ 41.8 ± 2.9 ms **(*)**	⬆ 176.2 ± 5.7 ms **(***)**	**No Change** 22.9 ± 2.3 ms **(NS)**
f_0 **(Hz)**	8.6 ± 0.5 Hz	⬆ 11.5 ± 0.5 Hz **(**)**	⬇ 1.8 ± 0.3 Hz **(***)**	**No Change** 8.7 ± 0.6 Hz **(NS)**
f_{ss} **(Hz)**	2.8 ± 0.3 Hz	⬆ 8.62 ± 0.6 Hz **(***)**	⬇ 0.93 ± 0.2 Hz **(**)**	**No Change** 2.88 ± 0.4 Hz **(NS)**

Table 4.1| Changes to young CGCs properties following suppression of I_A, I_{DR} or I_{Cl}. Symbols: Red upward facing arrow indicates a significant increase of the parameter, while red downward facing arrows indicate a significant decrease of the parameter. Black upward or downward facing arrows indicate that a substantial (>20% change) but not significant increase or decrease of the parameter, respectively. Data shown as mean ± SEM, *n=6* RCGCs for each treatment. *p<0.05, **p<0.01 and ***p<0.001 *vs*. control young CGCs. NS, not statistically significant.

4.4 Discussion

Experiments in this chapter had examined the role of I_A, I_{DR} and I_{Cl} in shaping the young CGC action potential and regulating firing frequency. Blocking I_A and I_{DR} with 4-AP and TEA, respectively, caused action potential broadening, reduced the fAHP amplitude, depolarised the RMP and suppressed SFA in young CGCs. However, inhibition of I_{DR} also increased the sAHP duration and ultimately decreased spontaneous CGC firing frequency. Although, suppression of I_{Cl} with NPPB also resulted in a decrease in the fAHP amplitude and depolarisation of the RMP, no changes were observed in other parameters that had been assessed including firing frequency.

4.4.1 Role of voltage-gated outward current in spontaneously elicited CGC action potentials

Inhibition of either I_A, I_{DR} or I_{Cl} significantly reduced the fAHP of the young CGC action potential, strongly suggesting that both voltage-gated outward K^+ and Cl^- currents have an important role in regulating this parameter in the *Lymnaea* CGCs. In mammalian neurons the Ca^{2+}-activated K^+ current, BK, has been cited by numerous studies as the principle mediator of the fAHP, whilst the involvement of voltage-gated K^+ channels has often been overlooked[259,292]. However, the few investigations that have examined voltage-gated K^+ currents in relation to the fAHP have also highlighted their importance[522,385,146,373]. For example, a study in rat neocortical neurons demonstrated that the fAHP was significantly reduced following the application of 4-AP, defying preconceptions that the fast inactivation properties of I_A precludes this current from having a significant role in regulating the fAHP[522]. Even in other invertebrate neurons such as *C. elegans*, I_A has been shown to have an important role in mediating the fAHP of action potentials[399].

In hippocampal mouse neurons, it has been shown that blocking I_{DR} with either TEA or guangxitoxin (specific I_{DR} blocker for K_v2 channels) significantly reduces the fAHP amplitude[264]. The role of I_{DR} has not been as extensively investigated in other invertebrate neurons. However, the findings in this study corroborated the work of both Staras *et al*. (2002) and Vavoulis *et al*. (2012) by showing that the fAHP of the young CGC action potential significantly reduces following inhibition of I_{DR}[457,416]. All results yielded with I_{DR}, however, needs to be interpreted with some caution as inhibition of this current will occur in other neurons of the CNS and also substantially broaden their action potentials. This will increase neurotransmitter release and subsequently enhance synaptic

inputs onto the CGCs. These inputs may then modulate other ionic currents in the CGCs to alter an array of action potential parameters, including the fAHP.

A few different experimental approaches could be implemented in the future to prevent changes in neurotransmitter release in the *Lymnaea* CNS, caused by the indirect effects of manipulating voltage-gated outward currents, from altering CGC properties. First, a Hodgkin-Huxley type of mathematical model of the CGCs could be developed- similar to that by Vavoulis *et al.* (2012)- to accurately assess the contribution of I_{DR} as well as other ionic currents to the CGC action potential in the absence of extrinsic interferences[457]. The Vavoulis *et al.* (2012) model will need to be modified to include ionic currents that were newly discovered in Chapter 3 (I_{Cl}, I_R and the TEA/4-AP/Cl⁻ insensitive current) and cannot be utilised until the model is capable of accurately reproducing the behaviour of the CGCs observed *in vitro*. Only then can the properties of I_{DR}, for example, be manipulated to examine its role in the CGC action potential waveform and firing frequency.

Another approach that could be performed is to chemically isolate the CGCs in the *Lymnaea* CNS. As demonstrated previously by Yeoman *et al.* (2008), for example, this can be accomplished by bathing preparations in a high Mg^{2+}/zero Ca^{2+} saline[507]. The lack of Ca^{2+} in the saline should be sufficient to block neurotransmitter release, which is dependent on Ca^{2+} influx *via* VGCCs[179]. The high Mg^{2+} concentration in this saline is an additive measure that will block Ca^{2+} influx by outcompeting it for its channels and thus assist in attenuating neurotransmission[107]. However, this method is not ideal as it would affect numerous Ca^{2+}-dependent events that are critically important for the proper functioning of neurons[294,447]. The resultant suppression of Ca^{2+}-dependent currents will also alter the action potential waveform, which may mask the effects that blocking I_{DR} or any other currents have on the CGCs and could make it more difficult to determine their roles.

Alternatively, experiments could be conducted on cultured isolated CGCs. The process of isolating CGCs from the *Lymnaea* CNS has been well characterised in numerous studies such as that by Straub *et al.* (2001) and Koert *et al.* (2001)[426,235]. Whilst this technique is relatively laborious, the guarantee that CGC firing properties are not altered by the actions of other neurons and the ability to still conduct both current and voltage clamp recordings significantly outweighs this minor limitation.

Overall, the findings yielded from the CGCs in this study as well those generated previously has now provided overwhelming evidence for the important and significant role of voltage-gated K^+ outward currents in regulating the fAHP of a neuronal action potential.

Whilst it is often regarded that voltage-gated outward Cl^- currents are involved in hyperpolarising neurons, no studies to date have shown that I_{Cl} actively contributes to the fAHP of action potentials[266,121]. To our knowledge, this is the first study to demonstrate that the outward I_{Cl} is involved in regulating the fAHP. However, as with I_{DR} some consideration needs to be taken into account when generating such statements as inhibition of I_{Cl} has been shown to significantly increase synaptic inputs onto neurons[519,56]. Interestingly, an increase in synaptic inputs was observed during recordings of the CGCs in the presence of NPPB. Again, this highlights the importance of future experiments to be conducted using cultured isolated CGCs or a computational CGC model.

This chapter also revealed that inhibition of I_{DR} caused a significant increase to the duration of the sAHP in young CGCs. This corroborated previous findings in mammalian hippocampal neurons that have shown blocking I_{DR} with TEA significantly increases the sAHP[391,120,425]. Initially, this may seem odd considering that delayed rectifiers are one of the major conduits for K^+ efflux in neurons and as such would be expected to have a significant role in hyperpolarising neurons by contributing to the development of the sAHP. Indeed, a few studies have also shown that enhancement rather than attenuation of I_{DR} increases the sAHP[264,232].

Numerous studies have demonstrated that the sAHP is primarily mediated by Ca^{2+}-activated K^+ channels conducting the I_{sAHP}[364,292,393]. Interestingly, suppression of I_{DR} has been linked to an increase in Ca^{2+} influx and it is believed that this may then increase the Ca^{2+}-dependent I_{sAHP}[369,227,391]. An investigation in *Archidoris montereyensis* (a mollusc) neurons, for example, revealed during electrophysiological and Ca^{2+} imaging experiments that I_{DR} inhibition facilitated greater Ca^{2+} influx by significantly extending the plateau phase of action potentials[6]. This occurs because broadening of the action potential increases the duration a cell spends above the activation threshold for voltage-gated Ca^{2+} currents, which then leads to an increase in Ca^{2+} influx. In mammalian neurons, it has been shown that this Ca^{2+} influx largely occurs *via* L-type channels and consequently augments I_{sAHP}[16,69,263].

Interestingly, in the young CGCs of this study there was a significant increase in the action potential half-width following suppression of I_{DR} that was also accompanied with prolongation of the plateau phase. Firstly, this indicates that I_{DR} has an important role in the repolarisation phase of the CGC action potential. This supports previous findings from mammalian and other invertebrate neurons that have demonstrated that a decrease in the rate of repolarisation is caused by a decrease in the I_{DR} conductance and *vice versa*[231,264,457]. Secondly, this strongly suggests that inhibition of I_{DR} in the CGCs causes an increase in the sAHP *via* action potential broadening, greater Ca^{2+} influx and an increase in the underlying I_{sAHP}[392].

Conversely, inhibition of I_A in young CGCs did not significantly alter the duration of the sAHP and this is probably due to its relatively fast inactivation kinetics. However, there was significant broadening of CGC action potentials and this supported previous studies demonstrating that I_A has an important role in regulating action potential repolarisation[13,231]. The observation that the sAHP duration did not significantly enhance despite significant broadening of the CGC action potential was also interesting. This suggests that the expected increase in Ca^{2+} influx *via* the broader action potential is not sufficient to activate enough Ca^{2+}-activated K^+ channels needed to considerably augment the I_{sAHP} underlying the sAHP[392].

Given that the sAHP is generated by the actions of multiple channels (including apamin-sensitive and insensitive Ca^{2+}-activated K^+ channels) and that it has been documented that 4-AP can block some apamin-insensitive Ca^{2+}-activated K^+ channels[6,344,17], it is not inconceivable that 4-AP may be blocking some Ca^{2+}-activated K^+ channels. This could explain the lack of significant increase in the sAHP, even if there is greater Ca^{2+} influx *via* the broader 4-AP treated CGC action potential.

The suppression of I_{Cl} was not associated with any significant alterations to the sAHP and unlike inhibition of I_A and I_{DR}, there was no significant change to the half-width of the CGC action potential. The lack of change to the sAHP following NPPB treatment was not unexpected as to date there have been no studies detailing the involvement of voltage-gated outward chloride channels regulating the sAHP in neurons.

Studies have shown that CLC4-6 (with the exception of CLC-7) have fast deactivation kinetics and this could explain their lack of involvement in mediating the sAHP[9]. However, considering it is generally thought that voltage-gated outward Cl^- channels are

involved in action potential repolarisation it was quite surprising to observe that there was no significant alteration to the CGC action potential half-width following NPPB treatment[467]. This may be due to the very small magnitude of I_{Cl} underlying the young CGC action potential. Alternatively, the lack of change may potentially be due to NPPB's capacity (as demonstrated in some mammalian neurons) to inhibit Ca^{2+} channels such as L-type channels, which would act to narrow the action potential[105,523].

Interestingly, it was observed that the "shoulder" of the young CGC action potential- a feature mediated by Ca^{2+} influx- was markedly reduced in the presence of NPPB. This strongly suggests that there may be a decrease in Ca^{2+} influx[449,395]. Performing Ca^{2+} imaging experiment in the future will help determine if this is true. Conversely, the lack of change in half-width may be due to NPPB increasing synaptic inputs onto the CGCs. This could counteract any potential increase to the half-width that may be caused by suppression of I_{Cl} by increasing the conductance of other currents involved in repolarisation such as I_A or I_{DR}.

A common alteration observed following suppression of either I_A, I_{DR} or I_{Cl} was significant depolarisation of the young CGC RMP. The findings with I_A and I_{DR} corroborated previous studies that have shown that these currents have a significant influence on regulating a negative RMP in neurons, particularly as they both activated near the RMP[233,47,237]. For example, in some mammalian and invertebrate neurons application of 4-AP or TEA to block I_A and I_{DR}, respectively, results in significant depolarisation of the RMP[237,497,474].

With regards to I_{Cl}, very few studies have examined the role of voltage-gated outward Cl^- channels in regulating the RMP. A study in rat hippocampal neurons, for example, demonstrated that inhibition of I_{Cl} significantly depolarised the RMP[473]. However, it is known that the activation threshold for I_{Cl} is significantly more positive than the RMP which, coupled with its relatively fast deactivation, would suggest that very little current is active around the RMP[9,490]. Additionally, the small magnitude of this current in the young CGCs supports this notion and suggests that this may be due to NPPB potentially blocking Ca^{2+} currents. Studies have shown that Ca^{2+}-activated K^+ channels can have an important role in regulating the RMP[306]. Thus, any potential block to Ca^{2+} influx by NPPB would decrease the conductance of these channels and subsequently lead to significant depolarisation of the RMP[306].

How do these changes to the action potential waveform following the suppression of either I_A, I_{DR} or I_{Cl} alter young CGC firing frequency? The inhibition of I_{Cl} with NPPB did not significantly alter CGC firing frequency despite the decrease in the fAHP and depolarisation of the RMP. This did not support previous studies in hippocampal neurons and dorsal root ganglion neurons, for example, which have shown that inhibition of I_{Cl} significantly increases firing frequency[331,473]. It was expected that the fAHP decrease and depolarisation of the RMP following I_{Cl} inhibition would have increased firing of the CGCs, as it should take less time for them to re-establish their RMP following action potential firing and subsequently less time to reach the threshold of the next action potential. As this did not happen, it suggests that the fAHP and RMP may not necessarily be important for regulating CGC firing frequency.

Given the number of ionic currents shown in our laboratory (this and prior investigations) and by others to influence the CGC RMP such as I_A, I_{DR}, I_{Cl} and $I_{Na(p)}$, for example, it is entirely plausible that the RMP may not be a fundamental regulator of CGC firing frequency[392,316,416]. The possible reason for this is that a change in any one of these currents may be compensated by changes to the properties of other currents involved in regulating the RMP in an attempt to stabilise and minimise significant alterations to CGC firing frequency. This may be particularly important in *Lymnaea* where *in vivo* and *in vitro* studies have demonstrated that CGC firing frequency is an important modulator of feeding frequency[508,506,507,336]. It may not be ideal in snails that depolarisation of the CGC RMP, or even hyperpolarisation, is accompanied with significant changes to firing frequency as this could cause snails to feed unnecessarily or attenuate feeding. Ultimately, this would likely affect the health and lifespan of the snails.

The notion that the RMP may not necessarily be important for regulating CGC firing frequency in young snails was supported by findings by Kemenes *et al.* (2006)[226]. This study revealed that spontaneous CGC firing rates of conditioned snails did not significant differ from unconditioned snails despite significant depolarisation of the RMP[226]. Whilst this demonstrates that depolarisation of the CGC RMP is a key event during memory formation, it also strongly suggests that it is important for CGC firing frequency to be kept relatively constant in young snails- regardless of changes to the RMP- possibly in order to regulate other associated behavioural outputs.

The suggestion that the fAHP and RMP may not be important for regulating CGC firing frequency may not be entirely true and could just be dependent by how much these

parameters are altered. It may be that further depolarisation of the RMP or further reduction of the fAHP amplitude would have resulted in a significant increase in CGC firing frequency, consistent with observations following injection of 2 nA depolarising pulse during SFA experiments.

Inhibition of I_A with 4-AP resulted in a slight (~26%), but not significant decrease in CGC firing frequency. Previous studies, particularly in cortical and hippocampal neurons have shown an increase in firing frequency following inhibition of I_A with 4-AP[283,133,262]. It would have been expected that the decrease in the fAHP and depolarisation of the CGC RMP caused by I_A inhibition would have significantly increased firing frequency, but for the same reasons discussed with I_{Cl} this may not necessarily be the situation and suggests (with caution) that both the fAHP and RMP may not be important determinants of CGC firing frequency.

Even if changes in the fAHP and RMP were to have increased CGC firing, it is likely that this would have been masked by the significant increase in the action potential half-width that also occurred following the attenuation of I_A. This suggests that half-width is an important parameter for regulating CGC firing frequency and supports other studies in mammalian neurons that have shown that alterations to the action potential half-width has a significant impact on neuronal firing rates[390,34]. However, the increase in the action potential half-width promotes a decrease in spontaneous CGC firing frequency and as such does not support previous studies that have reported an increase in firing rates following inhibition of I_A.

At present, the studies that have described the increase in spontaneous firing frequency following I_A inhibition have not measured the action potential half-width, whereas those that have reported action potential broadening have not examined firing frequency[283,133,262,457]. Thus, it could be that an increase in firing frequency is not associated with action potential broadening, whereas a decrease could be due to action potential broadening. This may be a reflection of different A-type K^+ channel subtypes with slightly different inactivation kinetics, for example, that are expressed by these neurons[283,133,262,457]. To date, this possibility has not been examined in any detail.

The changes to the action potential shape following I_{DR} suppression were associated with a significant decrease in CGC firing. This finding corroborated Staras *et al.* (2002) study, which also observed a decrease in CGC firing following the application of TEA[416].

Although, it is well regarded that I_{DR} is important for regulating neuronal firing in mammalian neurons, the effects of blocking this current on spontaneous firing frequency has not been extensively explored. Indeed, the very few studies that have examined this have also shown that suppressing I_{DR} leads to a decrease in neuronal firing[197,517]. For example, Colwell et al. (2005) demonstrated that I_{DR} inhibition caused a significant decrease to spontaneous firing frequency in mice suprachiasmatic nucleus (SCN) neurons[197]. Such studies also noted that the decrease in firing frequency following I_{DR} suppression was due to a significant increase in action potential half-width and a significant increase in the sAHP, which had also been observed in this study.

Overall, two important findings were yielded about the regulation of spontaneous CGC firing in this study. First, it was revealed that I_{DR} is a very important voltage-gated outward current for controlling young CGC firing frequency, whereas I_A has a much smaller influence and I_{Cl} has no involvement. Second, it appears that the half-width and the sAHP are particularly crucial parameters of the action potential waveform involved in regulating CGC firing frequency.

4.4.2 Changes to evoked CGC firing properties following inhibition of voltage-gated outward currents

The ionic profile mediating SFA in the CGCs has not been extensively examined. Thus, it was of interest in this study to assess whether I_A, I_{DR} and I_{Cl} were involved in regulating SFA in the young CGCs.

Inhibition of both I_A and I_{DR} significantly impeded SFA in the young CGCs. This supported previous studies that have shown suppression of either I_A or I_{DR} slows SFA, highlighting the importance of voltage-gated outward K^+ currents in this neuronal property. However, the means by which inhibition of I_{DR} changed SFA in the young CGCs was not consistent with previous observations in the literature[18,152].

In this study, blocking I_{DR} altered SFA by reducing both initial (f_0) and steady-state (f_{ss}) instantaneous firing frequencies. Other studies in rat sympathetic neurons or mouse hippocampal neurons, for example, have demonstrated that inhibition of I_{DR} causes an increase in both f_0 (Hz) and f_{ss} (Hz) as opposed to a decrease[18,152,159]. The decrease in f_0 (Hz) and f_{ss} (Hz) in the young CGCs following the inhibition of I_{DR} was due to a significant increase in half-width of the evoked spikes, by ~150 ms, when compared to the control. Interestingly, previous studies in hippocampal neurons noted that evoked

spikes were much narrower following I_{DR} inhibition. This narrowing was due to an increase in the activity of BK channels caused by an increase in Ca^{2+} influx into the cell, which promoted repolarisation[159]. Given that evoked spikes were significantly broader in the young CGCs following I_{DR} suppression alluded to the possibility that BK channels may not be expressed by the CGCs. Alternatively, the increase in synaptic inputs to the CGCs following the perfusion of TEA may be suppressing currents involved in repolarisation and thus diminishing the ability of young CGCs to counteract the increase in spike half-width caused by I_{DR} inhibition.

With regards to inhibition of I_A, it was found that the alterations to SFA were caused by an increase in the number of evoked spikes that corresponded with a significant increase in both f_0 (Hz) and f_{ss} (Hz) to similar rates. This corroborated previous studies in mammalian neurons, including those from the hippocampus and amygdala, that have demonstrated that attenuation of I_A with 4-AP increases both f_0 (Hz) and f_{ss} (Hz). These studies noted that this increase was due to a reduction in the amplitude of the fAHP and a decrease in the inter-spike interval, which enabled neurons to evoke more spikes in response to the depolarising stimulus. Indeed, observational analysis of the high frequency bursts generated by young CGCs treated with 4-AP revealed that there was a clear decrease in the fAHP and inter-spike interval. Whilst there was a significant increase in half-width due to the role of I_A in spike repolarisation, this increase from the control was not as extreme as with I_{DR} (~17 ms as opposed to ~150 ms) and thus, did not appear to have a significant influence on decreasing the frequency of evoked spikes. This highlights an important point raised previously in that many of the parameters involved in shaping the action potential can alter firing frequency, but the extent of this depends on the magnitude by which these parameters change.

Inhibition of I_{Cl} did not alter any of the SFA parameters in the young CGCs. No studies to date in mammalian or other invertebrate neurons have explored the involvement of voltage-gated outward Cl⁻ currents in SFA and thus, this is the first study to establish that I_{Cl} is not an important conductance required for the modulation of SFA in neurons.

Note, all data regarding the role of voltage-gated outward currents in regulating intrinsic CGC excitability must be interpreted with caution due to the experimental design limitation of this study by stimulating CGCs from their RMP and not from a defined membrane potential (**section 2.4.3**).

4.4.3 The role of voltage-gated outward currents in old and AAPH-treated young CGC action potentials

The aim of experiments in this chapter had been to establish the role of I_A, I_{DR} and I_{Cl} in regulating the CGC action potential waveform and firing frequency. As this was accomplished by blocking these currents, it was easier to ascertain the function of these currents *via* this manner in young CGCs rather than in the old or AAPH-treated CGCs due to the nature of changes exhibited by some of the currents in these CGCs. However, it would be interesting for future experiments (when more animals are available and samples are prepared) to manipulate voltage-gated outward currents in old and AAPH-treated young CGCs using either blocker or activators, where appropriate, to examine the role of these currents in the altered CGC action potential waveform.

Given that I_A increased in the CGCs with age and acute OS due to slower activation and inactivation, it would be possible for experiments to inhibit this current with 4-AP to investigate its role. With the action potentials narrower and the fAHP larger in both the old and AAPH-treated young CGCs, it is predicted that suppression of I_A would significantly broaden action potentials and decrease the fAHP amplitude. It is unlikely, however, that these CGCs will resemble a young control CGCs following the alterations to the action potential half-width and fAHP when I_A is blocked. This stems from the observations that the magnitude by which inhibition of I_A altered the action potential half-width and fAHP was substantially large in the young CGCs. Thus, it would be more sensible to lower the 4-AP concentration to decrease I_A in old and AAPH-treated young CGCs rather than block it completely and then examine whether reversal of the altered action potential waveform, with respect to these particular parameters, more accurately reflects a young control CGC.

It is also predicted that the RMP will depolarise in the old and AAPH-treated young CGCs following I_A inhibition. Whilst the RMP of old CGCs was significantly more hyperpolarised than the AAPH-treated young CGCs, it is unlikely that this is due to I_A as the properties of this current did not significantly differ between these CGCs. Thus, it is expected that the RMP of both old and AAPH-treated young CGCs will depolarise by approximately the same magnitude following I_A suppression.

It had been postulated that the slow inactivation kinetics of I_A with age and acute OS may contribute towards a very small increase in the early phase of the sAHP (**section 3.4.2**). Therefore, it is predicted that inhibition of I_A in these CGCs- unlike young CGCs- would

slightly reduce the sAHP duration. It is doubtful whether this would significantly reverse the decrease to spontaneous CGC firing frequency with age and acute OS, as the sAHP duration would still be extremely long due to alterations in other ionic currents[392]. Furthermore, the significant broadening of action potentials that is also likely to be encountered following I_A inhibition in old and AAPH-treated young CGCs would probably mask any effects that slightly reducing the sAHP may have on CGC firing frequency. Even if the 4-AP concentration was reduced to lessen broadening of action potentials, this consequently would decrease any potential reduction to the sAHP.

It is predicted, however, that there will be an increase in evoked firing rates following I_A inhibition in the old and AAPH-treated young CGCs. This is only likely to be a partial reversal, as it is has been reported previously that alterations to other ionic currents contribute significantly to the decrease in evoked CGC firing frequency with age[392].

As the properties of I_{DR} were not altered with age or acute OS, this current could be blocked with TEA in future experiments to explore its role in the CGC action potential. First, it is predicted that suppression of I_{DR} will (as in young CGCs) significantly decrease the fAHP and depolarise the RMP. Given that the fAHP increased by ~6 mV with age and acute OS and that I_{DR} inhibition in young CGCs caused a reduction by ~7 mV, it may be observed that the fAHP in the old and AAPH-treated CGCs bathed in TEA will no longer differ significantly from young control CGCs.

The same could also be observed with the RMP of the old CGCs, where there was a hyperpolarisation of ~13 mV and I_{DR} inhibition in young CGCs depolarised the RMP by ~14 mV. Despite this, there will be still be differences in the behaviour of the underlying ionic currents regulating these parameters in the old and AAPH-treated CGCs when compared to young CGCs.

Second, it is predicted that suppression of I_{DR} (*via* its direct effects and/or possible indirect effects; **section 4.4.1**) will further increase the sAHP duration in old and AAPH-treated CGCs as well as significantly broaden spontaneous and evoked action potentials. It is also postulated that these particular alterations to the action potential waveform will then further decrease both spontaneous and evoked firing rates in these CGCs.

With regards to I_{Cl}, this current was suppressed in the old and AAPH-treated young CGCs and so it is not possible to examine its role in the CGC action potential by blocking it. It may still be useful, however, to conduct this experiment for another reason and that is to

determine whether alterations to the young CGC action potential waveform following I_{Cl} inhibition with NPPB may have been caused by the potential indirect effects of this antagonist.

As knowledge about the indirect effects of NPPB is limited, it is predicted that NPPB will not alter the action potential waveform in the old and AAPH-treated young CGCs given that I_{Cl} is already suppressed in these CGCs. If there is a decrease in the fAHP and depolarisation of the RMP (as observed in young CGCs treated with NPPB) this would then strongly suggest, as previously postulated, that NPPB may be having indirect effects on Ca^{2+}-dependent currents and/or neurotransmitter release (**section 4.4.1**).

It would also be interesting to perfuse a voltage-gated Cl⁻ channel agonist over old and AAPH-treated young preparations to examine how the CGC action potential waveform is altered. If an agonist is successful in causing voltage-gated Cl⁻ channels to conduct a Cl⁻ current again in these CGCs (this is dependent on how the channels are modified), it is predicted based on findings from young CGCs (disregarding speculation about possible non-specific effects of NPPB) that the fAHP will increase and the RMP will hyperpolarise.

The biggest challenge of this approach is finding a suitable activator, as the selection of agonists currently available is extremely small when compared to Ca^{2+}-activated Cl⁻ channels and volume-regulated Cl⁻ channels. This is perhaps due to less information known about the pharmacology of voltage-gated Cl⁻ channels[462].

4.5 Conclusion

In conclusion, this chapter examined the role of I_A, I_{DR} and I_{Cl} in shaping the young CGC action potential waveform and regulating firing frequency. It was revealed that all these currents were involved in hyperpolarising the CGCs *via* the RMP and fAHP. It was also observed that both I_A and I_{DR} contributed to regulating the rate of action potential repolarisation in the CGCs. Moreover, it was identified that I_{DR} significantly influenced spontaneous CGC firing frequency predominately *via* its modulation of the CGC action potential half-width and sAHP. Importantly, this study also highlighted that future experiments need to be conducted on cultured isolated CGCs and/or on a computational CGC model to allow for the functions of various currents to be precisely characterised in the CGCs without potentially being altered by extrinsic processes.

Chapter 5: General Discussion

Experiments in this thesis utilised the pond snail, *Lymnaea stagnalis,* to investigate the mechanisms underlying neuronal ageing in a pair of modulatory interneurons, the cerebral giant cells. Evidence revealed that the increase in OS in the ageing cerebral ganglia was accompanied with a decrease in CGC firing frequency, alterations to the CGC action potential waveform and a decrease in feeding frequency in old snails. These age-related changes were largely mimicked in young preparations following the induction of acute OS with extracellular AAPH treatment. This suggested that OS may be responsible for mediating the age-related changes in the CGCs. In addition to these findings, the properties of the newly discovered I_{Cl}, I_R and TEA/4-AP/zero Cl$^-$ insensitive current were characterised along with I_A and I_{DR} in the old and AAPH-treated young CGCs. Interestingly, it appeared that the similar changes incurred to the voltage sensitivity and activation/inactivation kinetics of I_A with age and acute OS may profoundly alter the CGC action potential waveform.

5.1 What underlies changes to the CGC action potential waveform and the decrease in firing with age and acute OS?

Chapter 2 demonstrated that the decrease in spontaneous and evoked CGC firing frequency with age was associated with an increase in the amplitude and duration of the AHP, hyperpolarisation of the RMP, narrowing of the action potential and slowing of SFA. These age-related electrophysiological changes were mimicked in young CGCs following acute treatment with extracellular AAPH, with the exception of the RMP and SFA.

Experiments in Chapter 4 established using young CGCs that I_{DR} has a very important role in regulating all the action potential parameters that exhibited changes with age and acute OS. Despite this, I_{DR} could not be accountable for any of these alterations as Chapter 3 demonstrated that the properties of this current were not altered with age or acute OS. Likewise, the role of the newly identified I_{Cl} in modulating the RMP and fAHP (inhibition of this current depolarised the RMP and reduced the fAHP in young CGCs) could not be accountable for the hyperpolarised RMP or larger fAHP observed in the old and 3 mM AAPH-treated young CGCs because this current was suppressed.

Of all the voltage-gated outward currents examined in this thesis, there was strong evidence to suggest that the changes to the properties of I_A with age and acute OS may be responsible for some of the alterations to CGC firing properties. The first of these parameters was the action potential half-width. I_A is known to have an important role in regulating the half-width, as Chapter 4 showed that suppression of this current with 4-AP significantly broadened young CGC action potentials. AP-clamp experiments also corroborated this by demonstrating that I_A was the largest current present during the repolarisation phase of a young CGC action potential. Whilst the peak amplitude of I_A did not change with age or acute OS, the slower activation (due to weaker voltage sensitivity and altered activation kinetics) coupled with slower inactivation suggests that more I_A will be available during the repolarisation phase of the old and 3 mM AAPH-treated young CGC action potentials. This altered sequence of events is likely to increase the rate of repolarisation, which would explain the narrowing of action potentials in the old and 3 mM AAPH-treated young CGCs. AP-clamp experiments will need to be performed in these CGCs in the future to confirm if more I_A is active during the repolarisation phase.

The increase in the fAHP with age and acute OS could also be explained by the altered properties of I_A. Chapters 3 and 4 had shown that I_A was an important regulator of the fAHP as its amplitude was reduced following the inhibition of this current in young CGCs. Thus, the slower inactivation of I_A observed with age and acute OS indicates that a greater proportion of this current will still be active during the development of the fAHP and so could contribute to its increase in amplitude.

Contrary to the half-width and fAHP, the slow inactivation kinetics of I_A with age and acute OS is unlikely to be fully responsible for the increase to the sAHP. This is based on evidence from Chapter 3 where it was shown that I_A takes ~70 ms to completely inactivate compared to the typical duration of the sAHP, ~2000 ms, in both the old and 3 mM AAPH-treated young CGCs. Thus, I_A (if involved) could potentially only contribute to an increase in the early phase of the sAHP.

Interestingly, similar findings have been observed in *C. elegans* where slow inactivation of I_A in ageing neurons contributes towards a slight increase in the duration of the AHP[59,398]. This result along with the CGCs, suggests that other currents (not examined in this study) are predominately responsible for increasing the sAHP duration with age and acute OS. The currents most likely to be involved are Ca^{2+}-activated K^+ currents.

Scutt (2012) previously demonstrated that an increase in I_{sAHP}, due to reverse-mode NCX (Scutt G, personal communications), was significantly responsible for the sAHP increase in old CGCs[392]. Even studies in ageing mammalian neurons, such as those from the hippocampus, have consistently demonstrated that the age-related increase of the sAHP is due to an increase in I_{sAHP}[254,292,364]. Therefore, experiments following this thesis will need to conduct recordings of I_{sAHP} in the old and 3 mM AAPH-treated young CGCs to assess whether this current is responsible for increasing the sAHP duration.

Another parameter altered with age and acute OS that could partially be explained by the slow inactivation kinetics of I_A is SFA. Chapter 4 demonstrated that VGKCs have a very important role in modulating SFA in the CGCs, which had not been explored before in these neurons. I_A specifically regulates SFA in the CGCs by slowing down spiking frequency and is involved in determining both f_0 and f_{ss} (Hz). This strongly corroborated previous findings in mammalian neurons[141,424]. Thus, the increase in I_A with age and acute OS due to its slower inactivation kinetics could be responsible for the decrease in the number of evoked CGC spikes. Note, **section 2.4.3** addresses the limitation with the experimental design when investigating SFA and that some caution has to be taken with the current interpretation of these findings.

With regards to f_0 (Hz) and f_{ss} (Hz), however, these parameters only decreased with age and not acute OS. This strongly suggested that I_A does not decrease evoked firing in the old and AAPH-treated young CGCs by altering f_0 (Hz) and f_{ss} (Hz), as the properties of I_A had not differed between these CGCs. It may be that other currents involved in regulating f_0 (Hz) and f_{ss} (Hz) are altered with age, but not by acute OS. In mammalian neurons, a number of currents involved in modulating f_0 (Hz) have been identified[232,49]. This includes I_{DR}, BK and M-currents[159,49]. I_{DR} did not change with age and therefore cannot be accountable for this decrease in f_0 (Hz) with age. This leaves the possibility that alterations to a BK or an M-current (provided they are expressed by the CGCs) may be responsible for the age-related decrease in f_0 (Hz).

Based on previous findings in mammalian neurons, and most importantly in the ageing CGCs by Scutt (2012), the current likely responsible for the decrease in f_{ss} (Hz) with age is I_{sAHP}[159,137,392]. The slow activation and inactivation properties of I_{sAHP} is thought to be crucial in generating the adaptive (or accommodating) response *via* regulating f_{ss} (Hz)[159,137,392]. Despite this evidence, it is generally thought that differences between the old and 3 mM AAPH-treated young CGCs are due to differences in the properties of ionic

currents[159,137,392]. If an increase in I_{sAHP} was responsible for the decrease in f_{ss} (Hz) with age, this would suggest that this current could not be accountable for the increase in the sAHP as this parameter had not differed significantly between old and AAPH-treated young CGCs. This may be true, but it is also well known that I_{sAHP} is manifested by the action of multiple different Ca^{2+}-activated K^+ channels and as such it could be that some channels are specifically involved in regulating the sAHP, while others are responsible for modulating SFA[364,292]. Perhaps those underlying SFA are particularly sensitive to the various effects of age, but not acute OS and this results in the decrease observed to f_{ss} (Hz) in old CGCs.

As I_A did not differ between old and AAPH-treated young CGCs, it is unlikely that the altered properties of I_A is responsible for the hyperpolarised RMP observed only in the old CGCs. Notably, the involvement of I_A in regulating the CGC RMP was a surprising result of this thesis. The reason for this is that I_A in the CGCs undergoes pronounced steady-state inactivation at a relatively fast rate.

The finding that I_A is involved in regulating the RMP does not appear to be a unique feature to the *Lymnaea* CGCs. Whilst not common, there have been a few studies involving various cell types in mammalian models that have also suggested a similar role for I_A. This includes, for example, Purkinje neurons and dorsal root ganglion neurons as well as non-neuronal cells such as ventricular myocytes[13,311,370,486,12]. It has been observed in such cells that I_A activates near the RMP and that inhibition of this current depolarises the RMP[13,311,370,486,12]. It is the presence of an I_A window current over the potential range encompassing the RMP that is thought to enable this current to regulate the RMP[12,370,13].

The window current occurs due to significant activation and incomplete (or submaximal) inactivation and is reflective of the sustained availability of I_A[179,370,13]. It has been reported in mammalian models from analysis of window currents that up to one third of A-type K^+ channels are available around the RMP[370,311]. Available channels in this region can activate in response to subthreshold depolarisations to delay action potential firing and return the cell back to its RMP[13,311,12,370]. These observations in mammalian cells may explain how I_A in the CGCs can regulate the RMP, particularly as it was also shown in this thesis that I_A exhibited a window current around the CGC RMP and that inhibition of this current depolarised the RMP.

While I_A may not be responsible for hyperpolarising the RMP with age, other currents may be implicated. The role of I_R has yet to be established in the CGCs due to difficulties in finding an appropriate antagonist, but based on numerous mammalian and other invertebrate studies it is postulated that this current will be important in regulating the RMP of the CGCs[178,130]. Given that the properties of I_R did not significantly change with age (or acute OS for that matter), this current cannot be responsible for the age-related hyperpolarisation of the RMP.

Previous studies have shown that an increase in $I_{sAHP,}$ a decrease in $I_{Na(P)}$, enhancement of the Na^+/K^+-ATPase and/or reverse-mode of the NCX can hyperpolarise the RMP of neurons[145,14,393,364]. Therefore, changes to one or more these ionic currents/pumps could account for the hyperpolarised RMP of the old CGCs. Preliminary experiments conducted in our laboratory suggests that NCX operating in reverse-mode may be responsible for hyperpolarising the RMP of old CGCs. It was observed that application of Li^+, an NCX blocker, hyperpolarised the RMP of the 3 mM AAPH-treated young CGCs and depolarised the RMP of the old CGCs[393]. When the NCX is operating in forward mode, blocking this pump will hyperpolarise the RMP as Ca^{2+} efflux and Na^+ influx is prevented, whereas blocking reverse-mode NCX depolarises the RMP as Ca^{2+} influx is reduced[392,393]. Interestingly, Scutt (2012) observed similar findings in the old CGCs and this highlights the importance of investigating pumps in addition to ion channels as they too may have a crucial role in determining various parameters of an action potential[392].

The decrease in firing frequency with age and acute OS did not appear to be due to changes in the voltage-gated outward currents examined in this study. Chapter 4 showed that only inhibition of I_{DR} could significantly slow CGC firing frequency, but this current was unaltered in the old and AAPH-treated young CGCs. The slower inactivation of I_A with age and acute OS had the potential to contribute to the decrease in CGC firing, but current inactivation was complete ~70 ms after the start of the action potential and this meant that its contribution to the sAHP increase was not substantial.

Chapter 4 identified that a significant increase in the sAHP or half-width could cause a significant decrease in CGC firing frequency. As the half-width decreased and the sAHP increased in the old and AAPH-treated young CGCs, this strongly indicates that the latter of the two parameters is predominately responsible for decreasing firing frequency in these CGCs. This strongly suggests that I_{sAHP} is responsible for mediating the decrease in CGC firing with age and acute OS, as it is the largest conductance involved

in regulating the sAHP[392,364,254,292]. It would be interesting to record I_{sAHP} in the CGCs with increasing age and acute OS to assess if there is an increase in this current and if so, whether its potential effects on firing frequency can be reversed.

Based on findings from Chapter 3, it was postulated that the unidentified TEA/4-AP/zero Cl⁻ insensitive sustained current may be a pacemaker current that acts to depolarise the CGCs. Interestingly, this current increased with both age and acute OS suggesting that it could be opposing the increase in I_A or the potential increase in I_{sAHP}. It may be doing this to prevent extreme changes caused by such currents to CGC firing properties with age and acute OS that could potentially attenuate synaptic transmission, inhibit learning and memory and adversely impair feeding behaviour.

The overall findings from the electrophysiological recordings in this thesis provides overwhelming support for I_A as an instrumental mediator of many changes to the action potential waveform with age and acute OS. Whilst I_A may not be responsible for the decrease in CGC firing, it effects on other parameters such as the half-width and fAHP may cause detrimental alterations to processes such as neurotransmission with age and acute OS. To our knowledge, this is the first study that has comprehensively investigated the properties of I_A with age and has yielded some very important findings that highlight the importance of this current in neuronal ageing. This should direct future studies in neuronal ageing across all species to consider investigating this current alongside the widely examined Ca^{2+}-activated K^+ currents.

In this thesis, current clamp and AP-clamp experiments were conducted to examine the contribution of voltage-gated currents in the CGC action potential waveform. However, dynamic clamp is an alternative and very powerful technique that could also be utilised in the future to explore this further[96,402,365,354]. This particular electrophysiological configuration allows users to artificially introduce or negate ionic conductances (as well as synaptic inputs) in targeted cells[96,354,365,402,225]. Moreover, the artificial addition or subtraction of a conductance in dynamic clamp can mimic the effects of activating or inhibiting a current using pharmacology without the non-specific effects (a potential issue of this thesis; **section 4.4.1**) that can be encountered with some agents[96,354].

Dynamic clamp alters the conductance of a neuron by first measuring its membrane potential[354,96,225,379]. It then computes the driving force (difference between the neuron's membrane potential and E_{rev} of the conductance) and multiplies this by the required

amount of conductance[354,96,225,379]. The resultant current is then injected into the neuron[354,96,225,379]. Accurate dynamic clamp requires this cycle to be executed rapidly (typically >10 kHz), as this enables the simulated effects of ionic conductances to be reproduced as if they were actually located in the membrane[354,96,225,379]. Interestingly, Kemenes *et al.* (2011) and Samu *et al.* (2012) designed and performed dynamic clamp experiments using *Lymnaea* neurons including the CGCs[225,379]. Thus, it is possible that this technique could be successfully implemented to study the role of voltage-gated outward currents in the CGC action potential in subsequent investigations derived from this thesis.

5.2 The *Lymnaea* behavioural outputs associated with the CGCs

The CGCs have a well-established role in the *Lymnaea* CNS as important neurons involved in modulating the frequency of feeding rhythm[506,507,21,35,477]. For example, two seminal papers by Yeoman *et al.* (1994) revealed that suppression of the CGCs either by irradiation or injecting a hyperpolarising current significantly reduced SO-driven fictive feeding rhythms[506,508]. Another study by Kemenes *et al.* (1990) demonstrated that the frequency of feeding movements significantly reduced following injection of 5,6-dihydroxytryptamine into the snails, which lesioned the CGCs[222]. Given that the CGCs extensively synapse with many CPG neurons, motor neurons and muscles involved in generating feeding movements, it is strongly believed that an age-related decrease in CGC firing will impair *Lymnaea* feeding behaviour[336,35]. Indeed, evidence from Chapter 2 revealed that the decrease in CGC firing frequency with age was accompanied with a decrease in feeding frequency (fewer sucrose-evoked bites), which corroborated similar findings by Patel *et al.* (2006)[336]. Moreover, the manner in which feeding was altered in the old snails (increase in bite duration and inter-bite interval) supported similar observations made previously by Arundell *et al.* (2006)[21].

This study as well as the previous ageing *Lymnaea* studies have only correlated the decrease in CGC firing frequency to the decrease in feeding frequency. It may be that the age-related decrease in feeding frequency is not simply due to an age-related decrease in CGC firing, but also caused by alterations in other neurons or muscles involved in modulating feeding behaviour. To examine this further some of the following experiments will need to be conducted: 1) Record from old intact snails to determine CGC firing frequency during feeding movements[508]; 2) Record fictive feeding patterns (for example, SO-driven rhythms) in association with the CGCs in old CNSs[509,35,54], and; 3)

Record activity of nerves that are connected to the feeding muscles, as well as record the movement of the muscles themselves during feeding in old snails[201,21].

Whether OS is responsible for mediating the age-related decrease to feeding behaviour has proven difficult to determine. Whilst injecting young snails with 0.3 mM AAPH significantly reduced the number of sucrose-evoked bites, as observed in old snails, it more than doubled the inter-bite interval, decreased the bite duration and compromised mouth opening and radula protrusion. Furthermore, it was observed that 0.3 mM AAPH *in vivo* did not alter CGC firing properties. Young snails injected with 3 mM AAPH completely failed to evoke any bites when presented with the sucrose stimulus. This suggests that other neurons and muscles of the feeding system that may not be impaired with age are oxidised and hindered in both the 0.3 and 3 mM AAPH-treated young snails. This difference does not entirely rule out the possibility that OS is responsible for the age-related decrease to feeding, as this may simply be a reflection of the limitations associated with this current experimental approach.

When injecting snails with AAPH, or any pharmacological agent for that matter, all the cells in the snail body could be targeted by these agents and consequently the behavioural output may be altered in a different manner to what is typically observed with age. At present, the best technique to examine whether OS can accurately mimic the age-related decrease to feeding frequency will probably be to record fictive feeding rhythms in isolated young CNS preparations treated with extracellular AAPH[509,35,54].

In addition to feeding behaviour, a lot of interest surrounds the CGCs due to their important role in learning and memory. Studies have shown that the CGCs are specifically involved in the maintenance of LTM (or late consolidation) as they exhibit, for example, persistent depolarisation of the RMP approximately 18-24 hours following single trial food-reward classical conditioning[126,222]. Kemenes *et al*. (2006) revealed that this depolarisation of the CGC RMP in trained *Lymnaea* was accompanied by a reduction of the fAHP, but no changes to CGC firing frequency[226]. Interestingly, this was strongly reminiscent of the effects of the newly discovered I_{Cl} that when suppressed depolarised the CGC RMP, reduced the fAHP amplitude, but did not alter CGC firing.

It is postulated in this thesis that during LTM formation, I_{Cl} is inhibited in the CGCs to generate a long lasting depolarisation that mediates the late consolidation process. This is interesting as it highlights that changes in the AP waveform may not only be involved in

determining firing frequency, but can have independent effects that alter other important neuronal processes such as nonsynaptic neuronal plasticity during learning and memory. What is even more fascinating is that Wildering *et al.* (2012) demonstrated that with increasing age the persistent depolarisation of the CGC RMP is attenuated in trained snails, which consequently impairs LTM formation[226]. This loss of the persistent depolarisation in old CGCs could be explained by a loss of I_{Cl} observed in the old CGCs of this study. Whilst inhibition of I_{Cl} would be expected to depolarise the CGC RMP (Chapter 4), this may not be observed as it could be masked by changes to the NCX.

5.3 OS, a mechanism that explains ageing of the CGCs?

OS has been implicated in a plethora of studies as one of the main culprits responsible for driving neuronal ageing[139,470,476,364,59]. Consistently throughout this thesis, it has been observed that acute OS induced in young CGCs by extracellular AAPH mimics many of the changes that accompany ageing of the CGCs. This strongly suggests that OS could be responsible for mediating these alterations in the old CGCs. However, some of these age-related changes could not be mimicked by acute extracellular AAPH treatment.

This could be explained by a few reasons. First, it may be that the short exposure period to AAPH is not sufficient to alter the properties of some ion channels, as they may possess residues that are particularly resilient to oxidative modifications. To re-iterate an important point stated in Chapter 2, ageing is driven by chronic processes such as OS that manifest slowly throughout an organisms lifespan. Thus, not all the alterations observed with ageing occur immediately when an organism reaches the age that classifies them as being old. For example, in *Lymnaea* it is often observed that the RMP only becomes significantly more hyperpolarised a few weeks or even a few months after other age-related changes (such as decreased firing frequency) have occurred. This suggests that some of the ion channels or pumps that regulate the RMP are particularly robust and that only when OS reaches a certain threshold will this parameter be altered.

At present, the time course in which changes to each CGC action potential parameter occurs as *Lymnaea* age has not been extensively documented. Thus, it will be useful to conduct experiments examining the electrophysiological properties of the CGCs at more time points (perhaps every month) to begin constructing a timeline of when these age-related changes begin to develop and completely manifest. In addition, future experiments

will need to create a chronic model of OS in young preparations to assess whether this can fully mimic the ageing phenotype of the CGCs.

The second possible reason why young CGCs treated with acute extracellular AAPH did not mimic all the age-related changes may have been that some of these changes arise from the intracellular actions of ROS. Chapter 2 provided strong evidence to suggest that this was not the situation, as it was observed that when AAPH was injected into young CGCs any alterations that had occurred to firing properties did not mimic the age-related changes. In addition, preliminary experiments in our lab have shown that treating young CGCs with hydrogen peroxide (H_2O_2) does not induce an ageing-like phenotype. H_2O_2 is an interesting pro-oxidant to use as it only mediates its effects once it has crossed the plasma membrane (which it can do so freely or *via* aquaporins) as it needs to react with transition metals in order to generate ROS such as $^{\bullet}OH$[487,42]. These findings strongly suggest that intracellular OS does not have the capacity to alter CGC firing properties with age. Therefore, it appears that the production of ROS from extracellular sources are critically responsible for mediating the changes observed in the ageing CGCs by targeting its extracellular components. This extracellular generation of ROS in the *Lymnaea* CNS (**Figure 5.1**) is likely to come from glial cells, which are notorious for being very potent ROS producers in the ageing mammalian CNS, and/or other neurons[38,276].
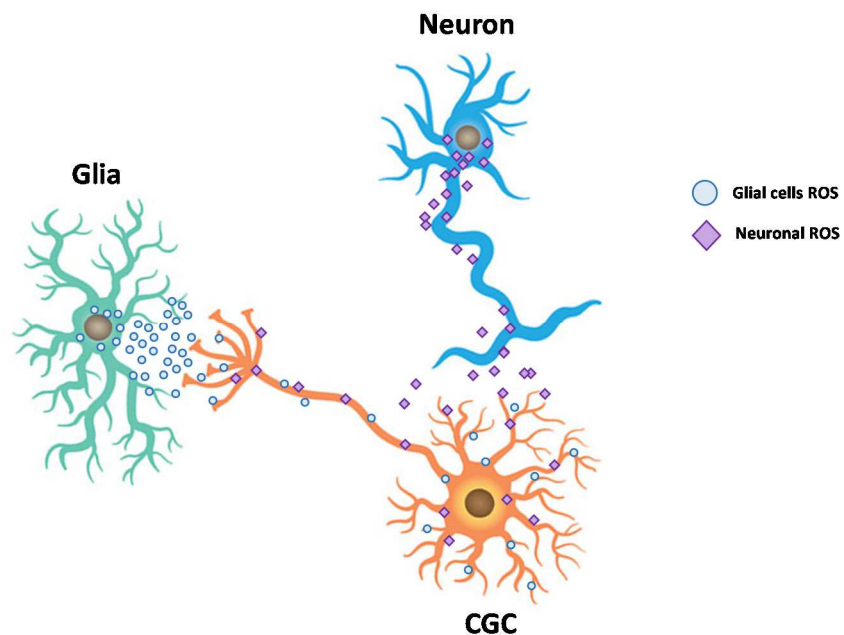
Figure 5.1| OS in the ageing *Lymnaea* CNS. Alterations to the CGCs with age could be driven by ROS generated from extracellular sources such as glial cells and/or other neurons.

Lastly, it may be that some of the alterations to the CGC action potential parameters with age are not caused by oxidative modifications. Changes in Ca^{2+} signalling or an increase in pro-inflammatory mediators have the capacity to alter neuronal properties and thus, could be accountable for some of the age-related changes in the CGCs independent of $OS^{[446,95,318]}$.

The aim of this entire thesis was to test the hypothesis that OS in *Lymnaea* drives the age-related changes to the CGC firing properties and action potential waveform. Very strong evidence has been presented indicating that OS may be responsible for driving the age-related changes in the CGCs. Specifically, the increase in OS markers in the ageing cerebral ganglia to the astonishing replication of many age-related electrophysiological changes in young CGCs treated with AAPH had strongly suggested that OS may be a key ageing mechanism in the CGCs. However, due to the challenges faced when attempting to reverse the effects of age on the CGC firing properties with short-term use of antioxidants (vitamins C and E), some caution must be exercised in conclusively stating that OS is responsible for mediating changes in the ageing CGCs. The next important experiment that will have to be conducted following this thesis will be to treat old CGCs with antioxidants for a much longer duration (several hours to a few days) to examine whether the effects of age can be reversed.

Based on experimental findings acquired throughout this thesis, **Figure 5.2** summarises the changes (both known and postulated) that occurs in the CGCs with increasing age and acute OS.

A.

Young CGCs

Extracellular

I_{sAHP} I_{sAHP} | I_{Cl} I_{Cl} | I_{DR} I_{DR} | I_A I_A | TEA/4-AP/zero Cl⁻ | I_R I_R | NCX

Below E_{rev}

Above E_{rev}

Intracellular

B.

Old CGCs

Extracellular

I_{sAHP} I_{sAHP} | I_{Cl} I_{Cl} | I_{DR} I_{DR} | I_A I_A | TEA/4-AP/zero Cl⁻ | I_R | NCX

Below E_{rev}

Above E_{rev}

Intracellular

C.

AAPH-treated young CGCs

Extracellular

I_{sAHP} I_{sAHP} | I_{Cl} I_{Cl} | I_{DR} I_{DR} | I_A I_A | TEA/4-AP/zero Cl⁻ | I_R I_R | NCX

Below E_{rev}

Above E_{rev}

Intracellular

A-type K⁺ channel | Delayed rectifier channel | Chloride channel | TEA/4-AP/zero Cl⁻ insensitive channel | Inward rectifier channel | Ca²⁺-activated K⁺ channel

Reverse mode NCX | Forward mode NCX | Malondialdehyde (MDA) | Protein Carbonyl (PC)

215

Figure 5.2| Overview of known and postulated changes to the CGCs with age and acute OS. (A) Young CGCs. I_A and I_{DR} are the principle voltage-gated outward currents regulating action potential repolarisation. These currents also have an important role in maintaining a negative RMP, slowing down SFA, mediating the fAHP and early sAHP. I_{Cl} appears to be involved in hyperpolarising young CGCs specifically *via* the RMP and fAHP. The TEA/4-AP/zero Cl⁻ insensitive current is postulated to have a pacemaking depolarising effect on the CGCs due to its extremely slow deactivation kinetics. Based on previous findings in mammalian and other invertebrate neurons, it is postulated that I_R has a role in regulating the RMP and inter-spike interval of the CGCs[79,130]. I_{sAHP} significantly mediates the CGC sAHP[392]. NCX operates in forward mode to reduce $[Ca^{2+}]_i$[393,19,203]. As a consequence, NCX has a slight depolarising effect on the CGCs as it mediates the influx of Na^+ and also prevents enhancement of the I_{sAHP} by facilitating Ca^{2+} efflux[393]. **(B-C) Old CGCs and 3 mM AAPH-treated young CGCs.** The increase in OS (MDA and PCs) with age and acute OS was associated with a shift in voltage sensitivity and slower activation/inactivation kinetics of I_A in these CGCs. The resultant increase in I_A is likely to increase the rate of repolarisation, which would help explain the narrowing of action potentials in these CGCs. Additionally, I_A may be responsible for mediating the increase to the fAHP and early sAHP. There were no changes to I_{DR} or I_R in these CGCs. I_{Cl} was suppressed, but this was masked by an increase in the TEA/4-AP/zero Cl⁻ insensitive current. The hypothesised depolarising effects of this latter current on the CGCs suggests that it may be acting in a compensatory capacity to prevent extreme changes to firing properties. Interestingly, the RMP of old CGCs was significantly hyperpolarised and could not be easily explained by the changes to the conductances examined in this study. Preliminary experiments revealed that NCX operating in reverse mode is involved in hyperpolarising the old CGC RMP, probably by increasing the conductance of Ca^{2+}-activated K^+ channels. It was found in 3 mM AAPH-treated young CGCs- where there were no changes to the RMP- that NCX was operating in forward mode.

5.4 Conclusion

Ageing of CGCs in *Lymnaea* is associated with a decrease in firing frequency, alterations to the action potential waveform and a decrease in feeding frequency. Underlying the electrophysiological changes were the altered kinetics and voltage sensitivity of I_A, the suppression of the previously uncharacterised I_{Cl} and an increase in the amplitude of the recently identified TEA/4-AP/zero Cl$^-$ insensitive current. There are no age-related alterations to the properties of I_{DR} or the newly discovered I_R. The increase in OS in the ageing CNS and the finding that acute OS induced in a young CNS mimicked the ageing CGC electrophysiological phenotype remarkably well, strongly suggests that OS may be a key instigator of changes in the CGCs with advancing age.

REFERENCES

1. Abel HJ, Lee JCF, Callaway JC, Foehring RC. Relationships between intracellular calcium and afterhyperpolarizations in neocortical pyramidal neurons. *J Neurophysiol* 2004;91:324–35.

2. Adams DJ, Smith SJ, Thompson SH. Ionic Currents in Molluscan Soma. *Annu Rev Neurosci* 1980;3:141–67.

3. Adibhatla RM, Hatcher JF. Phospholipase A(2), reactive oxygen species, and lipid peroxidation in CNS pathologies. *BMB Rep* 2008;41:560–7.

4. AGE UK. Later Life in the United Kingdom. *AGE UK* 2015.

5. Aggarwal SK, MacKinnon R. Contribution of the S4 segment to gating charge in the Shaker K+ channel. *Neuron* 1996;16:1169–77.

6. Ahmed Z, Connor JA. Measurement of calcium influx under voltage clamp in molluscan neurones using the metallochromic dye arsenazo III. *J Physiol* 1979;286:61–82.

7. Ahsan H, Ali A, Ali R. Oxygen free radicals and systemic autoimmunity. *Clin Exp Immunol* 2003;131:398–404.

8. Aksenov MYY, Aksenova MV V, Butterfield DAA, Geddes JWW, Markesbery WRR. Protein oxidation in the brain in Alzheimer's disease. *Neuroscience* 2001;103:373–83.

9. Alexander SP, Kelly E, Marrion N, Peters JA, Benson HE, Faccenda E, et al. The Concise Guide to PHARMACOLOGY 2015/16: Other ion channels. *Br J Pharmacol* 2015;172:5942–55.

10. Allyson J, Bi X, Baudry M, Massicotte G. Maintenance of synaptic stability requires calcium-independent phospholipase A_2 activity. *Neural Plast* 2012;2012:569149.

11. Alshuaib WB, Hasan SM, Cherian SP, Mathew MV, Hasan MY, Fahim MA. Reduced potassium currents in old rat CA1 hippocampal neurons. *J Neurosci Res* 2001;63:176–84.

12. Amberg GC, Baker SA, Koh SD, Hatton WJ, Murray KJ, Horowitz B, et al. Characterization of the A-type potassium current in murine gastric antrum. *J Physiol* 2002;544:417–28.

13. Amberg GC, Koh SD, Imaizumi Y, Ohya S, Sanders KM. A-type potassium currents in smooth muscle 2003;284:C583–95.

14. Anderson TR, Huguenard JR, Prince DA. Differential effects of Na+-K+ ATPase blockade on cortical layer V neurons. *J Physiol* 2010;588:4401–14.

15. Anderton BH. Ageing of the brain. *Mech Ageing Dev* 2002;123:811–7.

16. Andrade R, Foehring RC, Tzingounis A V. The calcium-activated slow AHP: cutting through the Gordian knot. *Front Cell Neurosci* 2012;6:47.

17. Andreasen M. Inhibition of slow Ca(2+)-activated K(+) current by 4-aminopyridine in rat hippocampal CA1 pyramidal neurones. *Br J Pharmacol* 2002;135:1013–25.

18. Angel-Chavez LI, Acosta-Gómez EI, Morales-Avalos M, Castro E, Cruzblanca H, Zhang Z. Forskolin Suppresses Delayed-Rectifier K+ Currents and Enhances Spike Frequency-Dependent Adaptation of Sympathetic Neurons. *PLoS One* 2015;10:e0126365.

19. Annunziato L, Pignataro G, Di Renzo GF. Pharmacology of brain Na+/Ca2+ exchanger: from molecular biology to therapeutic perspectives. *Pharmacol Rev* 2004;56:633–54.

20. Araque A, Navarrete M. Glial cells in neuronal network function. *Philos Trans R Soc Lond B Biol Sci* 2010;365:2375–81.

21. Arundell M, Patel BA, Straub V, Allen MC, Janse C, O'Hare D, et al. Effects of age on feeding behavior and chemosensory processing in the pond snail, Lymnaea stagnalis. *Neurobiol Aging* 2006;27:1880–91.

22. Ayala A, Muñoz MF, Argüelles S. Lipid peroxidation: production, metabolism, and signaling mechanisms of malondialdehyde and 4-hydroxy-2-nonenal. *Oxid Med Cell Longev* 2014;2014:360438.

23. Azpurua J, Eaton BA. Neuronal epigenetics and the aging synapse. *Front Cell Neurosci* 2015;9:208.

24. Banay-Schwartz M, Lajtha A, Palkovits M. Changes with aging in the levels of amino acids in rat CNS structural elements. I. Glutamate and related amino acids. *Neurochem Res* 1989;14:555–62.

25. Banks G, Kemenes I, Schofield M, O'Shea M, Korneev SA. Acetylcholine binding protein of mollusks is unlikely to act as a regulator of cholinergic neurotransmission at neurite-neurite synaptic sites in vivo. *FASEB J* 2009;23:3030–6.

26. Baranauskas G, Tkatch T, Surmeier DJ. Delayed Rectifier Currents in Rat Globus Pallidus Neurons Are Attributable to Kv2.1 and Kv3.1/3.2 K+ Channels. *J Neurosci* 1999;19.

27. Barnes CA, Rao G, McNaughton BL. Functional integrity of NMDA-dependent LTP induction mechanisms across the lifespan of F-344 rats. *Learn Mem* 1996;3:124–37.

28. Baumann A, Grupe A, Ackermann A, Pongs O. Structure of the voltage-dependent potassium channel is highly conserved from Drosophila to vertebrate central nervous systems. *EMBO J* 1988;7:2457–63.

29. Baumgartner W, Islas L, Sigworth FJ. Two-Microelectrode Voltage Clamp of Xenopus Oocytes: Voltage Errors and Compensation for Local Current Flow. *Biophys J* 1999;77:1980–91.

30. Bazinet RP, Layé S. Polyunsaturated fatty acids and their metabolites in brain function and disease. *Nat Rev Neurosci* 2014;15:771–85.

31. Bean BP. The action potential in mammalian central neurons. *Nat Rev Neurosci* 2007;8:451–65.

32. Beaulieu E, Ioffe J, Watson SN, Hermann PM, Wildering WC. Oxidative-stress induced increase in circulating fatty acids does not contribute to phospholipase A2-dependent appetitive long-term memory failure in the pond snail Lymnaea stagnalis. *BMC Neurosci* 2014;15:56.

33. Bedard K, Krause K-H. The NOX family of ROS-generating NADPH oxidases: physiology and pathophysiology. *Physiol Rev* 2007;87:245–313.

34. Begum R, Bakiri Y, Volynski KE, Kullmann DM. Action potential broadening in a presynaptic channelopathy. *Nat Commun* 2016;7:12102.

35. Benjamin PR. Distributed network organization underlying feeding behavior in the mollusk Lymnaea. *Neural Syst Circuits* 2012;2:4.

36. Benjamin PR. A Systems Approach to the Cellular Analysis of Associative Learning in the Pond Snail Lymnaea. *Learn Mem* 2000;7:124–31.

37. Bernèche S, Roux B. A Gate in the Selectivity Filter of Potassium Channels. *Structure* 2005;13:591–600.

38. von Bernhardi R, Eugenín-von Bernhardi L, Eugenín J. Microglial cell dysregulation in brain aging and neurodegeneration. *Front Aging Neurosci* 2015;7:124.

39. Bett GCL, Dinga-Madou I, Zhou Q, Bondarenko VE, Rasmusson RL. A model of the interaction between N-type and C-type inactivation in Kv1.4 channels. *Biophys J* 2011;100:11–21.

40. Bhanu MU, Mandraju RK, Bhaskar C, Kondapi AK. Cultured cerebellar granule neurons as an in vitro aging model: topoisomerase IIβ as an additional biomarker in DNA repair and aging. *Toxicol In Vitro* 2010;24:1935–45.

41. Bhattacharyya A, Chattopadhyay R, Mitra S, Crowe SE. Oxidative stress: an essential factor in the pathogenesis of gastrointestinal mucosal diseases. *Physiol Rev* 2014;94:329–54.

42. Bienert GP, Schjoerring JK, Jahn TP. Membrane transport of hydrogen peroxide. *Biochim Biophys Acta - Biomembr* 2006;1758:994–1003.

43. Biswas SK. Does the Interdependence between Oxidative Stress and Inflammation Explain the Antioxidant Paradox? *Oxid Med Cell Longev* 2016;2016:1–9.

44. Blaine JT, Ribera AB. Kv2 channels form delayed-rectifier potassium channels in situ. *J Neurosci* 2001;21:1473–80.

45. Bloodsworth A, O'Donnell VB, Freeman BA. Nitric Oxide Regulation of Free Radical- and Enzyme-Mediated Lipid and Lipoprotein Oxidation. *Arterioscler Thromb Vasc Biol* 2000;20:1707–15.

46. Blunck R, Batulan Z. Mechanism of electromechanical coupling in voltage-gated potassium channels. *Front Pharmacol* 2012;3:166.

47. Bocksteins E, Van de Vijver G, Van Bogaert P-P, Snyders DJ. Kv3 channels contribute to the delayed rectifier current in small cultured mouse dorsal root ganglion neurons. *Am J Physiol Cell Physiol* 2012;303:C406-15.

48. Bodhinathan K, Kumar A, Foster TC. Redox sensitive calcium stores underlie enhanced after hyperpolarization of aged neurons: role for ryanodine receptor mediated calcium signaling. *J Neurophysiol* 2010;104:2586–93.

49. Bordas C, Kovacs A, Pal B. The M-current contributes to high threshold membrane potential oscillations in a cell type-specific way in the pedunculopontine nucleus of mice. *Front Cell Neurosci* 2015;9:121.

50. Bordey A, Sontheimer H. Differential inhibition of glial K(+) currents by 4-AP. *J Neurophysiol* 1999;82:3476–87.

51. Boveris A, Navarro A. Brain mitochondrial dysfunction in aging. *IUBMB Life* 2008;60:308–14.

52. Bratic A, Larsson N-G. The role of mitochondria in aging. *J Clin Invest* 2013;123:951–7.

53. Bridge G, Rashid S, Martin SA. DNA mismatch repair and oxidative DNA damage: implications for cancer biology and treatment. *Cancers (Basel)* 2014;6:1597–614.

54. Brierley MJ, Yeoman MS, Benjamin PR. Glutamatergic N2v cells are central pattern generator interneurons of the lymnaea feeding system: new model for rhythm generation. *J Neurophysiol* 1997;78:3396–407.

55. Brini M, Carafoli E. The plasma membrane Ca^2+ ATPase and the plasma membrane sodium calcium exchanger cooperate in the regulation of cell calcium. *Cold Spring Harb Perspect Biol* 2011;3.

56. Brodal P. The central nervous system : structure and function. Oxford University Press; 2004.

57. Byerly L, Suen Y. Characterization of proton currents in neurones of the snail, Lymnaea stagnalis. *J Physiol* 1989;413:75–89.

58. Cai S-Q, Li W, Sesti F. Multiple modes of a-type potassium current regulation. *Curr Pharm Des* 2007;13:3178–84.

59. Cai S-Q, Sesti F. Oxidation of a potassium channel causes progressive sensory function loss during aging. *Nat Neurosci* 2009;12:611–7.

60. Caillard O, Miles R, Campanac E, Cudmore R, Giraud P. Pre & Postsynaptic Tuning of Action Potential Timing by Spontaneous GABAergic Activity. *PLoS One* 2011;6:e22322.

61. Campisi J. Aging, cellular senescence, and cancer. *Annu Rev Physiol* 2013;75:685–705.

62. Campisi J, d'Adda di Fagagna F. Cellular senescence: when bad things happen to good cells. *Nat Rev Mol Cell Biol* 2007;8:729–40.

63. Canas PM, Duarte JMN, Rodrigues RJ, Köfalvi A, Cunha RA. Modification upon aging of the density of presynaptic modulation systems in the hippocampus. *Neurobiol Aging* 2009;30:1877–84.

64. Capettini LSA, Cortes SF, Lemos VS. Relative contribution of eNOS and nNOS to endothelium-dependent vasodilation in the mouse aorta. *Eur J Pharmacol* 2010;643:260–6.

65. Carrasquillo Y, Burkhalter A, Nerbonne JM. A-type K+ channels encoded by Kv4.2, Kv4.3 and Kv1.4 differentially regulate intrinsic excitability of cortical pyramidal neurons. *J Physiol* 2012;590:3877–90.

66. Carter BC, Giessel AJ, Sabatini BL, Bean BP. Transient sodium current at subthreshold voltages: activation by EPSP waveforms. *Neuron* 2012;75:1081–93.

67. Catalá A. Five decades with polyunsaturated Fatty acids: chemical synthesis, enzymatic formation, lipid peroxidation and its biological effects. *J Lipids* 2013;2013:710290.

68. Catterall WA. Voltage-gated sodium channels at 60: structure, function and pathophysiology. *J Physiol* 2012;590:2577–89.

69. Catterall WA. Voltage-gated calcium channels. *Cold Spring Harb Perspect Biol* 2011;3:a003947.

70. Chen-Izu Y, Izu LT, Nanasi PP, Banyasz T. From Action Potential-Clamp to "Onion-Peeling" Technique – Recording of Ionic Currents Under Physiological Conditions n.d.

71. Chen J-H, Hales CN, Ozanne SE. DNA damage, cellular senescence and organismal ageing: causal or correlative? *Nucleic Acids Res* 2007;35:7417–28.

72. Chen KC, Nicholson C. Spatial buffering of potassium ions in brain extracellular space. *Biophys J* 2000;78:2776–97.

73. Chen X, Guo C, Kong J. Oxidative stress in neurodegenerative diseases. *Neural Regen Res* 2012;7:376–85.

74. Chew YL, Fan X, Götz J, Nicholas HR. Aging in the nervous system of Caenorhabditis elegans. *Commun Integr Biol* 2013;6:e25288.

75. Chinta SJ, Lieu CA, Demaria M, Laberge R-M, Campisi J, Andersen JK. Environmental stress, ageing and glial cell senescence: a novel mechanistic link to Parkinson's disease? *J Intern Med* 2013;273:429–36.

76. Choe S. Potassium channel structures. *Nat Rev Neurosci* 2002;3:115–21.

77. Christensen K, Doblhammer G, Rau R, Vaupel JW. Ageing populations: the challenges ahead. *Lancet* 2009;374:1196–208.

78. Citri A, Malenka RC. Synaptic plasticity: multiple forms, functions, and mechanisms. *Neuropsychopharmacology* 2008;33:18–41.

79. Clark RB, Kondo C, Belke DD, Giles WR. Two-pore domain K^+ channels regulate membrane potential of isolated human articular chondrocytes. *J Physiol* 2011;589:5071–89.

80. Cleophas TJM. Statistics applied to clinical trials. Springer; 2009.

81. Cooke MS, Evans MD, Dizdaroglu M, Lunec J. Oxidative DNA damage: mechanisms, mutation, and disease. *FASEB J* 2003;17:1195–214.

82. Cooper GM. The Mechanism of Oxidative Phosphorylation 2000.

83. Coppé J-P, Desprez P-Y, Krtolica A, Campisi J. The senescence-associated secretory phenotype: the dark side of tumor suppression. *Annu Rev Pathol* 2010;5:99–118.

84. Cressman JR, Ullah G, Ziburkus J, Schiff SJ, Barreto E. The influence of sodium and potassium dynamics on excitability, seizures, and the stability of persistent states: I. Single neuron dynamics. *J Comput Neurosci* 2009;26:159–70.

85. Crossley M. Neural mechanisms of decision making in the pond snail Lymnaea stagnalis. DPhil thesis. *Univ Sussex* 2013.

86. Curtin F, Schulz P. Multiple correlations and Bonferroni's correction. *Biol Psychiatry* 1998;44:775–7.

87. Dai D-F, Chiao YA, Marcinek DJ, Szeto HH, Rabinovitch PS. Mitochondrial oxidative stress in aging and healthspan. *Longev Heal* 2014;3:6.

88. Le Dain AC, Anderton PJ, Martin DK, Millar TJ. A tetraethylammonium-insensitive inward rectifier K+ channel in müller cells of the turtle (Pseudemys scripta elegans) retina. *J Membr Biol* 1994;141:239–45.

89. Dalle-Donne I, Rossi R, Giustarini D, Milzani A, Colombo R. Protein carbonyl groups as biomarkers of oxidative stress. *Clin Chim Acta* 2003;329:23–38.

90. Danbolt NC, Furness DN, Zhou Y. Neuronal vs glial glutamate uptake: Resolving the conundrum. *Neurochem Int* 2016;98:29–45.

91. Daoudal G, Debanne D. Long-term plasticity of intrinsic excitability: learning rules and mechanisms. *Learn Mem* 2003;10:456–65.

92. Dasgupta A, Zheng J, Bizzozero OA. Protein Carbonylation and Aggregation Precede Neuronal Apoptosis Induced by Partial Glutathione Depletion. *ASN Neuro* 2012;4:AN20110064.

93. Dawson R, Wallace DR, Meldrum MJ. Endogenous glutamate release from frontal cortex of adult and aged rats. *Neurobiol Aging* 10:665–8.

94. DeCoursey TE. Voltage-gated proton channels. *Cell Mol Life Sci* 2008;65:2554–73.

95. Deleidi M, Jäggle M, Rubino G. Immune aging, dysmetabolism, and inflammation in neurological diseases. *Front Neurosci* 2015;9:172.

96. Destexhe A, Bal T. Dynamic-Clamp: From Principles to Applications. *From Princ to Appl* 2009;1:443.

97. Devices M. Axon Guide to Electrophysiology & Biophysics Laboratory Techniques | Molecular Devices n.d.

98. Dew ITZ, Giovanello KS. Differential age effects for implicit and explicit conceptual associative memory. *Psychol Aging* 2010;25:911–21.

99. Dias V, Junn E, Mouradian MM. The role of oxidative stress in Parkinson's disease. *J Parkinsons Dis* 2013;3:461–91.

100. Dickstein DL, Weaver CM, Luebke JI, Hof PR. Dendritic spine changes associated with normal aging. *Neuroscience* 2013;251:21–32.

101. Ding S, Matta SG, Zhou F-M. Kv3-Like Potassium Channels Are Required for Sustained High-Frequency Firing in Basal Ganglia Output Neurons. *J Neurophysiol* 2011;105.

102. Disterhoft JF, Thompson LT, Moyer JR, Mogul DJ. Calcium-dependent afterhyperpolarization and learning in young and aging hippocampus. *Life Sci* 1996;59:413–20.

103. Dixit PD, Asthagiri D. Thermodynamics of ion selectivity in the KcsA K+ channel. *J Gen Physiol* 2011;137:427–33.

104. Doiron B, Longtin A, Turner RW, Maler L. Model of Gamma Frequency Burst Discharge Generated by Conditional Backpropagation. *J Neurophysiol* 2001;86.

105. Doughty JM, Miller AL, Langton PD. Non-specificity of chloride channel blockers in rat cerebral arteries: block of the L-type calcium channel. *J Physiol* 1998;507 (Pt 2):433–9.

106. Doyle DA, Morais Cabral J, Pfuetzner RA, Kuo A, Gulbis JM, Cohen SL, et al. The structure of the potassium channel: molecular basis of K+ conduction and selectivity. *Science* 1998;280:69–77.

107. Dribben WH, Eisenman LN, Mennerick S. Magnesium induces neuronal apoptosis by suppressing excitability. *Cell Death Dis* 2010;1:e63.

108. Driscoll I, Davatzikos C, An Y, Wu X, Shen D, Kraut M, et al. Longitudinal pattern of regional brain volume change differentiates normal aging from MCI. *Neurology* 2009;72:1906–13.

109. Duan H. Age-related Dendritic and Spine Changes in Corticocortically Projecting Neurons in Macaque Monkeys. *Cereb Cortex* 2003;13:950–61.

110. Duggan S, Rait C, Platt A, Gieseg SP. Protein and thiol oxidation in cells exposed to peroxyl radicals is inhibited by the macrophage synthesised pterin 7,8-dihydroneopterin. *Biochim Biophys Acta - Mol Cell Res* 2002;1591:139–45.

111. Eijkelkamp N, Linley JE, Baker MD, Minett MS, Cregg R, Werdehausen R, et al. Neurological perspectives on voltage-gated sodium channels. *Brain* 2012;135:2585–612.

112. Elliott CJH, Susswein AJ. Comparative neuroethology of feeding control in molluscs. *J Exp Biol* 2002;205:877–96.

113. Engelmann C, Haenold R. Transcriptional Control of Synaptic Plasticity by Transcription Factor NF-κB. *Neural Plast* 2016;2016:7027949.

114. England N. NHS: Our 2014-15 Annual Report. *NHS Engl* 2015.

115. Erraji-Benchekroun L, Underwood MD, Arango V, Galfalvy H, Pavlidis P, Smyrniotopoulos P, et al. Molecular aging in human prefrontal cortex is selective and continuous throughout adult life. *Biol Psychiatry* 2005;57:549–58.

116. Evangelisti C, Cenni V, Lattanzi G. Potential therapeutic effects of the MTOR inhibitors for preventing ageing and progeria-related disorders. *Br J Clin Pharmacol* 2016;82:1229–44.

117. Evason K, Huang C, Yamben I, Covey DF, Kornfeld K. Anticonvulsant Medications Extend Worm Life-Span. *Science (80-)* 2005;307:258–62.

118. Fan Z, Ji X, Fu M, Zhang W, Zhang D, Xiao Z. Electrostatic interaction between inactivation ball and T1–S1 linker region of Kv1.4 channel. *Biochim Biophys Acta - Biomembr* 2012;1818:55–63.

119. Farajnia S, Meijer JH, Michel S. Photoperiod Modulates Fast Delayed Rectifier Potassium Currents in the Mammalian Circadian Clock. *ASN Neuro* 2016;8.

120. Farajnia S, Meijer JH, Michel S. Photoperiod Modulates Fast Delayed Rectifier Potassium Currents in the Mammalian Circadian Clock. *ASN Neuro* 2016;8:175909141667077.

121. Farmer LM, Le BN, Nelson DJ. CLC-3 chloride channels moderate long-term potentiation at Schaffer collateral-CA1 synapses. *J Physiol* 2013;591:1001–15.

122. Farooqui AA, Horrocks LA. Phospholipase A2-generated lipid mediators in the brain: the good, the bad, and the ugly. *Neuroscientist* 2006;12:245–60.

123. Faure É, Starek G, McGuire H, Bernèche S, Blunck R. A limited 4 Å radial displacement of the S4-S5 linker is sufficient for internal gate closing in Kv channels. *J Biol Chem* 2012;287:40091–8.

124. Feng Z-P, Zhang Z, van Kesteren RE, Straub VA, van Nierop P, Jin K, et al. Transcriptome analysis of the central nervous system of the mollusc Lymnaea stagnalis. *BMC Genomics* 2009;10:451.

125. Fleischhauer R, Davis MW, Dzhura I, Neely A, Avery L, Joho RH. Ultrafast inactivation causes inward rectification in a voltage-gated K(+) channel from Caenorhabditis elegans. *J Neurosci* 2000;20:511–20.

126. Ford L, Crossley M, Williams T, Thorpe JR, Serpell LC, Kemenes G. Effects of Aβ exposure on long-term associative memory and its neuronal mechanisms in a defined neuronal network. *Sci Rep* 2015;5:10614.

127. Forman HJ, Torres M. Reactive oxygen species and cell signaling: respiratory burst in macrophage signaling. *Am J Respir Crit Care Med* 2002;166:S4-8.

128. Foster TC, Kumar A. Susceptibility to induction of long-term depression is associated with impaired memory in aged Fischer 344 rats. *Neurobiol Learn Mem* 2007;87:522–35.

129. Foster TC, Norris CM. Age-associated changes in Ca(2+)-dependent processes: relation to hippocampal synaptic plasticity. *Hippocampus* 1997;7:602–12.

130. Le Franc Y. Inward Rectifier Potassium Channels. Encycl. Comput. Neurosci., New York, NY: Springer New York; 2014, p. 1–4.

131. Franceschi C, Bonafè M, Valensin S, Olivieri F, De Luca M, Ottaviani E, et al. Inflamm-aging. An evolutionary perspective on immunosenescence. *Ann N Y Acad Sci* 2000;908:244–54.

132. Franceschi C, Campisi J. Chronic inflammation (inflammaging) and its potential contribution to age-associated diseases. *J Gerontol A Biol Sci Med Sci* 2014;69 Suppl 1:S4-9.

133. Fransén E, Tigerholm J. Role of A-type potassium currents in excitability, network synchronicity, and epilepsy. *Hippocampus* 2010;20:877–87.

134. Frohnert BI, Bernlohr DA. Protein carbonylation, mitochondrial dysfunction, and insulin resistance. *Adv Nutr* 2013;4:157–63.

135. Fusco D, Colloca G, Lo Monaco MR, Cesari M. Effects of antioxidant supplementation on the aging process. *Clin Interv Aging* 2007;2:377–87.

136. Fux J. Primary and Auxiliary Subunits of Sodium Channel Nav1 in Lymnaea Stagnalis 2014.

137. Gabbiani F, Krapp HG. Spike-frequency adaptation and intrinsic properties of an identified, looming-sensitive neuron. *J Neurophysiol* 2006;96:2951–62.

138. Gabuzda D, Yankner BA. Physiology: Inflammation links ageing to the brain. *Nature* 2013;497:197–8.

139. Gandhi S, Abramov AY. Mechanism of oxidative stress in neurodegeneration. *Oxid Med Cell Longev* 2012;2012:428010.

140. Gates KS. An overview of chemical processes that damage cellular DNA: spontaneous hydrolysis, alkylation, and reactions with radicals. *Chem Res Toxicol* 2009;22:1747–60.

141. Gean PW, Shinnick-Gallagher P. The transient potassium current, the A-current, is involved in spike frequency adaptation in rat amygdala neurons. *Brain Res* 1989;480:160–9.

142. Gemechu JM, Bentivoglio M. T Cell Recruitment in the Brain during Normal Aging. *Front Cell Neurosci* 2012;6:38.

143. Gemma C, Vila J, Bachstetter A, Bickford PC. Oxidative Stress and the Aging Brain: From Theory to Prevention 2007.

144. Gems D, Doonan R. The Nematode Caenorhabditis elegans: Oxidative Stress and Aging in the Nematode Caenorhabditis elegans n.d.

145. Genet S, Kado RT. Hyperpolarizing current of the Na/K ATPase contributes to the membrane polarization of the Purkinje cell in rat cerebellum. *Pflugers Arch Eur J Physiol* 1997;434:559–67.

146. Giese KP, Storm JF, Reuter D, Fedorov NB, Shao LR, Leicher T, et al. Reduced K+ channel inactivation, spike broadening, and after-hyperpolarization in Kvbeta1.1-deficient mice with impaired learning. *Learn Mem* 1998;5:257–73.

147. Gilly WF, Gillette R, Mcfarlane M. Fast and Slow Activation Kinetics of Voltage-Gated Sodium Channels in Molluscan Neurons. *J Neurophysiol* 1997;77:2373–84.

148. Giorgi C, Agnoletto C, Bononi A, Bonora M, De Marchi E, Marchi S, et al. Mitochondrial calcium homeostasis as potential target for mitochondrial medicine. *Mitochondrion* 2012;12:77–85.

149. Gkikas I, Petratou D, Tavernarakis N. Longevity pathways and memory aging. *Front Genet* 2014;5:155.

150. Gladyshev VN. The free radical theory of aging is dead. Long live the damage theory! *Antioxid Redox Signal* 2014;20:727–31.

151. Gleichmann M, Mattson MP. Neuronal calcium homeostasis and dysregulation. *Antioxid Redox Signal* 2011;14:1261–73.

152. Goh JW, Kelly MEM, Pennefather PS. Electrophysiological function of the delayed rectifier (I K) in bullfrog sympathetic ganglion neurones. *Arch Eur J Physiol* 1989;413:482–6.

153. Gomez-Isla T, Price JL, McKeel Jr. DW, Morris JC, Growdon JH, Hyman BT. Profound Loss of Layer II Entorhinal Cortex Neurons Occurs in Very Mild Alzheimer''s Disease. *J Neurosci* 1996;16:4491–500.

154. Görlach A, Bertram K, Hudecova S, Krizanova O. Calcium and ROS: A mutual interplay. *Redox Biol* 2015;6:260–71.

155. Grabe M, Bichet D, Qian X, Jan YN, Jan LY. K+ channel selectivity depends on kinetic as well as thermodynamic factors. *Proc Natl Acad Sci U S A* 2006;103:14361–6.

156. Greenamyre JT, MacKenzie G, Peng TI, Stephans SE. Mitochondrial dysfunction in Parkinson's disease. *Biochem Soc Symp* 1999;66:85–97.

157. Grissmer S, Nguyen AN, Cahalan MD. Calcium-activated potassium channels in resting and activated human T lymphocytes. Expression levels, calcium dependence, ion selectivity, and pharmacology. *J Gen Physiol* 1993;102:601–30.

158. Grizel A V, Glukhov GS, Sokolova OS. Mechanisms of activation of voltage-gated potassium channels. *Acta Naturae* 2014;6:10–26.

159. Gu N, Vervaeke K, Storm JF. BK potassium channels facilitate high-frequency firing and cause early spike frequency adaptation in rat CA1 hippocampal pyramidal cells. *J Physiol* 2007;580:859–82.

160. Guan B, Chen X, Zhang H. Two-Electrode Voltage Clamp. Methods Mol. Biol., vol. 998, 2013, p. 79–89.

161. Guo C, Sun L, Chen X, Zhang D. Oxidative stress, mitochondrial damage and neurodegenerative diseases. *Neural Regen Res* 2013;8:2003–14.

162. Guo D, Ramu Y, Klem AM, Lu Z. Mechanism of rectification in inward-rectifier K+ channels. *J Gen Physiol* 2003;121:261–75.

163. Gupta VK, Scheunemann L, Eisenberg T, Mertel S, Bhukel A, Koemans TS, et al. Restoring polyamines protects from age-induced memory impairment in an autophagy-dependent manner. *Nat Neurosci* 2013;16:1453–60.

164. Hajieva P, Bayatti N, Granold M, Behl C, Moosmann B. Membrane protein oxidation determines neuronal degeneration. *J Neurochem* 2015;133:352–67.

165. Hammond C (Constance), Preceded by: Hammond C (Constance). Cellular and molecular

neurophysiology. n.d.

166. Hands SL, Proud CG, Wyttenbach A. mTOR's role in ageing: protein synthesis or autophagy? *Aging (Albany NY)* 2009;1:586–97.

167. Hansson E, Olsson T, Rönnbäck L. On astrocytes and glutamate neurotransmission : new waves in brain information processing. Landes Bioscience; 1997.

168. Harman D. Aging: a theory based on free radical and radiation chemistry. *J Gerontol* 1956;11:298–300.

169. Hatakeyama D, Fujito Y, Sakakibara M, Ito E. Expression and distribution of transcription factor CCAAT/enhancer-binding protein in the central nervous system of Lymnaea stagnalis. *Cell Tissue Res* 2004;318:631–41.

170. Hedden T, Gabrieli JDE. Insights into the ageing mind: a view from cognitive neuroscience. *Nat Rev Neurosci* 2004;5:87–96.

171. Hegde ML, Hegde PM, Rao KS, Mitra S. Oxidative genome damage and its repair in neurodegenerative diseases: function of transition metals as a double-edged sword. *J Alzheimers Dis* 2011;24 Suppl 2:183–98.

172. Heginbotham L, Lu Z, Abramson T, Mackinnon R. Mutations in the K+ Channel Signature Sequence. *Biophys J* 1994;66:1061–7.

173. Hermann A, Sitdikova GF, Weiger TM. Oxidative Stress and Maxi Calcium-Activated Potassium (BK) Channels. *Biomolecules* 2015;5:1870–911.

174. Hermann PM, Lee A, Hulliger S, Minvielle M, Ma B, Wildering WC. Impairment of long-term associative memory in aging snails (Lymnaea stagnalis). *Behav Neurosci* 2007;121:1400–14.

175. Hermann PM, Park D, Beaulieu E, Wildering WC. Evidence for inflammation-mediated memory dysfunction in gastropods: putative PLA2 and COX inhibitors abolish long-term memory failure induced by systemic immune challenges. *BMC Neurosci* 2013;14:83.

176. Hermann PM, Watson SN, Wildering WC. Phospholipase A2 - nexus of aging, oxidative stress, neuronal excitability, and functional decline of the aging nervous system? Insights from a snail model system of neuronal aging and age-associated memory impairment. *Front Genet* 2014;5:419.

177. Hernandez L, Grasa L, Fagundes DS, Gonzalo S, Arruebo MP, Plaza MA, et al. Role of potassium channels in rabbit intestinal motility disorders induced by 2, 2'-azobis (2-amidinopropane) dihydrochloride (AAPH). *J Physiol Pharmacol* 2010;61:279–86.

178. Hibino H, Inanobe A, Furutani K, Murakami S, Findlay I, Kurachi Y. Inwardly Rectifying Potassium Channels: Their Structure, Function, and Physiological Roles. *Physiol Rev* 2010;90:291–366.

179. Hille B. Ion channels of excitable membranes. Sinauer; 2001.

180. Hochner B, Klein M, Schacher S, Kandel ER. Action-potential duration and the modulation of transmitter release from the sensory neurons of Aplysia in presynaptic facilitation and behavioral sensitization. *Proc Natl Acad Sci U S A* 1986;83:8410–4.

181. Holmgren M, Shin KS, Yellen G. The Activation Gate of a Voltage-Gated K+ Channel Can Be Trapped in the Open State by an Intersubunit Metal Bridge. *Neuron* 1998;21:617–21.

182. Horn R. How S4 segments move charge. Let me count the ways. *J Gen Physiol* 2004;123:1–4.

183. Horrigan FT. Perspectives on: conformational coupling in ion channels: conformational coupling in BK potassium channels. *J Gen Physiol* 2012;140:625–34.

184. Hoshi T, Heinemann S. Regulation of cell function by methionine oxidation and reduction. *J Physiol* 2001;531:1–11.

185. Hroudová J, Singh N, Fišar Z. Mitochondrial dysfunctions in neurodegenerative diseases: relevance to Alzheimer's disease. *Biomed Res Int* 2014;2014:175062.

186. Hsieh C-P. Redox modulation of A-type K+ currents in pain-sensing dorsal root ganglion neurons. vol. 370. 2008.

187. Hsieh H-L, Yang C-M. Role of redox signaling in neuroinflammation and neurodegenerative diseases. *Biomed Res Int* 2013;2013:484613.

188. Hu D, Serrano F, Oury TD, Klann E. Aging-dependent alterations in synaptic plasticity and memory in mice that overexpress extracellular superoxide dismutase. *J Neurosci* 2006;26:3933–41.

189. Humez S, Fournier F, Guilbault P. A voltage-dependent and pH-sensitive proton current in Rana esculenta oocytes. *J Membr Biol* 1995;147:207–15.

190. Humphries ESA, Dart C. Neuronal and Cardiovascular Potassium Channels as Therapeutic Drug Targets: Promise and Pitfalls. *J Biomol Screen* 2015;20:1055–73.

191. Huschenbett J, Zaidi A, Michaelis ML. Sensitivity of the synaptic membrane Na+/Ca2+ exchanger

and the expressed NCX1 isoform to reactive oxygen species. *Biochim Biophys Acta* 1998;1374:34–46.

192. Ikematsu N, Dallas ML, Ross FA, Lewis RW, Rafferty JN, David JA, et al. Phosphorylation of the voltage-gated potassium channel Kv2.1 by AMP-activated protein kinase regulates membrane excitability. *Proc Natl Acad Sci* 2011;108:18132–7.

193. Imbrici P, Grottesi A, D'Adamo MC, Mannucci R, Tucker SJ, Pessia M. Contribution of the central hydrophobic residue in the PXP motif of voltage-dependent K+ channels to S6 flexibility and gating properties. *Channels (Austin)* n.d.;3:39–45.

194. Islam MS. Transient receptor potential channels. Springer Science+Business Media; 2011.

195. Islas LD, Sigworth FJ. Voltage sensitivity and gating charge in Shaker and Shab family potassium channels. *J Gen Physiol* 1999;114:723–42.

196. Ito E, Otsuka E, Hama N, Aonuma H, Okada R, Hatakeyama D, et al. Memory trace in feeding neural circuitry underlying conditioned taste aversion in Lymnaea. *PLoS One* 2012;7:e43151.

197. Itri JN, Michel S, Vansteensel MJ, Meijer JH, Colwell CS. Fast delayed rectifier potassium current is required for circadian neural activity. *Nat Neurosci* 2005;8:650–6.

198. Itri JN, Vosko AM, Schroeder A, Dragich JM, Michel S, Colwell CS. Circadian regulation of a-type potassium currents in the suprachiasmatic nucleus. *J Neurophysiol* 2010;103:632–40.

199. Jäkel S, Dimou L. Glial Cells and Their Function in the Adult Brain: A Journey through the History of Their Ablation. *Front Cell Neurosci* 2017;11:24.

200. Janse C, Wildering WC, Popelier CM. Age-related changes in female reproductive activity and growth in the mollusc Lymnaea stagnalis. *J Gerontol* 1989;44:B148-55.

201. Jansen RF, Pieneman AW, Maat AT. Pattern generation in the buccal system of freely behaving Lymnaea stagnalis. *J Neurophysiol* 1999;82:3378–91.

202. Jastroch M, Divakaruni AS, Mookerjee S, Treberg JR, Brand MD. Mitochondrial proton and electron leaks. *Essays Biochem* 2010;47:53–67.

203. Jeffs GJ, Meloni BP, Bakker AJ, Knuckey NW. The role of the Na(+)/Ca(2+) exchanger (NCX) in neurons following ischaemia. *J Clin Neurosci* 2007;14:507–14.

204. Jessen KR. Glial cells. *Int J Biochem Cell Biol* 2004;36:1861–7.

205. Jeulin C, Fournier J, Marano F, Dazy A-C. Effects of hydroxyl radicals on outwardly rectifying chloride channels in a cultured human bronchial cell line (16HBE14o–). *Pflügers Arch - Eur J Physiol* 2000;439:331–8.

206. Jeyapalan JC, Sedivy JM. Cellular senescence and organismal aging. *Mech Ageing Dev* 129:467–74.

207. Jiang Y, Ruta V, Chen J, Lee A, MacKinnon R. The principle of gating charge movement in a voltage-dependent K+ channel. *Nature* 2003;423:42–8.

208. Jogini V, Roux B. Dynamics of the Kv1.2 voltage-gated K+ channel in a membrane environment. *Biophys J* 2007;93:3070–82.

209. Johns P, Johns P. Electrical signalling in neurons. Clin. Neurosci., Elsevier; 2014, p. 71–80.

210. Johnson SC, Rabinovitch PS, Kaeberlein M. mTOR is a key modulator of ageing and age-related disease. *Nature* 2013;493:338–45.

211. Joseph JA, Shukitt-Hale B, Casadesus G, Fisher D. Oxidative Stress and Inflammation in Brain Aging: Nutritional Considerations n.d.

212. Jow F, Zhang Z-H, Kopsco DC, Carroll KC, Wang K. Functional coupling of intracellular calcium and inactivation of voltage-gated Kv1.1/Kvbeta1.1 A-type K+ channels. *Proc Natl Acad Sci U S A* 2004;101:15535–40.

213. Jurk D, Wang C, Miwa S, Maddick M, Korolchuk V, Tsolou A, et al. Postmitotic neurons develop a p21-dependent senescence-like phenotype driven by a DNA damage response. *Aging Cell* 2012;11:996–1004.

214. Juusola M, Robinson HPC, De Polavieja GG. Coding with spike shapes and graded potentials in cortical networks. *BioEssays* 2007;29:178–87.

215. Kaczorowski CC, Disterhoft JF. Memory deficits are associated with impaired ability to modulate neuronal excitability in middle-aged mice. *Learn Mem* 2009;16:362–6.

216. Kadala A, Verdier D, Morquette P, Kolta A. Ion Homeostasis in Rhythmogenesis: The Interplay Between Neurons and Astroglia. *Physiology* 2015;30:371–88.

217. Kaltschmidt B, Kaltschmidt C. NF-kappaB in the nervous system. *Cold Spring Harb Perspect Biol* 2009;1:a001271.

218. Kann O, Kovács R. Mitochondria and neuronal activity. *Am J Physiol Cell Physiol* 2007;292:C641-57.

219. Katyal S, McKinnon PJ. DNA strand breaks, neurodegeneration and aging in the brain. *Mech Ageing Dev* 129:483–91.

220. Kelly ME, Dixon SJ, Sims SM. Outwardly rectifying chloride current in rabbit osteoclasts is activated by hyposmotic stimulation. *J Physiol* 1994;475:377–89.

221. Kemenes G, Elliot CJH, Benjamin PR. Chemical and Tactile Inputs to the Lymnaea Feeding System: Effects on Behaviour and Neural Circuitry. *J Exp Biol* 1986;122:113–37.

222. Kemenes G, Hiripi L, Benjamin PR. Behavioural and Biochemical Changes in the Feeding System of Lymnaea Induced by the Dopamine and Serotonin Neurotoxins 6-hydroxydopamine and 5,6-dihydroxytryptamine. *Philos Trans R Soc B Biol Sci* 1990;329:243–55.

223. Kemenes G, Staras K, Benjamin PR. Multiple Types of Control by Identified Interneurons in a Sensory-Activated Rhythmic Motor Pattern. *J Neurosci* 2001;21:2903–11.

224. Kemenes G, Staras K, Benjamin PR. In Vitro Appetitive Classical Conditioning of the Feeding Response in the Pond Snail Lymnaea stagnalis. *J Neurophysiol* 1997;78:2351–62.

225. Kemenes I, Marra V, Crossley M, Samu D, Staras K, Kemenes G, et al. Dynamic clamp with StdpC software. *Nat Protoc* 2011;6:405–17.

226. Kemenes I, Straub VA, Nikitin ES, Staras K, O'Shea M, Kemenes G, et al. Role of Delayed Nonsynaptic Neuronal Plasticity in Long-Term Associative Memory. *Curr Biol* 2006;16:1269–79.

227. Kemnitz CP. Dopaminergic Modulation of Spinal Neurons and Synaptic Potentials in the Lamprey Spinal Cord n.d.

228. Kempsell AT, Fieber LA. Aging in Sensory and Motor Neurons Results in Learning Failure in Aplysia californica. *PLoS One* 2015;10:e0127056.

229. Khalili-Araghi F, Jogini V, Yarov-Yarovoy V, Tajkhorshid E, Roux B, Schulten K. Calculation of the gating charge for the Kv1.2 voltage-activated potassium channel. *Biophys J* 2010;98:2189–98.

230. Kim CS, Coyne MD, Gwathmey JK. Voltage-dependent calcium channels in ventricular cells of rainbow trout: effect of temperature changes in vitro. *Am J Physiol - Regul Integr Comp Physiol* 2000;278.

231. Kim J, Wei D-S, Hoffman DA. Kv4 potassium channel subunits control action potential repolarization and frequency-dependent broadening in rat hippocampal CA1 pyramidal neurones. *J Physiol* 2005;569:41–57.

232. Kimm T, Khaliq ZM, Bean BP. Differential Regulation of Action Potential Shape and Burst-Frequency Firing by BK and Kv2 Channels in Substantia Nigra Dopaminergic Neurons. *J Neurosci* 2015;35:16404–17.

233. Kita T, Kita H, Kitai ST. Effects of 4-aminopyridine (4-AP) on rat neostriatal neurons in an in vitro slice preparation. *Brain Res* 1985;361:10–8.

234. Kocsis JD, Eng DL, Gordon TR, Waxman SG. Functional differences between 4-aminopyridine and tetraethylammonium-sensitive potassium channels in myelinated axons. *Neurosci Lett* 1987;75:193–8.

235. Koert CE, Spencer GE, van Minnen J, Li KW, Geraerts WP, Syed NI, et al. Functional implications of neurotransmitter expression during axonal regeneration: serotonin, but not peptides, auto-regulate axon growth of an identified central neuron. *J Neurosci* 2001;21:5597–606.

236. Kofuji P, Newman EA. Potassium buffering in the central nervous system. *Neuroscience* 2004;129:1045–56.

237. Koh SD, Ward SM, Dick GM, Epperson A, Bonner HP, Sanders KM, et al. Contribution of delayed rectifier potassium currents to the electrical activity of murine colonic smooth muscle. *J Physiol* 1999;515 (Pt 2:475–87.

238. Koivisto K, Reinikainen KJ, Hänninen T, Vanhanen M, Helkala EL, Mykkänen L, et al. Prevalence of age-associated memory impairment in a randomly selected population from eastern Finland. *Neurology* 1995;45:741–7.

239. Komatsuzaki T. Single-molecule biophysics : experiment and theory. J. Wiley & Sons; 2012.

240. Korneev SA, Straub V, Kemenes I, Korneeva EI, Ott SR, Benjamin PR, et al. Timed and targeted differential regulation of nitric oxide synthase (NOS) and anti-NOS genes by reward conditioning leading to long-term memory formation. *J Neurosci* 2005;25:1188–92.

241. Krapivinsky G, Medina I, Eng L, Krapivinsky L, Yang Y, Clapham DE. A novel inward rectifier K+ channel with unique pore properties. *Neuron* 1998;20:995–1005.

242. Kregel KC, Zhang HJ. An integrated view of oxidative stress in aging: basic mechanisms, functional effects, and pathological considerations. *Am J Physiol Integr Comp Physiol* 2007;292:R18–36.

243. Krishna MC, Dewhirst MW, Friedman HS, Cook JA, DeGraff W, Samuni A, et al. Hyperthermic

sensitization by the radical initiator 2,2'-azobis (2-amidinopropane) dihydrochloride (AAPH). I. In vitro studies. *Int J Hyperthermia* n.d.;10:271–81.

244. Kuang Q, Purhonen P, Hebert H. Structure of potassium channels. *Cell Mol Life Sci* 2015;72:3677–93.

245. Kumar A. Long-Term Potentiation at CA3-CA1 Hippocampal Synapses with Special Emphasis on Aging, Disease, and Stress. *Front Aging Neurosci* 2011;3:7.

246. Kumar A, Bodhinathan K, Foster TC. Susceptibility to Calcium Dysregulation during Brain Aging. *Front Aging Neurosci* 2009;1:2.

247. Kumar A, Foster TC. Neurophysiology of Old Neurons and Synapses. CRC Press/Taylor & Francis; 2007.

248. Kumar H, Lim H-W, More SV, Kim B-W, Koppula S, Kim IS, et al. The role of free radicals in the aging brain and Parkinson's Disease: convergence and parallelism. *Int J Mol Sci* 2012;13:10478–504.

249. Kumar M, Seeger W, Voswinckel R. Senescence-associated secretory phenotype and its possible role in chronic obstructive pulmonary disease. *Am J Respir Cell Mol Biol* 2014;51:323–33.

250. Labro AJ, Snyders DJ. Being flexible: the voltage-controllable activation gate of kv channels. *Front Pharmacol* 2012;3:168.

251. Labro AJ, Snyders DJ. Being Flexible: The Voltage-Controllable Activation Gate of Kv Channels. *Front Pharmacol* 2012;3:168.

252. Landfield PW, Pitler TA. Prolonged Ca2+-dependent afterhyperpolarizations in hippocampal neurons of aged rats. *Science* 1984;226:1089–92.

253. Laplante M, Sabatini DM. mTOR signaling in growth control and disease. *Cell* 2012;149:274–93.

254. Larsson HP. What determines the kinetics of the slow afterhyperpolarization (sAHP) in neurons? *Biophys J* 2013;104:281–3.

255. Latour A, Grintal B, Champeil-Potokar G, Hennebelle M, Lavialle M, Dutar P, et al. Omega-3 fatty acids deficiency aggravates glutamatergic synapse and astroglial aging in the rat hippocampal CA1. *Aging Cell* 2013;12:76–84.

256. Laurienti PJ, Blankenship JE. Parapodial swim muscle in Aplysia brasiliana. I. Voltage-gated membrane currents in isolated muscle fibers. *J Neurophysiol* 1996;76:1517–30.

257. Lecar H, Larsson HP, Grabe M. Electrostatic model of S4 motion in voltage-gated ion channels. *Biophys J* 2003;85:2854–64.

258. Lee JC-M, Simonyi A, Sun AY, Sun GY. Phospholipases A2 and neural membrane dynamics: implications for Alzheimer's disease. *J Neurochem* 2011;116:813–9.

259. Lee US, Cui J. BK channel activation: structural and functional insights. *Trends Neurosci* 2010;33:415–23.

260. Lenaz G. The Mitochondrial Production of Reactive Oxygen Species: Mechanisms and Implications in Human Pathology. *IUBMB Life (International Union Biochem Mol Biol Life)* 2001;52:159–64.

261. de Lera Ruiz M, Kraus RL. Voltage-Gated Sodium Channels: Structure, Function, Pharmacology, and Clinical Indications. *J Med Chem* 2015;58:7093–118.

262. Lin L, Sun W, Kung F, Dell'Acqua ML, Hoffman DA. AKAP79/150 impacts intrinsic excitability of hippocampal neurons through phospho-regulation of A-type K+ channel trafficking. *J Neurosci* 2011;31:1323–32.

263. Linz KW, Meyer R. Control of L-type calcium current during the action potential of guinea-pig ventricular myocytes. *J Physiol* 1998;513 (Pt 2):425–42.

264. Liu PW, Bean BP. Kv2 channel regulation of action potential repolarization and firing patterns in superior cervical ganglion neurons and hippocampal CA1 pyramidal neurons. *J Neurosci* 2014;34:4991–5002.

265. Lobo V, Patil A, Phatak A, Chandra N. Free radicals, antioxidants and functional foods: Impact on human health. *Pharmacogn Rev* 2010;4:118–26.

266. Lodish H, Berk A, Zipursky SL, Matsudaira P, Baltimore D, Darnell J. The Action Potential and Conduction of Electric Impulses 2000.

267. Long SB, Campbell EB, Mackinnon R. Crystal Structure of a Mammalian Voltage-Dependent Shaker Family K+ Channel. *Science (80-)* 2005;309:897–903.

268. Looney SW, Hagan JL. Analysis of Biomarker Data: A Practical Guide 2015:424.

269. Lopes KO, Sparks DL, Streit WJ. Microglial dystrophy in the aged and Alzheimer's disease brain is associated with ferritin immunoreactivity. *Glia* 2008;56:1048–60.

270. López-Bayghen E, Ortega A. Glial Glutamate Transporters: New Actors in Brain Signaling n.d.

271. López-Otín C, Blasco MA, Partridge L, Serrano M, Kroemer G. The hallmarks of aging. *Cell* 2013;153:1194–217.

272. de Lores Arnaiz GR, Ordieres MGL. Brain Na(+), K(+)-ATPase Activity In Aging and Disease. *Int J Biomed Sci* 2014;10:85–102.

273. Lü J-M, Lin PH, Yao Q, Chen C. Chemical and molecular mechanisms of antioxidants: experimental approaches and model systems. *J Cell Mol Med* 2010;14:840–60.

274. Lukowiak, Ringseis, Spencer, Wildering, Syed. Operant conditioning of aerial respiratory behaviour in Lymnaea stagnalis. *J Exp Biol* 1996;199:683–91.

275. Lunenfeld B, Stratton P. The clinical consequences of an ageing world and preventive strategies. *Best Pract Res Clin Obstet Gynaecol* 2013;27:643–59.

276. Luo X-G, Chen S-D. The changing phenotype of microglia from homeostasis to disease. *Transl Neurodegener* 2012;1:9.

277. Luo X-G, Ding J-Q, Chen S-D. Microglia in the aging brain: relevance to neurodegeneration. *Mol Neurodegener* 2010;5:12.

278. Ma Z, Lou XJ, Horrigan FT. Role of charged residues in the S1-S4 voltage sensor of BK channels. *J Gen Physiol* 2006;127:309–28.

279. MacKinnon R. Potassium channels. *FEBS Lett* 2003;555:62–5.

280. MacKinnon R, Cohen SL, Kuo A, Lee A, Chait BT. Structural conservation in prokaryotic and eukaryotic potassium channels. *Science* 1998;280:106–9.

281. MacKinnon R, Doyle DA. Prokaryotes offer hope for potassium channel structural studies. *Nat Struct Biol* 1997;4:877–9.

282. Magoski NS, Syed NI, Bulloch AG. A neuronal network from the mollusc Lymnaea stagnalis. *Brain Res* 1994;645:201–14.

283. Mahon S, Casassus G, Mulle C, Charpier S. Spike-Dependent Intrinsic Plasticity Increases Firing Probability in Rat Striatal Neurons *In Vivo*. *J Physiol* 2003;550:947–59.

284. Majumder S, Caccamo A, Medina DX, Benavides AD, Javors MA, Kraig E, et al. Lifelong rapamycin administration ameliorates age-dependent cognitive deficits by reducing IL-1β and enhancing NMDA signaling. *Aging Cell* 2012;11:326–35.

285. Männikkö R, Elinder F, Larsson HP. Voltage-sensing mechanism is conserved among ion channels gated by opposite voltages. *Nature* 2002;419:837–41.

286. Mantegazza M, Catterall WA. Voltage-Gated Na+Channels: Structure, Function, and Pathophysiology. National Center for Biotechnology Information (US); 2012.

287. Maqbool A, Lattke M, Wirth T, Baumann B. Sustained, neuron-specific IKK/NF-κB activation generates a selective neuroinflammatory response promoting local neurodegeneration with aging. *Mol Neurodegener* 2013;8:40.

288. Marder E, Prinz AA, Marder E, Harris-Warrick RM, Guckenheimer J. Current compensation in neuronal homeostasis. *Neuron* 2003;37:2–4.

289. Marmot M. MARMOT INDICATORS BRIEFINGS. 2017.

290. Martel M-A, Patenaude C, Ménard C, Alaux S, Cummings BS, Massicotte G. A novel role for calcium-independent phospholipase A in alpha-amino-3-hydroxy-5-methylisoxazole-propionate receptor regulation during long-term potentiation. *Eur J Neurosci* 2006;23:505–13.

291. Massaeli H, Sobrattee S, Pierce GN. The importance of lipid solubility in antioxidants and free radical generating systems for determining lipoprotein proxidation. *Free Radic Biol Med* 1999;26:1524–30.

292. Matthews EA, Linardakis JM, Disterhoft JF. The fast and slow afterhyperpolarizations are differentially modulated in hippocampal neurons by aging and learning. *J Neurosci* 2009;29:4750–5.

293. Matthews EA, Weible AP, Shah S, Disterhoft JF. The BK-mediated fAHP is modulated by learning a hippocampus-dependent task. *Proc Natl Acad Sci U S A* 2008;105:15154–9.

294. Mattson MP. Calcium and neurodegeneration. *Aging Cell* 2007;6:337–50.

295. Mattson MP, Magnus T. Ageing and neuronal vulnerability. *Nat Rev Neurosci* 2006;7:278–94.

296. Mazucanti CH, Cabral-Costa JV, Vasconcelos AR, Andreotti DZ, Scavone C, Kawamoto EM. Longevity Pathways (mTOR, SIRT, Insulin/IGF-1) as Key Modulatory Targets on Aging and Neurodegeneration. *Curr Top Med Chem* 2015;15:2116–38.

297. Merzetti EM, Staveley BE. Mitochondrial dynamics in degenerative disease and disease models. *Neurosci Discov* 2013;1:8.

298. Meyers, Lawrence S., Gamst, Gleen C. G. Performing data analysis using IBM SPSS(R). Wiley; 2013.

299. Miceli F, Soldovieri MV, Hernandez CC, Shapiro MS, Annunziato L, Taglialatela M. Gating Consequences of Charge Neutralization of Arginine Residues in the S4 Segment of Kv7.2, an Epilepsy-Linked K+ Channel Subunit. *Biophys J* 2008;95:2254–64.

300. Miller C. An overview of the potassium channel family. *Genome Biol* 2000;1:REVIEWS0004.

301. Mindell JA, Maduke M. ClC chloride channels. *Genome Biol* 2001;2:REVIEWS3003.

302. Miquel J, Economos AC, Fleming J, Johnson JE. Mitochondrial role in cell aging. *Exp Gerontol* 1980;15:575–91.

303. Mobasheri A, Avila J, Cózar-Castellano I, Brownleader MD, Trevan M, Francis MJ, et al. Na+, K+-ATPase isozyme diversity; comparative biochemistry and physiological implications of novel functional interactions. *Biosci Rep* 2000;20:51–91.

304. Mostany R, Anstey JE, Crump KL, Maco B, Knott G, Portera-Cailliau C. Altered synaptic dynamics during normal brain aging. *J Neurosci* 2013;33:4094–104.

305. Moyer JR, Thompson LT, Black JP, Disterhoft JF. Nimodipine increases excitability of rabbit CA1 pyramidal neurons in an age- and concentration-dependent manner. *J Neurophysiol* 1992;68:2100–9.

306. Moyer JR, Thompson LT, Black JP, Disterhoft JF. Nimodipine Increases Excitability of Rabbit CA1 Pyramidal Neurons in an Age-and Concentration-Dependent Manner. *JOURNALOF Neurophysiol* 1992;68.

307. Muller M, Felmy F, Schwaller B, Schneggenburger R, Frotscher M, Sakmann B, et al. Parvalbumin Is a Mobile Presynaptic Ca2+ Buffer in the Calyx of Held that Accelerates the Decay of Ca2+ and Short-Term Facilitation. *J Neurosci* 2007;27:2261–71.

308. Muñoz-Espín D, Serrano M. Cellular senescence: from physiology to pathology. *Nat Rev Mol Cell Biol* 2014;15:482–96.

309. Murakoshi H, Shi G, Scannevin RH, Trimmer JS. Phosphorylation of the Kv2.1 K+ channel alters voltage-dependent activation. *Mol Pharmacol* 1997;52:821–8.

310. Murphy GG, Fedorov NB, Giese KP, Ohno M, Friedman E, Chen R, et al. Increased Neuronal Excitability, Synaptic Plasticity, and Learning in Aged Kvβ1.1 Knockout Mice. *Curr Biol* 2004;14:1907–15.

311. Na Phuket TR, Covarrubias ML. Kv4 channels underlie the subthreshold-operating A-type K+-current in nociceptive dorsal root ganglion neurons. *Front Mol Neurosci* 2009;2:3.

312. Naranjo D, Moldenhauer H, Pincuntureo M, Díaz-Franulic I. Pore size matters for potassium channel conductance. *J Gen Physiol* 2016;148:277–91.

313. Negre-Salvayre A, Coatrieux C, Ingueneau C, Salvayre R. Advanced lipid peroxidation end products in oxidative damage to proteins. Potential role in diseases and therapeutic prospects for the inhibitors. *Br J Pharmacol* 2008;153:6–20.

314. Negro CA Del, Chandler SH. Physiological and Theoretical Analysis of K+ Currents Controlling Discharge in Neonatal Rat Mesencephalic Trigeminal Neurons. *J Neurophysiol* 1997;77.

315. Niki E. Interaction of ascorbate and alpha-tocopherol. *Ann N Y Acad Sci* 1987;498:186–99.

316. Nikitin ES, Kiss T, Staras K, O 'shea M, Benjamin PR, Kemenes G. Persistent Sodium Current Is a Target for cAMP-Induced Neuronal Plasticity in a State-Setting Modulatory Interneuron n.d.

317. Nikitin ES, Vavoulis D V, Kemenes I, Marra V, Pirger Z, Michel M, et al. Persistent sodium current is a nonsynaptic substrate for long-term associative memory. *Curr Biol* 2008;18:1221–6.

318. Nikoletopoulou V, Tavernarakis N. Calcium homeostasis in aging neurons. *Front Genet* 2012;3:200.

319. Noble WS. How does multiple testing correction work? *Nat Biotechnol* 2009;27:1135–7.

320. Norman GR, Streiner DL. Biostatistics : the bare essentials. B.C. Decker; 2008.

321. Norris CM, Halpain S, Foster TC. Reversal of age-related alterations in synaptic plasticity by blockade of L-type Ca2+ channels. *J Neurosci* 1998;18:3171–9.

322. Norris CM, Halpain S, Foster TC. Reversal of Age-Related Alterations in Synaptic Plasticity by Blockade of L-Type Ca2+ Channels. *J Neurosci* 1998;18.

323. Ogden D, Stanfield P. Patch clamp techniques for single channel and whole-cell recording n.d.

324. Oh MM, McKay BM, Power JM, Disterhoft JF. Learning-related postburst afterhyperpolarization reduction in CA1 pyramidal neurons is mediated by protein kinase A. *Proc Natl Acad Sci U S A* 2009;106:1620–5.

325. Oh MM, Oliveira FA, Disterhoft JF. Learning and aging related changes in intrinsic neuronal excitability. *Front Aging Neurosci* 2010;2:2.

326. Othman S Ben, Yabe T. USE OF HYDROGEN PEROXIDE AND PEROXYL RADICALS TO INDUCE OXIDATIVE STRESS IN NEURONAL CELLS. *Rev Agric Sci* 2015;3:40–5.

229

327. Ottschytsch N, Raes A, Van Hoorick D, Snyders DJ, Trigg LM, Rossum DB van, et al. Obligatory heterotetramerization of three previously uncharacterized Kv channel alpha-subunits identified in the human genome. *Proc Natl Acad Sci U S A* 2002;99:7986–91.

328. Padurariu M, Ciobica A, Mavroudis I, Fotiou D, Baloyannis S. Hippocampal neuronal loss in the CA1 and CA3 areas of Alzheimer's disease patients. *Psychiatr Danub* 2012;24:152–8.

329. Paiva CN, Bozza MT. Are reactive oxygen species always detrimental to pathogens? *Antioxid Redox Signal* 2014;20:1000–37.

330. Palaniappan APA. A SURPRISING CLARIFICATION OF THE MECHANISM OF ION-CHANNEL VOLTAGE- GATING n.d.

331. Pang R-P, Xie M-X, Yang J, Shen K-F, Chen X, Su Y-X, et al. Downregulation of ClC-3 in dorsal root ganglia neurons contributes to mechanical hypersensitivity following peripheral nerve injury. *Neuropharmacology* 2016;110:181–9.

332. Papazian DM, Timpe LC, Jan YN, Jan LY. Alteration of voltage-dependence of Shaker potassium channel by mutations in the S4 sequence. *Nature* 1991;349:305–10.

333. Partridge L. The new biology of ageing. *Philos Trans R Soc Lond B Biol Sci* 2010;365:147–54.

334. Partridge L. Rejuvenating ageing research. *Acad Med Sci* 2009.

335. Partridge L, Alic N, Bjedov I, Piper MDW. Ageing in Drosophila: the role of the insulin/Igf and TOR signalling network. *Exp Gerontol* 2011;46:376–81.

336. Patel BA, Arundell M, Allen MC, Gard P, O'Hare D, Parker K, et al. Changes in the properties of the modulatory cerebral giant cells contribute to aging in the feeding system of Lymnaea. *Neurobiol Aging* 2006;27:1892–901.

337. Patel BA, Arundell M, Parker KH, Yeoman MS, O'Hare D. Microelectrode investigation of neuroneal ageing from a single identified neurone. *Phys Chem Chem Phys* 2010;12:10065–72.

338. Pathak D, Guan D, Foehring RC. Roles of specific Kv channel types in repolarization of the action potential in genetically identified subclasses of pyramidal neurons in mouse neocortex. *J Neurophysiol* 2016;115.

339. Paul V, Ekambaram P. Involvement of nitric oxide in learning & memory processes. *Indian J Med Res* 2011;133:471–8.

340. Perez-Reyes E. Molecular Physiology of Low-Voltage-Activated T-type Calcium Channels. *Physiol Rev* 2003;83:117–61.

341. Perry SJ, Straub VA, Kemenes G, Santama N, Worster BM, Burke JF, et al. Neural modulation of gut motility by myomodulin peptides and acetylcholine in the snail Lymnaea. *J Neurophysiol* 1998;79:2460–74.

342. Peters A. Structural changes that occur during normal aging of primate cerebral hemispheres. *Neurosci Biobehav Rev* 2002;26:733–41.

343. Peters R. Ageing and the brain. *Postgrad Med J* 2006;82:84–8.

344. Petkova-Kirova P, Gagov H, Krien U, Duridanova D, Noack T, Schubert R. 4-aminopyridine affects rat arterial smooth muscle BK(Ca) currents by changing intracellular pH. *Br J Pharmacol* 2000;131:1643–50.

345. Petralia RS, Mattson MP, Yao PJ. Communication breakdown: the impact of ageing on synapse structure. *Ageing Res Rev* 2014;14:31–42.

346. Pham-Huy LA, He H, Pham-Huy C. Free radicals, antioxidants in disease and health. *Int J Biomed Sci* 2008;4:89–96.

347. Picton LD, Sillar KT. Mechanisms underlying the endogenous dopaminergic inhibition of spinal locomotor circuit function in Xenopus tadpoles. *Sci Rep* 2016;6:35749.

348. Pole A, Dimri M, P. Dimri G. Oxidative stress, cellular senescence and ageing. *AIMS Mol Sci* 2016;3:300–24.

349. Pongs O. Regulation of Excitability by Potassium Channels. Inhib. Regul. Excit. Neurotransmission, Berlin, Heidelberg: Springer Berlin Heidelberg; 2007, p. 145–61.

350. Potier B, Billard J-M, Rivière S, Sinet P-M, Denis I, Champeil-Potokar G, et al. Reduction in glutamate uptake is associated with extrasynaptic NMDA and metabotropic glutamate receptor activation at the hippocampal CA1 synapse of aged rats. *Aging Cell* 2010;9:722–35.

351. Power JM, Bocklisch C, Curby P, Sah P. Location and Function of the Slow Afterhyperpolarization Channels in the Basolateral Amygdala. *J Neurosci* 2011;31:526–37.

352. Power JM, Wu WW, Sametsky E, Oh MM, Disterhoft JF. Age-related enhancement of the slow outward calcium-activated potassium current in hippocampal CA1 pyramidal neurons in vitro. *J Neurosci* 2002;22:7234–43.

353. Pradeep AR, Ramchandraprasad M V, Bajaj P, Rao NS, Agarwal E. Protein carbonyl: An oxidative

stress marker in gingival crevicular fluid in healthy, gingivitis, and chronic periodontitis subjects. *Contemp Clin Dent* 2013;4:27–31.

354. Prinz AAA, Abbott LFF, Marder E. The dynamic clamp comes of age. vol. 27. 2004.

355. Purves D, Augustine GJ, Fitzpatrick D, Katz LC, LaMantia A-S, McNamara JO, et al. Mechanisms of Synaptic Plasticity in Relatively Simple Invertebrates 2001.

356. Qu Z, Hartzell HC. Anion permeation in Ca(2+)-activated Cl(-) channels. *J Gen Physiol* 2000;116:825–44.

357. Quattrocki EA, Marshall J, Kaczmarek LK. A Shab potassium channel contributes to action potential broadening in peptidergic neurons. *Neuron* 1994;12:73–86.

358. R. Wittenberg, H.Bo, A. Comas-Herrera JL-F et al. Care for older people. *Nuff Trust* 2012.

359. Radi R. Protein tyrosine nitration: biochemical mechanisms and structural basis of functional effects. *Acc Chem Res* 2013;46:550–9.

360. Ramos BP, Birnbaum SG, Lindenmayer I, Newton SS, Duman RS, Arnsten AFT. Dysregulation of Protein Kinase A Signaling in the Aged Prefrontal Cortex: New Strategy for Treating Age-Related Cognitive Decline. *Neuron* 2003;40:835–45.

361. Rao JS, Rapoport SI, Kim H-W. Altered neuroinflammatory, arachidonic acid cascade and synaptic markers in postmortem Alzheimer's disease brain. *Transl Psychiatry* 2011;1:e31.

362. Ray Sujata; Susan Davidson. Dementia and Cognitive Decline Evidence Review. *AGE UK* 2014.

363. Rezazadeh S, Kurata HT, Claydon TW, Kehl SJ, Fedida D. An activation gating switch in Kv1.2 is localized to a threonine residue in the S2-S3 linker. *Biophys J* 2007;93:4173–86.

364. Rizzo V, Richman J, Puthanveettil S V. Dissecting mechanisms of brain aging by studying the intrinsic excitability of neurons. *Front Aging Neurosci* 2014;6:337.

365. Robinson HPC, Kawai N. Injection of digitally synthesized synaptic conductance transients to measure the integrative properties of neurons. *J Neurosci Methods* 1993;49:157–65.

366. Rose RM, Benjamin PR. The relationship of the central motor pattern to the feeding cycle of Lymnaea stagnalis. *J Exp Biol* 1979;80:137–63.

367. Rosenthal JJC, Seeburg PH. A-to-I RNA editing: effects on proteins key to neural excitability. *Neuron* 2012;74:432–9.

368. Roux B. Ion Conduction and Selectivity in K+ Channels. *Annu Rev Biophys Biomol Struct* 2005;34:153–71.

369. Sabatini BL, Regehr WG. Control of Neurotransmitter Release by Presynaptic Waveform at the Granule Cell to Purkinje Cell Synapse n.d.

370. Sacco T, Tempia F. A-type potassium currents active at subthreshold potentials in mouse cerebellar Purkinje cells. *J Physiol* 2002;543:505–20.

371. Sachdev S, Davies KJA. Production, detection, and adaptive responses to free radicals in exercise. *Free Radic Biol Med* 2008;44:215–23.

372. Sadowska-Bartosz I, Bartosz G. Effect of antioxidants supplementation on aging and longevity. *Biomed Res Int* 2014;2014:404680.

373. Sah P, McLachlan EM. Potassium currents contributing to action potential repolarization and the afterhyperpolarization in rat vagal motoneurons. *J Neurophysiol* 1992;68:1834–41.

374. Sahoo N, Hoshi T, Heinemann SH. Oxidative modulation of voltage-gated potassium channels. *Antioxid Redox Signal* 2014;21:933–52.

375. Sakakibara M, Okuda F, Nomura K, Watanabe K, Meng H, Horikoshi T, et al. Potassium Currents in Isolated Statocyst Neurons and RPeD1 in the Pond Snail, Lymnaea stagnalis. *J Neurophysiol* 2005;94:3884–92.

376. Saki M, Prakash A. DNA damage related crosstalk between the nucleus and mitochondria. *Free Radic Biol Med* 2017;107:216–27.

377. Sakmann B, Neher E. Single-channel recording. Springer; 2009.

378. Salminen A, Kauppinen A, Kaarniranta K. Emerging role of NF-κB signaling in the induction of senescence-associated secretory phenotype (SASP). *Cell Signal* 2012;24:835–45.

379. Samu D, Marra V, Kemenes I, Crossley M, Kemenes G, Staras K, et al. Single electrode dynamic clamp with StdpC. *J Neurosci Methods* 2012;211:11–21.

380. Sanchez DY, Blatz AL. Voltage-dependent block of fast chloride channels from rat cortical neurons by external tetraethylammonium ion. *J Gen Physiol* 1992;100:217–31.

381. Sanchez DY, Blatz AL. Block of neuronal fast chloride channels by internal tetraethylammonium ions. *J Gen Physiol* 1994;104:173–90.

382. Sanchez G, Rodriguez MJ, Pomata P, Rela L, Murer MG. Neurobiology of Disease Reduction of

an Afterhyperpolarization Current Increases Excitability in Striatal Cholinergic Interneurons in Rat Parkinsonism n.d.

383. Sansom MSP. Potassium channels: Watching a voltage-sensor tilt and twist. *Curr Biol* 2000;10:R206–9.

384. Saransaari P, Oja SS. Age-related changes in the uptake and release of glutamate and aspartate in the mouse brain. *Mech Ageing Dev* 1995;81:61–71.

385. Sarria I, Ling J, Gu JG. Thermal sensitivity of voltage-gated Na+ channels and A-type K+ channels contributes to somatosensory neuron excitability at cooling temperatures. *J Neurochem* 2012;122:1145–54.

386. Sattelle DB, Buckingham SD. Invertebrate studies and their ongoing contributions to neuroscience. *Invert Neurosci* 2006;6:1–3.

387. Scala F, Fusco S, Ripoli C, Piacentini R, Li Puma DD, Spinelli M, et al. Intraneuronal Aβ accumulation induces hippocampal neuron hyperexcitability through A-type K(+) current inhibition mediated by activation of caspases and GSK-3. *Neurobiol Aging* 2015;36:886–900.

388. Schampel A, Kuerten S. Danger: High Voltage—The Role of Voltage-Gated Calcium Channels in Central Nervous System Pathology n.d.

389. Schott BH, Henson RN, Richardson-Klavehn A, Becker C, Thoma V, Heinze H-J, et al. Redefining implicit and explicit memory: the functional neuroanatomy of priming, remembering, and control of retrieval. *Proc Natl Acad Sci U S A* 2005;102:1257–62.

390. Schwartzkroin PA (Philip A., Elsevier Science (Firm). Encyclopedia of basic epilepsy research. Elsevier Academic Press; 2009.

391. Schwartzkroin PA, Prince DA. Effects of TEA on hippocampal neurons. *Brain Res* 1980;185:169–81.

392. Scutt G. Age-related changes to ionic currents and excitability in the cerebral giant cells of the pond snail, lymnaea stagnalis. University of Brighton, 2012.

393. Scutt G, Allen M, Kemenes G, Yeoman M. A switch in the mode of the sodium/calcium exchanger underlies an age-related increase in the slow afterhyperpolarization. *Neurobiol Aging* 2015;36:2838–49.

394. Segovia G, Porras A, Del Arco A, Mora F. Glutamatergic neurotransmission in aging: a critical perspective. *Mech Ageing Dev* 2001;122:1–29.

395. Selverston AI. Model neural networks and behavior. Plenum Press; 1985.

396. Senatore A, Zhorov BS, Spafford JD. Cav3 T-type calcium channels. *Wiley Interdiscip Rev Membr Transp Signal* 2012;1:467–91.

397. Seo AY, Joseph A-M, Dutta D, Hwang JCY, Aris JP, Leeuwenburgh C. New insights into the role of mitochondria in aging: mitochondrial dynamics and more. *J Cell Sci* 2010;123:2533–42.

398. Sesti F. Oxidation of K(+) Channels in Aging and Neurodegeneration. *Aging Dis* 2016;7:130–5.

399. Sesti F, Liu S, Cai S-Q. Oxidation of potassium channels by ROS: a general mechanism of aging and neurodegeneration? *Trends Cell Biol* 2010;20:45–51.

400. Shafi MM, Westover MB, Fox MD, Pascual-Leone A. Exploration and modulation of brain network interactions with noninvasive brain stimulation in combination with neuroimaging. *Eur J Neurosci* 2012;35:805–25.

401. Shah NH, Aizenman E. Voltage-gated potassium channels at the crossroads of neuronal function, ischemic tolerance, and neurodegeneration. *Transl Stroke Res* 2014;5:38–58.

402. Sharp AA, O'Neil MB, Abbott LF, Marder E. The dynamic clamp: artificial conductances in biological neurons. *Trends Neurosci* 1993;16:389–94.

403. Shen W, Hernandez-Lopez S, Tkatch T, Held JE, Surmeier DJ. Kv1.2-containing K+ channels regulate subthreshold excitability of striatal medium spiny neurons. *J Neurophysiol* 2004;91:1337–49.

404. Shibata R, Nakahira K, Shibasaki K, Wakazono Y, Imoto K, Ikenaka K. A-Type K ⁺ Current Mediated by the Kv4 Channel Regulates the Generation of Action Potential in Developing Cerebellar Granule Cells n.d.

405. Shih R-H, Wang C-Y, Yang C-M. NF-kappaB Signaling Pathways in Neurological Inflammation: A Mini Review. *Front Mol Neurosci* 2015;8:77.

406. Shoeb M, Ansari NH, Srivastava SK, Ramana K V. 4-Hydroxynonenal in the pathogenesis and progression of human diseases. *Curr Med Chem* 2014;21:230–7.

407. Shrivastava IH, Capener CE, Forrest LR, Sansom MS. Structure and dynamics of K channel pore-lining helices: a comparative simulation study. *Biophys J* 2000;78:79–92.

408. Shrivastava IH, Peter Tieleman D, Biggin PC, Sansom MSP. K+ versus Na+ Ions in a K Channel

Selectivity Filter: A Simulation Study. *Biophys J* 2002;83:633–45.

409. Simkin D, Hattori S, Ybarra N, Musial TF, Buss EW, Richter H, et al. Aging-Related Hyperexcitability in CA3 Pyramidal Neurons Is Mediated by Enhanced A-Type K+ Channel Function and Expression. *J Neurosci* 2015;35:13206–18.

410. Smith DO, Rosenheimer JL, Kalil RE. Delayed Rectifier and A-Type Potassium Channels Associated with Kv 2.1 and Kv 4.3 Expression in Embryonic Rat Neural Progenitor Cells. *PLoS One* 2008;3:e1604.

411. So MJ, Cho EJ. Phloroglucinol Attenuates Free Radical-induced Oxidative Stress. *Prev Nutr Food Sci* 2014;19:129–35.

412. Sonner PM, Stern JE. Functional role of A-type potassium currents in rat presympathetic PVN neurones. *J Physiol* 2007;582:1219–38.

413. Spector PS, Curran ME, Zou A, Keating MT, Sanguinetti MC. Fast inactivation causes rectification of the IKr channel. *J Gen Physiol* 1996;107:611–9.

414. Stadtman ER, Levine RL. Free radical-mediated oxidation of free amino acids and amino acid residues in proteins. *Amino Acids* 2003;25:207–18.

415. Standen NB (Nick B., Gray PTA (Peter TA., Whitaker MJ (Michael J., Plymouth Workshop. Microelectrode techniques : the Plymouth Workshop handbook. Company of Biologists; 1987.

416. Staras K, Gyoo'ri J, Kemenes G. Voltage-gated ionic currents in an identified modulatory cell type controlling molluscan feeding. *Eur J Neurosci* 2002;15:109–19.

417. Staras K, Kemenes G, Benjamin PR. Pattern-Generating Role for Motoneurons in a Rhythmically Active Neuronal Network. *J Neurosci* 1998;18:3669–88.

418. Staras K, Kemenes G, Benjamin PR. Electrophysiological and behavioral analysis of lip touch as a component of the food stimulus in the snail Lymnaea. *J Neurophysiol* 1999;81:1261–73.

419. Staras K, Kemenes G, Benjamin PR. Cellular Traces of Behavioral Classical Conditioning Can Be Recorded at Several Specific Sites in a Simple Nervous System. *J Neurosci* 1999;19:347–57.

420. Staras K, Kemenes G, Benjamin PR. Neurophysiological Correlates of Unconditioned and Conditioned Feeding Behavior in the Pond Snail Lymnaea stagnalis. *J Neurophysiol* 1998;79.

421. Starkstein SE, Kremer JL. Cerebral aging: neuropsychological, neuroradiological, and neurometabolic correlates. *Dialogues Clin Neurosci* 2001;3:217–28.

422. Stocker M, Krause M, Pedarzani P. An apamin-sensitive Ca2+-activated K+ current in hippocampal pyramidal neurons. *Proc Natl Acad Sci U S A* 1999;96:4662–7.

423. Stölting G, Fischer M, Fahlke C. CLC channel function and dysfunction in health and disease. *Front Physiol* 2014;5:378.

424. Storm JF. Potassium currents in hippocampal pyramidal cells. *Prog Brain Res* 1990;83:161–87.

425. Storm JF. Action potential repolarization and a fast after-hyperpolarization in rat hippocampal pyramidal cells. *J Physiol* 1987;385:733–59.

426. Straub VA, Benjamin PR. Extrinsic modulation and motor pattern generation in a feeding network: a cellular study. *J Neurosci* 2001;21:1767–78.

427. Straub VA, Staras K, Kemenes G, Benjamin PR. Endogenous and Network Properties of Lymnaea Feeding Central Pattern Generator Interneurons. *J Neurophysiol* 2002;88:1569–83.

428. Straub VA, Styles BJ, Ireland JS, O'Shea M, Benjamin PR. Central localization of plasticity involved in appetitive conditioning in Lymnaea. *Learn Mem* 11:787–93.

429. Streit WJ. Microglial senescence: does the brain's immune system have an expiration date? *Trends Neurosci* 2006;29:506–10.

430. Streit WJ, Braak H, Xue Q-S, Bechmann I. Dystrophic (senescent) rather than activated microglial cells are associated with tau pathology and likely precede neurodegeneration in Alzheimer's disease. *Acta Neuropathol* 2009;118:475–85.

431. Südhof TC, Rizo J. Synaptic vesicle exocytosis. *Cold Spring Harb Perspect Biol* 2011;3.

432. Sunada H, Lukowiak K, Ito E. Cerebral Giant Cells are Necessary for the Formation and Recall of Memory of Conditioned Taste Aversion in *Lymnaea*. *Zoolog Sci* 2017;34:72–80.

433. Sunada H, Takigami S, Lukowiak K, Sakakibara M. Electrophysiological characteristics of feeding-related neurons after taste avoidance Pavlovian conditioning in Lymnaea stagnalis. *Biophys (Nagoya-Shi, Japan)* 2014;10:121–33.

434. Takahira M, Hughes BA. Isolated bovine retinal pigment epithelial cells express delayed rectifier type and M-type K+ currents. *Am J Physiol* 1997;273:C790-803.

435. Tan FCC, Hutchison ER, Eitan E, Mattson MP. Are there roles for brain cell senescence in aging and neurodegenerative disorders? *Biogerontology* 2014;15:643–60.

436. Tanaka K, Hashimoto T, Tokumaru S, Iguchi H, Kojo S. Interactions between vitamin C and vitamin E are observed in tissues of inherently scorbutic rats. *J Nutr* 1997;127:2060–4.

437. Tank EMH, Rodgers KE, Kenyon C. Spontaneous age-related neurite branching in Caenorhabditis elegans. *J Neurosci* 2011;31:9279–88.

438. Taylor BE, Lukowiak K. The respiratory central pattern generator of Lymnaea: a model, measured and malleable. *Respir Physiol* 2000;122:197–207.

439. Tchkonia T, Zhu Y, van Deursen J, Campisi J, Kirkland JL. Cellular senescence and the senescent secretory phenotype: therapeutic opportunities. *J Clin Invest* 2013;123:966–72.

440. Thibault O, Gant JC, Landfield PW. Expansion of the calcium hypothesis of brain aging and Alzheimer's disease: minding the store. *Aging Cell* 2007;6:307–17.

441. Thibault O, Hadley R, Landfield PW. Elevated postsynaptic [Ca2+]i and L-type calcium channel activity in aged hippocampal neurons: relationship to impaired synaptic plasticity. *J Neurosci* 2001;21:9744–56.

442. Thibault O, Landfield PW. Increase in single L-type calcium channels in hippocampal neurons during aging. *Science* 1996;272:1017–20.

443. Tieleman DP, Shrivastava IH, Ulmschneider MR, Sansom MS. Proline-induced hinges in transmembrane helices: possible roles in ion channel gating. *Proteins* 2001;44:63–72.

444. Todorovic SM, Jevtovic-Todorovic V. Redox regulation of neuronal voltage-gated calcium channels. *Antioxid Redox Signal* 2014;21:880–91.

445. Toescu EC. Normal brain ageing: models and mechanisms. *Philos Trans R Soc Lond B Biol Sci* 2005;360:2347–54.

446. Toescu EC. Altered Calcium Homeostasis in Old Neurons 2007.

447. Toescu EC, Vreugdenhil M. Calcium and normal brain ageing. *Cell Calcium* 2010;47:158–64.

448. Tosato M, Zamboni V, Ferrini A, Cesari M. The aging process and potential interventions to extend life expectancy. *Clin Interv Aging* 2007;2:401–12.

449. Toth PT, Miller RJ. Calcium and sodium currents evoked by action potential waveforms in rat sympathetic neurones. *Doi.org* 1995;485:43–57.

450. Treptow W, Tarek M. K+ conduction in the selectivity filter of potassium channels is monitored by the charge distribution along their sequence. *Biophys J* 2006;91:L81-3.

451. Tripathi ON, Ravens U, Sanguinetti MC. Heart rate and rhythm : molecular basis, pharmacological modulation and clinical implications. Springer; 2011.

452. Tse F, Fraser D, Duffy S, MacVicar B. Voltage-activated K+ currents in acutely isolated hippocampal astrocytes. *J Neurosci* 1992;12.

453. University RCP of BM. Behavior and Its Neural Control in Gastropod Molluscs. Oxford University Press, USA; 2002.

454. Vanguilder HD, Yan H, Farley JA, Sonntag WE, Freeman WM. Aging alters the expression of neurotransmission-regulating proteins in the hippocampal synaptoproteome. *J Neurochem* 2010;113:1577–88.

455. Vardanyan V, Pongs O. Coupling of voltage-sensors to the channel pore: a comparative view. *Front Pharmacol* 2012;3:145.

456. Varma S, Rogers DM, Pratt LR, Rempe SB. Perspectives on: ion selectivity: design principles for K+ selectivity in membrane transport. *J Gen Physiol* 2011;137:479–88.

457. Vavoulis D V, Nikitin ES, Kemenes I, Marra V, Feng J, Benjamin PR, et al. Balanced plasticity and stability of the electrical properties of a molluscan modulatory interneuron after classical conditioning: a computational study. *Front Behav Neurosci* 2010;4:19.

458. Vavoulis D V, Straub VA, Kemenes I, Kemenes G, Feng J, Benjamin PR. Dynamic control of a central pattern generator circuit: a computational model of the snail feeding network. *Eur J Neurosci* 2007;25:2805–18.

459. Vehovszky A, Elliott CJH. Activation and Reconfiguration of Fictive Feeding by the OctopamineContaining Modulatory OC Interneurons in the Snail Lymnaea. *J Neurophysiol* 2001;86:792–808.

460. Verkerk AO, Schumacher CA, van Ginneken ACG, Veldkamp MW, Ravesloot JH. Role of Ca^{2+}-Activated Cl$^-$ Current in Ventricular Action Potentials of Sheep During Adrenoceptor Stimulation. *Exp Physiol* 2001;86:151–9.

461. Verkhratsky A. The endoplasmic reticulum and neuronal calcium signalling. *Cell Calcium* 32:393–404.

462. Verkman AS, Galietta LJ V. Chloride channels as drug targets. *Nat Rev Drug Discov* 2009;8:153–71.

234

463. Viña J, Borras C, Abdelaziz KM, Garcia-Valles R, Gomez-Cabrera MC. The Free Radical Theory of Aging Revisited: The Cell Signaling Disruption Theory of Aging. *Antioxid Redox Signal* 2013;19:779–87.

464. Vitureira N, Goda Y. Cell biology in neuroscience: the interplay between Hebbian and homeostatic synaptic plasticity. *J Cell Biol* 2013;203:175–86.

465. Vorbach C, Harrison R, Capecchi MR. Xanthine oxidoreductase is central to the evolution and function of the innate immune system. *Trends Immunol* 2003;24:512–7.

466. Vyjayanti VN, Rao KS. DNA double strand break repair in brain: reduced NHEJ activity in aging rat neurons. *Neurosci Lett* 2006;393:18–22.

467. Waldegger S, Jentsch TJ. From tonus to tonicity: physiology of CLC chloride channels. *J Am Soc Nephrol* 2000;11:1331–9.

468. Wang C-Y, Huang A-Q, Zhou M-H, Mei Y-A. GDF15 regulates Kv2.1-mediated outward K+ current through the Akt/mTOR signalling pathway in rat cerebellar granule cells. *Biochem J* 2014;460:35–47.

469. Wang K, Chai J. N-Type Inactivation in Voltage-Gated Potassium Channels. Encycl. Biophys., Berlin, Heidelberg: Springer Berlin Heidelberg; 2013, p. 1750–2.

470. Wang X, Michaelis EK. Selective neuronal vulnerability to oxidative stress in the brain. *Front Aging Neurosci* 2010;2:12.

471. Wang X, Proud CG. The mTOR pathway in the control of protein synthesis. *Physiology (Bethesda)* 2006;21:362–9.

472. Wang XJ. Calcium coding and adaptive temporal computation in cortical pyramidal neurons. *J Neurophysiol* 1998;79:1549–66.

473. Wang XQ, Deriy L V, Foss S, Huang P, Lamb FS, Kaetzel MA, et al. CLC-3 channels modulate excitatory synaptic transmission in hippocampal neurons. *Neuron* 2006;52:321–33.

474. Wang Z, Van den Berg RJ, Ypey DL. Resting membrane potentials and excitability at different regions of rat dorsal root ganglion neurons in culture. *Neuroscience* 1994;60:245–54.

475. Ward E V, Berry CJ, Shanks DR. Age effects on explicit and implicit memory. *Front Psychol* 2013;4:639.

476. Watson SN, Lee JR, Risling TE, Hermann PM, Wildering WC. Diminishing glutathione availability and age-associated decline in neuronal excitability. *Neurobiol Aging* 2014;35:1074–85.

477. Watson SN, Risling TE, Hermann PM, Wildering WC. Failure of delayed nonsynaptic neuronal plasticity underlies age-associated long-term associative memory impairment. *BMC Neurosci* 2012;13:103.

478. Watson SN, Wright N, Hermann PM, Wildering WC. Phospholipase A$_2$: the key to reversing long-term memory impairment in a gastropod model of aging. *Neurobiol Aging* 2013;34:610–20.

479. Weber JT. Altered calcium signaling following traumatic brain injury. *Front Pharmacol* 2012;3:60.

480. Weiger T, Dopico A, Hermann A. BK Channels: Integrators of cellular signals in health and disease. 1st ed. Frontiers Media SA; 2017.

481. West AP, Shadel GS, Ghosh S. Mitochondria in innate immune responses. *Nat Rev Immunol* 2011;11:389–402.

482. Wheeler DD, Ondo JG. Time course of the aging of the high affinity L-glutamate transporter in rat cortical synaptosomes. *Exp Gerontol* 1986;21:159–68.

483. White SH, Sturgeon RM, Magoski NS. Nicotine inhibits potassium currents in Aplysia bag cell neurons. *J Neurophysiol* 2016;115:2635–48.

484. Whyte KA, Hogg RC, Dyavanapalli J, Harper AA, Adams DJ. Reactive oxygen species modulate neuronal excitability in rat intrinsic cardiac ganglia. *Auton Neurosci* 2009;150:45–52.

485. Wildburger NC, Lin-Ye A, Baird MA, Lei D, Bao J. Neuroprotective effects of blockers for T-type calcium channels. *Mol Neurodegener* 2009;4:44.

486. Winkelman DLB, Beck CL, Ypey DL, O'Leary ME. Inhibition of the A-type K+ channels of dorsal root ganglion neurons by the long-duration anesthetic butamben. *J Pharmacol Exp Ther* 2005;314:1177–86.

487. Winterbourn CC. The Biological Chemistry of Hydrogen Peroxide. Methods Enzymol., vol. 528, 2013, p. 3–25.

488. Wladyka CL, Kunze DL. KCNQ/M-currents contribute to the resting membrane potential in rat visceral sensory neurons. *J Physiol* 2006;575:175–89.

489. Wong BS, Adler M. Tetraethylammonium blockade of calcium-activated potassium channels in clonal anterior pituitary cells. *Pflügers Arch Eur J Physiol* 1986;407:279–84.

490. Woodward OM, Willows AOD. Dopamine modulation of Ca2+ dependent Cl- current regulates

ciliary beat frequency controlling locomotion in Tritonia diomedea. *J Exp Biol* 2006;209.

491. Wright E. Older People's Day 2011. *Off Natl Stat* 2011.

492. Wu L-J. Voltage-Gated Proton Channel H $_\text{V}$ 1 in Microglia. *Neurosci* 2014;20:599–609.

493. Wu L-J, Wu G, Sharif MRA, Baker A, Jia Y, Fahey FH, et al. The voltage-gated proton channel Hv1 enhances brain damage from ischemic stroke. *Nat Neurosci* 2012;15:565–73.

494. Xiong J, Camello PJ, Verkhratsky A, Toescu EC. Mitochondrial polarisation status and [Ca2+]i signalling in rat cerebellar granule neurones aged in vitro. *Neurobiol Aging* 2004;25:349–59.

495. Xiong J, Verkhratsky A, Toescu EC. Changes in Mitochondrial Status Associated with Altered Ca2+ Homeostasis in Aged Cerebellar Granule Neurons in Brain Slices. *J Neurosci* 2002;22:10761–71.

496. Xu S, Cai Y, Wei Y. mTOR Signaling from Cellular Senescence to Organismal Aging. *Aging Dis* 2014;5:263–73.

497. Xu ZJ, Adams DJ. Resting membrane potential and potassium currents in cultured parasympathetic neurones from rat intracardiac ganglia. *J Physiol* 1992;456:405–24.

498. Yamamoto D, Suzuki N. Properties of single chloride channels in primary neuronal cultures of Drosophila. *Biochim Biophys Acta* 1989;986:187–90.

499. Yamazaki D, Horiuchi J, Nakagami Y, Nagano S, Tamura T, Saitoe M. The Drosophila DC0 mutation suppresses age-related memory impairment without affecting lifespan. *Nat Neurosci* 2007;10.

500. Yang J-L, Weissman L, Bohr VA, Mattson MP. Mitochondrial DNA damage and repair in neurodegenerative disorders. *DNA Repair (Amst)* 2008;7:1110–20.

501. Yellen G. The voltage-gated potassium channels and their relatives n.d.

502. Yellen G. The moving parts of voltage-gated ion channels. *Q Rev Biophys* 1998;31:239–95.

503. Yeoman M, Scutt G, Faragher R. Insights into CNS ageing from animal models of senescence. *Nat Rev Neurosci* 2012;13:435–45.

504. Yeoman MS, Benjamin PR. Two types of voltage-gated K(+) currents in dissociated heart ventricular muscle cells of the snail Lymnaea stagnalis. *J Neurophysiol* 1999;82:2415–27.

505. Yeoman MS, Brierley MJ, Benjamin PR. Central pattern generator interneurons are targets for the modulatory serotonergic cerebral giant cells in the feeding system of Lymnaea. *J Neurophysiol* 1996;75:11–25.

506. Yeoman MS, Kemenes G, Benjamin PR, Elliott CJ. Modulatory role for the serotonergic cerebral giant cells in the feeding system of the snail, Lymnaea. II. Photoinactivation. *J Neurophysiol* 1994;72:1372–82.

507. Yeoman MS, Patel BA, Arundell M, Parker K, O'Hare D. Synapse-specific changes in serotonin signalling contribute to age-related changes in the feeding behaviour of the pond snail, Lymnaea. *J Neurochem* 2008;106:1699–709.

508. Yeoman MS, Pieneman AW, Ferguson GP, Ter Maat A, Benjamin PR, Burke JF, et al. Modulatory role for the serotonergic cerebral giant cells in the feeding system of the snail, Lymnaea. I. Fine wire recording in the intact animal and pharmacology. *J Neurophysiol* 1994;72:1357–71.

509. Yeoman MS, Vehovszky A, Kemenes G, Elliott CJ, Benjamin PR. Novel interneuron having hybrid modulatory-central pattern generator properties in the feeding system of the snail, Lymnaea stagnalis. *J Neurophysiol* 1995;73:112–24.

510. Yu-Zhi L, Hai-Long A, Su-Hua Z, Hui Y, Yong Z, Hai-Lin Z. Electrostatic Interactions Determining the Selectivity of KcsA Channel and Its Mutants. *Chinese Phys Lett* 2010;27:88701.

511. Yu FH, Catterall WA. Overview of the voltage-gated sodium channel family. *Genome Biol* 2003;4:207.

512. Yu SP, Yeh CH, Gottron F, Wang X, Grabb MC, Choi DW. Role of the outward delayed rectifier K+ current in ceramide-induced caspase activation and apoptosis in cultured cortical neurons. *J Neurochem* 1999;73:933–41.

513. Yu W, Parakramaweera R, Teng S, Gowda M, Sharad Y, Thakker-Varia S, et al. Oxidation of KCNB1 Potassium Channels Causes Neurotoxicity and Cognitive Impairment in a Mouse Model of Traumatic Brain Injury. *J Neurosci* 2016;36:11084–96.

514. Zagotta W, Hoshi T, Aldrich R. Restoration of inactivation in mutants of Shaker potassium channels by a peptide derived from ShB. *Science (80-)* 1990;250:568–71.

515. Zaidi A. Plasma membrane Ca-ATPases: Targets of oxidative stress in brain aging and neurodegeneration. *World J Biol Chem* 2010;1:271–80.

516. Zakon HH. Adaptive evolution of voltage-gated sodium channels: The first 800 million years. *Proc Natl Acad Sci* 2012;109:10619–25.

517. Zhan X-Q, He Y-L, Yao J-J, Zhuang J-L, Mei Y-A. The antidepressant citalopram inhibits delayed rectifier outward K+ current in mouse cortical neurons. *J Neurosci Res* 2012;90:324–36.

518. Zhang G, Li J, Purkayastha S, Tang Y, Zhang H, Yin Y, et al. Hypothalamic programming of systemic ageing involving IKK-β, NF-κB and GnRH. *Nature* 2013;497:211–6.

519. Zhang W, Schmelzeisen S, Parthier D, Frings S, Möhrlen F. Anoctamin Calcium-Activated Chloride Channels May Modulate Inhibitory Transmission in the Cerebellar Cortex. *PLoS One* 2015;10:e0142160.

520. Zhao B, Rassendren F, Kaang B-K, Furukawa Y, Kubo T, Kandel ER, et al. A New Class of Noninactivating K+ Channels from Aplysia Capable of Contributing to the Resting Potential and Firing Patterns of Neurons. *Neuron* 1994;13:1205–13.

521. Zheng J, Trudeau MC. Handbook of ion channels. n.d.

522. Zhou FM, Hablitz JJ. Layer I neurons of rat neocortex. I. Action potential and repetitive firing properties. *J Neurophysiol* 1996;76:651–67.

523. Zhou S-S, Gao Z, Dong L, Ding Y-F, Zhang X-D, Wang Y-M, et al. Anion channels influence ECC by modulating L-type Ca(2+) channel in ventricular myocytes. *J Appl Physiol* 2002;93:1660–8.

524. Zhou Y, MacKinnon R. Ion Binding Affinity in the Cavity of the KcsA Potassium Channel [†]. *Biochemistry* 2004;43:4978–82.

525. Zhou Y, MacKinnon R. The occupancy of ions in the K+ selectivity filter: charge balance and coupling of ion binding to a protein conformational change underlie high conduction rates. *J Mol Biol* 2003;333:965–75.

526. Zhou Y, Morais-Cabral JH, Kaufman A, MacKinnon R. Chemistry of ion coordination and hydration revealed by a K+ channel-Fab complex at 2.0 A resolution. *Nature* 2001;414:43–8.

527. Zündorf G, Reiser G. Calcium dysregulation and homeostasis of neural calcium in the molecular mechanisms of neurodegenerative diseases provide multiple targets for neuroprotection. *Antioxid Redox Signal* 2011;14:1275–88.

528. Excitability and branching of neuroendocrine cells during reproductive senescence. *Neurobiol Aging* 1999;20:675–83.

529. Neurobiology and Behavior. Elsevier Science; 2013.

530. Physiology of Mollusca, Volume 2. Elsevier Science; 2013.

531. Chloride channels. *Br J Pharmacol* 2009;158:S130–4.